2009

STUDIES ON DRUG SOLUBILIZATION MECHANISM IN SIMPLE MICELLE SYSTEMS

Shaoxin Feng
University of Kentucky, sfenf2@uky.edu

ABSTRACT OF DISSERTATION

Shaoxin Feng

The Graduate School

University of Kentucky

2009

STUDIES ON DRUG SOLUBILIZATION MECHANISM IN SIMPLE MICELLE SYSTEMS

ABSTRACT OF DISSERTATION

A dissertation submitted in partial fulfillment of the requirements for the degree of Doctor of Philosophy in the College of Pharmacy at the University of Kentucky

By
Shaoxin Feng

Lexington, Kentucky

Director: Dr. Paul M. Bummer, Associate Professor of Pharmaceutical Sciences

Lexington, Kentucky

2009

ABSTRACT OF DISSERTATION

STUDIES ON DRUG SOLUBILIZATION MECHANISM IN SIMPLE MICELLE SYSTEMS

Poor aqueous solubilities of drug candidates limit the biopharmaceutical usefulness in either oral or parenteral dosage forms. Lipid assemblies, such as micelles, may provide a means of enhancing solubility. Despite their usefulness, little is known about the means by which micelles accomplish this result. The goal of the current dissertation is to provide the molecular level understanding of the mechanism by which simple micelle systems solubilize drugs. Specifically, the location, orientation and amount of the drug molecules in micelle systems are the focuses of the work.

Three series of model drugs, steroids, benzodiazepines and parabens, in three surfactant systems with anionic, cationic and neutral hydrophilic headgroups were studied. Solubilization power of each micelle system for each model drug was determined by equilibrium solubility. The observed strong surface activities of model drug at hydrocarbon/water interface and the ability of the drugs to compete with surfactants for the model oil/water interface lend support to the hypothesis that drug molecules are mainly solubilized in the interfacial region of the micelles. A surface-localized thermodynamic model that considered the surfactant-drug competition at micelle surface was successfully applied to predict the micelle/water partitioning coefficients. The predictions were made without the use of adjustable parameters in the case of both dilute and concentrated solutions. The orientation of drug at micelle surface was determined by matching calculated occupied areas by solutes at oil/water interface using molecular modeling method to the experimental values. To look into the micro-structure of micelles, two-dimensional and diffusion (or PGSE) NMR techniques were employed to detect the specific drug-surfactant interactions and the micelle sizes influenced by model drugs and electrolytes.

KEYWORDS: Simple Micelle Systems, Poorly Water-soluble Drugs, Solubilization, Thermodynamic Model, Surface Activity

Shaoxin Feng

November 17, 2009

STUDIES ON DRUG SOLUBILIZATION MECHANISM IN SIMPLE MICELLE SYSTEMS

By

Shaoxin Feng

Dr. Paul M. Bummer
Director of Dissertation

Dr. Robert Yokel
Director of Graduate Studies

November 17, 2009
Date

RULES FOR THE USE OF DISSERTATIONS

Unpublished dissertations submitted for the Doctor's degree and deposited in the University of Kentucky Library are as a rule open for inspection, but are to be used only with due regard to the rights of the authors. Bibliographical references may be noted, but quotations or summaries of parts may be published only with the permission of the author, and with the usual scholarly acknowledgments.

Extensive copying or publication of the dissertation in whole or in part also requires the consent of the Dean of the Graduate School of the University of Kentucky.

A library that borrows this dissertation for use by its patrons is expected to secure the signature of each user.

Name	Date

DISSERTATION

Shaoxin Feng

The Graduate School

University of Kentucky

2009

STUDIES ON DRUG SOLUBILIZATION MECHANISM IN SIMPLE MICELLE SYSTEMS

DISSERTATION

A dissertation submitted in partial fulfillment of the requirements for the degree of Doctor of Philosophy in the College of Pharmacy at the University of Kentucky

By
Shaoxin Feng

Lexington, Kentucky

Director: Dr. Paul M. Bummer, Associate Professor of Pharmaceutical Sciences

Lexington, Kentucky

2009

ACKNOWLEDGEMENTS

I would like to thank all the people who have accompanied and supported me and made their direct and indirect contributions to this dissertation in the past years.

First and foremost I would like to express my sincere appreciation to my research advisor, Dr. Paul M. Bummer, for his tremendous support throughout my graduate study. Dr. Bummer had been not only a scientist, but also a mentor, a great educator and a friend to me. His expertise and continuous guidance helped me develop skills in designing, executing and analyzing experiments, given my pure theoretical background. His approachable character and ever-present enthusiasm led to a lot of discussions with him, from which I got patient answers and fresh insights that covered various areas, such as experimental methodologies, instrumental problems, presentation preparations and even job-hunting strategies.

I would like to thank Dr. Bradley Anderson for his inspiring questions that helped keep my research in the right track. His preciseness and deep understanding in physical pharmacy helped me develop critical thinking that is important for a qualified scientist. I am also grateful for his kindness of letting me use many instruments in his lab. I would like to thank the members of my dissertation committee: Dr. Barbara Knutson and Dr. Tonglei Li, as well as Dr. Stefan Stamm, the outside examiner, for their technical expertise, insights, and knowledge to this work.

Special thanks go to Mr. John Layton and Dr. Anne-Frances Miller who generously helped me use the Pulsed Gradient Spin Echo NMR in the Department of Chemistry.

I would like to thank my labmates, Lin Song, Salin Gupta, Abebe Mengesha, and Dr. Anderson's group members (Vijay Jogoparthi, Michael DeHart, Dhaval Patel) for their help on my experiments. I also thank my friends, Xue Luo, Liming Zhao, Donghua Zhu, and Mikolaj Milewski, for their friendship which made the time in the graduate school unforgettable.

I would like to thank my parents for their love and support during the long years of my education. I thank my parents-in-law for their support in helping with the family. I also thank my son, Yihan (Leo), for all the joys he brought to the family which had brightened my life.

Last but not least, I thank my wife, Lingzhi Liu, for being there for me no matter what happens. Her love, dedication and persistent confidence in me have taken, and will always take the load off my shoulder.

TABLE OF CONTENTS

List of Tables

List of Figures

Chapter 1

Statement of Problem and Aims

Poor water solubility is a major limiting factor to the development of many pharmacotherapeutic agents. Micelles are well known to enhance the aqueous solubility of poorly-water soluble drugs and thus have the potential to enable drug delivery by the parenteral or oral routes. At present, fundamental understanding of the solubilization mechanism by micelles is lacking. As a consequence, the enhancement of drug delivery employing micelles has not reached its full potential.

The goal of this dissertation is to provide a molecular-level understanding of the mechanism by which micelle systems solubilize drug molecules. Specifically, the location and orientation of the drug molecules in micelle systems will be determined; the amount of the solute molecules in specific micelle systems could be predicted based on the interactions between solutes and surfactants in micelles. The mechanistic understanding of which micelle system could best solubilize a specific drug candidate can provide a guideline for selecting the optimal solubilizing ingredients and greatly speed up the drug formulation process.

The major hypothesis to be tested is**:** It is possible to predict micelle/water partitioning by accounting for solute-surfactant interactions that lead to localization at the micelle surface.

The specific aims employed to test this hypothesis are as follows:

1. Demonstrate that solubilization of model drugs in the core of the micelles is insufficient to predict micelle/water partitioning of the drugs.

2. Show experimentally that competition does occur between hydrophobic solutes and surfactants for a model oil/water interface.

3. Evaluate the ability of a surface-localized thermodynamic model to account for experimentally-determined micelle/water partitioning.

4. Determine the orientations of model drugs at the micelle surface by matching the calculated interfacial areas occupied by drugs at the oil/water interface to the experimental values.

5. Employing NMR spectroscopic techniques, probe the nature of the solute-surfactant molecular interactions in the micelles with the goal of determining how interactions will govern molecular location/orientation and thus solubilization of drugs.

Chapter 2

Background and Literature Review

2.1. Introduction

It has been estimated that 40 to 60 % of new drug candidates entering drug development programs possess poorly aqueous solubility. Poor solubility presents a major challenge for pharmaceutical formulation of both oral and parenteral products. The formulation scientist is often faced with the difficult task of either increasing the dissolution rates or enhancing the aqueous solubility of those poorly soluble drug candidates.

The importance of solubility has long been recognized by official compendia, such as the USP (USP, 2009). There are several ways to express absolute solubility of a solute, such as the number of parts of solvent required to dissolve one part of solute. For biopharmaceutical purposes, a solubility descriptor focusing on the clinical dose is appropriate. Based on biopharmaceutical classification system (BCS) (Amidon et al., 1995), a drug candidate is considered to have adequate solubility when its highest dose could be dissolved in 250mL or less of buffer within pH 1~7.5. If more than 250mL is required the drug candidate is defined as poorly soluble. BCS classifies drug candidates into 4 categories in terms of their aqueous solubilities and permeabilities through biological membrane (Figure 2.1). Class I drugs are both highly soluble and highly permeable and tend to have good oral bioavailabilities, assuming no issues with first-pass metabolism or chemical stability. Class II drugs have bioavailabilities limited by poor solubility. Poor solubility is also one characteristic of Class IV drugs as well. Formulation methods that enhance solubility could “move” class II drug candidates (low solubility,

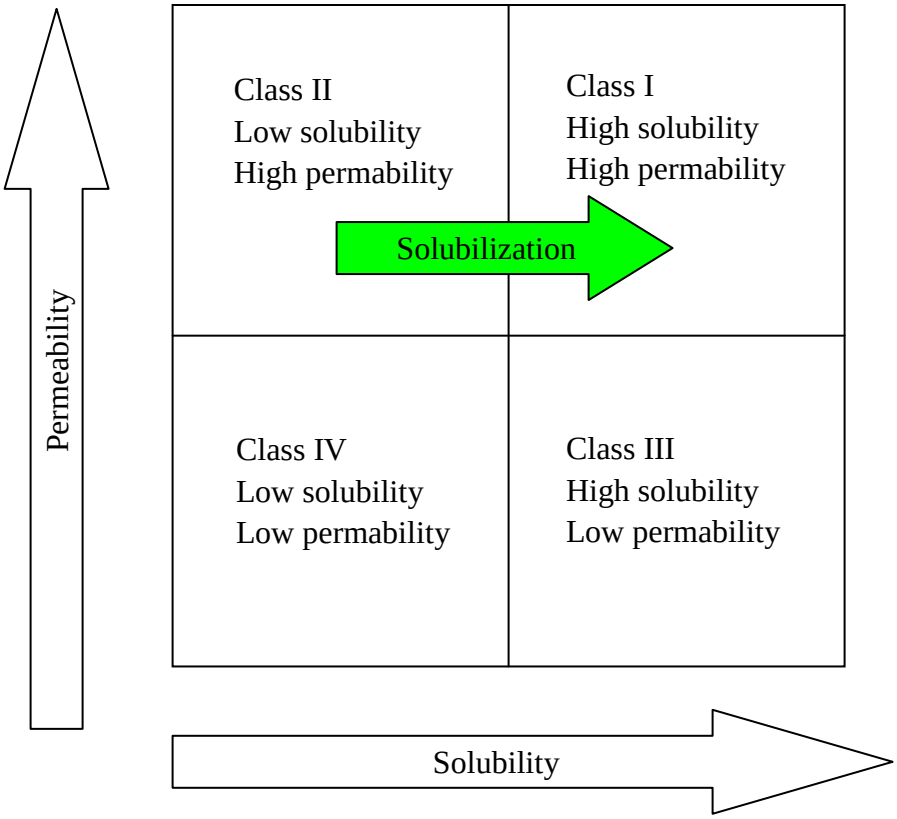

Figure 2.1 A schematic of biopharmaceutical classification system (BCS) (Adapted from Amidon et al. (Amidon et al., 1995)). Solubilization could shift BCS class II drug candidates into the BCS class I region.

high permeability) into class I (high solubility, high permeability) and enhance the corresponding bioavailabilities.

2.2. Means of Solubilization

There are many techniques used to improve aqueous solubility, such as pH adjustment, salt formation, co-solvents, complexation, amorphous solids and lipid assemblies (Yalkowsky, 1999). The techniques could be employed individually or in combination to provide synergistic effect of solubility enhancement (Li et al., 1999a; Li et al., 1999b; Li et al., 1998; Tongeree et al., 1999; Viernstein et al., 2003; Kawakami et al., 2004). All these methods are successful to some extent or another, but all do have disadvantages for oral or parenteral administration. Altering pH or salt formation makes use of higher solubility of ionic form of solute which could be obtained by decreasing pH for weak bases or increasing pH for weak acids, but the methods has potential issues of chemical stability of drugs and biocompatibility of pH extremes. Co-solvents technique uses the mixture of water and physiologically-acceptable organic solvents, such as propylene glycol, ethanol, glycerin etc., to improve solubility, but has the issue of pharmacological effect of organic solvents and possible precipitation of drugs upon dilution. Complexation could shift monomer forms of drugs into complexes with complexing agents, usually cyclodextrin, and improve solubility. The structure of drug must be such so as to interact strongly with the complexing agent. Slow releasing rate of drugs from the complexes is another potential limiting issue. Amorphous solids could be applied to enhance the “solubility”, as defined using free energy difference between amorphous and crystal form (Hancock and Parks, 2000), because of the higher free energy of the amorphous state. On the other hand, the high free energy of amorphous solids exhibit poor long term physical/chemical stability. Lipid assemblies make use of higher solubility of hydrophobic drugs in biocompatible lipid assemblies but excipient selection and drug releasing profiles are not yet well understood.

2.3. Family of Lipid Assemblies

One of the advantageous characteristics of the use of lipids to enhance the solubility of drugs in dosage forms is the wide variety of lipid assemblies that can be formed in an aqueous environment. The properties of lipid assemblies are modified by changing the composition of their components: water, surfactant, oil, and in some cases co-solvent. Figure 2.2 shows a general schematic phase diagram of lipid assemblies adapted from Bummer (Bummer, 2004). Lipid assemblies included here are micelles, mixed micelles, microemulsions, emulsions, liposomes, solid lipid nanoparticles, and self-dispersing systems. In all cases, the assemblies provide micro-environments that help solubilize drug molecules of varying properties. For example, micelles, as aggregations of surfactant molecules, may be treated as a separate phase when the surfactant concentration was above critical micelle concentration (CMC) in the absence of oil. Emulsions/microemulsions have oil-in-water or water-in-oil form depending on the surfactant properties and oil/water ratio. Liposomes use phospholipids bi-layer as the primary structure and may be classified as small unilamellar vesicles (SUV, size~50nm), large unilamellar vesicles (LUV, size 100~1000nm), multilamellar vesicles (MLV) and multivesicular liposomes (MVL) types. The drug molecules could be solubilized or loaded inside the liposomal vesicles or on lipid bi-layer membranes.

As indicated in Figure 2.2, the surfactant is a critical component of any lipid assemblies. Surfactant, as an abbreviation of “surface active agent”, is an organic compound that is amphiphilic comprising both hydrophilic groups (commonly referred to as “heads”) and hydrophobic groups (“tails”). Based on the electron charges of the hydrophilic head groups, surfactant are classified into 4 categories: anionic surfactants, such as sodium dodecyl sulfate (SDS), cationic surfactants, such as cetyl trimethylammonium bromide (CTAB), nonionic surfactants, such as polysorbate 80, and amphoteric (zwitterionic)

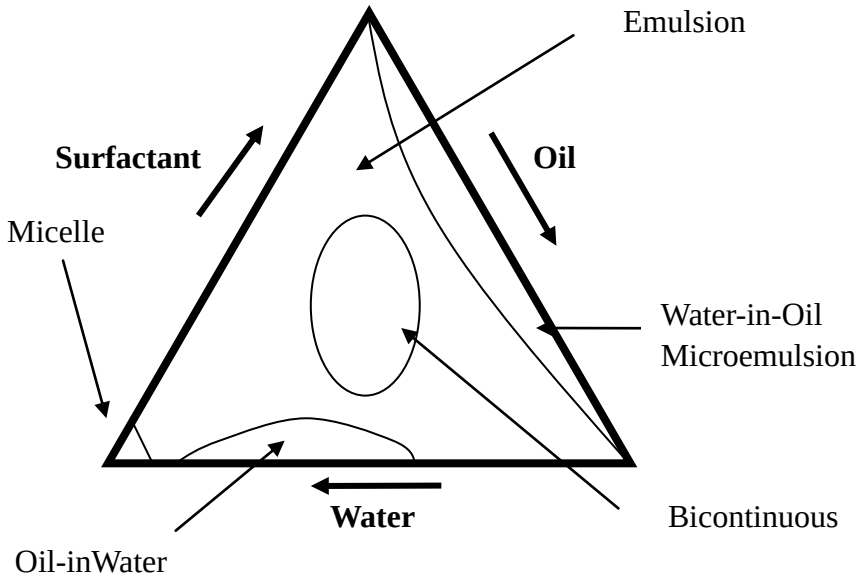

Figure 2.2 A schematic of phase diagram of lipid based systems. Adapted from Bummer (Bummer, 2004)

surfactants, such as phospholipids that contain anionic phosphate groups and cationic ammonium groups. In pharmaceutical preparations, the surfactants or any other excipients selected are often limited to be generally regarded as safe (GRAS) materials by Food and Drug Administration (Smolinske, 1992). Especially the use of the cationic agents is limited to topical antimicrobial preservatives rather than solubilizing agents because organic cations can be adsorbed at cell membrane in a nonspecific manner resulting in cell lysis. Anionic agents generally result in less hemolysis and SDS has been widely used as wetting agent, emulsifier and solubilizer in oral solid dosage forms. Zwitterionic surfactants, such as phospholipids, usually exhibit good biocompatibility. Phospholipids are mainly used to form liposomes that are often effective drug delivery systems for poorly soluble drugs and have controlled releasing profile and targeting capability (Joguparthi, 2007). Nonionic surfactants generally have the least toxicity profile and thus are the major class of surfactants used in pharmaceutical system through both oral and parenteral routes. Most commonly used nonionic surfactants have polyethylene glycol (PEG) chains as parts of hydrophilic heads, e.g. trade-marked products Tween series, Brij series, Cremophor EL and RH, TPGS etc.. Besides the solubilization function of PEGylated head groups, the PEG brushes on particle surfaces are believed to prevent the phagocytosis by blocking opsonins binding and increase the lifetime of the drug delivery vehicles in systemic circulation when administered parenterally (Allen et al., 1991).

Surfactants may also be classified in terms of technical applications. Each surfactant may be assigned a hydrophile-lipophile balance (HLB) value indicative of the relative polarity of parts of the molecules (Griffin, 1949; Griffin, 1954). The HLB value, as originally defined for nonionic surfactants, is weight percentage of hydrophilic groups (usually refer to polyethylene glycol) divided by 5 to narrow the range of values. Some ionic surfactants, such as SDS, could have greater HLB values than the theoretical maximum

number (20) because their hydrophilic behavior of the anionic head exceeds the polyethylene glycol group alone. HLB system is quite useful in assigning the major functions of surfactants: surfactants with HLB values between 3 and 6 are mainly used as water-in-oil emulsifiers; agents with HLB 8~18 are good oil-in-water emulsifiers; wetting agents usually have a HLB from 7 to 9; surfactants having HLB 15~20 can be used as solubilizers (Ansel et al., 1995).

Again referring to Figure 2.2, the oil is also a critical component of many (but not all) lipid assembly dosage forms. The oil phase of lipid assemblies is often a glyceride derived from plant sources, purified and chemically modified, either by PEGylation or hydrogenation to decrease the degrees of unsaturation for protection from oxidation. Typically triglycerides could be classified into 3 categories: short chain (<5 carbons), medium chain (6~12 carbons) and long chain (>12 carbons) for fatty acid portion. In commercial application of lipid-based delivery systems, the most frequently used oils are medium-chain (e.g. coconut oil, palm seed oil, etc.) and long-chain (e.g. corn oil, soybean oil, olive oil, sesame oil etc.) triglycerides because those oils could provide desirable physical and drug absorption properties (Hauss, 2007). Typically, triglycerides are employed, but a wide variety of commercially-modifed di- and mono-glycerides are also available.

2.4. Examples in the Literature of Use of Lipid Assemblies in Drug Delivery

Lipid-based drug delivery systems have received considerable interest in the recent years (Hauss, 2007; Pouton, 1997; Grove and Mullertz, 2007) because of their advantages in enhancing bioavailability of poorly-soluble hydrophobic drugs and possessing good biocompatibility. Besides the solubility improvement of poorly-soluble drugs by lipid-based system, there are several other factors that could help further increase the bioavailability and decrease the variability of absorption of poorly-soluble drugs: (1)

Some excipients such as Cremophor may increase absorption of drugs by inhibiting P-glycoprotein-mediated drug efflux and/or metabolism by GIT (GI tract) membrane-bind-cytochrome enzymes (Dintaman and Silverman, 1999; Chervinsky et al., 1993; Wandel et al., 2003). (2) Lymphatic transport could be promoted by long chain triglyceride, which delivers drug into lymph before entering the systemic circulation while avoiding hepatic first-pass metabolism (Khoo et al., 2003; Holm et al., 2003). (3) Permeability of drug through GIT membrane can be enhanced by surfactants through interfering with epithelial cell membrane (Whitehead and Mitragotri, 2008; Kitagawa and Ikarashi, 2003).

On the pharmaceutical market, there are already some commercially available formulations applying lipid based drug delivery systems through oral and parenteral routes (Strickley, 2004). For example, immunosuppressant cyclosporin A/Sandimmune® (Novartis) is formulated into oral soft gelatin capsules with Labrafil M-2125CS(surfactants) and corn oil; Anti-HIV drugs lopinavir & ritonavir/Kaletra® (Abbott) are formulated into oral soft gelatin capsules with oleic acid(oils) and Cremophor EL(surfactants); Antifungal antibiotics amphotericin B/Abelcet® (Enzon) employs liposomal formulations through IV injection using two kinds of phospholipids (dimyristoylphosphatidylcholine and dimyristoylphosphatidylglycol). Based on Strickley's survey on three markets, lipid-based system has occupied 3% (27 out of 839 products) of current drug market in the United States, 2% (21 out of 1254 products) in the United Kingdom, and 4% (8 out of 200 products) in Japan (Strickley, 2007).

2.5. Micelles as Drug Delivery Systems

Micelles are among the oldest lipid-based drug delivery systems. The earliest pharmaceutical application of micelles as solubilization agents was using soap solutions to solubilize cresols in preparation of Saponated Solutions of Cresol, U.S.P. and Lysol,

B.P. at the end of 19th century (Sjoblom, 1967). Surfactants, as emulsifying agents, had been applied in pharmaceuticals even earlier (Fishbein, 1945). It was not until 1950s that the pharmaceutical applications of micellar solubilization had received systematic attention (Sjoblom, 1967) and became extensively studied afterwards. In the current pharmaceutical market, many products use micelles as the drug delivery systems. For examples: anti-cancer drug paclitaxel/Taxol® (Bristol-Myers Squibb) uses Cremorphor EL micelles as the major delivery vehicles through IV infusion; Dutasteride/Avodart® (Glaxo SmithKline) is formulated into gelatin capsule that could form mixed micelles of mono- and diglycerides of caprylic/capric acid upon oral administration.

There are many advantages of micelles as a practical drug delivery system other than solubilization of poorly soluble drugs: micelles are thermodynamic stable (McBain and McBain, 1936); micelles may protect some unstable drugs from chemical degradation when the vulnerable functional groups of the drug are hided in the core region (Rodriguez et al., 2008); some polymeric micelles have tumor targeting function through enhanced permeation and retention (EPR) effect (Rangel-Yagui et al., 2005).

Micelles could also play an important role in other lipid-based delivery systems, such as self-emulsifying drug delivery system (SEDDS). Emulsions or microemulsions are formed by diluting SEDDS with aqueous fluids in GI tract. The digestability of the lipid component is thought to be essential in the drug release and absorption because indigestible lipids, such as paraffin oil, often actually inhibit the drug absorption by keeping the drug within the lipophilic reservoir (Palin and Wilson, 1984). The lipid digestion, mainly through lipolysis, will hydrolyze triglycerides to mono- or diglycerides and fatty acids that form mixed micelles with phospholipids and bile salts (Zangenberg, 2001a; Zangenberg, 2001b). The drugs solubilized in the mixed micelles are readily absorbed because of the large surface/volume ratio and fast exchange rate of the

monomers in and out of the micelles. The amount of the drug that could be solubilized in the mixed micelles would be critical in drug absorption.

2.6. Relevant Properties of Micelles

2.6.1. Physical and Chemical Properties of Micelles

There are several physicochemical properties of micelles that are critical in understanding their thermodynamic and kinetic behaviors. Typically, micelles exhibit critical behavior, that is, they form only when the concentration of the surfactant exceeds a characteristic value. This critical micelle concentration (CMC) can be modified by temperature and by the presence of other solutes. Micelles have a small size, normally around 5 to 100 nm (Rangel-Yagui et al., 2005). Light-scattering (Anacker and Ghose, 1968), small angle X-ray scattering (SAXS) (Svens and Rosenholm, 1973), small angle neutron scattering (SANS) (Lin et al., 1990), pulse gradient spin-echo NMR (Soderman et al., 2004) and other methods have been used to measure the micellar size and shape. Yalkowsky and Zografi found most micelles likely assume a spherical shape when the aggregation number, the number of surfactant molecules in the assembly, is below 100 (Yalkowsky and Zografi, 1972). The aggregation number may be modified by changing surfactant concentration or by other solutes (Turro and Yekta, 1978). At high surfactant concentration corresponding to high aggregation number, micelles may be subjected to a transition from spherical shape to elongated ellipsoidal shape (Imae et al., 1985; Reiss-Husson and Luzzati, 1964; Lin et al., 1990).

The kinetics of association and disassociation of surfactants forming a micelle are usually very rapid. The characteristic time for the surfactant monomers moving in and out of micelle is typically in the range of 10^{-8} to 10^{-3}s (Lindman and Wennerstrom, 1980). These bring a practical issue of possible precipitation of solubilizate among dilution of surfactants to below CMC that could affect drug performance. One exception is some

polymeric micelle could have much longer lifetime, in the order of hours, in the circulation system even the surfactant concentration is below CMC (Lavasanifar et al., 2002; Adams et al., 2003).

The micellar surfaces are found to be highly hydrated based on both experiments (Lindman and Brun, 1973; Mukerjee, 1964) and theoretical molecular dynamic simulations (Tieleman et al., 2000). For example, the hydration numbers per surfactant molecule in micelle are on the order of 9 for SDS, 5 for dodecyl trimethylammonium chloride (Mukerjee, 1964) and 8.7 for sodium caprylate (Lindman and Brun, 1973).

2.6.2. Molecular Organization in Micelles

The conventional representation of a micelle assumed the hydrocarbon chain was all-trans and directed radially inward shown in Figure 2.3. Apparently all the chain termini were located at the center of micelle which resulted in anomalously high density that was not physically appropriate. Dill et al. introduced an interphase model to describe the molecular arrangement in micelles that considered both chain continuity and steric constraint (Dill and Flory, 1981; Dill, 1982; Dill et al., 1984). The SANS and ^{13}C and ^{2}H NMR experiments supported the interphase model as opposed to the radial chain or oil droplet models. The interphase model inferred disordered alkyl chains near the micelle surface and much more ordered chains near the core of micelle. With rapid development in computational power, more explicit micellar structure was explored using molecular dynamic simulations (MacKerel, 1995; Bogusz et al., 2000; Moura and Freitas, 2005). The radial density distributions from micelle center for hydrocarbon chain, head group and water were clearly demonstrated. The interior of micelle was found to be less fluidic for hydrocarbon and be void of water that all agreed with Dill et al. (Dill et al., 1984).

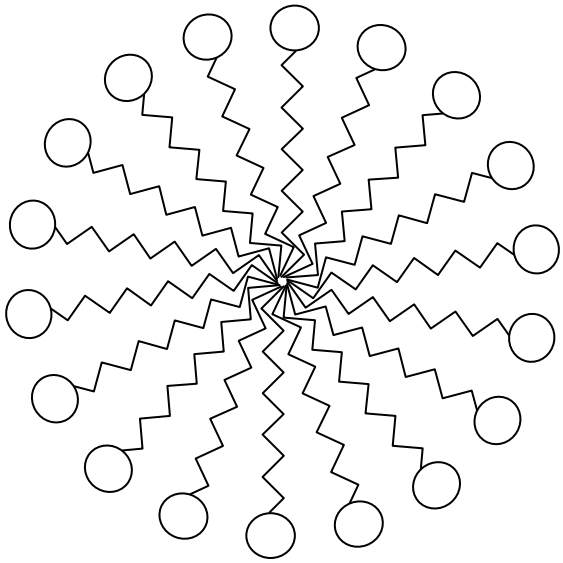

Figure 2.3 Conventional representation of a micelle. The circles represent the hydrophilic head groups of micelles, and the zigzags are the hydrocarbon chains of micelles.

2.6.3. Solubilization Capacity of Micelles

The surfactant solutions, such as soaps and bile salts, had been observed to be able to increase the solubility of water insoluble substances in as early as 19th century (Persoz, 1846; Kuehne, 1868; Engler and Dierckhoff, 1892). It was until 1930s when the solubilization phenomena by surfactants were rationalized using the hypothesis of the formation of colloidal particles or micelles (Smith, 1932; Blitzinger and Beier, 1933; McBain and McBain, 1936; Verzar, 1933). Hartley observed that solubilization of trans-azobenzene in solutions of cetylpyridinium salts only occurred when the concentration of surfactant was above the CMC (Hartley, 1938). Many studies have been done on micellar solubilization of pharmaceuticals and there were many review articles/book chapters covering the subject (Mulley, 1964; Sjoblom, 1967; Elworthy et al., 1968; Attwood and Florence, 1983; Rosen, 1989; Christian and Scamehorn, 1995; Yalkowsky, 1999).

Many factors had been found to be able to affect solubilization capacities of micelles, such as hydrocarbon chain length and headgroup of surfactants, polarity and hydrophobicity of solubilizates, temperature, pH, ionic strength, etc. Longer hydrocarbon chain length of surfactant usually produces higher solubilization capacity. The more nonpolar the solute, the more significant the increase in solubilization. For example, a series of drugs was solubilized in polysorbate 20, 40, 60 and 80 and the solubilization powers all increased to some extent with increasing the alkyl chain length of surfactants (Sjoblom, 1967; Attwood and Florence, 1983; Ong and Tamoukian, 1988). The solubilization capacity ratio between polysorbate 80 and polysorbate 20 systems had the following ranking order: vitamin A palmitate (4.5) > estrone (1.9) > timobesome acetate (1.6) > indomethacin (1.4). Vitamin A palmitate was apparently most nonpolar of the tested solutes. Timobesome acetate and indomethacin, having more polar functional groups, were most polar. When the alkyl chain length of surfactants was fixed, the

hydrophilic head group could also affect the solubilization capacity and the trend depended on the solute properties. Tokiwa (Tokiwa, 1968) used a series of surfactants with same hydrocarbon chain length to solubilize hydrocarbon and nonpolar compounds. Although it was expected that these solutes localized in the core of the miclle, Tokiwa found the solubilizing powers of the surfactants in the order of anionic < cationic <nonionic. For polar solutes that were solubilized in the palisade layer of the micelles, the results were somewhat different. Shihab et al. (Shihab et al., 1979) solubilized furosemide, a diuretic, in anionic SDS micelles, nonionic polysorbate 80 micelles and PEG polymers and observed the ranking order of the solubilization capacity to be SDS>polysorbate 80>PEG. With elevated temperature the micellar solubilization capacity would usually increase (Lundberg, 1980; Saket, 1996) with some exceptions, e.g., benzocaine in polysorbate systems had lower solubilization power at higher temperature (Hamid and Parrott, 1971). The complicated behavior was due to the two factors of the solubilization power, intrinsic solubility and micelle-water partitioning, which may have different trend with rising temperature: intrinsic solubility would increase with increasing temperature while the micelle-water partitioning coefficient was usually decreased with elevated temperature (Barry and El Eini, 1976; Saket, 1996). The overall effect depended on the competition between the two factors.

The above studies, although experimental, mainly observe some qualitative correlation between solubilization and varieties of micelle factors. Attempts to quantitatively predict the solubilization capacity are mainly of three approaches: linear free energy relationship (LFER), deconstruction method and thermodynamic modeling. Most commonly used LFER based methods utilize a correlation between micelle/water partitioning coefficient, $K_{m/w}$, of the solubilizate with its octanol/water partitioning coefficient, P_{oct}, in specific surfactant systems. The following linear equation is employed:

$$\log K_{m/w} = A + B \log P_{\text{oct}} \qquad (2.1)$$

where A, B are constants and have different values for different surfactants. This approach was applied to SDS (Valsaraj and Thibodeaux, 1990; Treiner and Mannebach, 1987), DTAB/CTAB (Treiner and Mannebach, 1987), polysorbate 80 (Alvarez-Munez and Yalkowsky, 2000), bile salt (Wiedmann and Kamel, 2002) and bile salt/egg PC mixed micelle (Wiedmann and Kamel, 2002) systems. Abraham et al. (Abraham et al., 1995) extended the method to include the volume term of the solubilizate:

$$\log K_{m/w} = A + B \log P_{\text{oct}} + C \cdot V_x \qquad (2.2)$$

where A, B, C are constants; V_x is the McGowan characteristic volume (McGowan, 1978) of the solute. They also extended the LFER-based equation to express micelle/water partitioning coefficient in SDS using the linear combination of a few molecular descriptors of the solute, such as excess molar refraction, polarizability, hydrogen-bond acidity and basicity, in the absence of logP_{oct} parameter. Some other LFER approaches to predict micelle/water partitioning considered the group contributions (Smith et al., 1987; Jafvert et al., 1994). Those correlation methods could be employed to predict the micelle/water partitioning of new compounds using their logP values and/or other solute properties. As with most LFER methods, the approach is semi-empirical and depends strongly on the training set of solubilizates.

The second method of predicting solubilization capacity is a deconstruction approach (Malcolmson and Lawrence, 1993), where the micelle is broken down into component parts. Octadecene was used to simulate the inner core of the micelle; dimethoxytetraethylene glycol (DMTG) was employed to simulate the poly(ethylene oxide) mantle region of Brij 96 micelles. Solubilities in the component parts were combined by weight fraction to predict micelle solubilization. This method could roughly estimate the relative importance of two micellar regions, core and surface, in solubilization. The overall prediction was not accurate. In addition, it may be difficult to

identify suitable solvent counterparts for some micelle hydrophilic head groups, such as that of SDS and DTAB.

The third method of predicting solubilization capacity is based on thermodynamic models (Mukerjee and Cardinal, 1978; Mukerjee, 1979; Gumkowski, 1986). In a two-location model, a micelle is divided into a core region that is hydrocarbon-like and a palisade region representing the surface of the micelle. The micelle/water partitioning coefficient of the solute could be expressed as the sum of two contributions from the two locations. Based on the Mukerjee model on bulk phase and surface adsorption phase, the micelle/water partitioning coefficient of solute could be expressed as:

$$K_{m/w} = K_{m/w,core} + K_{m/w,surface} = K_{h/w} \exp\left[-PV/RT\right] + \Gamma Af \qquad (2.3)$$

where $K_{h/w}$ is the hydrocarbon/water partitioning coefficient; P is the Laplace pressure (Mukerjee, 1979); V is the molar volume of the solute; R the ideal gas constant; T the temperature. For the surface solubilization term, Γ is the surface excess of drugs on hydrocarbon/water interface; A is the area per surfactant molecular on micellar surface; f is a competition factor between surfactant and drug at hydrocarbon/water interface.

The method had been applied to many organic molecules with simple structures, such as alkanols, ketones, amides and aromatics, in SDS and sodium decyl sulfate (SDeS) micelle systems and the predicted results showed good agreement with experimental values.

2.6.4. Location of Solutes in Micelles

Micelles could solubilize water-insoluble drugs in a range of microenvironments, from the hydrophobic core to the amphiphilic surface (palisade). Certainly then, the micellar solubilization mechanism must be critically-related to the location of the drug in the assemblies. The small size of these aggregates results in a very large surface-to-volume

ratio, therefore, the surface region has to be considered in any mechanistic picture of micellar solubilization. Many spectroscopic techniques, including fluorescence quenching (Bromberg and Temchenko, 1999; Lebedeva et al., 2007) UV/visible spectroscopy (Sabate et al., 2001; Goldenberg et al., 1993; Ramachandran et al., 1982; Vermathen et al., 2000), small angle X-ray diffraction (Svens and Rosenholm, 1973;) NMR (Nagaonkar and Bhagwat, 2006; Kim et al., 2001; Suratkar and Mahapatra, 2000; Vermathen et al., 2000; Bratt et al., 1990), EPR (Yoshioka, 1979; Lebedeva et al., 2007), and indirect method based on thermodynamic analysis (Mukerjee and Ko, 1992; Croy and Kwon, 2005; Donbrow et al., 1967), had been employed to probe the locus of drug solubilization in micelles. The field is too voluminous to review comprehensively and we cover only some of the more important works below.

Bromberg and Temchenko (Bromberg and Temchenko, 1999) used fluorescence spectroscopy combined with hydrophilic quenching (using Tl^+ as quencher) technique to probe the location of pyrene and steroids in Pluronic-poly(acrylic acid) micelles. They concluded that pyrene was mainly solubilized in the micellar core while only 60% of 17β-estradiol was located in the core region. Lebedeva et al. (Lebedeva et al., 2007) applied EPR and time resolved fluorescence quenching techniques (using 5- and 16-doxyl stearic acid methyl esters as quenchers) to study the location of pyrene in sodium dodecyl sulfate (SDS) micelles. At low aggregation number (N=53) of SDS micelles 33% of pyrene was found in the core region and the fraction decreased to 25% when the aggregation number was increased to 130. Sabate et al. (Sabate et al., 2001) employed UV/visible spectroscopy method to study the solubilization site of pinacyanol in DTAB, TTAB and HTAB micelles. They first built a correlation between ionization constant pKa of the solute and dielectric constant ε of bulk solvent. By measuring the pKa of the solute in micelles using UV/vis method the effective dielectric constant of its microenvironment was determined to be that between water and hydrocarbon, which

indicated the solubilizate was on average located in an environment with characteristics between micellar core and outer aqueous solution. Svens and Rosenholm (Svens and Rosenholm, 1973) utilized small angle X-ray diffraction technique to examine the locations of N,N'-dimethylaniline, decanol and p-xylene in sodium octanoate micelles by measuring the radii of the core and polar (palisade) regions of the micelles. N,N'-dimethylaniline was found at the polar layer because the radius of the polar region increased in the presence of the solubilizate but the radius of the core was not affected by the solubilization process. Based on the same principle, p-xylene was mainly solubilized in the core region while the location of dodecanol was concentration-dependent.

NMR is an important technique in studying the location of solutes in micelles. The technique includes approaches that focus on chemical shifts, spin-lattice /spin-spin relaxation times, and intermolecular interactions based on 2D NMR spectra. Nagaonkar and Bhagwat (Nagaonkar and Bhagwat, 2006) employed proton NMR spectroscopy to detect the solubilization site of isophorone in SDS micelles. By monitoring the change of chemical shifts of different protons in isophorone, part of the solute was not affected and believed to be located in aqueous environment while remainder of the solute was affected significantly indicating its location close to the micellar core. The NMR approach was also focused on the chemical shifts of surfactant molecule, which were measured in pure micelle system compared to those in micelle+solubilizate system. The largest change in chemical shift of hydrogen atoms of surfactant molecules corresponds to the closest contact to solute molecule. Using the position of those hydrogen atoms of the carbon chain, the depth of penetration of the drugs into micelle core could be determined (Suratkar and Mahapatra, 2000). ^{1}H spin-lattice relaxation time (T_1) and spin-spin relaxation time (T_2) could also be used in molecular location determination (Ueno and Asano, 1997). In general, the relaxation rates depend on the motional behavior of functional groups in solution where restricting motion corresponds to shorter relaxation

time. Ueno and Asano employed the relaxation time approach to study the orientation of bile salt sodium glycochenodeoxycholate (NaGCDC) at the NaGCDC/octaoxyethylene glycol mono n-decyl ether ($C_{10}E_8$) mixed micelle systems (Ueno and Asano, 1997). The increased T_1 and T_2 values of 19-methyl group at lower mole fraction of NaGCDC suggested 19-methyl group became free due to the hydrogen-bonding breakage between two NaGCDC molecules in the mixed micelle. In contrast, the motion of 18-methyl group was restricted at the lower mole fraction of NaGCDC. Those results suggested that α-plane of the bile salt oriented toward the water phase and the β-plane together with 19-methyl group oriented toward the center of the core; the 18-methyl group was located near the boundary between ethylene oxide and hydrocarbon chain of the $C_{10}E_8$ molecule in mixed micelles. 2-Dimensional NMR, nuclear Overhauser effect spectroscopy (NOESY) and rotating-frame Overhauser effect spectroscopy (ROESY) were applied to detect inter-molecular interactions (Hawrylak and Marangoni, 1999; Matsuoka et al., 2007; Heins et al., 2007; Bachofer et al., 1991). Hawrylak and Marangoni studied the solubilization sites of butanol and benzene in SDS and DTAB micelles using NOESY (Hawrylak and Marangoni, 1999). The cross peaks between α-protons of the SDS and the 1-butanol molecule indicated the hydroxyl group of butanol was close to the headgroup of SDS at the micelle surface. The cross peaks between the methyl protons of the butanol and the hydrocarbon chain protons of SDS suggested the hydrocarbon chain of butanol was pointed inwards towards the center of the micelle.

2D NMR method is highly specific on the inter-molecular interactions that provide molecule level understanding of micellar solubilization. As of yet, the applications of the technique to micellar solubilization of pharmaceuticals are limited (Matsuoka et al., 2007; Heins et al., 2007). Applying 2D NOESY and ROESY NMR methods would be a powerful tool to study the solublization of model drugs in micelle systems in order to obtain microscopic information of micellar solubilization.

As shown earlier, the groups of Bromberg (Bromberg and Temchenko, 1999) and Lebedeva (Lebedeva et al., 2007) used fluorescence quenching method to determine the pyrene to be in the micellar core or part in hydrocarbon core and part at the surface of micelles. One reason for the controversies is the location of solutes has a subtle different definition for different experimental technique. For thermodynamics based technique the location is for the whole molecule: if one part of the molecule was at surface the whole molecule is considered to be at surface. But for UV/vis, fluorescence and NMR methods the location of drug is functional group specific: only the polar part or the fluorescent part of the molecules is focused in ultraviolet or fluorescence spectroscopy respectively. Hence, the conclusion about fractions of drug molecules located in different regions of micelles would be different using different experiments. Thermodynamics based method usually claim a larger fraction of solubilizates at the micellar surface compared to spectroscopy based methods.

Mukerjee and Ko (Mukerjee and Ko, 1992) observed a significant discrepancy between micelle/water and hydrocarbon/water partitioning coefficients of ethyl o-, m- and p-aminobenzoates in a series of micelles (octyl glucoside, SDS, DM, zwig 3-12 and HTAC): the micelle/water partitioning coefficients were much higher than the hydrocarbon/water partitioning constants which indicated the core region was insufficient to solubilize the drugs, i.e. the first term in Eq. 2.3 was negligible, and micelle surface should be the major solubilization locus. Croy and Kwon (Croy and Kwon, 2005) studied the micelle/water partitioning of nystatin in polysorbate 80 and cremophor EL systems as a function of drug concentrations (solubilization isotherm). The results showed a good fit with the Langmuir adsorption isotherm indicating the drug was solubilized at the core-corona interface, in an adsorbed state.

Based on those studies on solubilization sites in micelles, attempts have been mad to correlate the locus of the solubilization and the chemical structures of the solubilizates: Saturated aliphatic and alicyclic hydrocarbons that were nonpolar molecules were solubilized in the inner core of the micelles (Rosen, 1989; Attwood and Florence, 1983; Lindblom et al., 1973). Semi-polar or polar solubilizates, such as alkanols, acids, and amines, were oriented radially in the micelle with the polar group at the micellar surface (Rosen, 1989; Attwood and Florence, 1983; Lee et al., 1990; Christian and Scamehorn, 1995). For the aromatic hydrocarbons, such as benzene, naphthalene and pyrene, there is still no general agreement regarding their loci in micelle systems (Mukerjee and Cardinal, 1978; Nakagawa, 1967; Eriksson and Gillberg, 1966; Bromberg and Temchenko, 1999; Lebedeva et al., 2007). For example, Mukerjee and Cardinal (Mukerjee and Cardinal, 1978) showed a moderate surface activity of benzene at the heptane-water interface which provided an explanation of its location mainly at the micellar surface (in the "adsorbed" state). They also pointed out the hydrocarbon core could not provide sufficient solubilization power based on the micelle-water and hydrocarbon-water partitioning properties.

2.7. Unanswered Questions

Controversy continues to surround the question s to the nature of the properties that promote solute localization in the core. The weaker argument (covering narrow range of solubilizate) is that only nonpolar molecules reside in the core region (Rosen, 1989; Attwood and Florence, 1983). The stronger argument (covering a broader range of solubilizates) suggests that hydrophobic molecules have a tendency to reside in the core, in addition to other locations (Rangel-Yagui et al., 2005; Suratkar and Mahapatra, 2000). Hydrophobic molecules often possess larger nonpolar regions with fewer polar functional groups. Whether those small polar contributions would affect drug location in micelles would be important to rational application of the dosage form.

Mukerjee's group have shown many organic molecules with simple chemical structures exhibit some surface activities at oil-water interface. It is unclear whether hydrophobic drug molecules with complicated chemical structures are surface active at oil/water interface although they do not possess surface activity at water-/air interface. If so, further studies of the strength of the surface activity, its correlation with chemical structures and the interaction/competition between the drugs and surfactants at the oil-water interface as a model micelle surface would provide deeper mechanistic understanding of micellar solubilization process.

Mukerjee et al. had laid a solid foundation of applying thermodynamic model, especially the surface adsorption model, to micellar solubilization mechanism studies. There are still some questions to be clarified:

1) Most of the test solutes were organic molecules with simple chemical structures. One exception was the solubilization studies on imaging probe molecules, OTEMPO and TEMPO in SDS micelles (Pyter et al., 1982). The surfactants chosen were limited to SDS and SDeS. It will be valuable to systematically study several series of drug molecules with complicated structures in micelle systems with different electron charges.

2) One of the major assumptions in derivation of two-state model was the dilute condition of solute. In many of the solubilization isotherm studies, the micelle/water partitioning coefficient is significantly dependent upon solute concentration (Christian et al., 1986; Lee et al., 1990; Goto and Endo, 1978). To remove the assumption, the micelle/water partitioning at saturated concentration of drug would be important in pharmaceutical applications where solute concentration is often high.

3) In the early two-state model studies, some controversial values for occupied areas at the oil/water interface by solute molecules were employed, e.g. 17.4$Å^2$ was used for both

benzene and pyrene molecules (Gumkowski, 1986). The area term is critical to predicting the amount and the orientation of solute at oil/water interface. As we illustrate in Chapter 5, inaccuracies in the value of the occupied area can result in misinterpretation of the solubilization data and weaken the strength of the model.

2.8. Summary

Micelle solution is a practical means of enhancing the solubility of poorly-soluble drugs and facilitating both administration and bioavailability.

While several general rules have been developed, at present the mechanism of solubilization of poorly-soluble drugs by micelles is not understood. This lack of fundamental knowledge forces formulators to adopt an inefficient and labor-intensive search for the optimal combination of solubilizing ingredients. A mechanistic understanding of which micelle system could best solubilize a specific drug candidate would greatly speed up the drug formulation process.

Chapter 3

Solubilization Capacity of Simple Micelle Systems and its Relation to the Partitioning of Model Drugs between Hydrocarbon and Water.

3.1. INTRODUCTION

The application of micelles as drug delivery vehicles has become increasingly popular with growing number of commercially available products utilizing micelles in the formulations. Even for conventional oral delivery vehicles, such as tablets and capsules, when the formulations reach the gastrointestinal tract the bile salts/phospholipids mixed micelles produced by the human body serve as a natural delivery system to help carry and transport the drug molecules into systemic circulation. One of the important advantages of micelles as drug delivery vehicles is their ability to enhance the solubility of poorly water-soluble drugs which account for a significant fraction (>40%) of drug candidates. Although micellar solubilization of drug substances has been studied for some time, and many factors that influence the solubilization power of micelles have been identified, the mechanism of the solubilization by micelles is not fully understood. The most notable gap in our knowledge is the inability to predicting the amount of a drug solubilized in a specific micelle system. This current work is designed to probe the solubilization mechanism at the molecular level and in a quantitative manner.

To understand the mechanism by which micelles solubilize poorly water-soluble drugs, one of the critical factors is the location of the drugs in micelles. It has been well-recognized that micelles present at least two regions for drug solubilization, a lipophilic “core” and an anisotropic “surface” region. The core is nonpolar and hydrocarbon-like. The surface, called palisade region, may be likened to an interface between oil (hydrocarbon) and aqueous phases. Many techniques, such as UV, NMR,

fluorescence, etc., had been employed to study the location of drug substances in difference micelle systems. In this study, a thermodynamics based model was employed so as to evaluate the location of the drug and to provide quantitative partitioning information of the drug in different regions.

We started with an assumption that poorly-water soluble drug molecules were mainly solubilized in the core region of the micelle. The distribution of solutes between hydrocarbon and water could then serve as a simulation of partitioning between micellar core and aqueous phase. Experimentally, the hydrocarbon/water and the micelle/water partitioning coefficients were measured and compared to each other. If the assumption about micellar core as the solubilization region is true, the above two partitioning coefficient would be comparable.

Related to the assumption of drugs solubilized in the core, another factor should be considered: the Laplace pressure effect (Mukerjee, 1979; Gumkowski, 1986). As a result of the presence of surface tension at the micelle surface and the small size of the micelle, the micellar interior is subject to a Laplace pressure which is expressed as following:

$$P = 2\gamma / r \tag{3.1}$$

where P is the Laplace pressure; γ is the surface tension at micelle surface and r is the micelle size. This equation is based on an assumption that the micelle has a spherical shape. Since the solute molecule has to create a spatial vacancy at micelle core, it must overcome a larger energy barrier under higher pressure. Therefore the presence of Laplace pressure will lower the solubilization capacity of micelle core region. To quantify the Laplace pressure effect, the following equation is applied:

$$K_{m/w} = K_{h/w} \exp\left[-PV/RT\right] \tag{3.2}$$

where $K_{m/w}$ is the micelle/water partitioning coefficient; $K_{h/w}$ is the hydrocarbon/water partitioning coefficient; V is the molar volume of the solute; R is the ideal gas constant and T is the temperature.

Experiments on micelle/water and hydrocarbon/water partitioning were carried out to test the accuracy of Eq. (3.2) in order to clarify whether the core region is the major locus of the solubilization in micelles. In these studies, three independent series of drugs were chosen as model solutes. In each series, 3 or 4 compounds were selected in order to probe the effect of functional groups on solubilization phenomena. In sum total there were 11 compounds: 4 steroids (progesterone, testosterone, 17β-estradiol and 11α-hydroxyprogesterone), 4 benzodiazepines (diazepam, temazepam, oxazepam and prazepam) and 3 parabens (methylparaben, ethylparaben and butylparaben). The chemical structures of those molecules are shown in Figure 3.1. So as to cover a broad range of micelle/water partitioning coefficient two series exhibit poor aqueous solubility and the third series exhibits relatively higher solubility were employed. Three micelle systems were employed as model simple micelle system: anonic sodium dodecyl sulfate (SDS), cationic dodecyltrimethylammonium bromide (DTAB) and nonionic dodecyl β-D-maltoside (DM). All three surfactants have the same hydrocarbon chain length (12 carbons) and differ only by the charge on the headgroups. The chemical structures of the surfactants are shown in Figure 3.2. An n-alkane, dodecane, was employed as a good model of hydrocarbon as a simulation of micellar core since dodecane have the same alkyl chain length with the hydrophobic tails of three model surfactants.

3.2. MATERIALS AND METHODS

3.2.1. Materials:

Progesterone (>99%), testosterone (>98%), 17β-estradiol (>98%), diazepam, temazepam, oxazepam, prazepam, methylparaben (>99%), ethylparaben (>99%), butylparaben

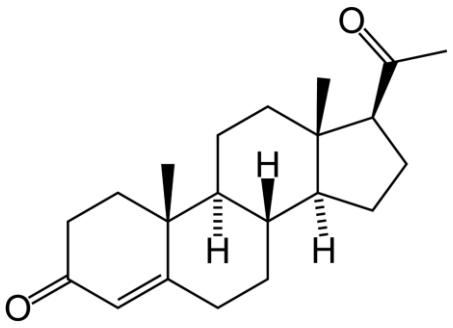

Progesterone

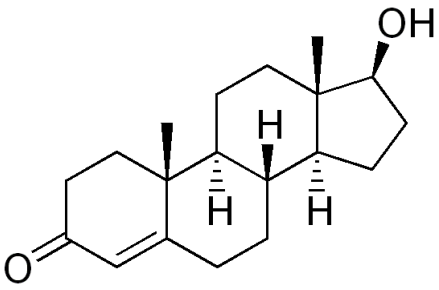

Testosterone

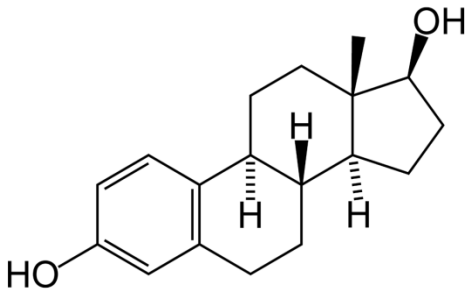

17β-estradiol

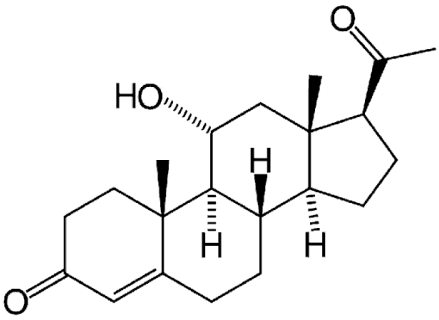

11α-hydroxyprogesterone

Figure 3.1a The chemical structures of model steroids.

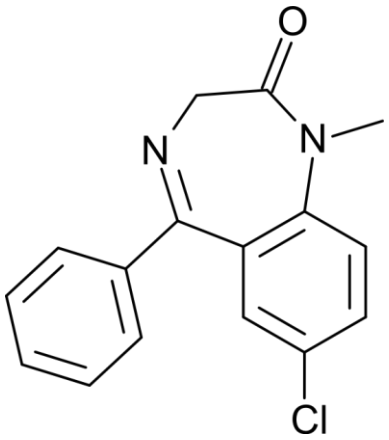

Diazepam

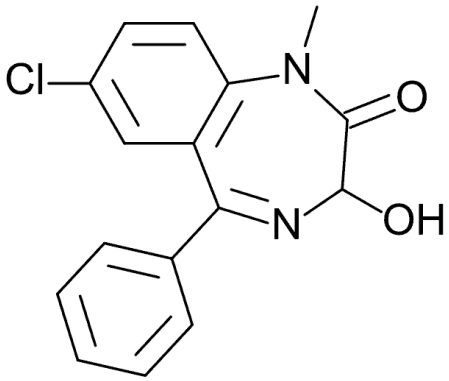

Temazepam

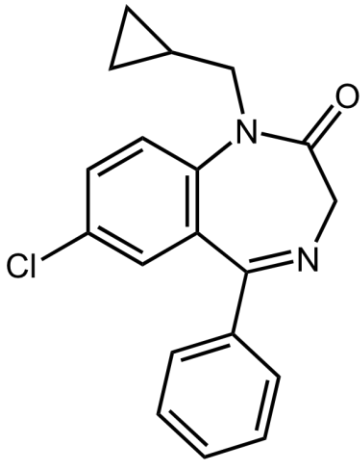

Prazepam

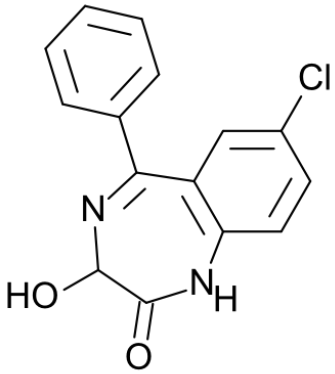

Oxazepam

Figure 3.1b The chemical structures of model benzodiazepines.

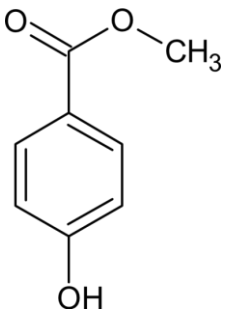

Methylparaben

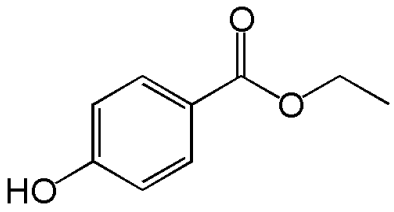

Ethylparaben

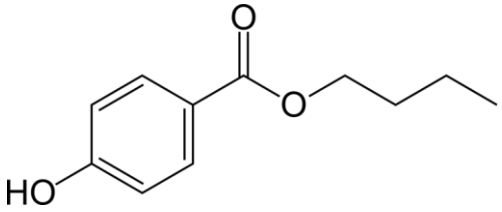

Butylparaben

Figure 3.1c The chemical structures of model parabens.

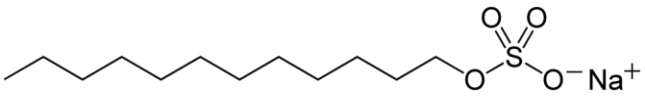

Sodium dodecyl sulfate

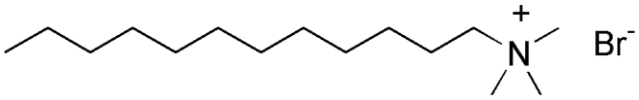

Dodecyltrimethylammonium bromide

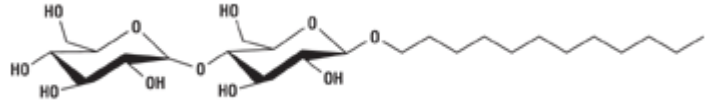

Dodecyl β-D-maltoside

Figure 3.2 The chemical structures of model surfactants.

(>99%), sodium dodecyl sulfate (>99%), dodecyltrimethylammonium bromide (>99%) and dodecyle β-D-maltoside (>98%) were obtained from Sigma-Aldrich (St. Louis, MO). 11α-hydroxyprogesterone (>95%) was from Janssen Chimica (New Brunswick, NJ).

3.2.2. Solubility Measurements in Aqueous Solutions:

The conventional shake-flask method was applied to measure the solubility of all model drugs in aqueous solutions in the presence and absence of surfactant: An extra amount of drugs was placed into aqueous solution with known concentration of surfactants and the system was rotated for 3~5 days at room temperature (24±1^{o}C) to reach equilibrium. Solutions were filtered using 0.2μm hydrophilic PTFE filter (Millipore Inc.) and the filtrates were diluted appropriately and assayed for drug concentration determinations by reverse phase HPLC methods (assays shown later in the chapter).

3.2.3. Solubility Determinations in Hydrocarbon Solutions:

Dodecane was chosen as a model hydrocarbon medium. The conventional shake-flask method was employed to measure the solubility of model drugs in dodecane: An excess amount of drug was placed into dodecane and the system was rotated for 3~5 days at room temperature (24±1^{o}C) to reach equilibrium. Solutions were filtered using 0.2μm hydrophobic PTFE filter (Pall corp.) and the filtrates were diluted appropriately and assayed for drug concentrations by normal phase HPLC methods (assays shown later in the chapter).

3.2.4. Micelle/water Partitioning Coefficient Determinations:

In a micelle-containing solution, drugs are dissolved both in the aqueous phase and in the micelle solutions. If it is assumed that solubility in the aqueous phase is independent of the presence of micelles, the total solubility of drug as a function of surfactant concentration has the following relationship:

$$S_{tot} = S_w + (C_{\text{surfactant}} - CMC) * \kappa \quad (3.3)$$

where S_{tot} and S_w are total and aqueous solubilities of drug (mole fraction based); $C_{surfactant}$ and CMC are surfactant concentration and critical micelle concentration (CMC, mole fraction based); κ is the slope of the ascending line and is defined as solubilization capacity (or solubilization power), in unit of moles of drug per mole of surfactant.

Under the condition where the surfactant concentration is much greater than the CMC, Eq. (3.3) becomes:

$$S_{tot} = S_w + C_{\text{surfactant}} * \kappa \quad (3.4)$$

If the micelle is considered as a "pseudo-phase", a micelle/water partitioning coefficient, $K_{m/w}$, can be defined as mole fraction of drugs in micelles divided by the mole fraction of drugs in aqueous phase. The relationship can be expressed as:

$$K_{m/w} = \frac{\kappa/(\kappa + 1)}{S_w} \quad (3.5)$$

3.2.5. Hydrocarbon/water Partitioning Coefficient Determination:

In the literature, there are two methods that were used to determine the $K_{h/w}$, solubility ratio and direct partitioning.

The solubility ratio (in mole fraction units) can be described by following equation:

$$K_{h/w} = \frac{S_h}{S_w} \quad (3.6)$$

where S_h is the solubility of drugs in model hydrocarbon, dodecane. The solubility ratio method assumes that both the aqueous phase and the oil phase act as near-ideal solutions of the drug. For instance, the drug is assumed not to self associate in either phase. The

method is also based on the assumption that saturated drugs have the same activities at different media. This assumption may not be true when the drug molecule could form different solvates in different media. One example is the testosterone crystal which has anhydrous form in dodecane but forms a hydrate in aqueous media. In those cases where the assumptions are not met, the direct partitioning method will be employed.

3.2.6. Direct Partitioning Coefficient Determinations

A known amount of drug was placed into 1:1 (v/v) mixture of dodecane and water. The system was rotated for 2 days and all the solid material was dissolved. The drug concentrations in aqueous solutions and dodecane solutions were analyzed using reverse phase HPLC and normal phase HPLC methods respectively. In some instances it was necessary to dilute the sample prior to HPLC analysis.

The partition coefficient (direct) would be determined:

$$K_{h/w} = \frac{\text{conc. in hydrocarbon}}{\text{conc. in water}} \qquad (3.7)$$

3.2.7. HPLC Methods

Waters HPLC system including 717plus autosampler, 610 pump and 486 UV detector was employed in the reverse phase experiments. Waters LCMod1 HPLC system was employed to run the normal phase measurements. SRI PeakSimple V3.21 software was utilized to analyze the collected chromatograms. Column and samples were all held at room temperature (24±1^{o}C). All mobile phases were pre-mixed and degassed before use. The assay protocols used in reverse phase and normal phase HPLC for all model drugs are listed in Table 3.1. In the table, the retention times and the response factors of the drugs are shown as well. All the assays were validated for precision and linearity test by standard protocols. The measured drug concentrations were all within the linear range of the respective calibration curves. No carry over was observed in any assays.

The HPLC chromatograms for all the assays are shown in Figure 3.3~3.13. In a majority of the chromatograms the peaks of the interested compounds exhibit symmetric shapes. Only the normal phase HPLC assays for temazepam and oxazepam result in significant tailing. These assays were not optimized in terms of the peak shape because there was only one interested compound and no peak overlaps from other components.

Table 3.1 Reverse phase and normal phase HPLC assays for all model drugs

Progesterone:

	Reverse phase	Normal phase
Column	Supelcosil ABZ+plus C18	Alltech® Allsphere Silica 5u
Mobile phase	50% acetonitrile/ 50% H_2O	95% hexane/ 5% 2-propanol
Injection volume	20μL	20μL
Detection wavelength	240nm	240nm
Flow rate	1.5mL/min	1.5mL/min
Retention time	11.1min	7.2min
Response factor (mV×min×mL/μg)	37.9±0.7	50.0±0.7

Testosterone:

	Reverse phase	Normal phase
Column	Supelcosil ABZ+plus C18	Alltech® Allsphere Silica 5u
Mobile phase	50% acetonitrile/ 50% H_2O	95% hexane/ 5% 2-propanol
Injection volume	20μL	20μL
Detection wavelength	240nm	240nm
Flow rate	1.5mL/min	1.5mL/min
Retention time	6.2min	9.1min
Response factor (mV×min×mL/μg)	43.6±0.2	37.3±0.8

17 β-estradiol:

	Reverse phase	Normal phase
Column	Alltech® Alltima C18 5u	Alltech® Allsphere Silica 5u
Mobile phase	50% acetonitrile/ 50% H_2O	95% hexane/ 5% 2-propanol
Injection volume	20μL	40μL
Detection wavelength	280nm	280nm
Flow rate	1.0mL/min	1.5mL/min
Retention time	12.0min	3.4min
Response factor (mV×min×mL/μg)	7.56±0.14	15.1±0.2

Table 3.1 (continued) Reverse phase and normal phase HPLC assays for all model drugs

11α-hydroxyprogesterone:

	Reverse phase	Normal phase
Column	Supelcosil ABZ+plus C18	Alltech® Allsphere Silica 5u
Mobile phase	50% acetonitrile/ 50% H_2O	80% hexane/ 20% 2-propanol
Injection volume	20μL	20μL
Detection wavelength	240nm	240nm
Flow rate	1.0mL/min	1.5mL/min
Retention time	6.2min	6.4min
Response factor (mV×min×mL/μg)	53.8±0.6	31.3±0.2

Diazepam:

	Reverse phase	Normal phase
Column	Supelcosil ABZ+plus C18	Alltech® Allsphere Silica 5u
Mobile phase	50% acetonitrile/ 50% H_2O	90% hexane/ 10% 2-propanol
Injection volume	20μL	20μL
Detection wavelength	240nm	240nm
Flow rate	1.0mL/min	1.5mL/min
Retention time	8.1min	3.9min
Response factor (mV×min×mL/μg)	91.7±0.4	52.0±0.6

Temazepam:

	Reverse phase	Normal phase
Column	Supelcosil ABZ+plus C18	Alltech® Allsphere Silica 5u
Mobile phase	50% acetonitrile/ 50% H_2O	80% hexane/ 20% 2-propanol
Injection volume	20μL	20μL
Detection wavelength	240nm	240nm
Flow rate	1.0mL/min	1.5mL/min
Retention time	6.4min	4.2min
Response factor (mV×min×mL/μg)	88.7±0.1	46.1±0.2

Table 3.1 (continued) Reverse phase and normal phase HPLC assays for all model drugs

Prazepam:

	Reverse phase	Normal phase
Column	Supelcosil ABZ+plus C18	Alltech® Allsphere Silica 5u
Mobile phase	50% acetonitrile/ 50% H_2O	90% hexane/ 10% 2-propanol
Injection volume	20μL	20μL
Detection wavelength	240nm	240nm
Flow rate	1.0mL/min	1.5mL/min
Retention time	12.8min	2.8min
Response factor (mV×min×mL/μg)	77.7±0.9	44.6±0.5

Oxazepam:

	Reverse phase	Normal phase
Column	Supelcosil ABZ+plus C18	Alltech® Allsphere Silica 5u
Mobile phase	50% acetonitrile/ 50% H_2O	80% hexane/ 20% 2-propanol
Injection volume	20μL	200μL
Detection wavelength	240nm	240nm
Flow rate	1.0mL/min	1.5mL/min
Retention time	5.8min	3.3min
Response factor (mV×min×mL/μg)	89.7±1.1	511±9

Methylparaben:

	Reverse phase	Normal phase
Column	Supelcosil ABZ+plus C18	Alltech® Allsphere Silica 5u
Mobile phase	50% acetonitrile/ 50% H_2O	97.5% hexane/2.5% 2-propanol
Injection volume	20μL	20μL
Detection wavelength	254nm	254nm
Flow rate	1.5mL/min	1.5mL/min
Retention time	3.4min	5.0min
Response factor (mV×min×mL/μg)	78.1±0.3	68.9±1.0

Table 3.1 (continued) Reverse phase and normal phase HPLC assays for all model drugs
Ethylparaben:

	Reverse phase	Normal phase
Column	Supelcosil ABZ+plus C18	Alltech® Allsphere Silica 5u
Mobile phase	50% acetonitrile/ 50% H_2O	97.5% hexane/2.5% 2-propanol
Injection volume	20μL	20μL
Detection wavelength	254nm	254nm
Flow rate	1.5mL/min	1.5mL/min
Retention time	4.3min	4.5min
Response factor (mV×min×mL/μg)	72.8±0.4	63.2±1.3

Butylparaben:

	Reverse phase	Normal phase
Column	Supelcosil ABZ+plus C18	Alltech® Allsphere Silica 5u
Mobile phase	50% acetonitrile/ 50% H_2O	97.5% hexane/2.5% 2-propanol
Injection volume	20μL	20μL
Detection wavelength	254nm	254nm
Flow rate	1.5mL/min	1.5mL/min
Retention time	8.8min	4.0min
Response factor (mV×min×mL/μg)	63.4±0.3	54.8±0.7

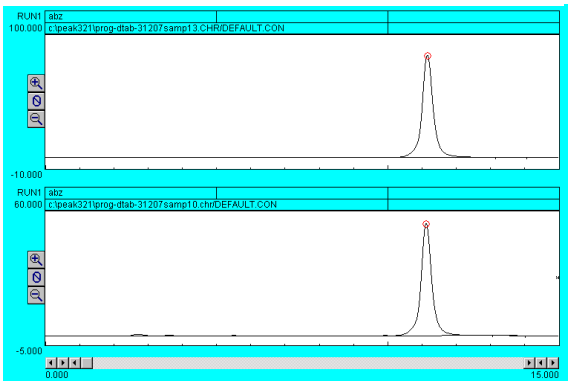

Figure 3.3a, Reverse phase HPLC chromatograms of progesterone: the top chromatogram is the standard solution with drug concentration of 51ug/mL; the bottom curve represents 20-fold dilution of the saturated drug in 10mg/mL DTAB solution.

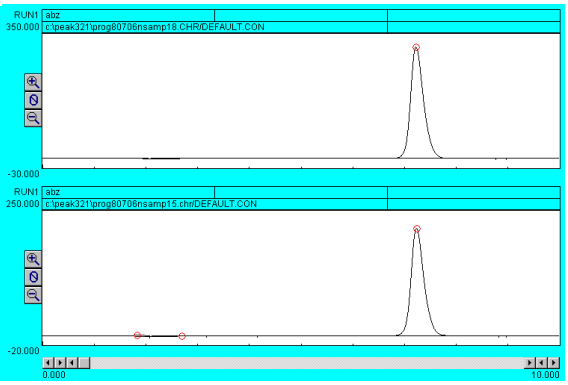

Figure 3.3b, Normal phase HPLC chromatograms of progesterone: the top chromatogram is the standard solution with drug concentration of 105ug/mL; the bottom curve is 40-fold dilution of the saturated drug in dodecane.

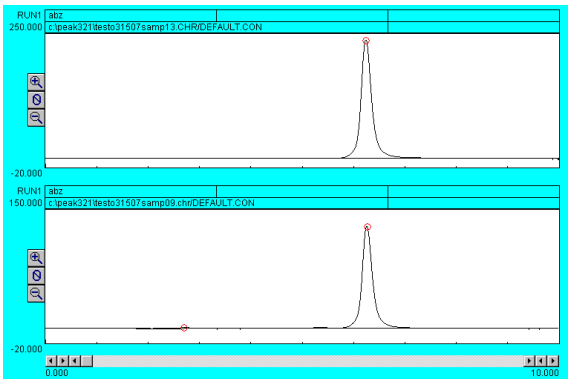

Figure 3.4a, Reverse phase HPLC chromatograms of testosterone: the top chromatogram is the standard solution with drug concentration of 81ug/mL; the bottom curve represents two-fold dilution of the saturated drug in 5mg/mL DTAB solution.

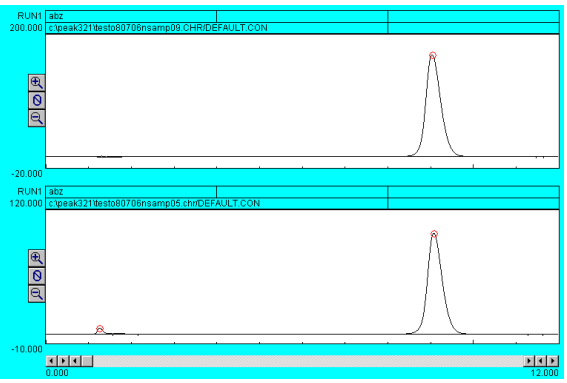

Figure 3.4b, Normal phase HPLC chromatograms of testosterone: the top chromatogram is the standard solution with drug concentration of 104ug/mL; the bottom curve is 5-fold dilution of the saturated drug in dodecane.

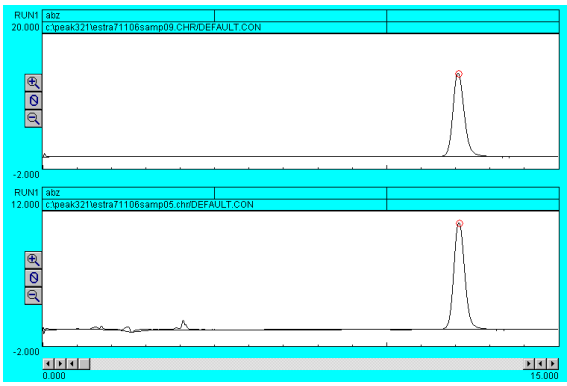

Figure 3.5a, Reverse phase HPLC chromatograms of 17β-estradiol: the top chromatogram is the standard solution with drug concentration of 40ug/mL; the bottom curve represents two-fold dilution of the saturated drug in 5mg/mL SDS solution.

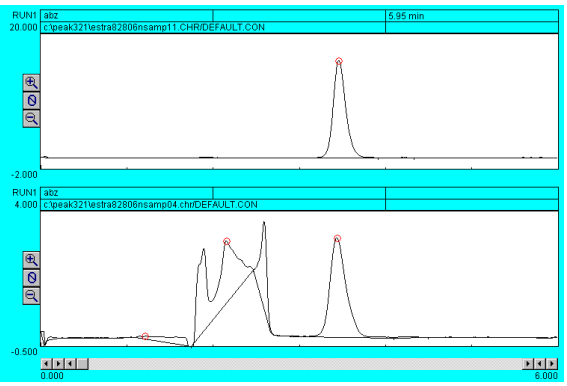

Figure 3.5b, Normal phase HPLC chromatograms of 17β-estradiol: the top chromatogram is the standard solution with drug concentration of 10ug/mL; the bottom curve is the saturated drug in dodecane.

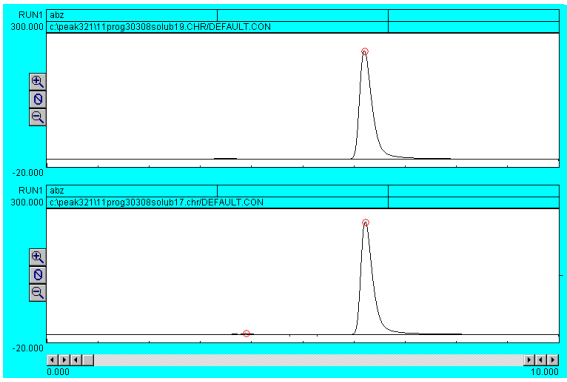

Figure 3.6a, Reverse phase HPLC chromatograms of 11α-hydroxy-progesterone: the top chromatogram is the standard solution with drug concentration of 84ug/mL; the bottom curve represents the saturated drug in 1.0mg/mL DM solution.

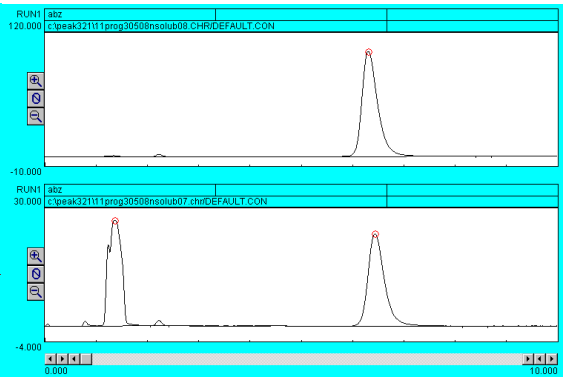

Figure 3.6b, Normal phase HPLC chromatograms of 11α-hydroxy-progesterone: the top chromatogram is the standard solution with drug concentration of 67ug/mL; the bottom curve is the saturated drug in dodecane.

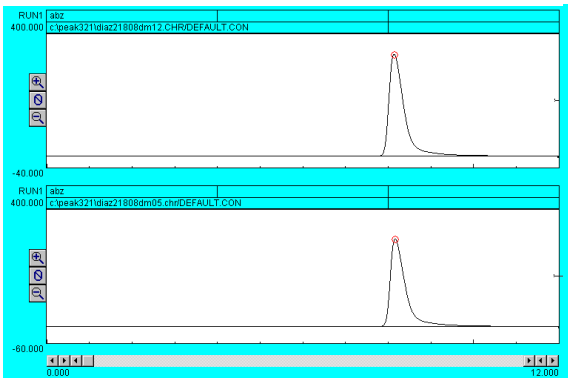

Figure 3.7a, Reverse phase HPLC chromatograms of diazepam: the top chromatogram is the standard solution with drug concentration of 88ug/mL; the bottom curve represents the saturated drug in 1.0mg/mL DM solution.

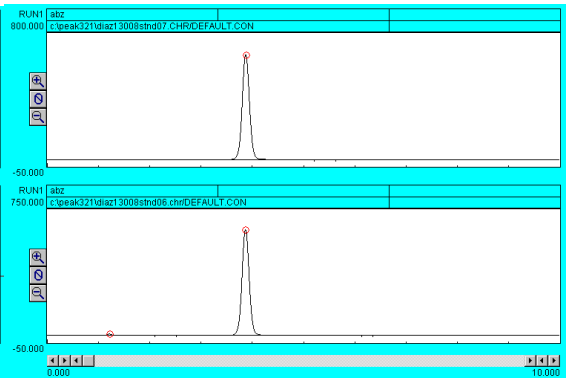

Figure 3.7b, Normal phase HPLC chromatograms of diazepam: the top chromatogram is the standard solution with drug concentration of 119ug/mL; the bottom curve is 10-fold dilution of the saturated drug in dodecane.

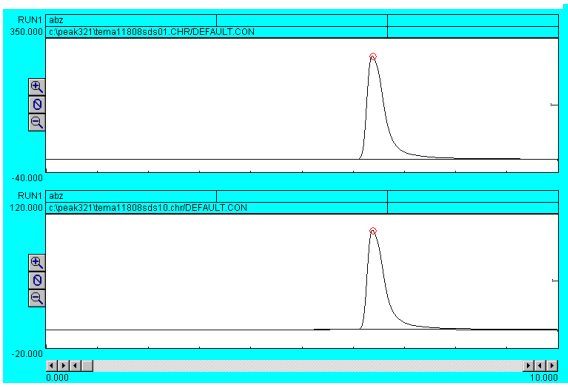

Figure 3.8a, Reverse phase HPLC chromatograms of temazepam: the top chromatogram is the standard solution with drug concentration of 82ug/mL; the bottom curve represents 20-fold dilution of the saturated drug in 2.5mg/mL SDS solution.

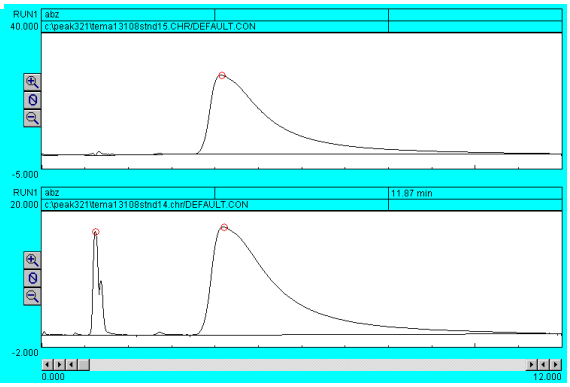

Figure 3.8b, Normal phase HPLC chromatograms of temazepam: the top chromatogram is the standard solution with drug concentration of 57ug/mL; the bottom curve is 3-fold dilution of the saturated drug in dodecane.

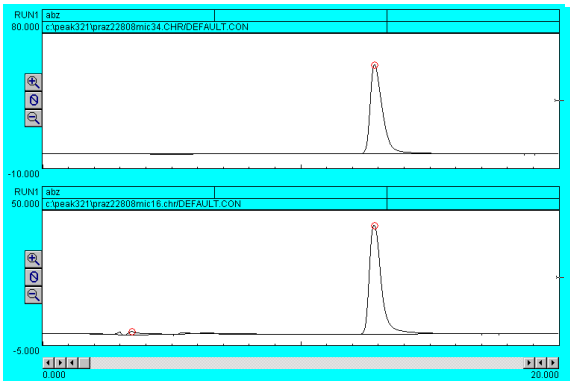

Figure 3.9a, Reverse phase HPLC chromatograms of prazepam: the top chromatogram is the standard solution with drug concentration of 24ug/mL; the bottom curve represents the saturated drug in 5mg/mL DTAB solution.

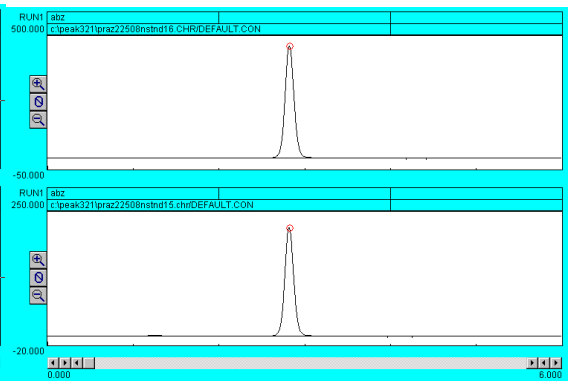

Figure 3.9b, Normal phase HPLC chromatograms of prazepam: the top chromatogram is the standard solution with drug concentration of 73ug/mL; the bottom curve is 40-fold dilution of the saturated drug in dodecane.

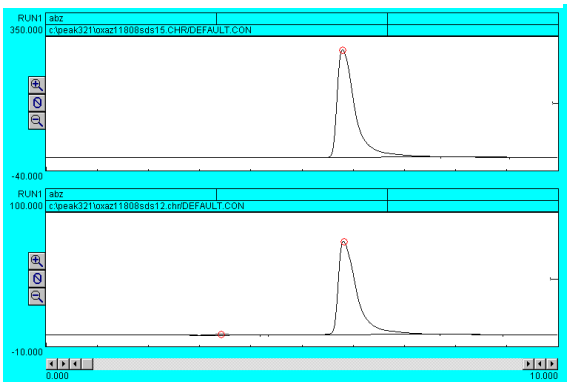

Figure 3.10a, Reverse phase HPLC chromatograms of oxazepam: the top chromatogram is the standard solution with drug concentration of 81ug/mL; the bottom curve represents 5-fold dilution of the saturated drug in 2.5mg/mL SDS solution.

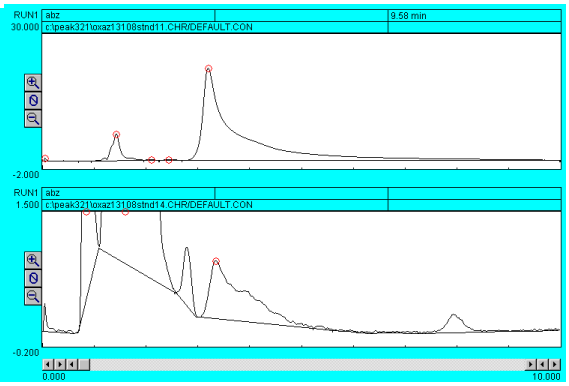

Figure 3.10b, Normal phase HPLC chromatograms of oxazepam: the top chromatogram is the standard solution with drug concentration of 1.8ug/mL; the bottom curve is the saturated drug in dodecane.

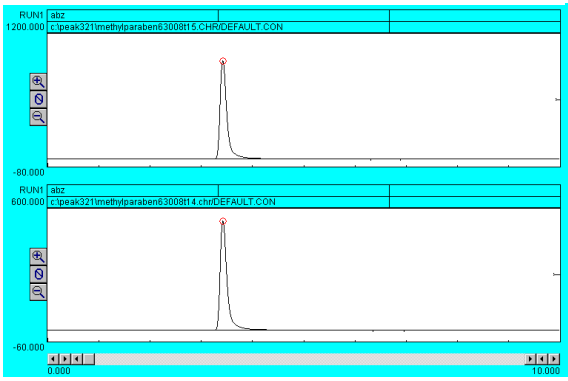

Figure 3.11a, Reverse phase HPLC chromatograms of methylparaben: the top chromatogram is the standard solution with drug concentration of 107ug/mL; the bottom curve represents 40-fold dilution of the saturated drug in 2.5mg/mL SDS solution.

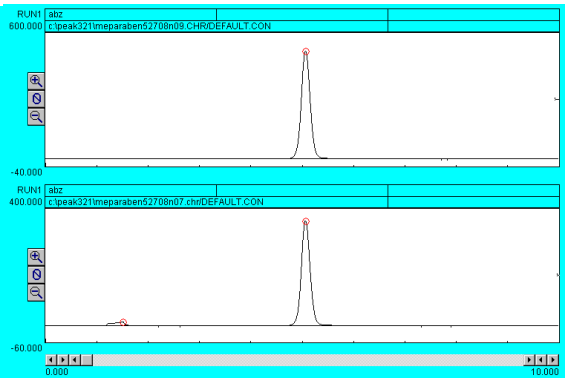

Figure 3.11b, Normal phase HPLC chromatograms of methylparaben: the top chromatogram is the standard solution with drug concentration of 86ug/mL; the bottom curve is the saturated drug in dodecane.

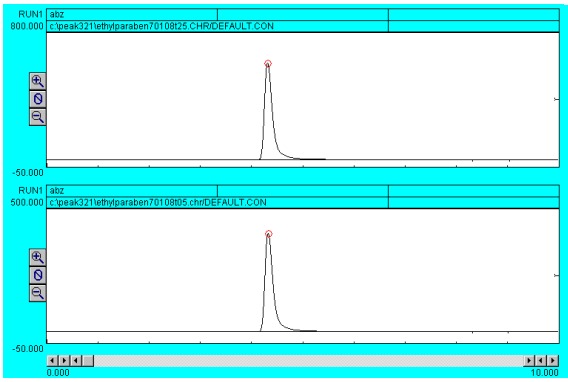

Figure 3.12a, Reverse phase HPLC chromatograms of ethylparaben: the top chromatogram is the standard solution with drug concentration of 91ug/mL; the bottom curve represents 20-fold dilution of the saturated drug in 2.5mg/mL SDS solution.

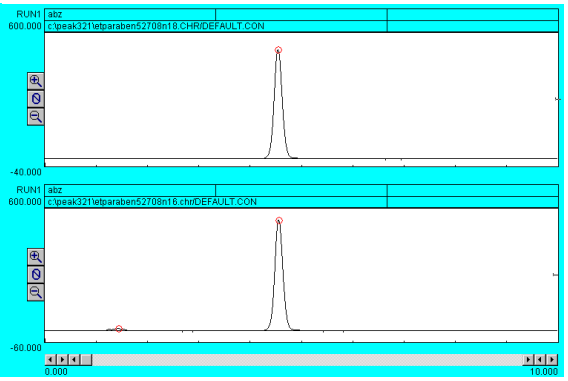

Figure 3.12b, Normal phase HPLC chromatograms of ethylparaben: the top chromatogram is the standard solution with drug concentration of 87ug/mL; the bottom curve is the saturated drug in dodecane.

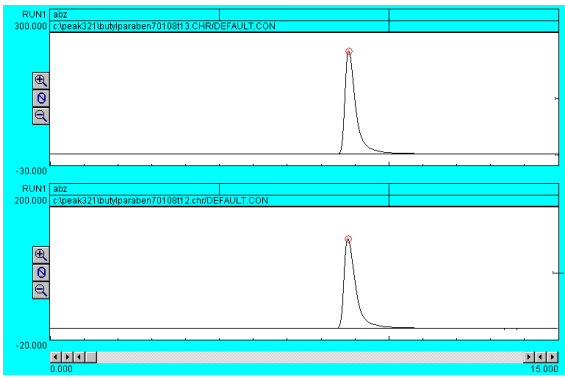

Figure 3.13a, Reverse phase HPLC chromatograms of butylparaben: the top chromatogram is the standard solution with drug concentration of 87ug/mL; the bottom curve represents 15-fold dilution of the saturated drug in 2.5mg/mL SDS solution.

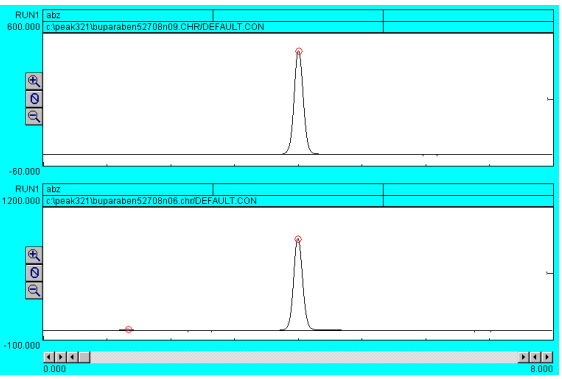

Figure 3.13b, Normal phase HPLC chromatograms of butylparaben: the top chromatogram is the standard solution with drug concentration of 90ug/mL; the bottom curve is 3-fold dilution of the saturated drug in dodecane.

3.3. RESULTS AND DISCUSSION

3.3.1. Solubilization of Model Drugs in Three Micelle Systems

The aqueous solubility results for the steroids, benzodiazepines and parabens are shown in Tables 3.2~3.4. In all cases, the aqueous solubility results were in good agreement with those found in the literature (Yalkowski and He, 2003). The most water-soluble solute was methylparaben and the least soluble was 17β-estradiol.

The solubility results in dodecane for the three solute sets are also shown in Tables 3.2~3.4. Dodecane solubility results in the literature are rare, so comparisons to results in Table 3.2 to 3.4 are difficult. None the less, the data presented in Tables 3.2 to 3.4 may be evaluated directly. For progesterone, testosterone, diazepam, prazepam and butylparaben solubility in dodecane is greater than in water. 17β-estradiol and temazepam show approximately equal solubility in water and dodecane. All other compounds are less soluble in dodecane compared to water. The dodecane/water partitioning coefficients of model drugs are listed in Table 3.2~3.4.

The solubilization capacities and associated micelle/water partitioning coefficients (calculated by Eq. (3.3) and (3.5), respectively) are also listed in Tables 3.2~3.4. For butylparaben, κ and $K_{m/w}$ values in DTAB and DM were not determined because the solutions became cloudy that suggested there may be a phase transition.

The experimental octanol/water partitioning property $\log P_{oct}$ values from literatures (Johnson et al., 1995; Kamlet et al., 1988; Hansch et al., 1995) are also shown in those tables. From the $\log P_{oct}$ values, most of the model compounds are quite hydrophobic.

Table 3.2, Critical parameters of model steroids: $logP_{oct}$, aqueous solubility, solubility in dodecane, hydrocarbon/water partitioning coefficient ($K_{h/w}$), solubilization capacity (κ) and micelle/water partitioning coefficients ($K_{m/w}$) in SDS, DTAB and DM micelle systems.

	Progesterone	Testosterone	17β-estradiol	11α-hydroxyprogesterone
$logP_{oct}$ (exp.)	3.77	3.31	3.86	2.36
Aqueous solubility (M)	$(2.79\pm0.14)\times10^{-5}$	$(8.42\pm0.28)\times10^{-5}$	$(6.23\pm0.33)\times10^{-6}$	$(1.77\pm0.09)\times10^{-4}$
Solubility in dodecane (M)	$(9.13\pm0.51)\times10^{-3}$	$(1.06\pm0.06)\times10^{-3}$	$(8.9\pm1.7)\times10^{-6}$	$(5.08\pm0.48)\times10^{-5}$
$K_{h/w}$	$(3.80\pm0.10)\times10^{3}$	51.2±2.9	10.6±0.6	3.62±0.39
κ (SDS)	0.227±0.008	0.209±0.006	0.0245±0.0003	0.276±0.010
$K_{m/w}$ (SDS)	$(3.69\pm0.21)\times10^{5}$	$(1.14\pm0.05)\times10^{5}$	$(2.13\pm0.12)\times10^{5}$	$(6.75\pm0.39)\times10^{4}$
κ (DTAB)	0.099±0.007	0.089±0.005	0.0479±0.0016	0.129±0.003
$K_{m/w}$ (DTAB)	$(1.79\pm0.15)\times10^{5}$	$(5.40\pm0.31)\times10^{4}$	$(4.07\pm0.25)\times10^{5}$	$(3.57\pm0.19)\times10^{4}$
κ (DM)	0.0501±0.006	0.0491±0.0078	0.0157±0.0014	0.0441±0.0018
$K_{m/w}$ (DM)	$(9.49\pm1.23)\times10^{4}$	$(3.09\pm0.48)\times10^{4}$	$(1.37\pm0.14)\times10^{5}$	$(1.32\pm0.09)\times10^{4}$

Errors are based on 95% confidence intervals.

Table 3.3, Critical parameters of model benzodiazepines: $logP_{oct}$, aqueous solubility, solubility in dodecane, hydrocarbon/water partitioning coefficient ($K_{h/w}$), solubilization capacity (κ) and micelle/water partitioning coefficients ($K_{m/w}$) in SDS, DTAB and DM micelle systems.

	Diazepam	Temazepam	Oxazepam	Prazepam
logP (exp.)	2.99	2.19	2.24	3.73
Aqueous solubility (M)	$(1.60\pm0.05)\times10^{-4}$	$(3.46\pm0.02)\times10^{-4}$	$(7.34\pm0.15)\times10^{-5}$	$(1.83\pm0.09)\times10^{-5}$
Solubility in dodecane (M)	$(3.91\pm0.18)\times10^{-3}$	$(4.16\pm0.10)\times10^{-4}$	$(2.06\pm0.63)\times10^{-7}$	$(4.27\pm0.17)\times10^{-3}$
$K_{h/w}$	308±17	15.1±0.4	0.0353±0.0108	$(2.94\pm0.19)\times10^{3}$
κ (SDS)	0.349±0.014	0.416±0.014	0.166±0.003	0.154±0.007
$K_{m/w}$ (SDS)	$(8.93\pm0.39)\times10^{4}$	$(4.70\pm0.11)\times10^{4}$	$(1.08\pm0.03)\times10^{5}$	$(4.03\pm0.26)\times10^{5}$
κ (DTAB)	0.0928±0.0016	0.116±0.003	0.0499±0.0023	0.0298±0.0013
$K_{m/w}$ (DTAB)	$(2.94\pm0.10)\times10^{4}$	$(1.67\pm0.04)\times10^{4}$	$(3.58\pm0.18)\times10^{4}$	$(8.76\pm0.57)\times10^{4}$
κ (DM)	0.0647±0.0012	0.0640±0.0024	0.0267±0.0010	0.0220±0.0002
$K_{m/w}$ (DM)	$(2.10\pm0.07)\times10^{4}$	$(9.63\pm0.35)\times10^{3}$	$(1.96\pm0.08)\times10^{4}$	$(6.51\pm0.33)\times10^{4}$

Errors are based on 95% confidence intervals.

Table 3.4, Critical parameters of model parabens: $\log P_{oct}$, aqueous solubility, solubility in dodecane, hydrocarbon/water partitioning coefficient ($K_{h/w}$), solubilization capacity (κ) and micelle/water partitioning coefficients ($K_{m/w}$) in SDS, DTAB and DM micelle systems.

	Methylparaben	Ethylparaben	Butylparaben
logP (exp.)	1.96	2.47	3.57
Aqueous solubility (M)	$(1.39\pm0.01)\times10^{-2}$	$(5.13\pm0.07)\times10^{-3}$	$(1.06\pm0.03)\times10^{-3}$
Solubility in dodecane (M)	$(4.00\pm0.16)\times10^{-4}$	$(5.47\pm0.37)\times10^{-4}$	$(2.45\pm0.09)\times10^{-3}$
$K_{h/w}$	0.362±0.015	1.34±0.09	29.0±1.3
κ (SDS)	0.559±0.035	0.475±0.015	0.643±0.009
$K_{m/w}$ (SDS)	$(1.42\pm0.06)\times10^{3}$	$(3.48\pm0.09)\times10^{3}$	$(2.04\pm0.06)\times10^{4}$
κ (DTAB)	0.771±0.027	0.656±0.035	n.d.
$K_{m/w}$ (DTAB)	$(1.73\pm0.04)\times10^{3}$	$(4.28\pm0.15)\times10^{3}$	n.d.
κ (DM)	0.412±0.052	0.359±0.006	n.d.
$K_{m/w}$ (DM)	$(1.16\pm0.10)\times10^{3}$	$(2.85\pm0.05)\times10^{3}$	n.d.

Errors are based on 95% confidence intervals.

n.d.=not determined.

The detailed solubilization results of 11 model drugs in SDS, DTAB and DM surfactant systems at room temperature are shown in Figures 3.14~3.22. The typical solubilization profiles expected in the presence of surfactants were obtained: at low surfactant concentration the drug solubility was constant and equal to the aqueous solubility. At surfactant concentrations above the CMC (critical micelle concentration) the solubility increased linearly as a function of surfactant concentration. From the solubilization profiles, two critical parameters could be extracted: the aqueous solubility and the solublization capacity by the slope of the ascending line. Then the micelle/water partitioning coefficient could be calculated from the solubilization capacity and aqueous solubility based on Eq. (3.5).

During the measurements of the hydrocarbon/water partitioning coefficients, two different techniques had been employed: solubility ratio and direct partitioning methods. For some compounds, such as testosterone and 17β-estradiol, there was statistically significant discrepancy between the results from different methods. The likely reason for this difference is that both of the drugs can form different crystals in dodecane and aqueous media: they exhibit an anhydrous form in dodecane and hydrated (testosterone) or hemi-hydrated (17β-estradiol) form in water. Therefore the saturated solutions in the two media are in equilibrium with different crystalline forms and the solubility ratio method becomes inappropriate. Other model compounds, such as progesterone, diazepam, temazepam, etc., have no reported solvate form and are expected to keep the same polymorph at the two media.

To evaluate the micelle core as the locus of solubilization of model drugs, the hydrocarbon/water partitioning coefficients were compared to micelle/water partitioning coefficients. The data in Tables 3.2~3.4 clearly show that in all cases micelle/water partitioning coefficients, $K_{m/w}$, are much larger than hydrocarbon/water partitioning

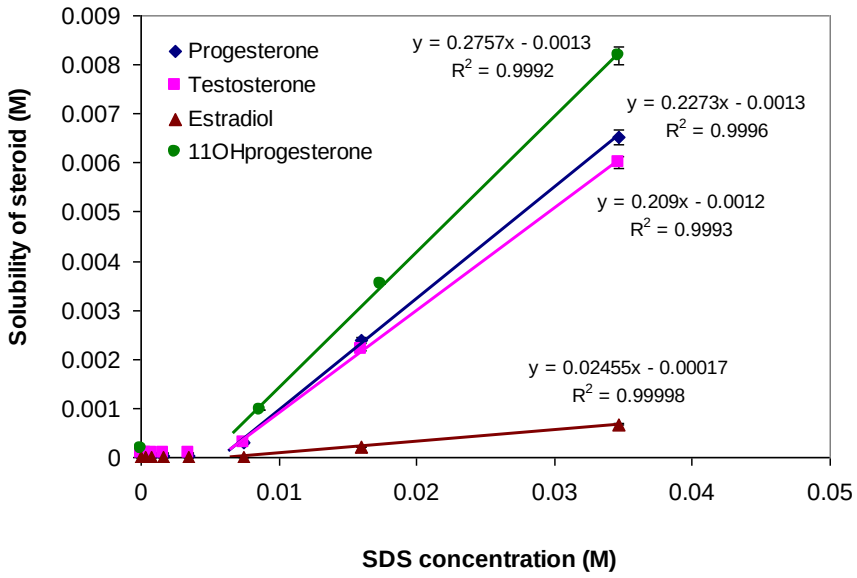

Figure 3.14, Solubilities of 4 model steroids as a function of SDS concentration.

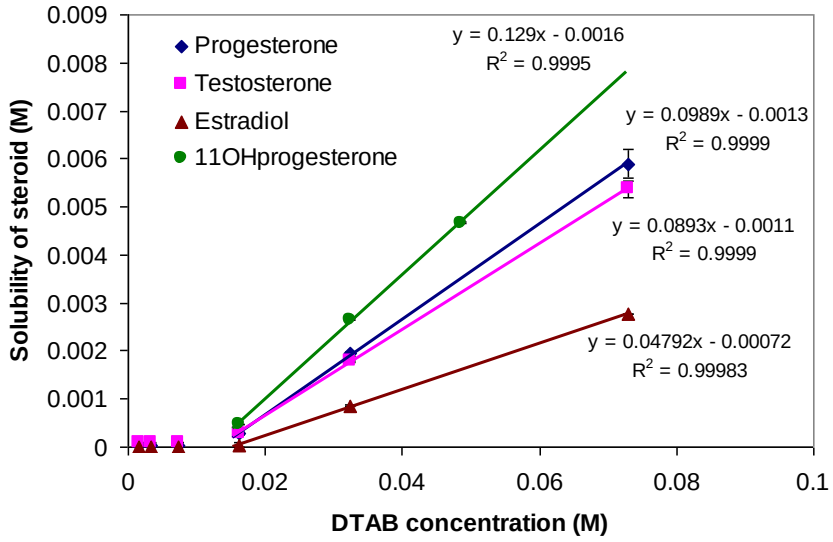

Figure 3.15, Solubilities of 4 model steroids as a function of DTAB concentration.

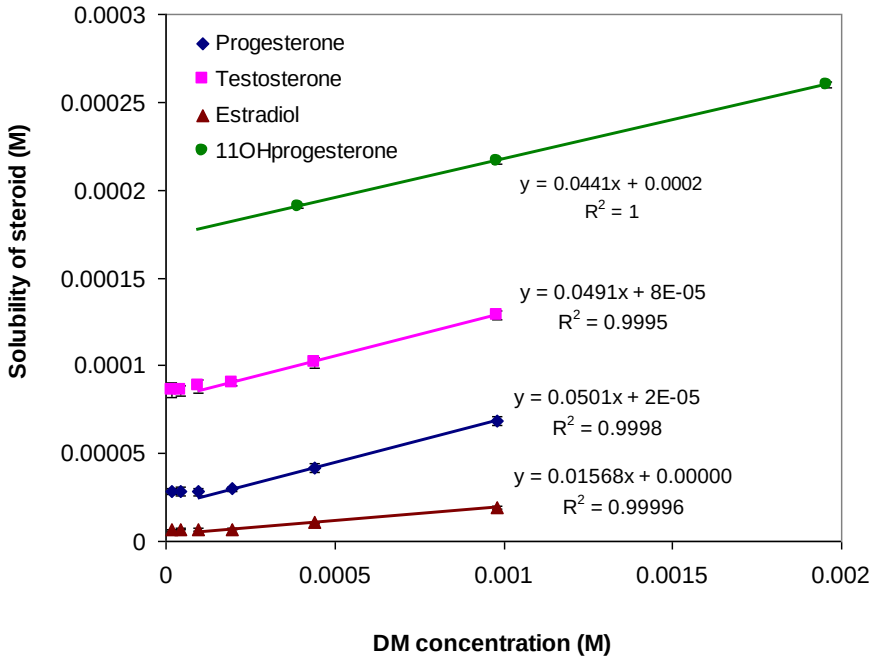

Figure 3.16, Solubilities of four model steroids as a function of DM concentration.

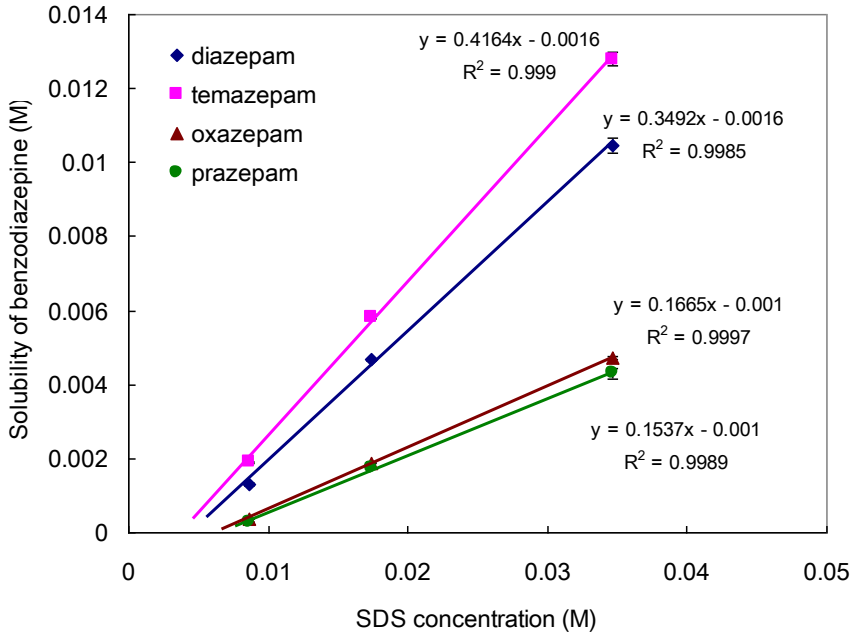

Figure 3.17, Solubilities of four benzodiazepines as a function of SDS concentration.

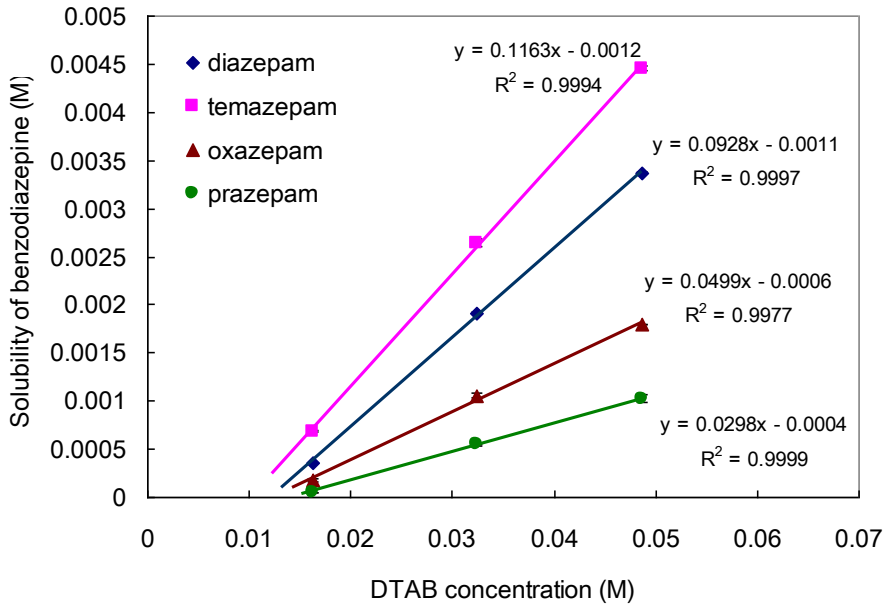

Figure 3.18, Solubilities of four benzodiazepines as a function of DTAB concentration.

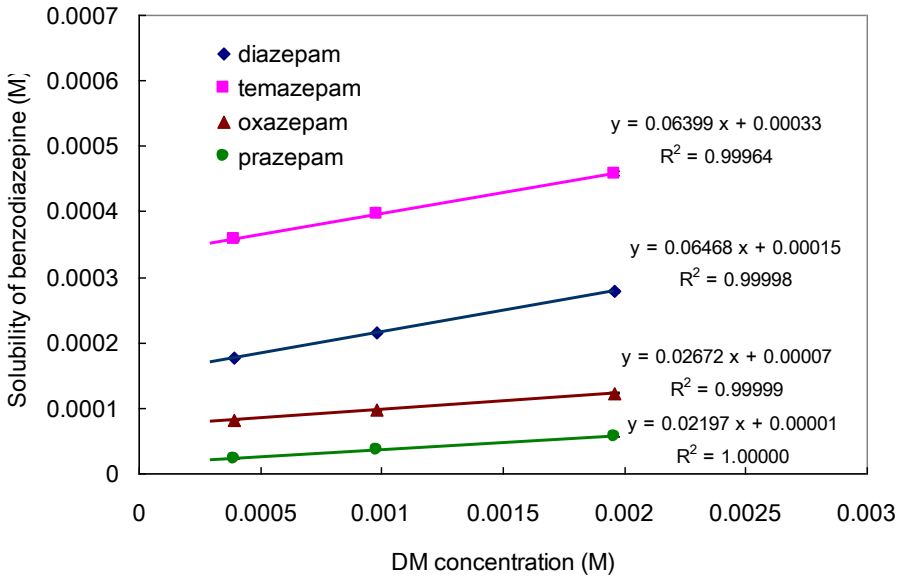

Figure 3.19, Solubilities of four benzodiazepines as a function of DM concentration.

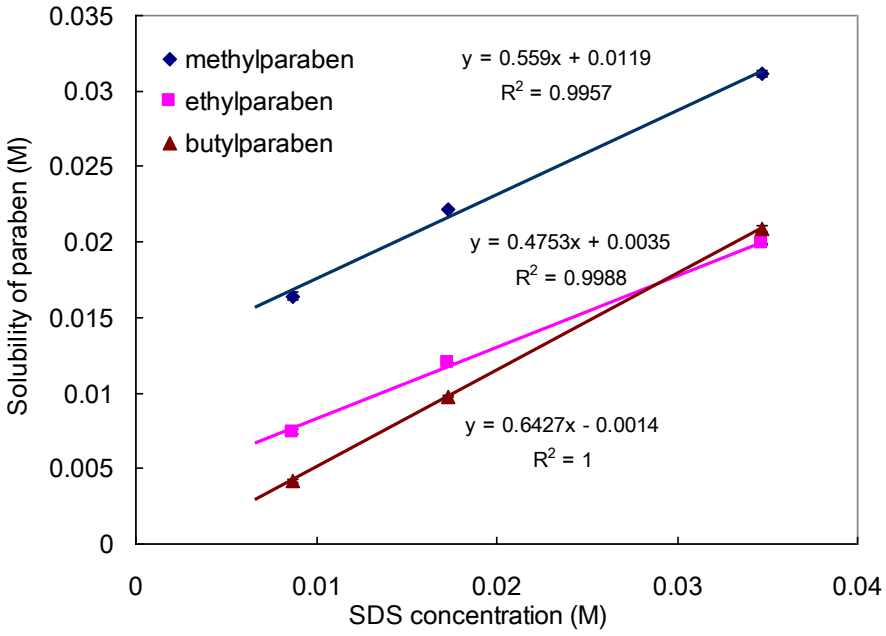

Figure 3.20, Solubilities of three parabens as a function of SDS concentration.

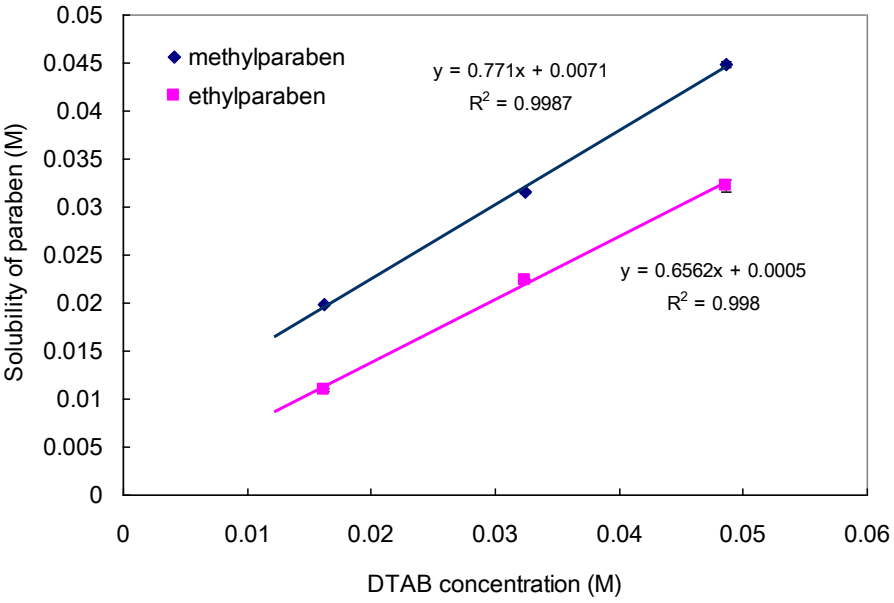

Figure 3.21, Solubilities of two parabens as a function of DTAB concentration.

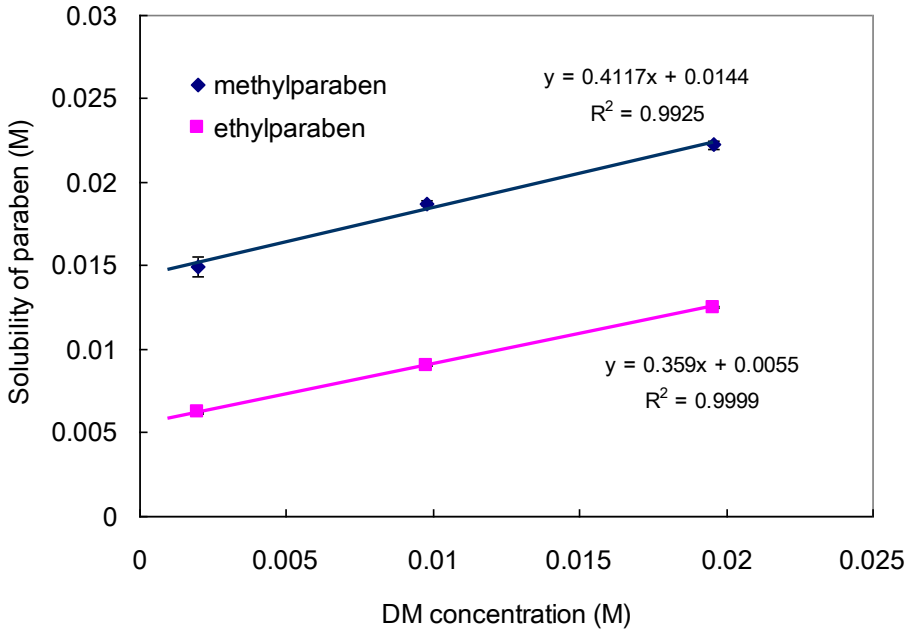

Figure 3.22, Solubilities of two parabens as a function of DM concentration.

coefficients, $K_{h/w}$. In most cases, $K_{m/w}$ is at least 2 orders of magnitude larger than $K_{h/w}$, which suggests there is less than 1% of the solutes are exclusively solubilized in the micellar core. The closest agreement between $K_{h/w}$ and $K_{m/w}$ is when progesterone is solubilized in DM micelles with the ratio $K_{m/w}/K_{h/w}=25$. When the Laplace pressure effect is taken into account the differences between $K_{h/w}$ and $K_{m/w}$ are even greater. The factor $\exp[-PV/RT]$ in Eq. (3.2) is always less than 1 and ranges from 0.01 to 0.3 in our systems. Detailed information on Laplace pressure is presented in Chapter 5. After considering the Laplace pressure effect, the ratio $\frac{K_{h/w}\exp[-PV/RT]}{K_{micelle/water}}$ has a maximum of 0.4% for progesterone solubilized in DM micelles. The Eq. (3.2) will not hold in any of our studied systems, which indicates the assumption of micelle core as major solubilization locus is not true.

If we relax the requirement that the Eq. (3.2) holds, the possible correlations between micelle/water partitioning coefficients and hydrocarbon/water partitioning constants can be examined. Using SDS micelle system as an example, the relationships between $K_{h/w}$ and $K_{m/w}$ of 11 model drugs are shown in Figure 3.23. From the scattered pattern, there is no identifiable correlation between the two properties. The hydrocarbon/water partitioning coefficients cover 5 orders of magnitude from 0.04 (oxazepam) to 3.8×10^3 (progesterone) while micelle/water partitioning constants span only 2.5 orders of magnitude from 1.4×10^3 (methylparaben) to 4.0×10^5 (prazepam).

Our results are consistent with reports that only completely nonpolar molecule may reside in the micellar core (Rosen, 1989; Attwood and Florence, 1983). High hydrophobicity is not the sufficient condition that makes hydrophobic solutes stay in the core region of the micelles. Although many hydrophobic molecules have the major part of the structure nonpolar and have only very small fraction of polar groups, those small polar fraction

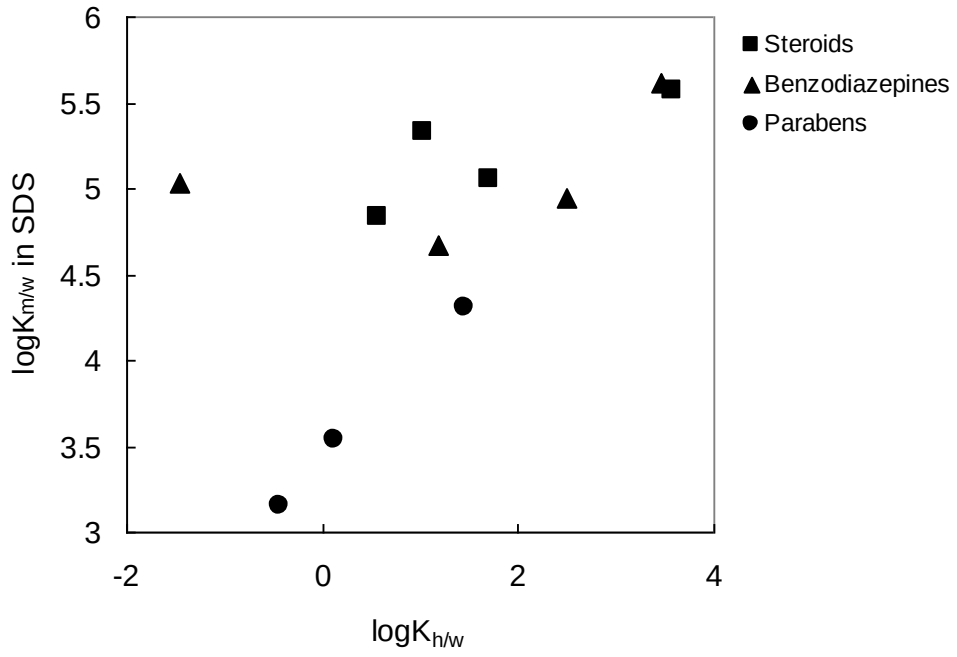

Figure 3.23, The relationships between hydrocarbon/water partition coefficient, $K_{h/w}$, and micelle/water partition coefficient, $K_{m/w}$, in aqueous SDS solutions for three series of drugs, steroids, benzodiazepines and parabens.

would affect the location of the molecules and drive them away from the hydrocarbon-like core.

This analysis had been applied to simple alkanols, ketones, amides and aromatics by Gumkowski (Gumkowski, 1986). Relatively complicated molecules, ethyl p- o- and m-aminobenzoates were also studied (Mukerjee and Ko, 1992). They found the micelle core is not the major locus of those compounds solubilized in the micelles. Our studies extended the objects to more pharmaceutical important molecules with complicated chemical structures and drew a similar conclusion: all of the model drugs are not mainly located at the micellar core region.

Different methods may have different definition when they were applied to determine the location of solutes in the micelle systems. In the thermodynamics based method, a molecule that has part of it at the micelle surface will be defined as staying at surface. Our conclusion that majority of drug molecules are not in the micellar core does not mean any part of the drug molecules cannot be at the micelle core. The hydrophobic part of the solute is still likely buried in the core region. From this viewpoint there is actually no qualitative conflict between thermodynamics based method and spectroscopy methods.

3.3.2. Effect of Salts on the Micelle/water Partitioning Coefficients

Three model drugs, progesterone, diazepam and methylparaben, each representing a series of solutes, were solubilized in SDS, DTAB and DM micelle systems in the presence of 0.15M NaCl to study the effect of the salts on the micelle/water partitioning coefficients. In Figures 3.24~3.27, the drug solubilities as a function of surfactant concentration in the presence and absence of 0.15M NaCl are shown. The quantitative results of aqueous solubility, solubilization power of micelles, and micelle/water

partitioning coefficient for three model drugs are summarized in Table 3.5. The statistical analyses were carried out using Scientist® software to provide the 95% confidence intervals. For comparison, the results corresponding to the solubilization of the three model drugs in the absence of salts from Table 3.2~3.4 are included.

In anionic SDS solutions, for all three model drugs, the solubilization power shows a significant decrease in the presence of salt compared to that in the absence of salt. The aqueous solubilities of progesterone and diazepam in 0.15M NaCl solutions were not significantly different from the measured solubilities in the absence of salt. On the other hand the aqueous solubility of methylparaben in 0.15M NaCl was decreased to 13.0±0.1mM compared to the intrinsic aqueous solubility of 13.9±0.1mM without salts. The decreasing solubility could be attributed to salting out effect. The calculated micelle/water partitioning coefficients based on the solubilization power and aqueous solubility through Eq. (3.5) exhibited a significant decrease by 36% (progesterone), 19% (diazepam) and 24% (methylparaben) with the introduction of 0.15M NaCl.

In cationic DTAB solutions, the solubilization power toward all three model drugs was significantly decreased by adding 0.15M NaCl. The micelle/water partition coefficients of progesterone and diazepam were reduced by 22% and 12% respectively in the presence of salts. The $K_{m/w}$ of methylparaben showed no statistically significant difference in the presence and absence of salt. This observation may be due to the nearly-saturated adsorption of methylparaben at DTAB micelle surface. The solubilization power of DTAB toward methylparaben was so large (>0.7) that the micelles consisted of a mole fraction of drugs nearly as much as that of surfactant. The effect of drug concentration on the solubilization isotherm will be further discussed in a later chapter.

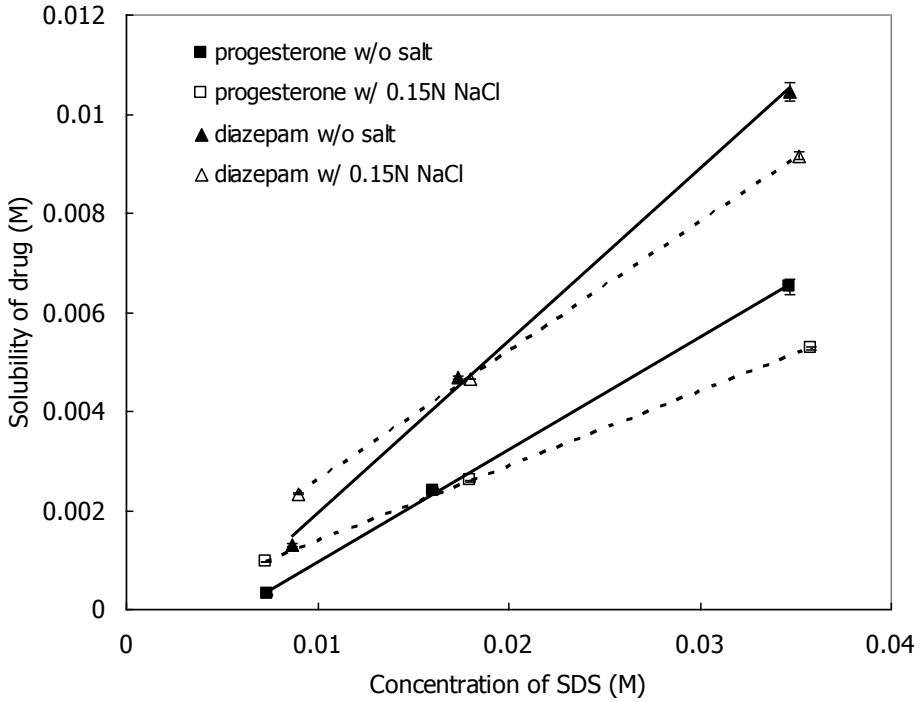

Figure 3.24, Solubilities of progesterone and diazepam as a function of SDS concentration in the absence and presence of 0.15M NaCl.

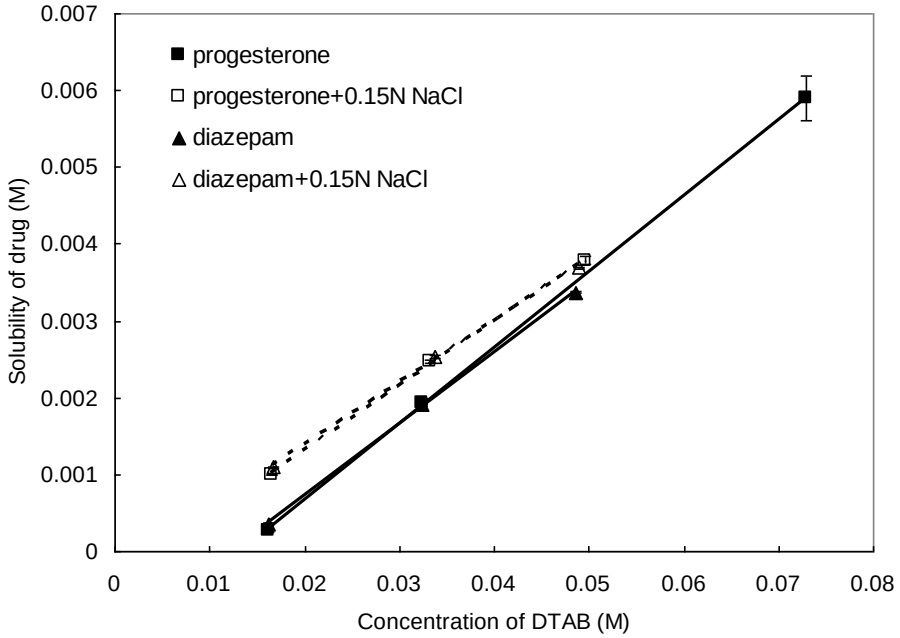

Figure 3.25, Solubilities of progesterone and diazepam as a function of DTAB concentration in the absence and presence of 0.15M NaCl.

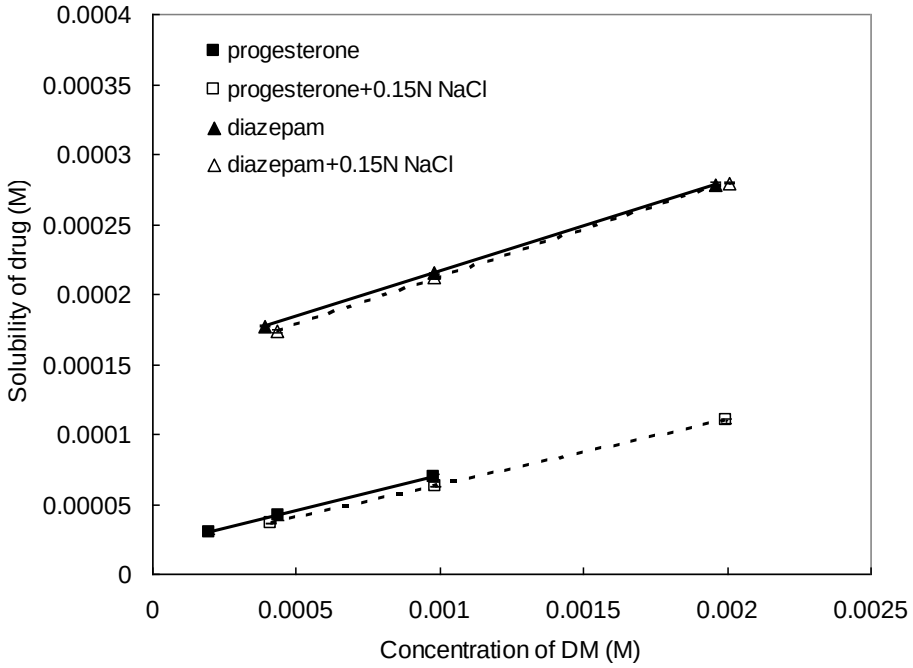

Figure 3.26, Solubilities of progesterone and diazepam as a function of DM concentration in the absence and presence of 0.15M NaCl.

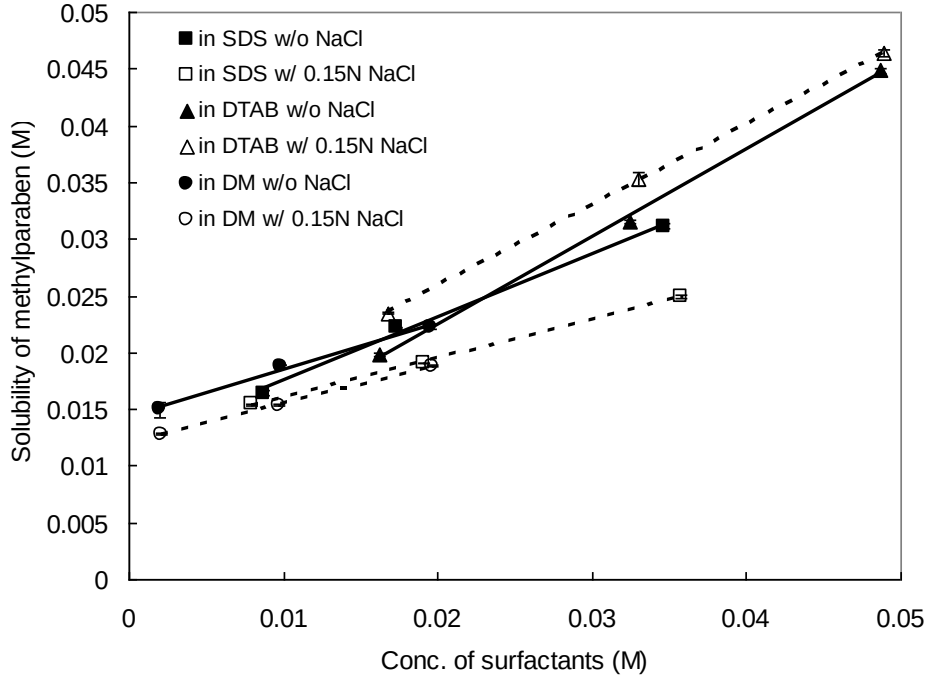

Figure 3.27, Solubilization results of methylparaben in three surfactant systems, SDS (square), DTAB (triangle) and DM (circle), in the absence and presence of 0.15M NaCl.

Table 3.5, Aqueous solubility, solubilization capacity (κ) and micelle/water partitioning coefficient ($K_{m/w}$) of three model drugs in SDS, DTAB and DM micelle systems in the absence and presence of 0.15M NaCl. Experimental data in the absence of salts are from Table 3.2~3.4.

	Progesterone	Diazepam	Methylparaben
Aqueous solubility (M)	$(2.79\pm0.14)\times10^{-5}$	$(1.60\pm0.05)\times10^{-4}$	$(1.39\pm0.01)\times10^{-2}$
Aqueous solubility w/0.15N NaCl (M)	$(3.09\pm0.22)\times10^{-5}$	$(1.59\pm0.03)\times10^{-4}$	$(1.30\pm0.01)\times10^{-2}$
κ (SDS)	0.227±0.008	0.349±0.014	0.559±0.035
κ (SDS) w/0.15N NaCl	0.151±0.002	0.261±0.003	0.341±0.008
$K_{m/w}$ (SDS)	$(3.69\pm0.21)\times10^{5}$	$(8.93\pm0.39)\times10^{4}$	$(1.42\pm0.06)\times10^{3}$
$K_{m/w}$ (SDS) w/0.15N NaCl	$(2.35\pm0.17)\times10^{5}$	$(7.21\pm0.15)\times10^{4}$	$(1.08\pm0.02)\times10^{3}$
κ (DTAB)	0.099±0.007	0.093±0.002	0.771±0.027
κ (DTAB) w/0.15N NaCl	0.084±0.003	0.080±0.002	0.714±0.023
$K_{m/w}$ (DTAB)	$(1.79\pm0.15)\times10^{5}$	$(2.94\pm0.10)\times10^{4}$	$(1.73\pm0.04)\times10^{3}$
$K_{m/w}$ (DTAB) w/0.15N NaCl	$(1.39\pm0.11)\times10^{5}$	$(2.59\pm0.08)\times10^{4}$	$(1.78\pm0.04)\times10^{3}$
κ (DM)	0.050±0.006	0.065±0.001	0.412±0.052
κ (DM) w/0.15N NaCl	0.046±0.001	0.067±0.001	0.340±0.009
$K_{m/w}$ (DM)	$(9.49\pm1.23)\times10^{4}$	$(2.10\pm0.07)\times10^{4}$	$(1.16\pm0.10)\times10^{3}$
$K_{m/w}$ (DM) w/0.15N NaCl	$(7.95\pm0.59)\times10^{4}$	$(2.19\pm0.05)\times10^{4}$	$(1.08\pm0.02)\times10^{3}$

Errors are based on 95% confidence intervals.

In nonionic DM solutions, the presence of salts had no statistically-significant effect on the micelle/water partition coefficients of all three model drugs. The results suggest that moderate concentrations of electrolytes have negligible influence on the solubilization behavior of nonionic micelles.

To determine the location of model drugs in micelles in the presence of salts, the same approach introduced in section 3.3.1 was employed: the micelle/water partitioning coefficients, $K_{m/w}$, was compared to hydrocarbon/water partitioning coefficient multiplied by a factor representing Laplace pressure effect, $K_{h/w}\exp(-PV/RT)$. The results in the absence of salts showed the term $K_{m/w}$ was at least 2 orders of magnitude greater than term $K_{h/w}\exp(-PV/RT)$ in all studied micelle systems. The minimum ratio between these two terms was 250 (when progesterone was solubilized in DM micelles). In the presence of salts, the greatest influence on $K_{m/w}$ was a 36% decrease. After taking salt effect into account, the micelle/water partitioning coefficient was still at least 2 orders of magnitude greater than term $K_{h/w}\exp(-PV/RT)$ in all studied drug-surfactant systems. Therefore, the micelle surface or palisade region was the major location of model drugs when solubilized in the three micelle systems in the absence and presence of salts.

3.4. CONCLUSION

The measured micelle/water partitioning coefficients were much larger than hydrocarbon/water partitioning constants, which indicated the core region of micelle was insufficient to solubilize the model hydrophobic drugs based on the thermodynamic model (Eq.(2.3)). This conclusion holds for 3 series of model drugs in 3 micelle systems in the absence and presence of salts. The model drugs have broad range in terms of hydrophobicity, as measured by logP, and aqueous solubility. In all the cases, partitioning solely into the micelle core seems insufficient to explain partitioning into a micelle.

Chapter 4

Oil/water Interface Activities of Hydrophobic Drugs in the Presence and Absence of Surfactants

4.1. INTRODUCTION

Micellar solubilization has been shown to be important both in considering micelles as drug delivery vehicles of poorly water-soluble drugs and in understanding *in vivo* absorption of hydrophobic drug molecules. Currently, the physicochemical factors controlling the solubilization capacity of micelles are poorly understood. This work is designed to probe the mechanism of solubilization by micelle systems with the goal of quantitative prediction of the micellar solubilization for specific drug-surfactant mixtures.

Location of the drugs in micelles is likely to be a critical factor in understanding the micellar solubilization phenomena. As a result of the small size of micelles, and the accompanying large surface/volume ratio, many studies have considered the surface region of micelles to be the major location of some solutes (Lebedeva et al., 2007; Sabate et al., 2001; Svens and Rosenholm, 1973; Nagaonkar and Bhagwat, 2006; Yoshioka, 1979); Malcolmson and Lawrence, 1993; Mukerjee and Ko, 1992; Croy and Kwon, 2005; Donbrow et al., 1967). In the previous chapter, we employed a thermodynamics-based solubility method to show that solubilization in the micellar core alone is insufficient to explain our experimental data. The conclusion, drawn from 11 model drugs solubilized in 3 micelle systems, indirectly suggests the micelle surface is the major location of the drugs solubilized in micelles.

In this chapter, the characteristics of adsorption of model drugs to model interface are probed. Here, we view the micelle surface as a hydrocarbon/water interface populated

by the surfactant molecules. For a drug to be solubilized at the micellar surface, it is expected to be surface active at the hydrocarbon/water interface even in the presence of surfactants. The surface activity of the model drugs will be measured at the water/air, oil/air and oil/water interfaces. The introduction of surfactants to the system will be used to observe the extent to which drugs and surfactants modulate the oil/water interfacial tension. Later a thermodynamic model will be utilized to quantitatively simulate the observed phenomena.

Dodecane/water was chosen as the model hydrocarbon/water interface to mimic the hydrocarbon chain of the model surfactants. Poorly-soluble steroids were chosen to demonstrate the ability of drugs to adsorb to the model oil/water interface. Three surfactants, anionic sodium dodecyl sulfate (SDS), cationic dodecyl trimethyl ammonium bromide (DTAB) and nonionic dodceyl maltoside (DM), were used to detect their interactions with the drug molecules at oil/water interface.

It should be kept in mind that many differences exist between a micelle surface and a flat hydrocarbon/water interface. Among the most obvious differences between the two is that the micelle surface is highly curved. In the current chapter, The curvature effect will be explored in the following chapter by invoking the Laplace pressure concept.

4.2. MATERIALS AND METHODS

4.2.1. Materials

Progesterone (>99%), testosterone (>98%), 17β-estradiol (>98%), sodium dodecyl sulfate (>99%), dodecyltrimethylammonium bromide (>99%) and dodecyl β-D-maltoside (>98%) were obtained from Sigma-Aldrich (St. Louis, MO). Progesterone, testosterone, SDS and DTAB were purified before use while 17β-estradiol and dodecyl β-D-maltoside were used as received.

4.2.2. Methods

4.2.2.1. Surface Tension Measurement

DuNouy ring method was used to measure the liquid/air and liquid/liquid interfacial tension. The method was first developed by duNouy in 1919 (duNouy, 1919). In this method, the interfacial tension is measured with the aid of platinum-iridium ring pulled through the interface (Figure 4.1). The force necessary to detach the ring at the interface is proportional to the interfacial tension.

The relationship between the interfacial tension and the applied force could be expressed using the formula:

$$\gamma = \frac{\mathrm{F}}{4\pi \cdot \mathrm{R}} \times \beta \qquad (4.1)$$

F is the applied force pulling the ring; R is the radius of the metal ring and β is the correction factor that could be calculated using Zuidema and Waters's empirical equation (Zuidema and Waters, 1941):

$$\beta = 0.725 + \left[\left(\frac{0.01452\ F}{C^2(\rho_1 - \rho_2)} \right) + 0.04534 - \frac{1.679\, r}{R} \right]^{0.5} \qquad (4.2)$$

Here, r is the radius of metal wire; C is the circumference of the metal ring which is equal to $2\pi\mathrm{R}$; ρ_1 and ρ_2 are the densities of lower and upper layers of liquid. The parameters of the above equation were obtained by fitting the formula to experimentally determined correction factors by Harkins and Jordan (Harkins and Jordan, 1930).

Our experiments were carried out in a water-jacketed beaker where the temperature was controlled at 25.0±0.1^{o}C. The parameters used were: circumference C=6.005cm; the ratio r/R =0.01859; $\rho_1 = 0.997\ g/cm^3$ (water at 25^{o}C) and $\rho_2 = 0.748\ g/cm^3$ for dodecane or 0.001 g/cm^3 for air.

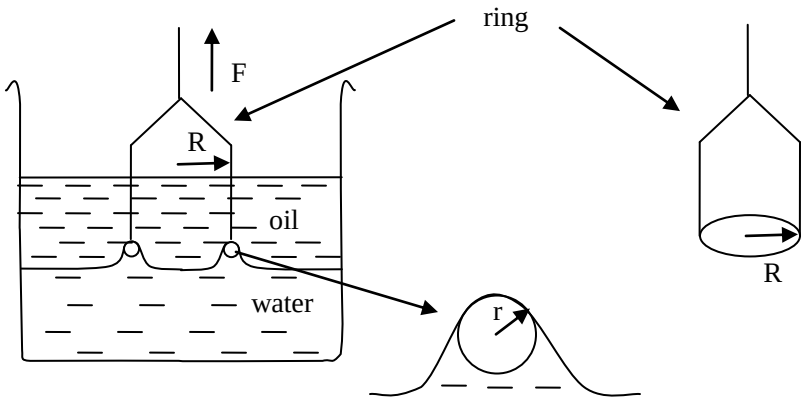

Figure 4.1, A schematic of the duNouy ring method. The ring is pulled up through the oil/water interface with a force F that is proportional to the interfacial tension.

When the drugs were present, an excess amount of drugs was added to water and hydrocarbon solvents (dodecane or octane) separately. Both systems were rotated for 3~5 days at room temperature (24±1^{o}C) to reach equilibrium. Aqueous solutions were filtered using 0.2μm hydrophilic PTFE filter (Millipore Inc.) and the hydrocarbon solutions were filtered using 0.2μm hydrophobic PTFE filter (Pall corp.). The filtrates were employed in water/air and hydrocarbon/air interfacial tension measurements respectively. The mixtures of the two filtered solutions (hydrocarbons at top layer and aqueous solutions at bottom layer) were used in hydrocarbon/water interfacial tension measurements.

The surfactants were dissolved in aqueous phase to make solutions with known concentrations, e.g. 0.1, 1.0 and 10 mg/mL SDS solutions. Because of negligible solubility in hydrocarbons, the surfactants were not prepared in oil phase. The aqueous solutions containing surfactants were mixed with dodecane for dodecane/water interfacial tension determinations. When also present, an excess amount of the drug solid was placed into aqueous solutions with known concentration of surfactants. The aqueous solutions were rotated for 3~5 days to reach equilibrium before being filtered using 0.2μm hydrophilic PTFE filter. The filtrate was mixed with drug-saturated dodecane prepared as shown above to measure the dodecane/water interfacial tensions.

Since testosterone can form different crystal forms, an anhydrous form in oil and a hydrate in water, the saturated aqueous and dodecane solutions prepared separately could not keep the same activity of the drug in the two media. Therefore the oil/water interfacial tension measurement would have a starting point where the oil/water partitioning of the drug was far from equilibrium and the kinetics of partitioning could affect the interfacial tension determinations. To avoid the complexity, a direct partitioning method was used in sample preparations: the dodecane and aqueous solutions in the presence or absence of surfactants were pre-mixed and excess testosterone was placed

into the mixture. The system was rotated for 3~5 days at room temperature to reach equilibrium. The two liquid layers were filtered using 0.2μm hydrophilic (for aqueous layer) and hydrophobic (for oil layer) PTFE filters separately and were mixed again for dodecane/water interfacial tension measurements.

4.2.2.2. Purification of Steroids and Surfactants:

Solid state adsorption method reported by Rosen to purify SDS (Rosen, 1981) was employed. This method was also applied to the purification of DTAB and two model drugs (progesterone and testosterone).

Purification of SDS and DTAB: About 1g SDS or DTAB was combined with 100mL deionized water and the solution was passed through a Sep-Pak® Plus C18 column (wetted with methanol and double distilled water before use). The first 15mL solution was discarded and the next 70 mL eluted solution was collected and freeze-dried using the following lyophilization cycle:

1. Freeze to -40^{o}C and maintain for 4h
2. Apply vacuum (100mT)
3. Increase temperature to -20^{o}C and maintain for 2h
4. Increase temperature to 0^{o}C and maintain for 8h
5. Increase temperature to 20^{o}C and maintain for 10h

After the purification, the surface tensions as a function of surfactant concentration were measured with the results shown in Figure 4.2 ad 4.3. For the purified surfactants, the figures clearly show the elimination of the local minimum near the CMC compared to the curves from unpurified surfactants.

Surface tension versus surfactant concentration curve was also measured for dodecyl β-D-maltoside with the results shown in Figure 4.4. The absence of local minimum in the

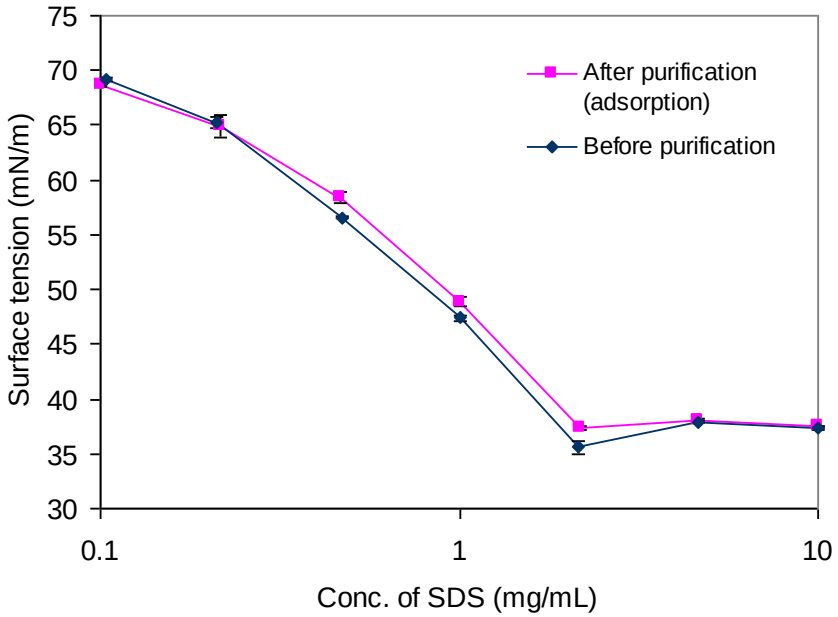

Figure 4.2, Surface tension vs. concentration of SDS in aqueous solutions before and after purification by solid adsorption method. Some error bars are smaller than the symbols.

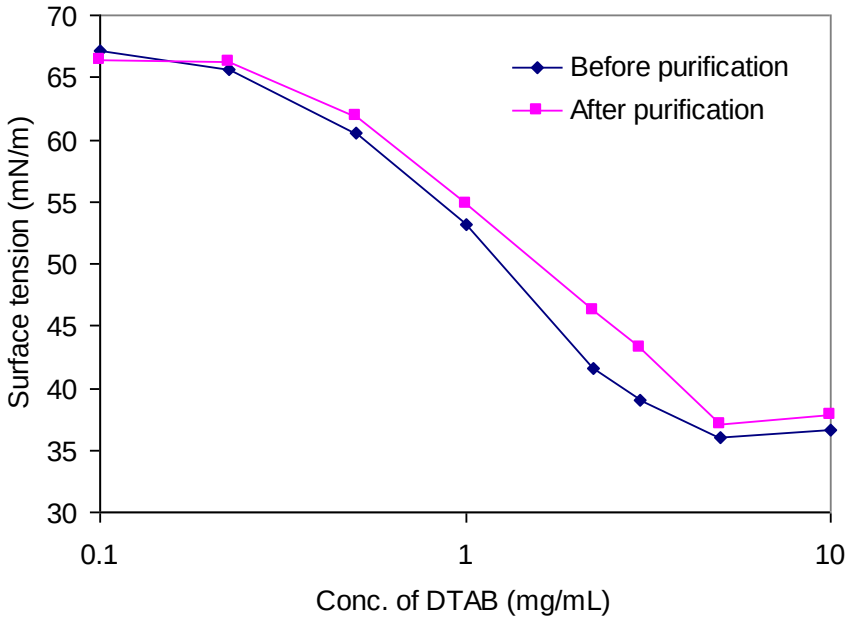

Figure 4.3, Surface tension vs. concentration of DTAB in aqueous solutions before and after purification by solid adsorption method.

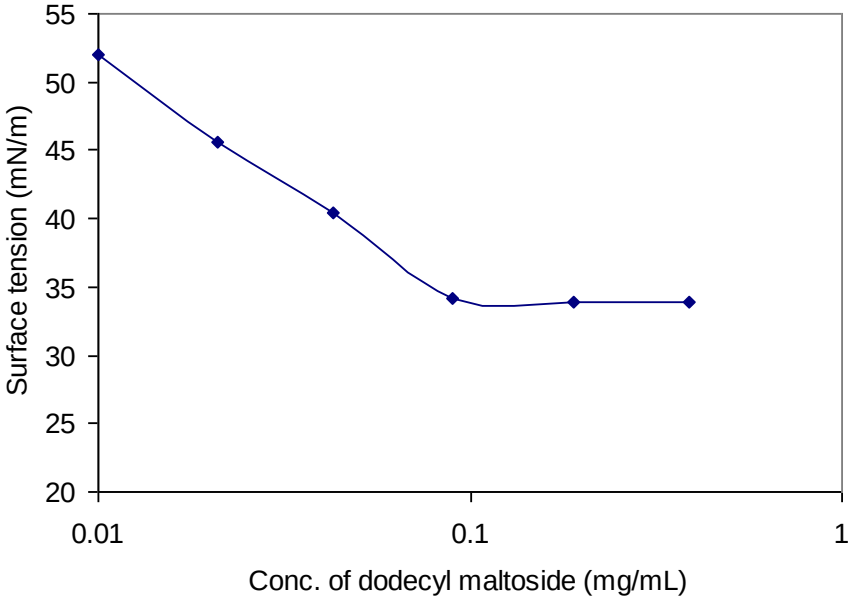

Figure 4.4. Surface tension vs. concentration of dodecyl β-D-maltoside in aqueous solutions

curve indicates high purity of the materials received from the vendor. The purification step for DM was deemed unnecessary.

Purification of progesterone and testosterone: The drugs were dissolved in hexane (20mL 1.5mg/mL for progesterone and 200mL 0.125mg/mL for testosterone) and the solutions were passed through Sep-Pak® Plus C18 columns (wetted with methanol before use). The eluent solutions were dried under a stream of nitrogen gas. After the purification, the HPLC chromatograms (Figure 4.5 and 4.6) showed significant suppressions of two impurity peaks for progesterone and one impurity peak for testosterone. The putative impurities were found to exhibit be less than 0.1% of main peaks (based on AUC ratio).

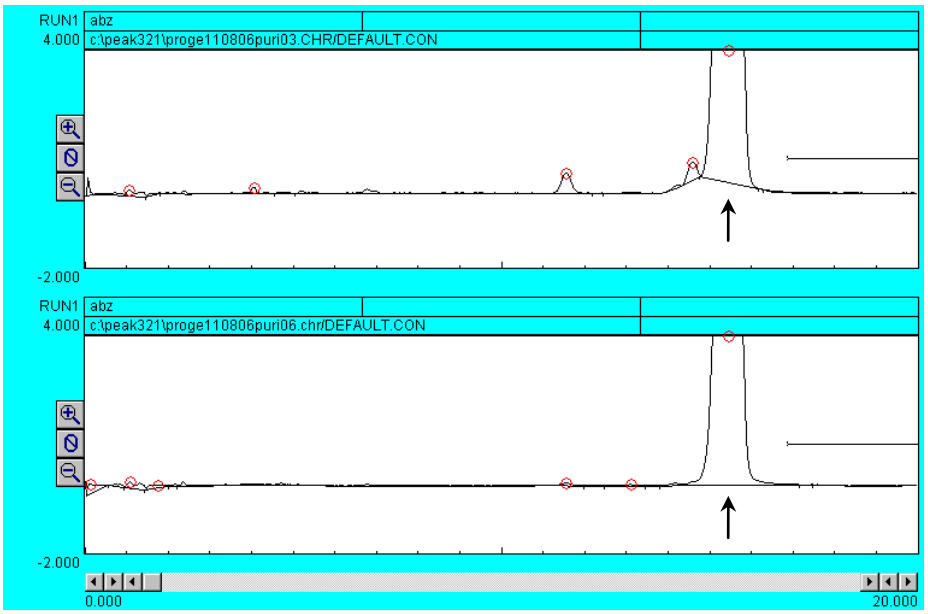

Figure 4.5, HPLC chromatograms of progesterone before (upper curve) and after (lower curve) purification. The arrow shows the main progesterone elution band.

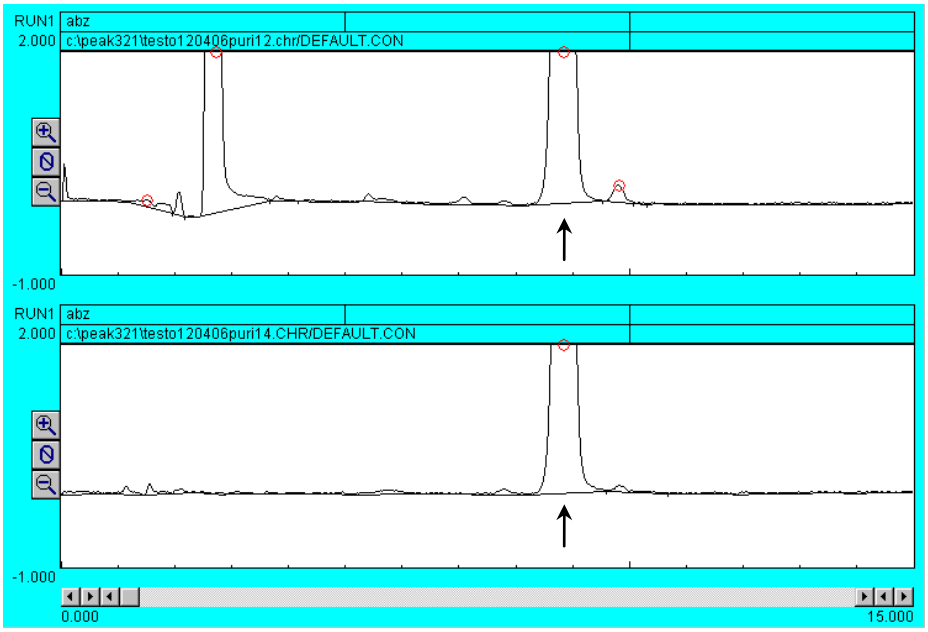

Figure 4.6, HPLC chromatograms of testosterone before (upper curve) and after (lower curve) purification. The arrow shows the main testosterone elution band.

4.3. RESULTS

4.3.1. Interfacial Studies in the Absence of Surfactants

The surface tensions of the water/air, oil/air and oil/water interfaces were measured in the presence and absence of steroids. Saturated solutions of the drugs were employed for water and oil phases. The results are summarized in Table 4.1. At the air/water interface and at the air/oil interface, the presence of 17β-estradiol showed no statistically significant effect on the surface tension. The presence of progesterone or testosterone showed only a weak effect on the surface tension at air/water interface and no effect at the air/oil interface. These results indicate that the model drugs are not significantly surface active at the water/air and oil/air interfaces. However, there was a dramatic change in the oil/water interfacial tension upon the addition of the drugs. In the absence of model drugs, the tension of the dodecane/water interface was 51.2 mN/m, a value close to that reported previously (Zeppieri et al., 2001; Gillap et al., 1968). In the presence of saturated solutions of progesterone (P), testosterone (T) or 17β-estradiol (E) the oil/water interfacial tensions were reduced to 28.9, 33.5, and 44.6 mN/m, respectively. Clearly, the progesterone showed the greatest influence on the interfacial tension by almost a factor of 2 compared to that in the absence of the drug. Thus it seems that these steroids do possess an ability to accumulate at the oil/water interface. Shown in the last column of Table 4.1 are the effects of hydrocarbon chain length on the hydrocarbon/water interface properties. A similar trend was observed in octane/water interface system compared to dodecane/water interface. All model steroids show a strong surface activity at the octane/water interface.

During the measurement of dodecane/water interfacial tension in the presence of the steroids, the direct partitioning was employed. The reason for this approach was that both testosterone and 17β-estradiol form different crystalline forms in aqueous and dodecane environments (see Chapter 3, Section 3.3.1). The direct partitioning method could

guarantee the same activity of the drugs in contacted phases. Despite the surface activity expressed by the steroids, no evidence of emulsification was observed.

4.3.2. Interfacial Studies in the Presence of Surfactants

4.3.2.1 Sodium Dodecyl Sulfate (SDS)

In Table 4.2, the interfacial tensions of the dodecane-water system in the presence of both SDS and steroids are listed. Addition of 0.1 mg/mL SDS to the control system (no drug) resulted in an interfacial tension of 40.1 mN/m. On the other hand, addition of 0.1 mg/mL SDS to the steroid-oil-water systems reduced the interfacial tensions to 24.2 (P), 30.4 (T) and 36.6 mN/m (E), respectively. The ability of the drugs to lower the interfacial tension, even in the presence of SDS, suggests that all three model drugs have some ability to compete with the surfactant for this interface. At the 1.0 mg/mL concentration of SDS, the interfacial tensions of the progesterone (12.9 mN/m) and testosterone (16.3 mN/m) systems were less than those of the SDS-oil-water system (19.4 mN/m) by about 6.5 and 3.1 mN/m, respectively. The 17β-estradiol exhibited no ability to make a statistically significant change in dodecane/water interfacial tension in the presence of 1mg/mL SDS. When the concentration of SDS was increased to 10 mg/mL, a value higher than the CMC of SDS (2.2mg/mL), the oil/water interfacial tension in the presence of 17β-estradiol was no different from control, indicating that the ability of the drug to effect interfacial tension was overwhelmed by higher surfactant concentration. On the other hand, saturated progesterone and testosterone were still able to compete with SDS for oil/water interface and further lower the interfacial tension from 7.86 (control, no drug) to 6.29 (P) and 7.68 mN/m (T). The surface tension of the air/water interface was only slightly decreased by progesterone or testosterone and unchanged by the presence of 17β-estradiol (shown in Table 4.1). The lack of effect at the air/water interface suggests

Table 4.1, Interfacial tensions in the absence and presence of model drugs

	Interfacial tension (mN/m)*			
	Water/air	Dodecane/air	Dodecane/water	Octane/water
No drug	71.2±0.6	24.2±0.5	51.2±1.0	47.5
Progesterone	65.2±1.8	23.8±1.1	28.9±0.8	23.7
Testosterone	66.8±0.7	23.6±0.9	33.5±0.5	27.8
17β-estradiol	69.9±1.3	24.8±0.2	44.6±0.4	42.7

*n=3, except for octane/water interface n=1.

Table 4.2, Dodecane/water interfacial tensions in the absence and presence of saturated model steroids (progesterone, testosterone, 17β-estradiol) and sodium dodecyl sulfate (SDS) solutions. Three concentrations of SDS were used: 0.1, 1.0 and 10.0mg/mL.

Dodecane/water interfacial tension (mN/m)*	No surfactant	0.1mg/mL SDS	1.0mg/mL SDS	10mg/mL SDS
No drug	51.2±0.7	40.1±1.3	19.4±0.6	7.86±0.03
Progesterone	28.9±0.8	24.2±0.2	12.9±0.3	6.29±0.03
Testosterone	33.5±0.5	30.4±0.1	16.3±0.1	7.68±0.13
17β-estradiol	44.6±0.4	36.6±2.0	18.8±0.6	7.84±0.19

*n=3.

that the surface tension decrease observed at the oil/water interface is not due to highly surface-active impurities in the systems.

4.3.2.2. Dodecyltrimethylammonium Bromide (DTAB)

In Table 4.3, the interfacial tensions of the dodecane-water system in the presence of both DTAB and steroids are listed. Addition of 0.1 mg/mL DTAB to the control system (no drug) resulted in an interfacial tension of 41.1 mN/m. On the other hand, addition of 0.1 mg/mL DTAB to the steroid-oil-water system reduced the interfacial tensions to 21.1 (P), 22.7 (T) and 32.2 mN/m (E), respectively. The ability of the drugs to lower the interfacial tension, even in the presence of DTAB, suggests that all three model drugs have some ability to compete with the surfactant for this interface. At the 1.0 mg/mL concentration of DTAB, the interfacial tensions of the progesterone (15.1 mN/m), testosterone (19.0 mN/m) and 17β-estradiol systems (20.9 mN/m) were less than those of the DTAB-oil-water system (25.8 mN/m) by about 10.7, 6.8 and 4.9 mN/m, respectively. When the concentration of DTAB was increased to 10 mg/mL, a value higher than the CMC of DTAB (4.9mg/mL), the ability of model drugs to compete for the interface was further weakened: the interfacial tensions of the steroid-DTAB-oil-water system dropped to 6.59 (P), 7.35 (T) and 7.43 mN/m (E) from 8.11 mN/m for control DTAB-oil-water system.

4.3.2.3. Dodecyl β-D-Maltoside (DM)

In Table 4.4, the interfacial tensions of the dodecane-water system in the presence of both DM and steroids are listed. Addition of 0.003mg/mL DM to the control system (no drug) resulted in an interfacial tension of 31.2 mN/m. On the other hand, addition of 0.003mg/mL DM to the steroid-oil-water system reduced the interfacial tensions to 24.2 (P), 26.9 (T), and 30.0 mN/m (E), respectively. The ability of the drugs to lower the interfacial tension, even in the presence of DM, suggests that all three model drugs have

Table 4.3, Dodecane/water interfacial tensions in the absence and presence of saturated model steroids (progesterone, testosterone, 17β-estradiol) and dodecyl trimethylammonium bromide (DTAB) solutions. Three concentrations of DTAB were used: 0.1, 1.0 and 10.0mg/mL.

Dodecane/water interfacial tension (mN/m)*	No surfactant	0.1mg/mL DTAB	1.0mg/mL DTAB	10mg/mL DTAB
No drug	51.2±0.7	41.1±1.7	25.8±0.5	8.11±0.02
Progesterone	28.9±0.8	21.1±0.5	15.1±0.4	6.59±0.17
Testosterone	33.5±0.5	22.7±0.2	19.0±0.9	7.35±0.07
17β-estradiol	44.6±0.4	32.2±1.7	20.9±0.9	7.43±0.03

*n=3

Table 4.4, Dodecane/water interfacial tensions in the absence and presence of saturated model steroids (progesterone, testosterone, 17β-estradiol) and dodecyl β-D-maltoside (DM) solutions. Three concentrations of DM were used: 0.003, 0.03 and 0.3mg/mL.

Dodecane/water interfacial tension (mN/m)*	No surfactant	0.003mg/mL DM	0.03mg/mL DM	0.3mg/mL DM
No drug	51.2±0.7	31.2±0.4	12.7±0.2	4.92±0.06
Progesterone	28.9±0.8	24.2±0.6	11.3±0.3	4.22±0.16
Testosterone	33.5±0.5	26.9±1.0	11.8±0.4	4.59±0.11
17β-estradiol	44.6±0.4	30.0±0.4	12.7±0.2	4.89±0.06

*n=3

some ability to compete with the surfactant for this interface. At the 0.03mg/mL concentration of DM, the interfacial tensions of the progesterone (11.3 mN/m) and testosterone (11.8 mN/m) systems were less than those of the SDS-oil-water system (12.7 mN/m) by about 1.4 and 0.9 mN/m. The 17β-estradiol system exhibited no statistically significant change in dodecane/water interfacial tension in the presence of either 0.03mg/mL or 0.3 mg/mL DM, indicating that the ability of the drugs to compete for the interface was overwhelmed by higher surfactant concentration. On the other hand, saturated progesterone and testosterone were still able to compete with DM for oil/water interface and further lower the interfacial tension from 4.92 (control, no drug) to 4.22 (P) and 4.59 mN/m (T).

4.3.3. Thermodynamic Model of Dodecane/water Interfacial Tension in the Presence of Drug and Surfactant

The above experimental results clearly show competition between surfactants and model drugs in a concentration-dependent manner at the oil/water interface. As of yet, the molecular basis for this proposed competition is not known. In this section, we will subject interfacial tension data to a thermodynamic analysis to probe the energetics of the putative competition. We will focus attention on the free energy of transfer to the interface of the surfactants and of the model solutes and will attempt to predict interfacial tension of mixtures based on the ΔG_{trans} of the component members.

4.3.3.1. Introduction-Models for Surface Adsorption

There are two main theoretical approaches to build the equilibrium relationship between adsorption and surface tension (Lucassen-Reynders, 1981). The two-dimensional gas model was first introduced by Langmuir (Langmuir, 1917) while a two-dimensional solution model was proposed by Butler (Butler, 1932). Both of the models employ a monolayer assumption for treatment of the interface. The 2-D gas model considers only

the surfactant at the interface, while the 2-D solution model explicitly includes the surfactants and the solvents at the interface. The 2-D gas approach works best for insoluble surfactants while the 2-D solution approach has advantages for soluble surface-active compounds (Lucassen-Reynders, 1981). In our studied systems, clearly the 2-D solution approach would be more appropriate because the surfactants employed are quite soluble in the aqueous phase.

Shown in Appendix 1 is the derivation, proposed by Butler, for relating bulk concentration, interfacial tension and surface transfer free energy.

4.3.3.2. Application of Butler Model to Single Solute Systems

The goal of this section is to employ interfacial tension data to calculate both the free energy of transfer to interface from the bulk and the partial molar interfacial area occupied by solute (surfactant or drug).

To determine the transfer free energies to interface for ionic surfactants (SDS and DTAB), the experimental dodecane-water interfacial tensions at three surfactant concentrations in Tables 4.2 and 4.3 were fitted to Eq. (A1.7). Several parameters required by the model could be obtained from the literature. The value employed for the occupied interfacial area of water was 7.62Å²/molecule taken from Gumkowski (Gumkowski, 1986) which was based on average hard sphere diameter of water ranging from 2.50~2.93 Å (Pierotti, 1965). The area occupied per molecule by SDS and DTAB, two extensively studied surfactant systems, at oil/water interface were determined by fitting the experimental π-A curves (Haydon and Taylor, 1960) using the π-A relationship, Eq. (A1.13), derived from 2-D solution model.

$$\pi = \frac{RT}{a_{water}} \ln\left(1 + \frac{2a_{water}}{A - a_{surfact}}\right) \qquad \text{(A1.13)}$$

where π is the surface pressure; A is the interfacial area per surfactant; a_{water} is surface area occupied by water. Figures 4.7 and 4.8 show the experimental π-A curves for three sodium alkyl sulfates and three alkyl trimethylammonium bromides in decane/water or petroleum ether/water interfacial systems from literatures (Haydon and Taylor, 1960). The SDS and DTAB data were collected employing petroleum ether whereas other systems, sodium octylsulfate (SOS), sodium decylsulfate (SDeS), octyltrimethylammonium bromide (OTAB) and decyltrimethylammonium bromide (DeTAB), were collected employing decane. Surprisingly the π-A curves for three alkyl sulfate surfactants in two different oil/water interfaces were essentially indistinguishable indicating that the occupied areas of the surfactants were not sensitive to the chain length of the hydrophobic tail and the type of oil phase. For this reason, we extrapolated the results to SDS in dodecane/water interface. In Figure 4.7, the fitted π-A curve using Eq. (A1.13) is also shown. Clearly the fitting was very good and the fitted occupied area by each SDS molecule was 32.0±0.6 Å². Similarly, in Figure 4.8, the π-A curves for three alkyl trimethylammonium bromide surfactants in two different oil/water interfaces were overlapped with each other. The fitted π-A curve applying Eq. (A1.13) is in good agreements with experiments. The estimated occupied area by DTAB at oil/water interface was 37.1±0.6 Å²/molecule.

The activity coefficient $f^{l}_{surfact}$ for ionized surfactants (SDS and DTAB) in Eq. (A1.7) could be calculated in terms of the ionic strength, *I*, using Debye-Huckel equation:

$$-\log f^{l}_{surfact} = \frac{0.509\sqrt{I}}{\sqrt{I}+1} \qquad (4.3)$$

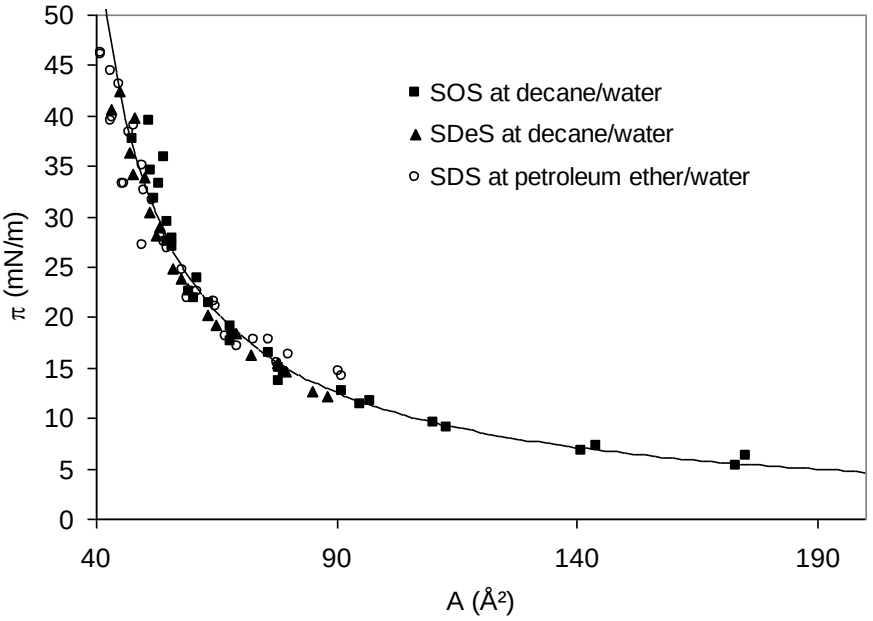

Figure 4.7, The experimental oil/water interfacial pressure in the presence of sodium alkyl sulfate surfactants as a function of area per surfactant molecule by Haydon and Taylor (Haydon and Taylor, 1960). The solid curve is fitted according to Eq. (A1.13).

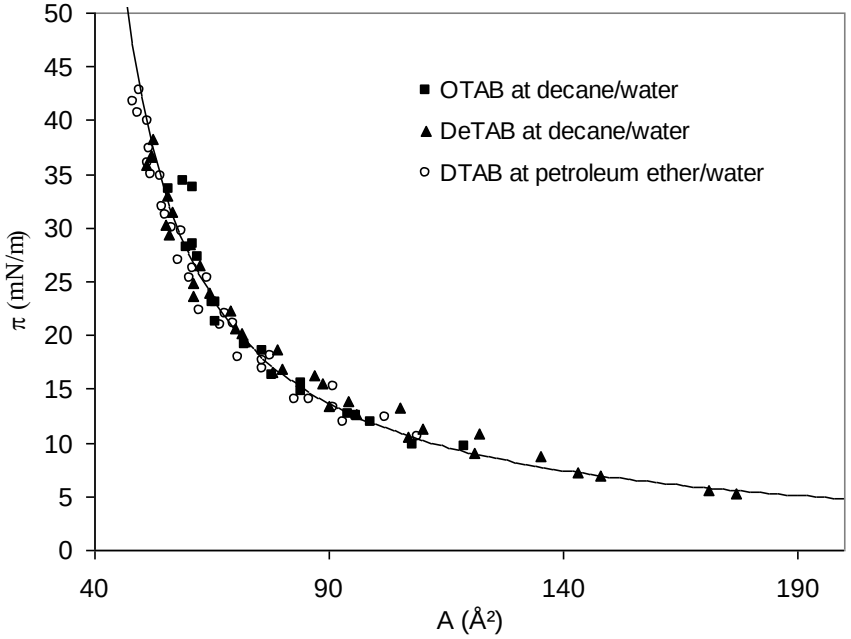

.

Figure 4.8, The experimental oil/water interfacial pressure in the presence of alkyl trimethylammonium bromide surfactants as a function of area per surfactant molecule by Haydon and Taylor (Haydon and Taylor, 1960). The solid curve is fitted according to Eq. (A1.13).

At concentrations greater than CMC, the CMC was employed in the simulations because the concentration of surfactant monomers was critical in determining the surface properties. In addition, it is know that inclusion of hydrophobic solutes, such as dodecane, can significantly lower the CMC. To account for this effect, the CMCs of SDS and DTAB micelles in the presence of saturated dodecane (6.9mM for SDS, Bonfillon et al., 1994 and 12.5mM for DTAB, Medrzycka and Zwierzykowski, 2000) were employed in the calculations.

The fitted ΔG_{trans} values using Eq. (A1.7) and the parameters mentioned above were -23.5±0.8 for SDS and -22.8±1.2 kJ/mol for DTAB. These surfactants have the same free energy of transfer to the oil/water interface.

For nonionic surfactant DM and neutral drugs, Eq. (A1.8) was employed to fit the experimental dodecane/water interfacial tension versus surfactant/drug concentration curves. The experimental and fitted $\gamma_{dodecane/water} \sim C$ (concentration of either drug or surfactant) curves for DM, progesterone and testosterone are shown in Figures 4.9~4.11. The fitted parameters are listed in Table 4.5. Apparently the fitted curves coincide with the experimental data very well. Statistical analysis was applied using Scientist® software to provide the 95% confidence intervals for the fitted two parameters that are also shown in Table 4.5. When applied to 17β-estradiol in dodecane/water interface system the fitting to the model was poor. The lack of fit is likely the result of poor reproducibility in measuring interfacial tensions especially when the drug concentrations were very low (<1μg/mL) (the results will be shown in Section 5.3.1, Figure 5.6). Therefore, in our simulation, the 17β-estradiol results were not considered.

Table 4.5, Critical parameters used in simulations. The parameters are the results of fitting interfacial tension data to the Butler model.

	a (Å^2)	ΔG_{trans}(kJ/mol)
SDS	32.0±0.6[a]	-23.45±0.84[b]
DTAB	37.1±0.6[a]	-22.83±1.22[b]
DM	41.41±2.75[c]	-42.07±0.58[c]
Progesterone	61.3±4.8[c]	-42.12±0.48[c]
Testosterone	59.6±5.1[c]	-36.17±0.37[c]

[a]Values from fitting Eq. (A1.13)
[b]Values from fitting Eq. (A1.7)
[c]Values from fitting Eq. (A1.8)

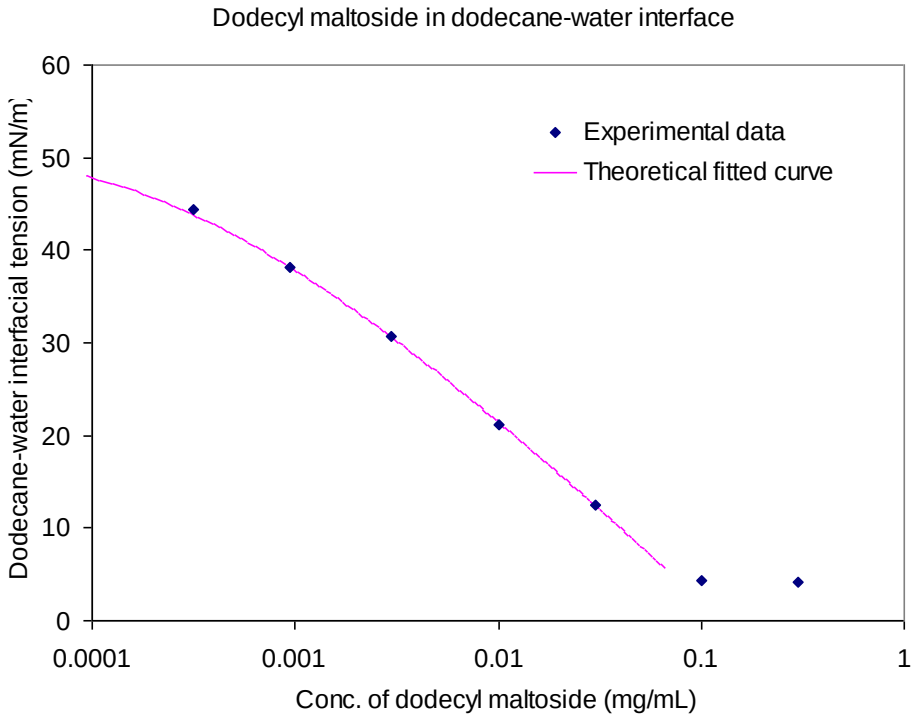

Figure 4.9, Dodecane/water interfacial tension as a function of dodecyl β-D-maltoside concentration in water. The solid line is the fitted theoretical curve.

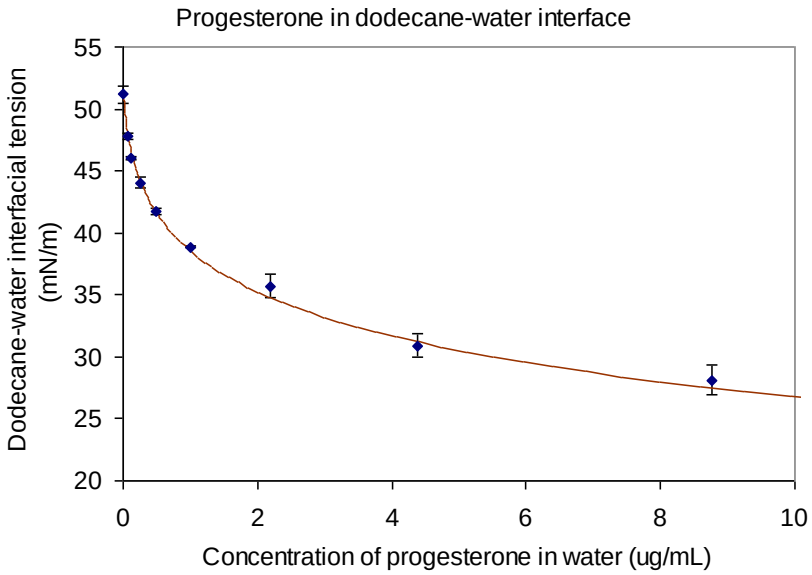

Figure 4.10, Dodecane/water interfacial tension as a function of progesterone concentration in water. The solid line is the fitted theoretical curve.

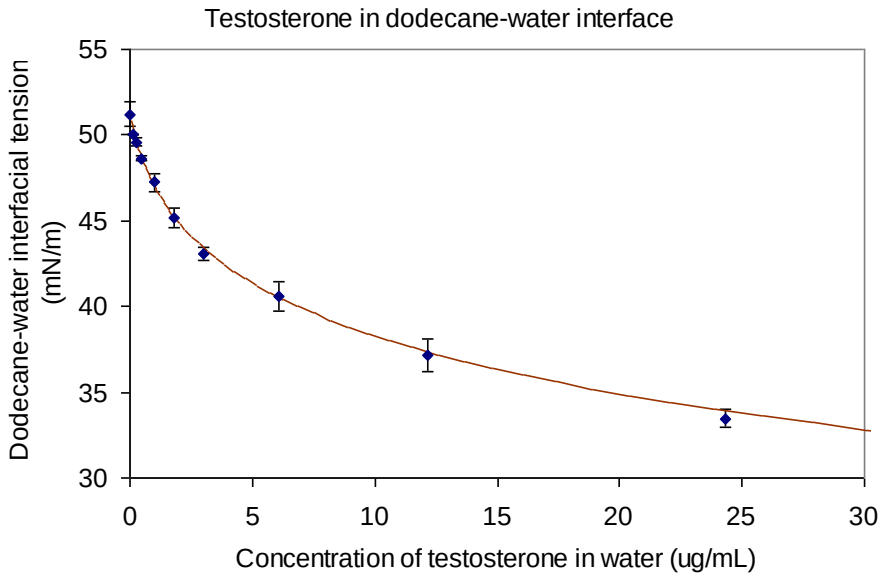

Figure 4.11, Dodecane/water interfacial tension as a function of testosterone concentration in water. The solid line is the fitted theoretical curve.

4.3.3.3. Application of Butler Model to Two Solute (Surfactant and Drug) Systems

The goal of the section is to predict surface tension by employing ΔG_{trans} and area occupied by each solute at the interface in the 2D solution model in the presence of drug and surfactant. These predicted values are then compared to experimental values (Tables 4.2~4.4).

For systems containing ionic surfactants SDS and DTAB and neutral molecules (steroids), Eq. (A1.9) was applied. For systems containing nonionic surfactant DM and steroids, Eq. (A1.10) was applied. Once the surface pressure, π, at any given drug and surfactant concentrations was solved, the surface tension could be simply calculated using $\gamma = \gamma_0 - \pi$. As mentioned in the previous section, the CMC of surfactant was employed in the simulations when the concentration of surfactant was higher than its CMC. The CMCs of SDS and DTAB in the presence of dodecane were taken from the literature (Bonfillon et al., 1994; Medrzycka and Zwierzykowski, 2000) with values shown in section 4.3.3.2. The CMC of DM in the presence of dodecane was determined by the point of intersection between the two segments of γ~C curve (Fig. 4.9) above and below CMC. The determined CMC using this method was 0.14mM. The computation was divided into two groups. In the first group only three components, water, dodecane and either surfactant or drug were considered. The experimental data were used in fitting the parameters, $\Delta G_{trans,drug/surfact}$ and $a_{drug/surfact}$, much like a training set. Eq. (A1.7) and (A1.8) were fitted with appropriate data to determine free energy of transfer and area occupied per molecule for the surfactant or the drug at the doecane/water interface.

The second group of calculations considered all four components, water, dodecane, surfactant and drug. Eq. (A1.9) and (A1.10) were employed to predict the surface tensions for mixtures of surfactant and drug. The comparisons between calculated and

experimental surface tensions are shown in Figure 4.10 for part I and in Figure 4.11 for part II.

It is not surprising that the prediction of surface tension in the first is very close to experimental results (see Figure 4.12). For the second group of calculations, where the surfactant and drug are both present, the overall predictions are overall good but with a few points that exhibited somewhat greater deviations (see Figure 4.13). To better illustrate the results, the quantitative data and their corresponding conditions are listed in Table 4.6. From the table, the calculated values for SDS and DM systems are quite close to measured surface tensions. Significant deviations of the model from experimental results are observed for DTAB at low concentration. The greatest differences between experiments and predictions are 10.2 mN/m for saturated testosterone in 0.1mg/mL DTAB. The other three data points that had large deviations are progesterone in 0.1mg/mL DTAB (5.7 mN/m), progesterone (6.1 mN/m) and testosterone (5.1 mN/m) in 1.0mg/mL DTAB. One possible reason for the deviations is the assumption used in the surface adsorption model, that there is no specific interactions between the drug and surfactant and the two solutes are ideally competing with each other for the oil/water interface. In following chapters it will be shown that the assumption of no interaction between drug and surfactant may not hold.

4.4. DISCUSSION

The experiments clearly showed, in all three surfactant systems differing in electronic charge, model steroids can successfully compete for the oil/water interface.

In our studies, the ability of model drugs from saturated solution to compete with surfactants has the rank order: progesterone > testosterone > 17β-estradiol. Therefore the progesterone has the greatest surface activity and 17β-estradiol has the least surface

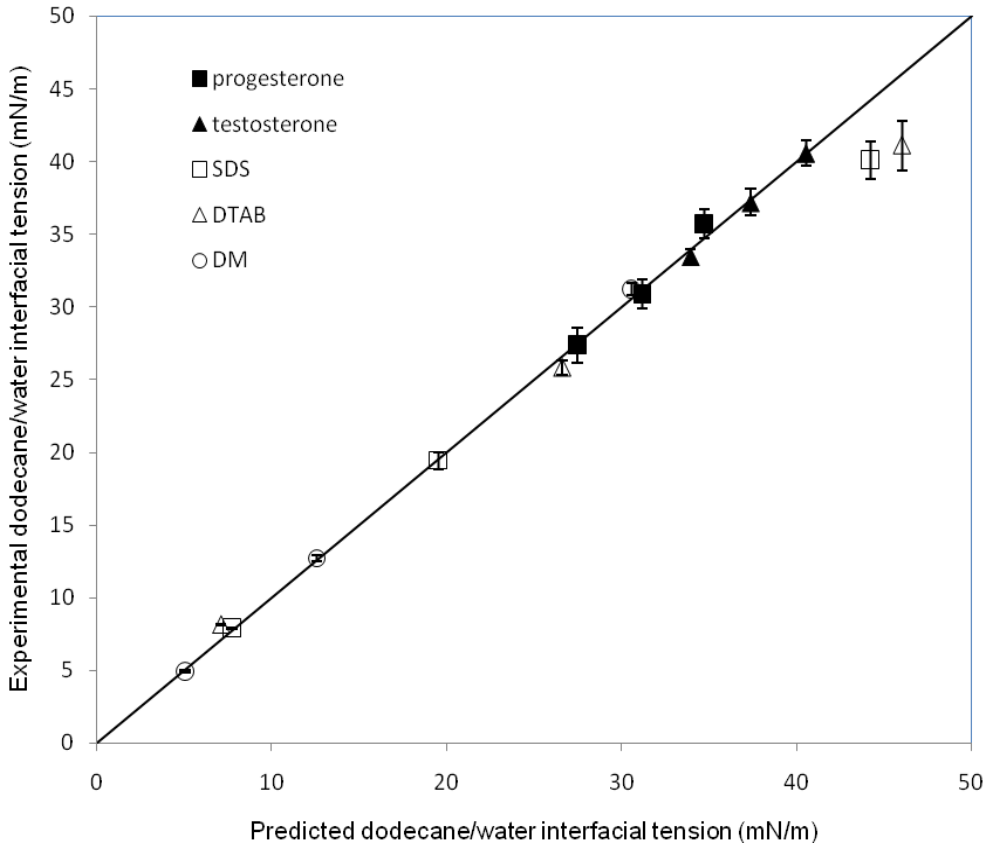

Figure 4.12, Comparison between experimental and theoretical fitted dodecane/water interfacial tensions in the presence of pure surfactants (SDS, DTAB or DM) or pure steroids (progesterone or testosterone).

Table 4.6, Comparison between experimental and predicted dodecane/water interfacial tensions in the presence of both surfactants and drugs. The predicted values were obtained using the Eq. (A1.9) and (A1.10). Experimental data are from Table 4.2 to 4.4.

Interfacial tension (mN/m)	Progesterone		Testosterone	
	Experimental	Predicted	Experimental	Predicted
0.1mg/mL SDS-dodecane	24.2±0.2	26.5	30.4±0.1	32.4
1.0mg/mL SDS-dodecane	12.9±0.3	16.8	16.3±0.1	18.5
10mg/mL SDS-dodecane	6.29±0.03	7.13	7.68±0.13	7.51
0.1mg/mL DTAB-dodecane	21.1±0.5	26.8	22.7±0.2	32.9
1.0mg/mL DTAB-dodecane	15.1±0.4	21.2	19.0±0.9	24.1
10.0mg/mL DTAB-dodecane	6.59±0.17	6.61	7.35±0.07	6.93
0.003mg/mL DM-dodecane	24.2±0.6	24.3	26.9±1.0	27.8
0.03mg/mL DM-dodecane	11.3±0.3	11.9	11.8±0.4	12.3
0.3mg/mL DM-dodecane	4.22±0.16	4.75	4.59±0.11	4.87

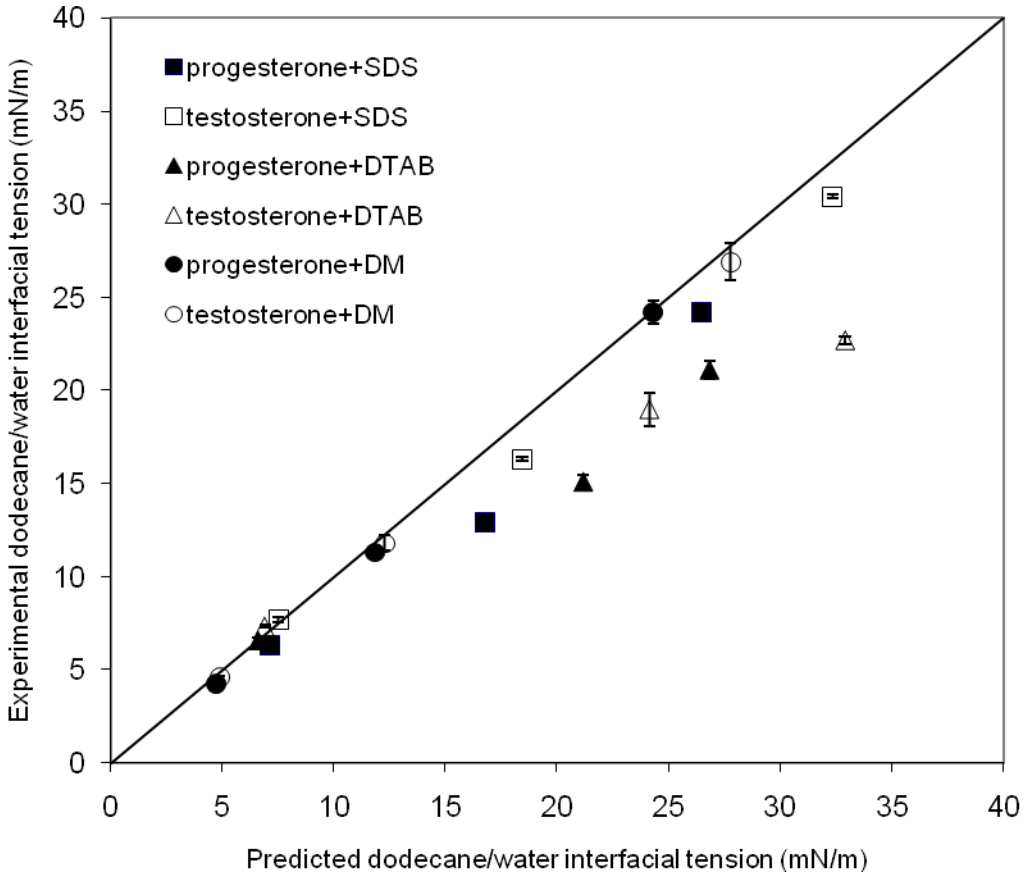

Figure 4.13, Comparison between experimental and predicted dodecane/water interfacial tensions in the presence of both surfactants (SDS, DTAB or DM) and model steroids (progesterone or testosterone).

activity at oil/water interface. This rank order correlates well with the solubilization capacity of the model drugs in all three micelle systems. In those micelle systems, progesterone always has the greatest solubilization power and 17β-estradiol has the least solubilization capacity. The correlation is consistent with the conclusion of Chapter 3 that the micellar solubilization is mainly localized to the micelle surface.

When the three different surfactants are compared, the surface tensions at dodecane/water interface at concentrations near their CMCs are 7.86 (SDS), 8.11 (DTAB) and 4.92 (DM) mN/m. Therefore the surface activities of surfactants at their CMC have the following ranking order: DM > SDS $\cong$ DTAB. This order has an inverse correlation with the solublization capacity of the micelle. DM micelle system always has the lowest solubilization power in the three micelle systems. For progesterone and testosterone, the solubilization power has the order SDS > DTAB > DM. For 17β-estradiol, the ranking order of solubilization capacity becomes DTAB > SDS > DM. The correlation also supports the hypothesis that these drugs are mainly solubilized in the hydrocarbon/water interface of the micelle.

The above correlations between solubilization in micelles and surface activity are only qualitative. There is significant difference between flat oil/water interface we studied in this chapter and highly curved micelle surface. The high surface curvature could change the surface packing density of both surfactants and drugs. The Laplace pressure, which likely offers molecule a greater energy barrier for entry onto the micelle surface as compared to a flat interface, may be the physical basis of the effect of curvature. In the next chapter we will consider the curvature effect and apply the surfactant-drug co-adsorption model to predict the micelle/water partitioning properties.

It is likely that results obtained on flat oil/water interface will more closely correlate to real lipid assembly systems when the particle size of oil or water droplets is large. If so, the present work could be applicable to other lipid-based drug delivery system, such as emulsions and liposomes. The modification of oil/water interface properties can influence the emulsification efficiency or particle size of oil droplets in emulsions. In turn, it will affect the performance of lipid-based drug delivery systems (Malcolmson and Lawrence, 1993; Craig et al., 1993). The studies on the behavior of drugs and surfactants on flat surface are important to provide intrinsic interface properties of drugs and surfactants and their interactions as a means of understanding lipid-based drug delivery systems. The larger the surface/volume ratio, the greater influences the drug-surfactant competition will make on solubilization.

Besides the experimental studies of competition of drug-surfactant for the model oil/water interface, a thermodynamic model (2-D solution model) was applied to simulate the interface adsorption phenomena. The parameters used were obtained by fitting to dodecane/water interface properties in the presence of only one type of molecules, either the surfactants or the model drugs. When the surfactants and drugs were mixed together, the interfacial tension was calculated under an assumption that there is no specific interaction between drug and surfactant molecules. In another word, the drug and surfactant are ideally competing with each other at the oil/water interface without any synergistic or antagonistic effect. Overall the predictions were good with a few exceptions when the steroids were mixed with low concentration of DTAB. This suggested the simulation method and the assumption used are valid in most cases. For DTAB-drug mixtures, the measured surface tensions were lower than predicted values which indicated the steroids may have attractive interactions with DTAB molecules that make synergistic effect in lowering the surface tensions.

From the negative sign of the transfer free energies of surfactants and model steroids, the oil/water interface is always more energetically favorable than the bulk aqueous phase. The transfer free energy from water to interface and the partitioning coefficient between interface and water have the following relationship under dilute solution condition.

$$K_{interface/water} = \exp\left(-\Delta G_{water \rightarrow interface} / RT\right) \quad (4.4)$$

The lower the ΔG value the more surface active the molecule (with constant low concentration). From Table 4.5, progesterone and dodecyl β-D-maltoside have the largest surface activity, testosterone is the next, while SDS and DTAB have the lowest surface activity. The results are quite surprising because they show some hydrophobic molecules are very surface active at oil/water interface and are even more surface active than conventional surfactants. The total surface activity of the model drugs is probably limited by low aqueous solubility while the surfactants have much higher solubility and monomer concentrations.

The study of 17β-estradiol at dodecane/water interface was plagued by large variations in the surface tension results. The problem may be due to the slow adsorption to the oil/water interface when the drug concentrations in both oil and aqueous phases are quite low (<1μg/mL). This slow adsorption kinetics may interfere with the effect of even small amount of impurities that could gradually lower the interfacial tension over long period of time up to hours (Mysels, 1986).

The success of employing a thermodynamic model in simulating the competing adsorption at oil/water interface will encourage us to apply the model to micelle surface where the curvature effect is considered using Laplace pressure concept.

4.5. CONCLUSION

Hydrocarbon/water interfacial tension can be significantly decreased in the presence of hydrophobic drugs, while the model steroids exhibit little or no surface activity in hydrocarbon/air or water/air interface. The hydrophobic drugs can compete with surfactant molecules for the oil/water interface. The ability of saturated drugs to compete for oil/water interface depends on the concentrations of the surfactant. The competition phenomena can be quantitatively simulated using a thermodynamic model.

Chapter 5

Surface-localized Thermodynamic Model Used to Predict the Micelle/water Partitioning Coefficient

5.1. INTRODUCTION

The capacity of micelle systems to solubilize poorly water-soluble drugs is one of the most important parameters when considering these lipid assemblies as drug delivery vehicles. The ability to quantitatively predict the micelle/water partitioning coefficients based on physicochemical properties of drug and surfactant would guide formulators to choose effective solubilizer and speed up the formulation process.

Currently, the majority of the predictions of micelle/water partitioning coefficients are based on empirical linear free energy relationship (LFER). The most frequently used method is the linear relationship between logarithm of micelle/water partitioning constants and the $\log P_{octanol/water}$ values for a specific micelle system (Valsaraj and Thibodeaux, 1990; Treiner and Mannebach, 1987; Alvarez-Munez and Yalkowsky, 2000; Wiedmann and Kamel, 2002). While LFERs are successful in correlating solubility with molecular descriptors, the method is strongly dependent on the members of the "training set". Both Valsaraj et al. (Valsaraj and Thibodeaux, 1990) and Treiner et al. (Treiner and Mannebach, 1987) have published successful correlation for solubilization of solutes in SDS micelles based on training sets of molecules of simple structure. If the $K_{m/w}$ data in Table 3.2~3.4 for steroids, benzodiazepines and parabens are plotted on those very same graphs, (Fig. 5.1), the correlation is much less successful, most likely because the structures of the drugs are significantly different than those of solutes of the training sets.

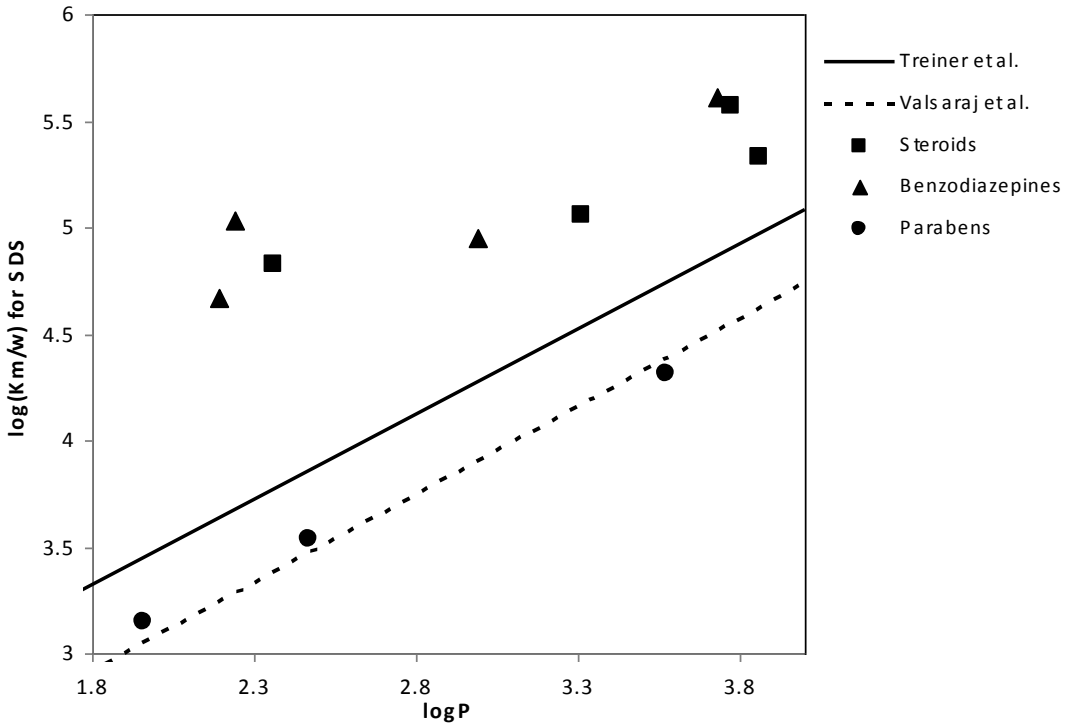

Figure 5.1. Correlation between logarithm of micelle/water partitioning coefficient for SDS, $K_{m/w}$, and $logP_{octanol/water}$. The solid line is from Treiner and Mannebach (Treiner and Mannebach, 1987) and the dotted line is from Valsaraj and Thibodeaux (Valsaraj and Thibodeaux, 1990). The plotted points are experimental data taken from the present work in Tables 3.2~3.4.

Mukerjee et al. (Mukerjee and Cardinal, 1978; Mukerjee, 1979) first applied a two-state thermodynamic model to simulate the micelle/water partitioning by considering both surface and core regions as solubilization loci. The results showed the micelle surface played an important role in solubilization and the agreement between predictions and theory are quite good in the model anionic micelle systems. The limitations of the work include the simple molecular structures of model compounds, such as alkanols, ketones, amides and aromatics, as well as surfactant selection (only anionic). In this Chapter, we will use a surface-localized thermodynamic model adapted from Mukerjee's two-state model to predict the micelle/water partitioning coefficients of three series of model drugs in three micelle systems with different charges. Then we will extend the model beyond the dilute condition to simulate the micellar solubilization at high drug concentration, a condition of critical importance in pharmaceutical formulation work.

5.2. MATERIALS AND METHODS

5.2.1. Materials

Progesterone (>99%), testosterone (>98%), 17 β-estradiol (>98%), diazepam, temazepam, oxazepam, prazepam, methylparaben (>99%), ethylparaben (>99%), butylparaben (>99%), sodium dodecyl sulfate (>99%), dodecyltrimethylammonium bromide (>99%), dodecyle β-D-maltoside (>98%) and dodecane (>99%) were obtained from Sigma-Aldrich (St. Louis, MO). 11α-hydroxyprogesterone (>95%) was from Janssen Chimica (New Brunswick, NJ).

5.2.2. Purification of Dodecane:

In order to remove surface active impurities dodecane was purified using a double-washing method. The dodecane was washed using methanol: about 40mL dodecane was mixed with 40mL methanol in separating funnel. The system was shaken for 1 minute and permitted to rest for 5 minutes. The liquid separated to form two layers.

The bottom layer containing methanol was removed. The top dodecane-rich layer was further washed 4 times with fresh methanol. The second washing step was carried out with deionized water. The washing was designed to remove impurities in dodecane that were soluble in methanol and the second step could remove methanol any water-soluble impurities.

The dodecane/water interfacial tension was measured for unpurified and purified solvent as a function of time. The results are shown in Figure 5.2. Generally, with unpurified dodecane, the oil/water interfacial tension tended to decrease markedly as a function of time (Mysels, 1986). For purified dodecane, the drop of dodecane/water interfacial tension over 40 hours was only about 0.5 mN/m.

5.2.3. Surface-localized Thermodynamic Model

A detailed derivation of the surface-localized thermodynamic model is included in Appendix 2.

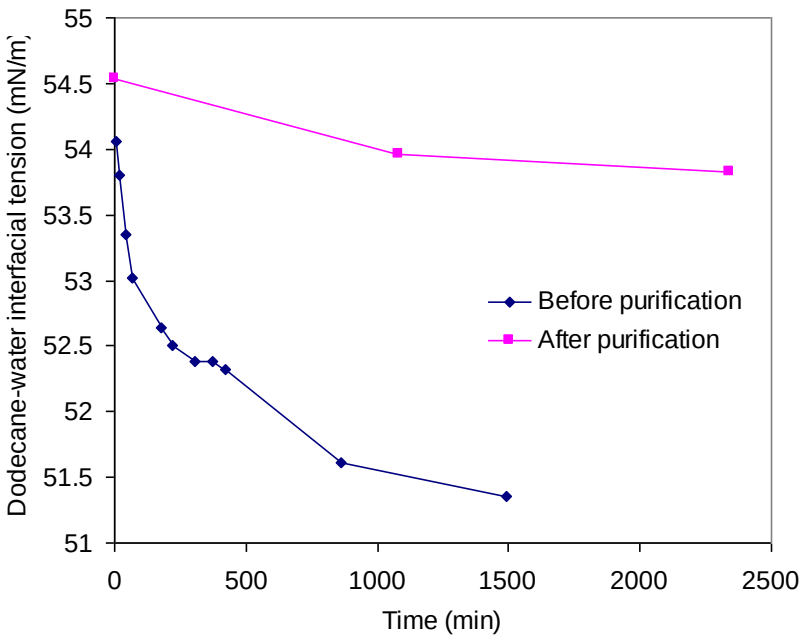

Figure 5.2, Dodecane/water interfacial tension as a function of time before and after purification of dodecane.

5.3. RESULTS AND DISCUSSION

5.3.1. Drug Solute-Specific Parameters of Solubilization in Micelles

The molar volumes of the model drugs are required in evaluating the effect of Laplace pressure, e.g. Eq.(A2.4). The volumes were estimated based on the occupied volumes of the molecules in crystalline phases from the crystal structures found in Cambridge Structure Database (Allen, 2002). The volume of each model drugs is listed in Table 5.1. Based on the model there are two other key parameters related to the drug substances solubilized in micelles: the first is the transfer free energy from aqueous solution to hydrocarbon/water interface, $\Delta G_{\text{water}\rightarrow\text{interface}}$; and the second is the area occupied by drug molecule at the oil/water interface, a_{drug}. To determine these key parameters independently the dodecane/water interfacial tensions were measured as a function of drug concentration. The ratio of drug concentrations between hydrocarbon and water phases were set to be equal to hydrocarbon/water partitioning coefficient determined in Chapter 3. From these data, a_{drug} and $\Delta G_{\text{water}\rightarrow\text{interface}}$ could be determined by fitting the results to Eq. (A1.8) using Scientist® software.

The measured dodecane/water interfacial tensions as a function of drug concentration in aqueous phase are shown in Figures 5.3 (for steroids), 5.4 (for benzodiazepines), 5.5 (for parabens) and 5.6 (17β-estradiol and oxazepam). In those figures, the fitted curves based on surface adsorption model, Eq. (A1.8), are also shown as solid lines. The results in Figure 5.7 demonstrate the relationship between the γ~C curve and the fitted parameters, $\Delta G_{\text{water}\rightarrow\text{interface}}$ and a_{drug}. The initial slope of interfacial tension as a function of drug concentration (Fig. 5.7a) is related to the transfer free energy term (Eq. (A2.6)):

$$slope = -\frac{RT}{a_{water}} \exp\left[-\frac{\Delta G_{\text{water}\rightarrow\text{interface}}}{RT}\right].$$

Table 5.1, Volumes of each molecules of model drugs based on reported crystal structures.

Drug	V(Å^3)
Progesterone	441.3
Testosterone	406.9
11α-hydroxyprogesterone	450.7
Diazepam	344.3
Temazepam	356.7
Prazepam	417.7
Methylparaben	182.7
Ethylparaben	213.8
Butylparaben	259.2
17β-estradiol	370.2
Oxazepam	330.5

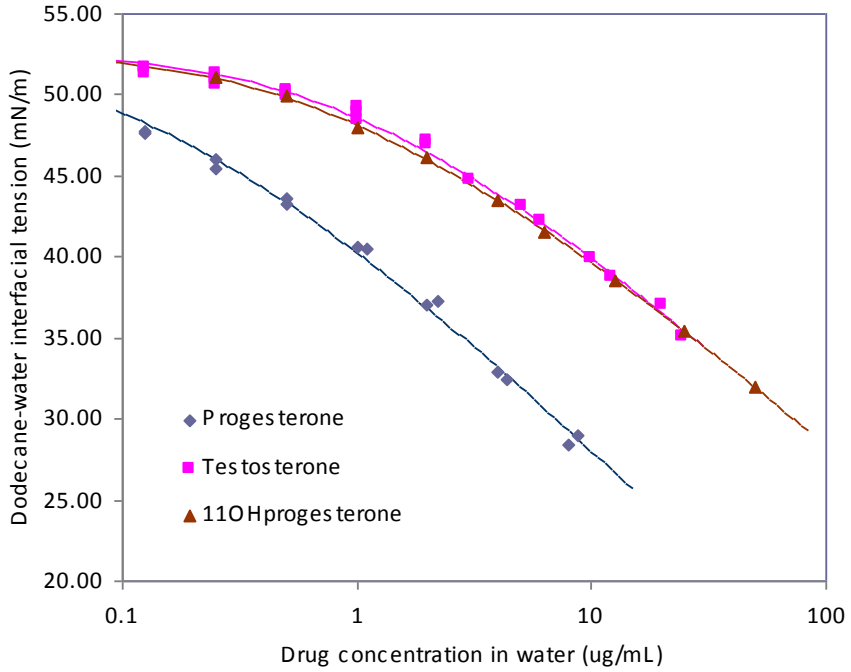

Figure 5.3, Dodecane/water interfacial tensions as a function of drug concentration in aqueous phase for 3 model steroids. The markers are experimental data and the solid lines are fitted curves based on surface adsorption model, Eq.(A1.8).

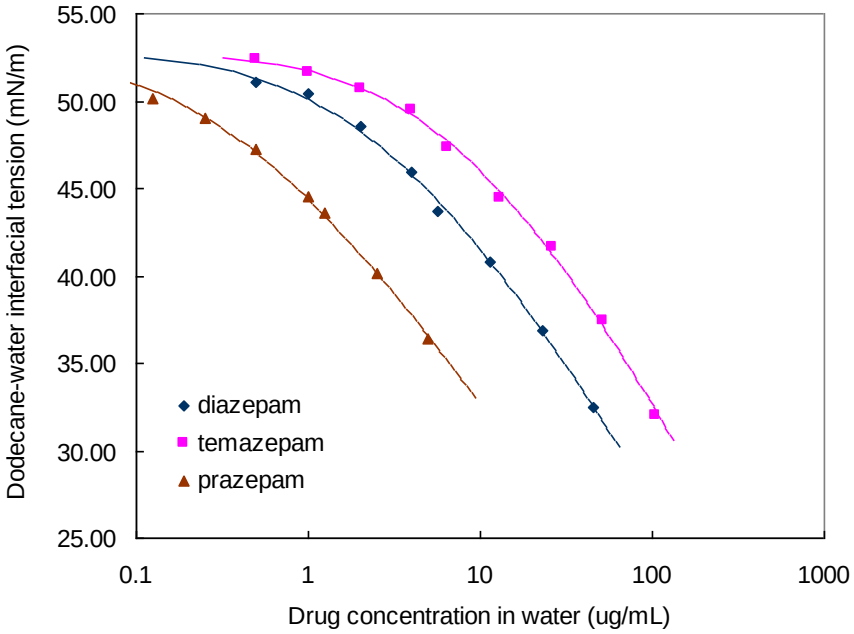

Figure 5.4, Dodecane/water interfacial tensions as a function of drug concentration in aqueous phase for 3 model benzodiazepines. The markers are experimental data and the solid lines are fitted curves based on surface adsorption model, Eq.(A1.8).

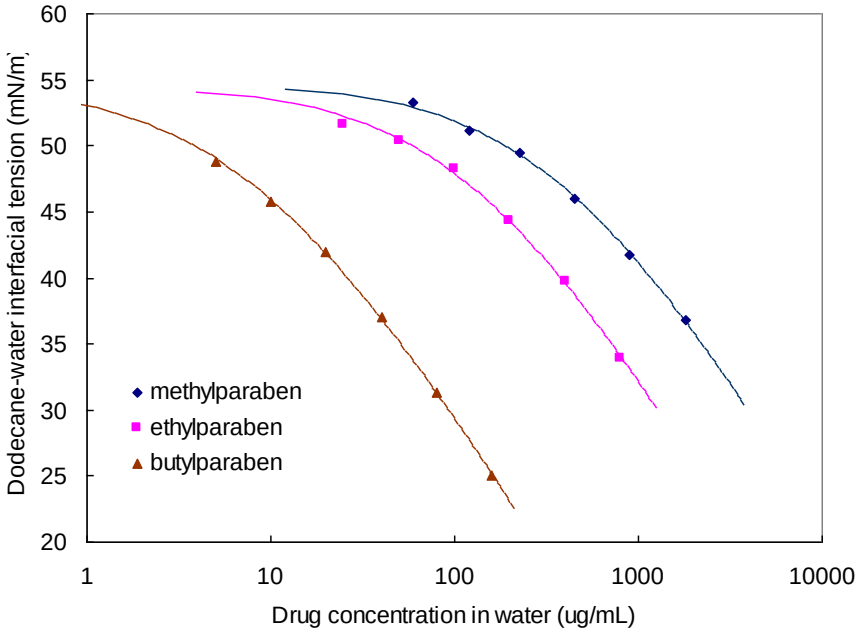

Figure 5.5, Dodecane/water interfacial tensions as a function of drug concentration in aqueous phase for 3 model parabens. The markers are experimental data and the solid lines are fitted curves based on surface adsorption model, Eq.(A1.8).

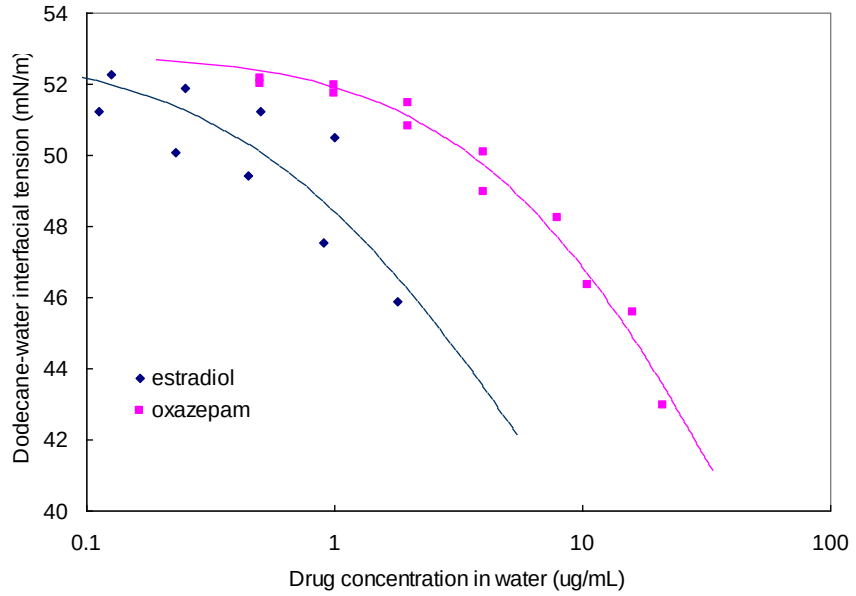

Figure 5.6, Dodecane/water interfacial tensions as a function of drug concentration in aqueous phase for 17β-estradiol and oxazepam. The markers are experimental data and the solid lines are fitted curves based on surface adsorption model, Eq.(A1.8).

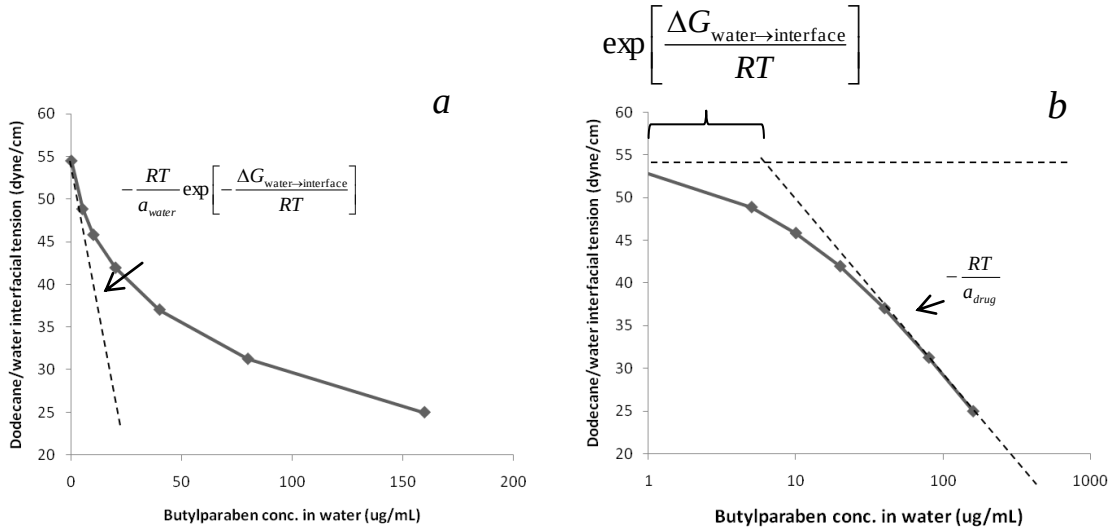

Figure 5.7, A schematic of relationship between the two key parameters of drug substances, $\Delta G_{\text{water}\to\text{interface}}$, a_{drug} and the oil/water interfacial tension versus drug concentration (a) or logarithm of drug concentration (b).

In the γ~logC plot (Fig. 5.7b), the linear limit is approached at high concentration. The slope of the line is related to the area occupied by the drug at the interface: $slope = -\frac{RT}{a_{drug}}$. The linear region will intersect the x-axis at a surface tension equal to γ_0. The intercept of the x-axis is equal to $\exp\left[\frac{\Delta G_{\text{water}\rightarrow\text{interface}}}{RT}\right]$. It should be kept in mind that the concentration of the drug must be mole fraction which is unitless. From the relationship, the transfer free energy value depends on the position of the γ~logC curve: a shift to the right of the curve corresponds to a larger transfer free energy.

The fitting results in Fig 5.3~5.6 are very satisfactory for all cases except for 17β-estradiol and oxazepam. For these latter two drugs the measured interfacial tensions exhibited poor reproducibility which we believe contributed to the unsatisfactory nature of the fit. The fitted parameters are shown in Table 5.2. Scientist® software package was employed to carry out the statistical analysis and provide the 95% confidence intervals for those parameters. Not surprisingly, in all cases, the transfer free energies were negative. From the results in the table, progesterone has the largest negative transfer free energy from water to dodecane/water interface which indicates that the drug is energetically favored to reside at the interface. To further illustrate the comparison, the γ~C curves for 9 drugs are shown in Figure 5.8. In the figure, the curves have the rank order, from left to right, progesterone, prazepam, 11α-hydroxyprogesterone, testosterone, diazepam, temazepam ≈ butylparaben, ethylparaben and methylparaben. This rank order is the same as that of transfer free energies from low to high, as indicated in Fig. 5.7. Based on physical picture, the higher the surface activity, the lower transfer free energy and the smaller the concentration necessary to lower the dodecane/water interfacial tensions by the same amount.

Table 5.2, Fitted transfer free energy $\Delta G_{water \rightarrow interface}$ and occupied area at oil/water interface for all model drugs. Listed are average values +/- 95% confidence intervals.

Drug	$\Delta G_{water \rightarrow interface}$(kJ/mol)	a(Å²)
Progesterone	-41.78±0.45	58.0±4.4
Testosterone	-36.18±0.34	59.8±4.9
11α-hydroxyprogesterone	-37.05±0.17	64.8±1.9
Diazepam	-34.41±0.32	46.2±3.7
Temazepam	-31.94±0.33	41.3±3.7
Prazepam	-39.38±0.40	54.0±5.7
Methylparaben	-21.27±0.33	31.9±4.0
Ethylparaben	-24.21±0.43	31.8±4.6
Butylparaben	-31.41±0.16	34.1±1.2
17β-estradiol	-36.31±2.91	57.4±105.3
Oxazepam	-31.34±0.74	42.1±17.5

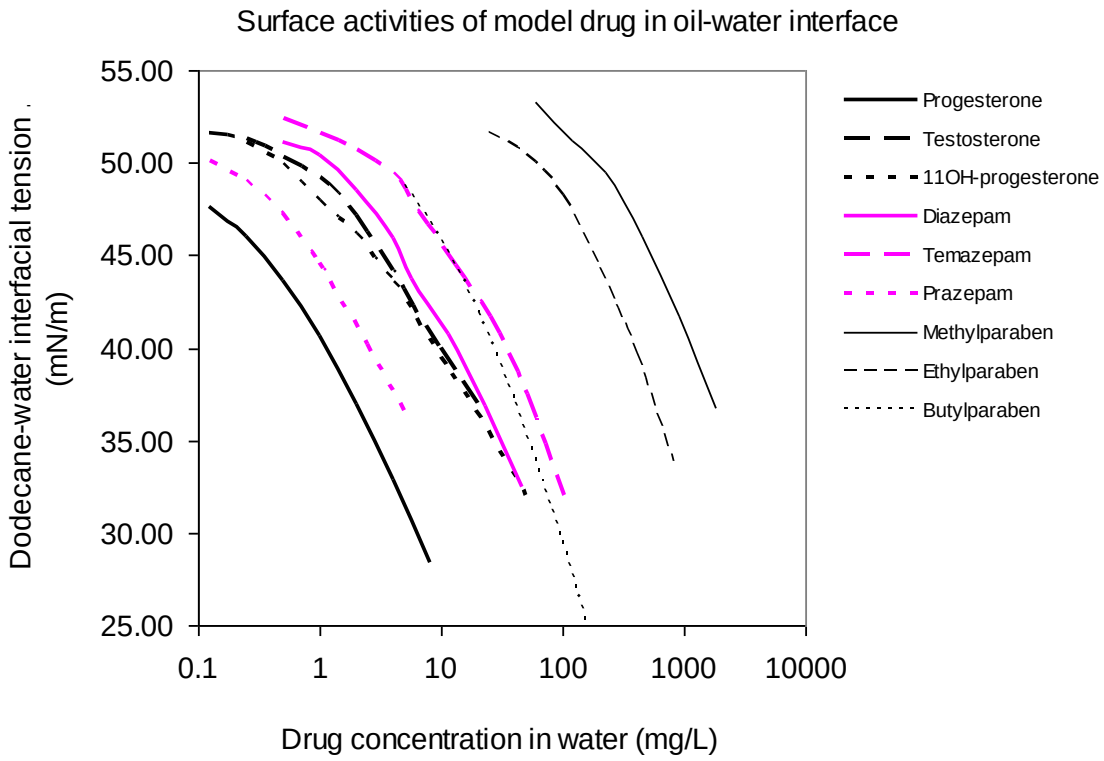

Figure 5.8, Summary of dodecane/water interfacial tensions as a function of drug concentration in aqueous phase for 9 model drugs. All curves are experimental data in the absence of fitted theoretical lines.

If we compare the surface activities of the members of the same series of the model drugs (structures are shown in Chapter 3), the effect of some functional groups could be hypothesized. The addition of hydroxyl group to a molecule can significantly decrease its oil/water interfacial activities: For example, the transfer free energy of 11α-hydroxyprogesterone is less negative than that of progesterone and the interfacial activity of temazepam is much lower than that of diazepam. When testosterone is compared to progesterone the hydroxyl group appears to lower the interfacial activity to a greater extent than the acetyl group. The addition of hydrocarbon moiety to the molecule appears to increase the interfacial activity: For example, by adding a cyclopropyl group to diazepam, prazepam exhibits greater interfacial activity. Similarly, by lengthening the alkyl group, the surface activity of parabens exhibits the rank order methylparaben < ethylparaben < butylparaben.

The negative sign of the transfer free energies listed in Table 5.2 suggests the dodecane/water interface is more energetically favorable than bulk aqueous phase for all the model drugs. The transfer free energy from hydrocarbon to oil/water interface can also be estimated from the following equation:

$$\Delta G_{\text{hydrocarbon}\rightarrow\text{interface}} = \Delta G_{water\rightarrow\text{interface}} + RT \ln K_{h/w} \qquad (5.1)$$

The values of $\Delta G_{\text{hydrocarbon}\rightarrow\text{interface}}$ are shown in Table 5.3. When the structure ~ $\Delta G_{\text{hydrocarbon}\rightarrow\text{interface}}$ relationships are examined, it appears that the hydroxyl group has significant influence on decreasing the transfer free energy from oil to interface. On the other hand, the addition of hydrocarbon group surprisingly makes very small changes to the oil to interface transfer free energy. For example, $\Delta G_{\text{hydrocarbon}\rightarrow\text{interface}}$ of 11α-hydroxyprogesterone and temazepam are significantly lower than those of progesterone and diazepam, respectively. The $\Delta G_{\text{hydrocarbon}\rightarrow\text{interface}}$ values are relatively

Table 5.3, Estimated transfer free energy from hydrocarbon to oil/water interface, $\Delta G_{hydrocarbon \rightarrow interface}$, for model drugs

Drug	$\Delta G_{dodecane \rightarrow interface}$(kJ/mol)
Progesterone	-21.36±0.46
Testosterone	-26.43±0.37
11α-hydroxyprogesterone	-33.86±0.32
Diazepam	-20.22±0.35
Temazepam	-25.21±0.34
Prazepam	-19.59±0.43
Methylparaben	-23.79±0.35
Ethylparaben	-23.48±0.46
Butylparaben	-23.07±0.19
17β-estradiol	-30.46±2.91
Oxazepam	-39.62±1.06

constant when comparing diazepam with prazepam, or among the methyl-, ethyl- and butylparabens. Unsurprisingly, these results suggest the hydrocarbon regions of the model drugs likely remain in the hydrocarbon phase when the molecules are located at the hydrocarbon/water interface.

5.3.2. Surfactant-Specific Parameters Used in the Thermodynamic Model

In this section, we discuss the rational behind the choice of surfactant-specific parameters employed in Equations (A2.13) and (A2.14). The parameters used for surfactants and micelles included minimum occupied area by surfactant molecules (a), radius (r) and aggregation number (N_{aggre}) of the micelles, area per surfactant molecule (A) and surface pressure (π) at micelle surface, and Laplace pressure acting on the micelles (P). The first three parameters (a, r, and N_{aggre}) are summarized in Table 5.4. Parameters, A, π and P, can be calculated from a, r, and N_{aggre}.

The areas occupied by SDS or DTAB at the hydrocarbon/water interface were reported in Chapter 4 to be 32.0 (for SDS) and 37.1Å^2 (for DTAB) by fitting Eq. (A1.13) to experimental π-A curves from literatures (Haydon and Taylor, 1960). The occupied area by DM at dodecane/water interface was determined by fitting Eq. (A1.8) to experimental γ~C curve, Fig. 4.9, with the fitted value of 41.4 Å^2.

The aggregation number of SDS micelles was 51 from Thevenot et al. (Thevenot et al., 2005) employing time-dependent static light scattering method. For cationic surfactant DTAB, the aggregation number was 56 from Rafati et al. (Rafati et al., 2003) using potentiometric technique. The aggregation number of nonionic surfactant DM was 113 by Bucci et al. (Bucci et al., 1991) using small angle neutron scattering method.

Table 5.4, The parameters of surfactants and the corresponding micelles used in the surface-localized model. The data with asterisk are independent and obtained from literatures (detail information is in main text). The other data are derivative from those independent parameters.

	SDS	DTAB	DM
$a_{surfact}$ (Å²)	32.0±0.6	37.1±0.6	41.4±2.7
r (Å)	19.7*	18.4*	22.4*
N_{aggr}	51*	56*	113*
$A=4\pi r^2/N_{aggr}$ (Å²)	95.6	76	55.8
π (mN/m)	11.6	17.9	22.9
$P=2(\gamma_0-\pi)/r$ (atm)	405	366	257

The radii of the micelles were estimated as being equal to the length of single surfactant molecule. The radii of SDS, DTAB and DM micelles were 19.7, 18.4 and 22.4Å respectively. The molecular structures of SDS and DTAB were obtained from the corresponding crystal structure from Cambridge Structure Database (Allen, 2002). Unfortunately, there is no reported crystal structure for dodecyl β-D-maltoside, but the molecular structure of methyl β-maltoside was available and served as an analogue of head group of DM. The maximum inter-atomic distance of dodecyl sulfate molecule was 18.4Å between one oxygen atom in sulfate group and one hydrogen atom in terminal methyl group. By considering the atomic radii of those atoms, the total length of the molecule was about 19.7Å. Using the same principle, the length of DTAB molecule was close to 18.4Å based on the maximum inter-atomic distance of 17.9Å between two hydrogen atoms in methyl group of head group and in terminal methyl group of hydrocarbon tail. For dodecyl β-D-maltoside, the length of hydrocarbon chain was 14.6Å and the maximum inter-atomic distance of maltoside head group was 11.3Å. The head group and the alkyl tail were connected with each other through a carbon-oxygen bond that could rotate easily and the angle between the long axes of the head group and hydrocarbon chain varied from 95^o to 147^o. The average angle was 119^o and the average value of the maximum inter-atomic distances of the DM molecule for different configurations was 22.4Å. The distance was chosen as the radius of DM micelles without considering the atomic radii because the DM micelles had a large hydrophilic head group that let us choose a slightly smaller length compared to the total length of the molecule without lose of accuracy.

The areas occupied per surfactant molecule at the micelle surface were calculated based on geometry, $A=4\pi r^2/N_{aggre}$. The surface pressure, $\pi=\gamma_0-\gamma$, at the micelle surface was determined by the π-A relationship, Eq.(A1.13) for anionic surfactants (SDS or DTAB) or

Eq.(A1.15) for nonionic surfactants (DM). The parameters used in these equations were determined in Section 4.3.3.2.

The Laplace pressure was calculated using equation: $P=2\gamma/r=2(\gamma_0-\pi)/r$ based on assumption that the micelle has spherical shape.

5.3.3. Application of Surface-localized Model to Predict the Micelle/water Partitioning

The micelle/water partitioning coefficients of dilute solutes can be predicted based on the surface-localized model described in Appendix 2. The model describes micellar solubilization as the co-localization of drug and surfactant at highly curved interface. The calculated micelle/water partitioning coefficients of 9 model drugs in 3 micelle systems are compared to experimental data (Chapter 3) with the results shown in Figure 5.9. Oxazepam and 17β-estradiol were not included because there were poor estimations of their interfacial activities at hydrocarbon-water interface. When butylparaben was solubilized in DTAB and DM solutions, the solutions became cloudy, suggesting that the Krafft point had been exceeded. Therefore there is no experimental micelle/water partitioning coefficient for butylparaben in the two surfactant systems. It is clear that the predictions for the remaining 25 surfactant/drug combinations are in good agreement with the experimental result. It should be noted a broad range of the micelle/water partitioning constants that cover three orders of magnitude are included. There is no result that has a deviation greater than a factor of 2, and a majority of the data points (19 out of 25) have deviations within a factor of 1.5. The R-square is equal to 0.959.

Although the surface-localized model has a complicated final expression, e.g. Eq. (A2.13) or (A2.14), the calculated micelle/water partitioning coefficient can be analyzed by

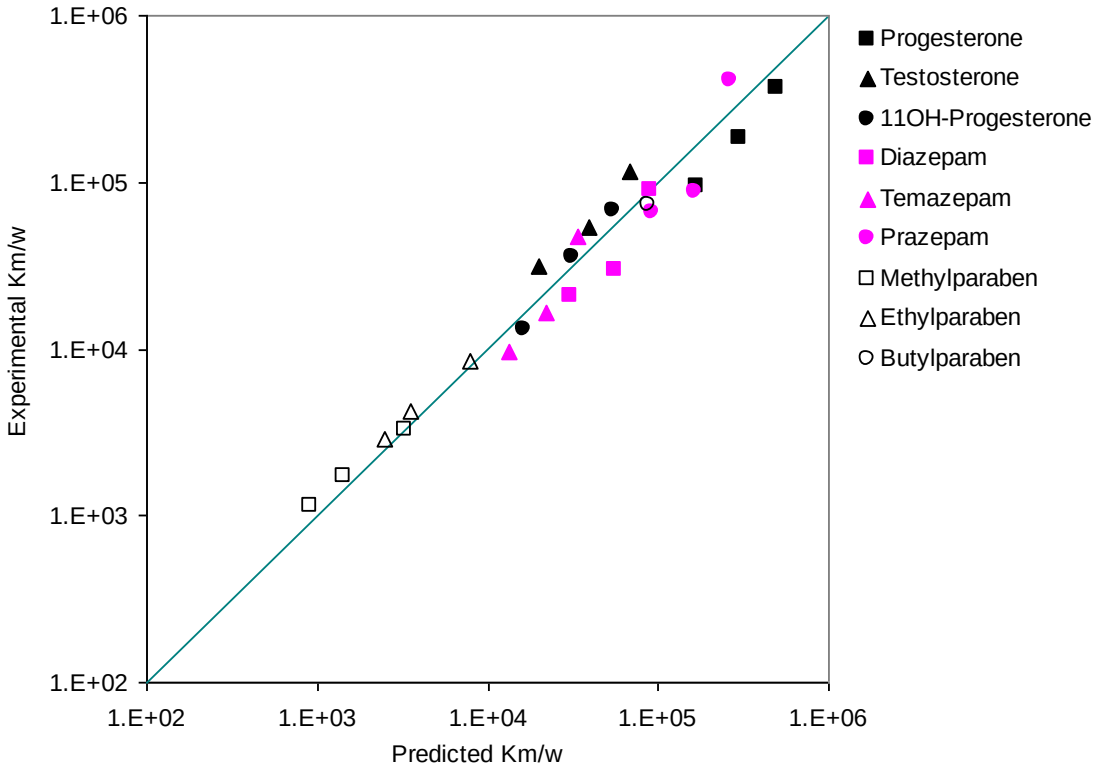

Figure 5.9, Comparison between experimental and predicted micelle/water partitioning coefficients ($K_{m/w}$) of 9 model drugs in 3 surfactant systems.

separating the expression into several components in terms of the basic relationship Eq.(A2.4):

$$K_{m/w} = \frac{\Gamma}{X_w} \cdot A \cdot f \cdot \exp[-PV/RT] + K_{h/w} \exp[-PV/RT] \qquad (5.2)$$

The values for terms, $\frac{\Gamma}{X_w}$, A, f, $\exp[-PV/RT]$ and $K_{h/w} \exp[-PV/RT]$ (also labeled as $K_{m/w,core}$), are explicitly listed in Table 5.5 along with the predicted and experimental $K_{m/w}$ values. P=2γ/r. Firstly, the contributions of the core region to the solubilization, $K_{h/w} \exp[-PV/RT]$, are compared to the total micelle/water partitioning constants. The fraction of solubilization by micellar core (as determined by dividing $K_{h/w} \exp[-PV/RT]$ by $K_{m/w}$(calc.)) has a range from 6.9×10^{-7} (11α-hydroxyprogesterone in SDS micelles) to 2.6×10^{-3} (prazepam in DM micelles). The results clearly show that core-localized solubilization is insufficient to explain experimental results and that the micelle surface is likely the dominant solubilization site.

The contributions of Laplace pressure on solubilization capacity, $\exp[-PV/RT]$, vary from 0.011 (11α-hydroxyprogesterone in SDS) to 0.32 (methylparaben in DM). Apparently the term exerts a significant influence on the total partitioning properties and can not be ignored. The Laplace pressure in the three micelle systems has the rank order: SDS > DTAB > DM, and correlates well with the differences in surface pressure at the micelle surface and the size of micelles. DM micelle has the greatest diameter and the largest surface pressure resulting in the lowest interfacial tension at micelle surface. Those two factors result in DM exhibiting the lowest Laplace pressure. For drug substances, the larger the molar volume, the more significant influence the Laplace pressure makes on solubilization capacity. Accordingly, 11α-hydroxyprogesterone was most affected and methylparaben was least influenced by Laplace pressure.

Table 5.5, The predicted micelle/water partitioning coefficients, $K_{m/w}$(calc.), their components, exp(-PV/RT), Γ/X_w, A, *f*, $K_{m/w,\ core}$ (=$K_{h/w}$exp(-PV/RT)), and experimental micelle/water partitioning coefficients, $K_{m/w}$(exp.), for 9 model drugs solubilized in 3 micelle systems.

		exp(-PV/RT)	Γ/X_w ($Å^{-1}$)	A (Å)	*f*	$K_{m/w,\ core}$	$K_{m/w}$(calc.)	$K_{m/w}$(exp.)
Progesterone	SDS	0.01225	2.79E+06	95.6	0.1609	46.50	5.25E+05	(3.69±0.13)E+05
Testosterone	SDS	0.01726	2.90E+05	95.6	0.1529	0.88	7.33E+04	(1.14±0.05)E+05
11OH-prog*	SDS	0.01115	4.13E+05	95.6	0.1328	0.04	5.84E+04	(6.75±0.39)E+04
Diazepam	SDS	0.03224	1.42E+05	95.6	0.2245	9.92	9.84E+04	(8.93±0.39)E+04
Prazepam	SDS	0.0155	1.06E+06	95.6	0.1801	45.53	2.82E+05	(4.03±0.26)E+05
Temazepam	SDS	0.02849	5.24E+04	95.6	0.2575	0.43	3.68E+04	(4.70±0.11)E+04
Methylparaben	SDS	0.16159	7.05E+02	95.6	0.3357	0.06	3.66E+03	3.24E+03
Ethylparaben	SDS	0.11849	2.31E+03	95.6	0.3366	0.16	8.82E+03	8.51E+03
Butylparaben	SDS	0.07533	4.23E+04	95.6	0.3155	2.19	9.62E+04	7.24E+04
Progesterone	DTAB	0.01863	2.79E+06	76	0.0574	70.73	2.27E+05	(1.79±0.13)E+05
Testosterone	DTAB	0.02541	2.90E+05	76	0.0531	1.30	2.98E+04	(5.40±0.31)E+04
11OH-prog*	DTAB	0.01711	4.13E+05	76	0.0428	0.06	2.29E+04	(3.57±0.19)E+04
Diazepam	DTAB	0.04472	1.42E+05	76	0.096	13.76	4.64E+04	(2.94±0.10)E+04
Prazepam	DTAB	0.02305	1.06E+06	76	0.0683	67.72	1.27E+05	(8.76±0.57)E+04
Temazepam	DTAB	0.03999	5.24E+04	76	0.1185	0.61	1.89E+04	(1.67±0.04)E+04
Methylparaben	DTAB	0.19224	7.05E+02	76	0.1783	0.07	1.84E+03	(1.73±0.04)E+03
Ethylparaben	DTAB	0.14519	2.31E+03	76	0.1791	0.19	4.57E+03	(4.28±0.15)E+03

*Abbreviation of 11α-hydroxyprogesterone

Table 5.5 (cont.), The predicted micelle/water partitioning coefficients, $K_{m/w}$(calc.), their components, exp(-PV/RT), Γ/X_w, A, *f*, $K_{m/w,\ core}$ (=$K_{h/w}$exp(-PV/RT)), and experimental micelle/water partitioning coefficients, $K_{m/w}$(exp.), for 9 model drugs solubilized in 3 micelle systems.

		exp(-PV/RT)	Γ/X_w (Å^{-1})	A (Å)	*f*	$K_{m/w,\ core}$	$K_{m/w}$	$K_{m/w}$(exp.)
Progesterone	DM	0.06167	2.79E+06	55.8	0.0156	234.2	1.50E+05	(9.49±1.18)E+04
Testosterone	DM	0.07663	2.90E+05	55.8	0.0141	3.92	1.75E+04	(3.09±0.48)E+04
11OH-prog*	DM	0.05812	4.13E+05	55.8	0.0107	0.21	1.43E+04	(1.32±0.09)E+04
Diazepam	DM	0.1138	1.42E+05	55.8	0.0301	35.02	2.72E+04	(2.10±0.07)E+04
Prazepam	DM	0.07158	1.06E+06	55.8	0.0195	210.3	8.24E+04	(6.51±0.33)E+04
Temazepam	DM	0.10524	5.24E+04	55.8	0.0395	1.59	1.21E+04	(9.63±0.35)E+03
Methylparaben	DM	0.31556	7.05E+02	55.8	0.0667	0.11	8.28E+02	(1.16±0.10)E+03
Ethylparaben	DM	0.25931	2.31E+03	55.8	0.067	0.35	2.24E+03	(2.85±0.05)E+03

*Abbreviation of 11α-hydroxyprogesterone

The area per molecule term "A" can be best envisioned as the inverse of the density of surfactant molecules at the micelle surface. A larger value for "A" corresponds to a lower density of surfactants at the micellar surface. Since the drug is hypothesized to co-adsorb with surfactant for the oil/water interface, the lower surfactant density of surfactant will permit drug molecules to more easily adsorb to the micelle surface and thus increase the micelle/water partitioning coefficient.

The term, Γ/X_w, represents the surface activities of the solutes at an oil/water interface in the absence of surfactants. This term reflects the transfer free energy of the solute from water to hydrocarbon/water interface (Eq.(A2.7)). A broad range for the model drugs from $7x10^2$ (methylparaben) to $3x10^6$ $Å^{-1}$ (progesterone) is evident.

The relative adsorption potential, *f*, is defined as a ratio between surface density of drugs in the presence and absence of surfactant. The factor reflects the ability of the drug to co-adsorb with surfactants at the oil/water interface. Since the ability of the drug to get into oil/water interface in the absence of surfactants has been included in the Γ/X_w term, the *f* factor takes into account the effect of the presence of the surfactants. The magnitude of the *f* factor is between 0.011 (11α-hydroxyprogesterone in DM) and 0.34 (methyl- and ethylparabens in SDS). From Eq. (A2.11) and (A2.12), the *f* factor is affected mainly by two parameters: surface pressure of the surfactant at micelle surface and minimum occupied area by the drug. High surface pressure, due to the stronger surface activity of the surfactant, will make adsorption of drug molecules onto the oil/water interface more difficult. When we compare the three surfactants, the *f* factor has the order of SDS > DTAB > DM because of the surface pressure has the reverse ranking order.

The second component of the adsorption potential is the occupied surface area by the drug molecule. When the drug must clear a larger area in order to move onto the oil/water interface, it has a weaker ability to compete with surface active agents for the interface. The rank order of relative adsorption factors in the same micelle system is reversely correlated to the occupied areas by the drug molecules: methylparaben ≈ ethylparaben > butylparaben > temazepam > diazepam > prazepam > progesterone > testosterone > 11α-hydroxyprogesterone.

To assess the relative importance of those terms, the units must be identical. The Γ/X_w term is combined with "A" term to form a unitless term $\Gamma*\mathrm{A}/X_w$ to compare to the other two unitless terms, $\exp[-PV/RT]$ and f. The $\Gamma*\mathrm{A}/X_w$ term ranges from $3.9\mathrm{x}10^4$ to $2.7\mathrm{x}10^8$ and thus makes the greatest contribution to total micelle/water partitioning coefficients. The Laplace pressure effect and the relative adsorption factor are within two orders of magnitude and make significant, but not the dominant, contributions to the micellar solubilization.

5.3.4. Sensitivity of Parameter Selections to the Prediction of Micelle/water Partition Coefficient

As is evident in Table 5.4, there are a number of physical parameters that are critical to the application of the thermodynamic model outlined in Equation (A2.13) and (A2.14). Most notable of these critical parameters are size of the micelle, as defined by radius, aggregation number, and the interfacial areas occupied by water and drugs. In this section, the sensitivity of the thermodynamic model to the values selected for these critical parameters is evaluated. The strategy is to vary each parameter individually over a range of physically-relevant values and to observe the extent to which $K_{m/w}$ is influenced by the variation. It is important here to realize that the values of the parameters are not being "floated" to fit an optimal result, but rather are being systemically-varied to illustrate the

ultimate effect on $K_{m/w}$ by a range of possible values. The following table lists the "independent" parameters to be tested, parameters depending on the choice of those independents, and the corresponding section number.

Independent parameter to be tested	Parameters dependent on choice of independents	Section number
r (radius of micelle)	A (micelle surface area per surfactant) π (surface pressure) P (Laplace pressure)	5.3.4.1
N_{aggre} (aggregation number of micelle)	r (radius of micelle) A (micelle surface area per surfactant) π (surface pressure) P (Laplace pressure)	5.3.4.2
a_{water} (interfacial area occupied by water)	$a_{surfact}$ (interfacial area occupied by surfactant) a_{drug} (area occupied by drug) ΔG_{trans} (free energy of transfer for drug from water to oil/water interface)	5.3.4.3
a_{drug} (interfacial area occupied by drug)	ΔG_{trans} (free energy of transfer for drug from water to oil/water interface)	5.3.4.4

5.3.4.1. Sensitivity of Predicted $K_{m/w}$ Values to the Radii of Micelles

In evaluating the surface-localized model (see results in Table 5.4), radii of the micelles were based on the dividing oil/water interface at the micelle surface and were calculated from the lengths of those surfactant molecules including head groups (see Section 5.3.2). Although experimentally-determined micellar radii are available in the literature, these values were not employed in the model simulations. The experimental values are obtained by different detecting techniques, such as dynamic light scattering, small-angle X-ray diffraction, small-angel neutron scattering, gel filtration and diffusivity measurements (Anacker and Ghose, 1968; Svens and Rosenholm, 1973; Lin et al., 1990; Soderman et al., 2004). Typically, the results exhibit a broad range of values. More importantly, the experimental radii tend to include effects of bound water and electrolytes

and are not defined solely at the dividing oil/water interface, as is defined in the thermodynamic model.

The sensitivity of the thermodynamic model to the radii of micelles was tested by varying the parameter '*r*' without changing any other independent parameters. Some dependent parameter would surely be modified due to the changing micellar size, such as Laplace pressure, area per surfactant molecule at micelle surface and the surface pressure. The radii of SDS micelles were varied from 17 to 20.7Å. A small radius would correspond to more efficient packing of surfactant molecules in the micelles and a large radius would indicate looser structures of the micelles. Three model drugs, progesterone, diazepam and methylparaben, were chosen to run the sensitivity test with the results shown in Figure 5.10. Here, the ratios of $K_{m/w}$ at the test radius to the $K_{m/w}$ at the radius of 19.7Å (Table 5.4) were calculated. Clearly the $K_{m/w}$ value increases with larger micellar size because the looser micellar structure is expected to provide larger interfacial volume with which to solubilize drugs. The micelle/water partitioning constants are quite sensitive to the choice of the micellar radius. The calculated $K_{m/w}$ increases 28~50% with each 1Å increment of micellar radius. Solubilization of progesterone is most sensitive to the radii and methylparaben is the least sensitive among the three model drugs. Progesterone occupies the largest area at the micelle surface and has the largest molecular volume among the model drugs and it seems likely that progesterone is more sensitive to the available space in the micelle surface as compared to the other two drugs.

Figures 5.11 and 5.12 show the sensitivities of predicted $K_{m/w}$ in DTAB and DM micelles to the radii of those micelles. The size ranges for DTAB and DM are 17~20Å and 20.7~24Å respectively. Again, the micelle/water partitioning coefficient is sensitive to the choice of the micellar radius. For DTAB micelles, one angstrom increment could produce

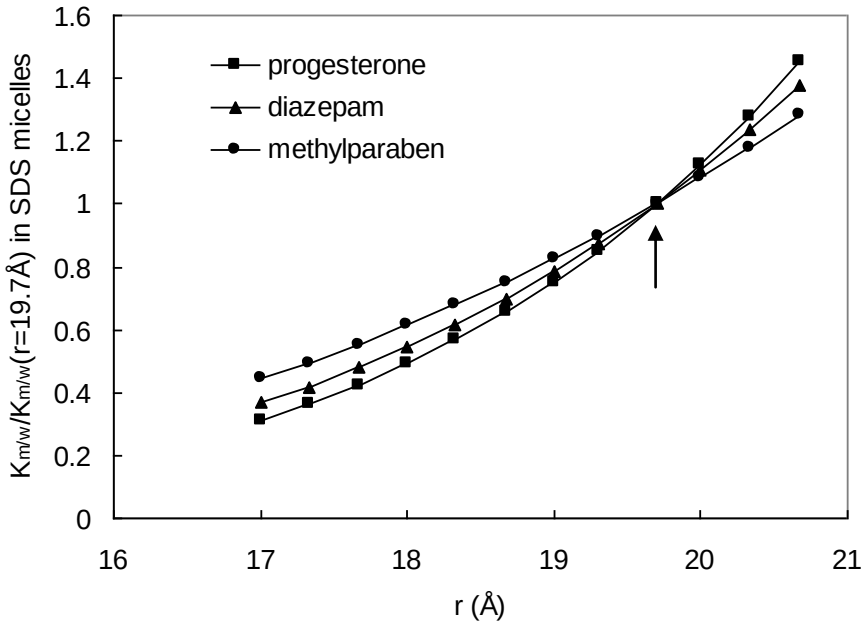

Figure 5.10, The sensitivity of calculated micelle/water partitioning coefficient in SDS micelle systems to the radius of SDS micelles. The arrow marks the radius employed in the evaluation of the thermodynamic model, Table 5.4.

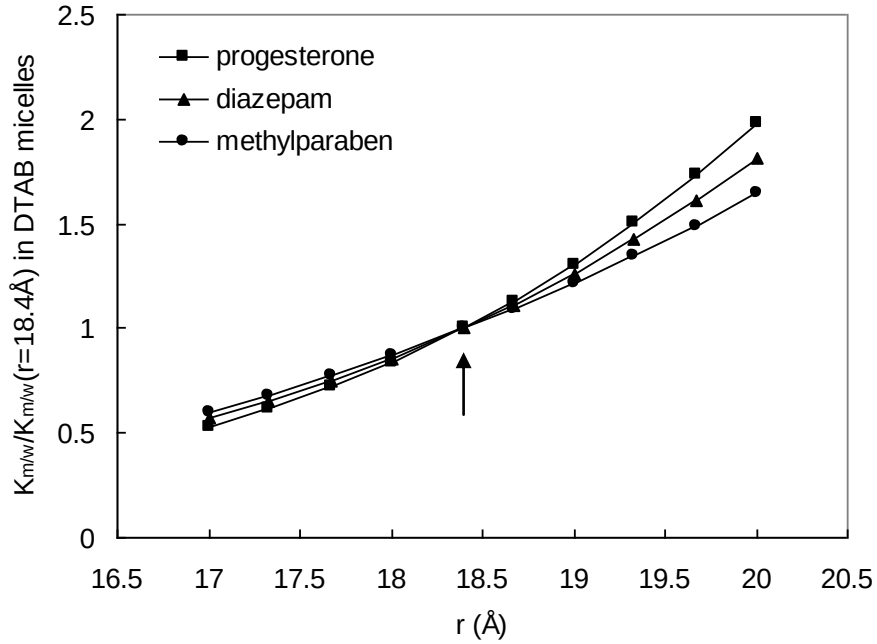

Figure 5.11, The sensitivity of calculated micelle/water partitioning coefficient in DTAB micelle systems to the radius of DTAB micelles. The arrow marks the radius employed in the evaluation of the thermodynamic model, Table 5.4.

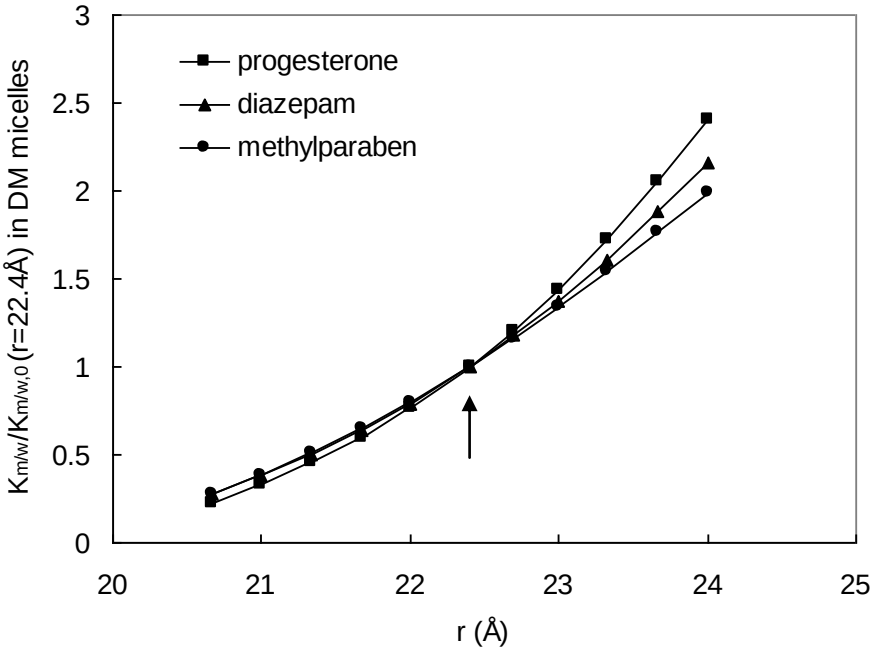

Figure 5.12, The sensitivity of calculated micelle/water partitioning coefficient in DM micelle systems to the radius of DM micelles. The arrow marks the radius employed in the evaluation of the thermodynamic model, Table 5.4.

40~56% enhancement in $K_{m/w}$ value. For nonionic DM micelles, increasing 1Å of 'r' would raise $K_{m/w}$ by 67~88%.

When we compare the three micelle systems, the solubilization by DM micelle is the most sensitive to the micellar size and SDS micelle system is the least sensitive. One possible reason is the different packing efficiency of those micelles: The packing of nonionic surfactant is more compact than ionic surfactants due to the absence of repulsion forces due to the uncharged headgroup. When the two charged micelles are compared to each other, the positive charge of DTAB between head groups is screened to some extent by the methyl groups in the head, while the negative charges of SDS are on the surface of the head group and the repulsive interactions between head groups would be stronger. Therefore the DTAB micelles are more efficiently packed than SDS micelles. The more tightly packed micelles would be more sensitive to the space available for solubilization of model drugs.

It is clear from the sensitivity analysis that the predicted $K_{m/w}$ is strongly dependent on the value of the 'r' term and that the dividing oil/water interface of the micelles has to be selected carefully.

5.3.4.2. Sensitivity of Predicted $K_{m/w}$ Values to Aggregation Number of Micelles

Many experimental studies on micelles have shown an increase in the aggregation number with increasing surfactant concentrations (Rafati et al., 2003; Bucci et al., 1991). There is experimental evidence for a relation between aggregation number and concentration of surfactant in our studied systems. For examples, SDS micelles have a aggregation number of 76 at 50mM and the number increases to 88 at 150mM (Bucci et al., 1991); the aggregation number of DTAB micelles is 56 at 15mM and rises to 62 at

92mM (Rafati et al., 2003); DM micelles have values of N=113 at 50mM and N=129 at 150mM (Bucci et al., 1991).

To test the sensitivity of $K_{m/w}$ on the aggregation number 'N', an appropriate relationship between the radius of micelles and the 'N' must be written. There are two approaches to deal with the effect of increasing surfactant concentration. One approach is to assume that micelles grow larger, while maintaining a spherical shape, as the total surfactant concentration in the system is increased. This approach assumes that the density of surfactant molecules in a micelle remains constant with increasing micelle size. The second approach assumes that the micelles take on the shape of a prolate ellipsoid. In this case, curvature restricts the size of the micelle. With a restriction on the size of the micelle, increasing the aggregation number of micelles must result in greater density of surfactant molecules in a micelle.

Based on the growing-sphere approach, the r~N relationship can be simply expressed as:

$$r/r_0 = \left[N/N_0\right]^{1/3} \qquad (5.3)$$

For an ellipsoidal shaped micelle, the additional surfactant molecules have more efficient packing as compared to spherical shaped micelle. One surfactant molecule in spherical micelles mainly occupies a cone shape with the volume equal to $\frac{1}{3}Sr$, where the S is the occupied surface area by each molecule and r is the length of the molecule. On the other hand, an additional surfactant molecule in an ellipsoid shaped micelle occupies a pie-shaped wedge with the volume equal to $\frac{1}{2}Sr$. Since the core region is limited by the packing of the hydrocarbon chain and had a constant density, the cone shape is not able to pack as efficiently on the surface compared with the pie-shape. The additional molecules were assumed to have a density of 1.5 times of the original density. The length of the three principle axes of the prolate ellipsoid is

$$a = r_0 \frac{N_0 + 2/3 \cdot (N - N_0)}{N_0} \qquad (5.4)$$
$$b = c = r_0$$

The total surface area of a prolate ellipsoid is

$$S = 2\pi \left(b^2 + \frac{a^2 b \arccos \frac{b}{a}}{\sqrt{a^2 - b^2}} \right) \qquad (5.5)$$

The average curvature could use the following approximation:

$$\text{average curvature} = \frac{1}{r_0} \left[\frac{N_0 + 2/3 \cdot (N - N_0)}{N_0} \right]^{-1/3} \qquad (5.6)$$

The approximation had an error of <1.7% when the axial ratio of the ellipsoid was below 2. The curvature was employed in estimating the Laplace pressure in prolate ellipsoid-shaped micelle.

Listed in Table 5.6 are the predicted micelle/water partitioning constants as a function of aggregation number for SDS and DTAB and Table 5.7 for DM. Aggregation numbers 75 and 100 were tested for ionic surfactants and N=120 and 130 were used for DM micelles. For purpose of comparison, the values of the $K_{m/w}$ calculated with the parameters listed in Table 5.4 are included. In the case of SDS micelles, the calculated $K_{m/w}$ of three steroids and three benzodiazepines increase significantly with large aggregation number under spherical shape condition. On the other hand, only a small variation in partition coefficients is observed with increasing aggregation number when the micelle assumes a prolate shape. The biggest deviations are 45% for spherical-shape micelles and 14% for prolate-shape micelles. When parabens are solubilized in SDS micelles, spherical shape micelles would produce smaller changes of $K_{m/w}$ with large aggregation number compared to those from ellipsoidal shape micelles. The deviations based on sphere shape are <12% compared to <30% based on prolate shape.

Table 5.6, Sensitivity of micelle/water partitioning coefficients in SDS and DTAB micelle systems to the aggregation number of the micelles

		Km/w Original	Km/w spherical		Km/w ellipsoidal	
			N_{aggre}=75	N_{aggre}=100	N_{aggre}=75	N_{aggre}=100
Progesterone	SDS	5.25E+05	6.88E+05	7.62E+05	5.25E+05	5.12E+05
Testosterone	SDS	7.33E+04	8.97E+04	9.46E+04	6.81E+04	6.30E+04
11OH-prog*	SDS	5.84E+04	7.49E+04	8.11E+04	5.60E+04	5.27E+04
Diazepam	SDS	9.84E+04	1.17E+05	1.23E+05	9.27E+04	8.74E+04
Prazepam	SDS	2.82E+05	3.63E+05	3.99E+05	2.81E+05	2.74E+05
Temazepam	SDS	3.68E+04	4.58E+04	5.00E+04	3.69E+04	3.65E+04
Methylparaben	SDS	3.66E+03	3.57E+03	3.33E+03	2.97E+03	2.56E+03
Ethylparaben	SDS	8.82E+03	9.07E+03	8.79E+03	7.56E+03	6.75E+03
Butylparaben	SDS	9.62E+04	1.06E+05	1.07E+05	8.72E+04	8.09E+04
Progesterone	DTAB	2.27E+05	2.54E+05	2.46E+05	1.99E+05	1.61E+05
Testosterone	DTAB	2.98E+04	3.11E+04	2.80E+04	2.39E+04	1.75E+04
11OH-prog*	DTAB	2.29E+04	2.47E+04	2.27E+04	1.88E+04	1.39E+04
Diazepam	DTAB	4.64E+04	4.88E+04	4.57E+04	3.95E+04	3.16E+04
Prazepam	DTAB	1.27E+05	1.41E+05	1.37E+05	1.12E+05	9.19E+04
Temazepam	DTAB	1.89E+04	2.11E+04	2.11E+04	1.76E+04	1.55E+04
Methylparaben	DTAB	1.84E+03	1.67E+03	1.40E+03	1.38E+03	1.00E+03
Ethylparaben	DTAB	4.57E+03	4.36E+03	3.84E+03	3.65E+03	2.82E+03

*Abbreviation of 11α-hydroxyprogesterone

Table 5.7, The sensitivity of micelle/water partitioning coefficients in DM micelle systems to the aggregation number of the micelles

		Km/w Original	Km/w spherical		Km/w ellipsoidal	
			N_{aggre}=120	N_{aggre}=130	N_{aggre}=120	N_{aggre}=130
Progesterone	DM	1.50E+05	1.39E+05	1.24E+05	1.26E+05	9.68E+04
Testosterone	DM	1.75E+04	1.59E+04	1.37E+04	1.42E+04	1.04E+04
11OH-prog*	DM	1.43E+04	1.30E+04	1.12E+04	1.16E+04	8.36E+03
Diazepam	DM	2.72E+04	2.54E+04	2.27E+04	2.32E+04	1.82E+04
Prazepam	DM	8.24E+04	7.71E+04	6.92E+04	7.02E+04	5.49E+04
Temazepam	DM	1.21E+04	1.16E+04	1.07E+04	1.08E+04	8.99E+03
Methylparaben	DM	8.28E+02	7.57E+02	6.61E+02	6.97E+02	5.40E+02
Ethylparaben	DM	2.24E+03	2.08E+03	1.85E+03	1.93E+03	1.54E+03

*Abbreviation of 11α-hydroxyprogesterone

In DTAB micelle systems, for all model drugs, the effect of increasing aggregation number on predicted $K_{m/w}$ values is less under spherical-shape micelle condition compared to those from the ellipsoid shape. With spherical micelle shape, the deviations of $K_{m/w}$ are within 10% for steroids and benzodiazepines and are 24% and 16% for two parabens when aggregation number changed from 56 to 100. When the micelles are assumed to be in the prolate shape, the greatest deviations of $K_{m/w}$ are 41% for steroids and benzodiazepines and 46% for parabens.

In DM micelle systems, the predicted $K_{m/w}$ decrease with increasing aggregation number no matter what the shape of the micelles. The spherical-shape micelles do exhibit smaller changes of $K_{m/w}$ compared to ellipsoidal micellar shape. The greatest deviations from original values are 22% for spherical shape and 42% for prolate shape.

As has been seen in Figures 3.14~3.22, the experimental partition coefficients are insensitive to surfactant concentration and therefore the aggregation number. Under these conditions, it is likely the DTAB and DM micelles will maintain a sphere shape while SDS micelles will transform to prolate shape with increasing aggregation number. As an example, almost doubling the size of the micelles of SDS and DTAB only produces <30% change in $K_{m/w}$ values. For DM micelles, the sensitivity of $K_{m/w}$ to N_{aggre} is a slightly larger: a 15% increase in aggregation number resulted in 22% decrease in micelle/water partition constants. For nonionic surfactant, the increasing of aggregation number with increasing surfactant concentration is less than that observed in ionic surfactant systems. Therefore, the sensitivity of $K_{m/w}$ to the surfactant concentration is small.

5.3.4.3. Sensitivity of Predicted $K_{m/w}$ Values to Occupied Interfacial Areas by Water Molecules

In the thermodynamic model being tested, the occupied areas by water molecules, a_{water}, and by surfactant molecules, $a_{surfact}$, are correlated. This can be seen by examining Figures 4.7 and 4.8 where Eq. (A1.13) was used to fit the two parameters to the experimental π-A curves of SDS and DTAB. When two parameters are directly correlated to each other, testing one parameter is sufficient in evaluating model sensitivity. Here we have chosen to test the effect of the occupied area by water molecules. As with other studies, the choice of the parameter must be physically realistic and not be freely adjustable. The size of the water molecule was well known. The commonly employed value is about 10Å² (Lucassen-Reynders, 1981). Gumkowski's value, a_{water}=7.62Å², (Gumkowski, 1986) had been used in our early studies. In this section, an area of 10Å² is employed to test the sensitivity of the predicted $K_{m/w}$ to the area occupied by water. Due to the correlation between a_{water} and $a_{surfact}$, Eq. (A1.13) was fit to experimental π-A curves for SDS and DTAB shown in Figures 4.7 and 4.8 using a_{water}=10Å². The fitted values of $a_{surfact}$ were 33.8±0.6Å² for SDS and 38.9±0.6Å² for DTAB. For nonionic surfactant DM, Eq. (A1.8) was employed to fit to experimental γ-C curve for DM, Fig. 4.9, using the test a_{water} value and the fitted $a_{surfact}$ became 42.3±2.1Å². Compared to original values in Table 5.4, the changes were less than 2Å² indicating the parameter $a_{surfact}$ is not very sensitive to the occupied interfacial area of water molecules.

The areas occupied by surfactants are not the only parameters that correlate with the area of water. The transfer free energy and interfacial area occupied by model drugs also correlate with a_{water}. As mentioned in Section 5.3.1, these two parameters were determined by fitting to the experimental γ~C curves, Fig.5.3~5.6, using Eq.(A1.8) where parameter a_{water} was present. Table 5.8 shows the fitted transfer free energies and occupied interfacial areas of 9 model drugs using a_{water}=10Å². Compared to parameter set

with a_{water}=7.62Å², Table 5.2, the ΔG_{trans} drops by ~0.67kJ/mol while a_{drug} increases by about 1.1Å². Applying the new parameter set corresponding to relatively large area of water molecules (10Å²), the predicted micelle/water partitioning coefficients for 9 model drugs in 3 surfactant systems are listed in Table 5.9. In the table, the calculated $K_{m/w}$ values using the initial parameter set with a_{water}=7.62Å² are also listed for comparison. The last column of the table shows the ratios between the predictions using two different parameters sets. Clearly the ratios are very close to 1. The greatest deviation of these ratios from a value of 1 is only 1.1% indicating the model predictions of $K_{m/w}$ are not very sensitive to the choice of occupied interfacial areas by water molecules or surfactant molecules.

5.3.4.4. Sensitivity of Predicted $K_{m/w}$ Values to Interfacial Areas Occupied by Solubilized Drugs

Once the a_{water} term is fixed, the occupied interfacial area of drugs, a_{drug}, and the transfer free energy of the model drugs, $\Delta G_{water \rightarrow interface}$, become a directly correlated parameter pair. In this section, only a_{drug} will be adjusted to test the sensitivity of $K_{m/w}$ predictions. Just like the water molecules, molecular structures of drug substances limit their range of possible occupied areas at oil/water interface. In the following chapter, a molecular simulation technique will be used to calculate the theoretical maximum and minimum areas occupied by the drug molecules assuming the molecule could assume any orientation. The results are listed in Table 6.2. In the model sensitivity test, four areas were chosen for each model drug: the theoretical maximum area, the theoretical minimum area, an area 10% larger than experimental fitted value, and an area 10% smaller than experimental area. Using these areas, the transfer free energies, $\Delta G_{water \rightarrow interface}$, were fitted using Eq.(A1.8). A Scientist® software was employed to run the statistical analysis.

Table 5.8, Fitted transfer free energies $\Delta G_{water \rightarrow interface}$ and occupied areas at oil/water interface for the model drugs using a_{water}=10Å²

Drug	$\Delta G_{water \rightarrow interface}$(kJ/mol)	a_{drug}(Å²)
Progesterone	-42.45±0.45	59.1±4.4
Testosterone	-36.85±0.34	60.9±4.9
11α-hydroxyprogesterone	-37.72±0.17	65.9±1.9
Diazepam	-35.08±0.32	47.2±3.7
Temazepam	-32.61±0.33	42.4±3.7
Prazepam	-40.05±0.40	55.1±5.7
Methylparaben	-21.94±0.33	33.0±4.0
Ethylparaben	-24.88±0.43	32.9±4.6
Butylparaben	-32.08±0.16	35.1±1.2

Table 5.9, Calculated micelle/water partitioning coefficients using new parameter set (Table 5.8) corresponding to a_{water}=10Å² compared to predictions using old parameters with a_{water}=7.62Å².

		Km/w a=7.62Å²	Km/w a=10Å²	Ratio*
Progesterone	SDS	5.25E+05	5.29E+05	1.007
Testosterone	SDS	7.33E+04	7.39E+04	1.008
11OH-prog^	SDS	5.84E+04	5.89E+04	1.008
Diazepam	SDS	9.84E+04	9.92E+04	1.008
Prazepam	SDS	2.82E+05	2.84E+05	1.007
Temazepam	SDS	3.68E+04	3.70E+04	1.006
Methylparaben	SDS	3.66E+03	3.68E+03	1.007
Ethylparaben	SDS	8.82E+03	8.87E+03	1.006
Butylparaben	SDS	9.62E+04	9.70E+04	1.009
Progesterone	DTAB	2.27E+05	2.28E+05	1.004
Testosterone	DTAB	2.99E+04	3.00E+04	1.005
11OH-prog^	DTAB	2.30E+04	2.31E+04	1.005
Diazepam	DTAB	4.65E+04	4.68E+04	1.007
Prazepam	DTAB	1.27E+05	1.27E+05	1.004
Temazepam	DTAB	1.89E+04	1.90E+04	1.004
Methylparaben	DTAB	1.84E+03	1.85E+03	1.005
Ethylparaben	DTAB	4.58E+03	4.60E+03	1.004
Progesterone	DM	1.50E+05	1.51E+05	1.009
Testosterone	DM	1.75E+04	1.77E+04	1.010
11OH-prog^	DM	1.43E+04	1.44E+04	1.010
Diazepam	DM	2.72E+04	2.75E+04	1.011
Prazepam	DM	8.24E+04	8.30E+04	1.008
Temazepam	DM	1.21E+04	1.22E+04	1.006
Methylparaben	DM	8.28E+02	8.34E+02	1.008
Ethylparaben	DM	2.24E+03	2.26E+03	1.007

* Equal to $K_{m.w}$ at 10Å² divided by $K_{m/w}$ at 7.62Å²

^ Abbreviation of 11α-hydroxyprogesterone

The chosen occupied areas by drugs and the corresponding transfer free energies are shown in Table 5.10. The 95% confidence intervals of $\Delta G_{water \rightarrow interface}$ are also listed. It is not surprising that the error of $\Delta G_{water \rightarrow interface}$ becomes larger when the chosen area deviates from the fitted areas. For example, the errors of the transfer free energies are about 0.20kJ/mol for progesterone areas within ±10% of fitted areas. The error increases to 1.02kJ/mol when the maximum area of progesterone molecules is chosen. Open cells Table 5.10 represent those physically-impossible conditions were the test areas are less than the theoretical lower limits.

The micelle/water partition coefficients were calculated using the parameters in Table 5.10 with the results shown in Table 5.11. When the areas of the drugs are within 10% of the fitted optimal areas, the calculated micelle/water partition coefficients exhibit small deviations, between -17% and 19%, from the original values. When the minimum areas of the drugs are employed, the calculated $K_{m/w}$ values have greater deviations, between -22% and 74%, from the original results. If the maximum areas of model drugs are chosen, the predicted $K_{m/w}$ values have the greatest deviations, between -70% and 106%, from the original values. Because the maximum areas of all model drugs are further away from the fitted values than are the minimum areas, it is not surprising that the $K_{m/w}$ predictions using maximum areas of the drugs result in greater deviations from the values based on fitted occupied areas of the drugs compared to the predictions using minimum areas. To demonstrate the effect of a_{drug} term on the calculated $K_{m/w}$, Figure 5.13a shows the distributions of the ratios $K_{m/w}/K_{m/w}(a_{drug,exp})$ for four groups of interfacial areas occupied by drug substances. Clearly, employing maximum occupied areas of model drugs results in a broad distribution of results. In log units, the deviations range from -0.5 log unit (factor of 3) to 0.3 log unit (factor of 2). The average of the ratios also shifts to -0.15 log unit corresponding to 30% decrease of the micelle/water partition coefficient. Both groups with ±10% from the experimental areas have very tight distribution and the

Table 5.10, The dependence of free energy of transfer for model drugs from water to oil/water interface on varying interfacial area occupied by the drugs at oil/water interface. In order to test the sensitivity of calculated $K_{m/w}$ on a_{drug}, four interfacial areas were chosen: maximum area, minimum area and ±10% deviations from the experimental area.

Drug	Parameters	a_{max}	$a_{exp.}$ +10%	$a_{exp.}$ -10%	a_{min}
Progesterone	a(Å²)	104.4	63.8	52.2	39.6
	$\Delta G_{water \rightarrow interface}$ (kJ/mol)	-45.87 ±1.02	-42.33 ±0.20	-41.22 ±0.19	-39.89 ±0.38
Testosterone	a(Å²)	95.8	65.8	53.8	39.5
	$\Delta G_{water \rightarrow interface}$ (kJ/mol)	-38.16 ±0.50	-36.55 ±0.17	-35.79 ±0.15	-34.75 ±0.28
11α-hydroxy progesterone	a(Å²)	104.8	71.3	58.3	40.2
	$\Delta G_{water \rightarrow interface}$ (kJ/mol)	-39.95 ±1.06	-37.57 ±0.18	-36.52 ±0.18	-34.86 ±0.59
Diazepam	a(Å²)	86.2	50.8	-	42.7
	$\Delta G_{water \rightarrow interface}$ (kJ/mol)	-37.22 ±1.17	-34.78 ±0.18	-	-34.13 ±0.15
Temazepam	a(Å²)	84.9	45.5	-	-
	$\Delta G_{water \rightarrow interface}$ (kJ/mol)	-34.94 ±1.22	-32.28 ±0.17	-	-
Prazepam	a(Å²)	86.4	59.4	-	50.9
	$\Delta G_{water \rightarrow interface}$ (kJ/mol)	-41.36 ±0.75	-39.73 ±0.18	-	-39.17 ±0.14
Methylparaben	a(Å²)	62.0	35.1	28.7	24.5
	$\Delta G_{water \rightarrow interface}$ (kJ/mol)	-23.28 ±0.98	-21.51 ±0.15	-21.02 ±0.14	-20.67 ±0.24
Ethylparaben	a(Å²)	70.6	35.0	28.6	25.6
	$\Delta G_{water \rightarrow interface}$ (kJ/mol)	-27.09 ±1.38	-24.49 ±0.18	-23.93 ±0.16	-23.65 ±0.23
Butylparaben	a(Å²)	82.9	37.5	30.7	25.4
	$\Delta G_{water \rightarrow interface}$ (kJ/mol)	-36.60 ±2.35	-31.82 ±0.17	-30.99 ±0.16	-30.30 ±0.39

Errors are based on 95% confidence intervals.

Table 5.11, Calculated micelle/water partitioning coefficients using new parameter set (Table 5.10) corresponding to varying interfacial areas occupied by drugs at oil/water interface.

		Km/w Original	Km/w $a_{drug,max}$	Km/w a_{drug}+10%	Km/w a_{drug}-10%	Km/w $a_{drug,min}$
Progesterone	SDS	5.25E+05	7.41E+05	5.57E+05	4.93E+05	4.11E+05
Testosterone	SDS	7.33E+04	5.91E+04	7.19E+04	7.42E+04	7.29E+04
11OH-prog*	SDS	5.84E+04	6.11E+04	6.00E+04	5.67E+04	4.83E+04
Diazepam	SDS	9.84E+04	9.91E+04	1.00E+05	-	9.69E+04
Prazepam	SDS	2.82E+05	2.52E+05	2.79E+05	-	2.83E+05
Temazepam	SDS	3.68E+04	3.62E+04	3.75E+04	-	-
Methylparaben	SDS	3.66E+03	3.53E+03	3.68E+03	3.62E+03	3.54E+03
Ethylparaben	SDS	8.82E+03	9.45E+03	9.02E+03	8.62E+03	8.37E+03
Butylparaben	SDS	9.62E+04	1.98E+05	1.03E+05	8.93E+04	7.85E+04
Progesterone	DTAB	2.27E+05	1.58E+05	2.20E+05	2.33E+05	2.35E+05
Testosterone	DTAB	2.98E+04	1.39E+04	2.67E+04	3.30E+04	4.04E+04
11OH-prog*	DTAB	2.29E+04	1.30E+04	2.13E+04	2.46E+04	2.76E+04
Diazepam	DTAB	4.64E+04	2.54E+04	4.40E+04	-	4.81E+04
Prazepam	DTAB	1.27E+05	6.90E+04	1.15E+05	-	1.33E+05
Temazepam	DTAB	1.89E+04	9.56E+03	1.81E+04	-	-
Methylparaben	DTAB	1.84E+03	1.12E+03	1.76E+03	1.91E+03	1.99E+03
Ethylparaben	DTAB	4.57E+03	2.71E+03	4.45E+03	4.69E+03	4.77E+03
Progesterone	DM	1.50E+05	5.89E+04	1.35E+05	1.65E+05	1.94E+05
Testosterone	DM	1.75E+04	5.23E+03	1.45E+04	2.09E+04	3.04E+04
11OH-prog*	DM	1.43E+04	4.95E+03	1.22E+04	1.65E+04	2.32E+04
Diazepam	DM	2.72E+04	9.11E+03	2.44E+04	-	2.95E+04
Prazepam	DM	8.24E+04	3.02E+04	7.02E+04	-	8.99E+04
Temazepam	DM	1.21E+04	3.59E+03	1.10E+04	-	-
Methylparaben	DM	8.28E+02	3.48E+02	7.63E+02	8.95E+02	9.81E+02
Ethylparaben	DM	2.24E+03	8.25E+02	2.10E+03	2.39E+03	2.53E+03

*Abbreviation of 11α-hydroxyprogesterone

averages are within 5% from the unity. When minimum occupied areas are used, the ratios are between -0.11 and 0.24 log units. The average value is increased by 10%. In Figure 5.13b, the ratios $K_{m/w}/K_{m/w}(a_{drug,exp.})$ were calculated by changing a_{drug} term only without adjusting the transfer free energy term. When the maximum occupied areas of model drugs are employed, the predicted micelle/water partition coefficients are decreased dramatically. The average drop in the ratios is -0.7 log unit corresponding to 80% decreases. If the minimum occupied areas of solutes are used, the predicted $K_{m/w}$ values are increased with the average increment of 64%. For ±10% variations in a_{drug} the micelle/water partition coefficients are also significantly shifted: ~18% drop for $a_{drug}=1.1a_{drug,exp.}$ and ~22% increase for $a_{drug}=0.9a_{drug,exp}$.

Based on above analyses, if the correlations between two parameters, a_{drug} and ΔG_{trans} are considered, the predicted micelle/water partition coefficients are not sensitive to the occupied areas of model drugs when those areas are within 10% of their experimental values. On the other hand, if the chosen areas are far removed from the fitted areas, such as the maximum occupied areas, the predictions result in significant deviations up to a factor of 2 or 3 from the original calculations. If we ignore the correlations between the interfacial areas occupied by model drugs and transfer free energies of the drugs and only adjust the area term, the calculated $K_{m/w}$ values are much more sensitive than those with consideration of the correlations: even ±10% variations in a_{drug} term could produce ~ ±20% changes in the micelle/water partition coefficients.

Recalling that the determinations of ΔG_{trans} and a_{drug}, and the sensitivity of $K_{m/w}$ to these two parameters the requirement for highly accurate experimental result of γ~C is critical to the success of the prediction of $K_{m/w.}$

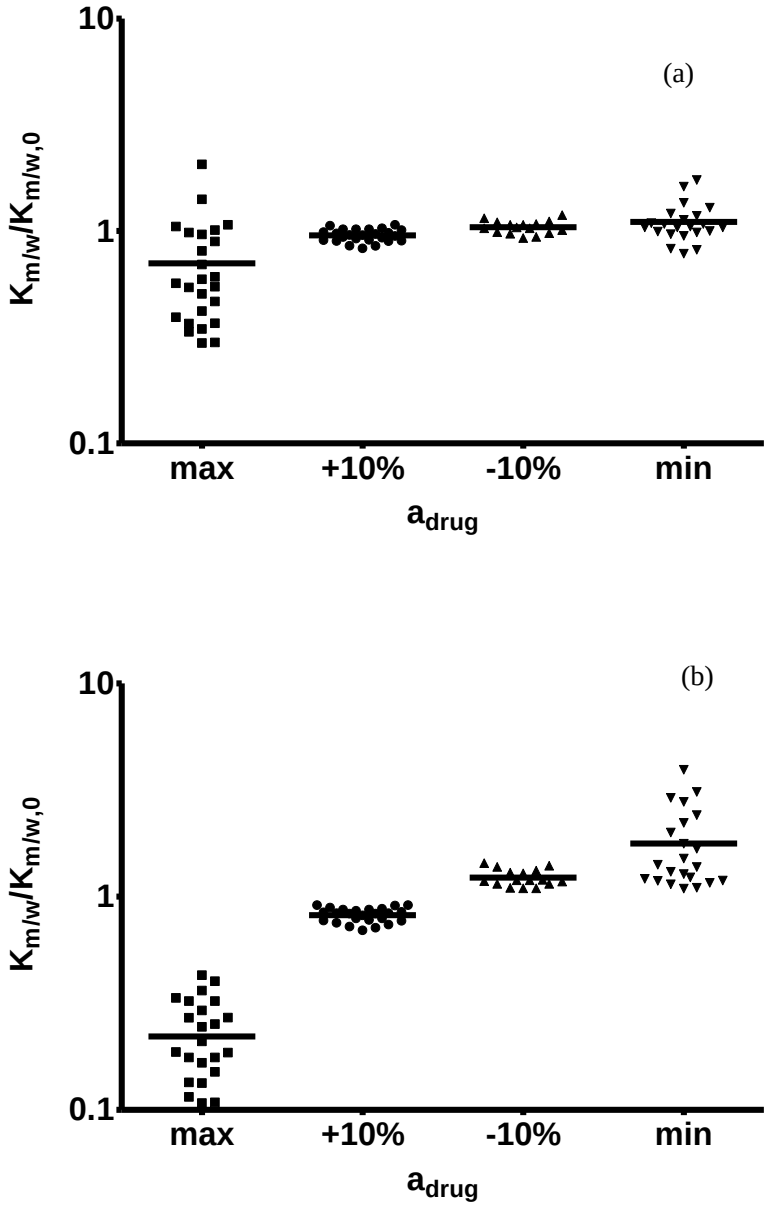

Figure 5.13a,b, The ratio of calculated micelle/water partitioning coefficient ($K_{m/w}$) using varying parameter, a_{drug}, and the micelle/water partitioning coefficient ($K_{m/w,0}$) using experimentally determined interfacial area occupied by drugs (a_{drug}). Four groups of a_{drug} values were chosen: the maximum and minimum interfacial areas, ±10% variations from $a_{drug,exp}$. (a) Another parameter, ΔG_{trans}, was allowed to vary with changing a_{drug} to best fit the oil/water interface adsorption experiment of drugs (Fig. 5.3~5.5); (b) The parameter ΔG_{trans} was fixed with changing a_{drug} in the calculations of $K_{m/w}$.

5.3.5. Effect of Salt on the Micelle/water Partitioning Coefficients

In section 3.3.2, the $K_{m/w}$ values of three model drugs, progesterone, diazepam and methylparaben, in ionic micelle systems (SDS and DTAB) were observed to decrease in the presence of 0.15N NaCl. The reduction of $K_{m/w}$ of model drugs in ionic micelles could be explained by the changes in micelle structure due to the added salt. Literature referneces (Hiemenz and Rajagopalan, 1997; Ueno and Asano, 1997) show the increase of aggregation number of ionic micelles by addition of NaCl. From our NMR studies on diffusivity of micelles in Chapter 7, the micelles show significant decreases in size. According to our surface-localized model, the increasing N_{aggre} with decreased r will decrease the area per surfactant at micelle surface, A, and increase the surface pressure, π. These changes indicate there is less space on the micelle surface to solubilize drug molecules. The large surface density of surfactant molecules makes the adsorption of drug less favorable. Equations (A2.4) and (A2.14) clearly demonstrate that reducing A and increasing π will result in smaller values for $K_{m/w}$.

5.3.6. Solubilization Isotherm Simulations - Moving Beyond the Dilute Solution Condition

The above simulations were based on dilute condition of the solubilizates. On the other hand, the solubilization capacity of a micelle system which was related to saturated condition of the solute was more relevant in practical design of drug delivery system. Indeed, the majority of measured micelle/water partition coefficients are carried out under saturated conditions. In this section, the $K_{m/w}$ values at finite solute concentrations will be studied. We extend the surface-localized model to finite solute concentrations. The detailed derivations are shown in Appendix 2.2. Unlike the dilute condition where the final results of $K_{m/w}$ have a clear expression as Eq.(A2.13) and (A2.14), the calculated $K_{m/w}$ at finite solute concentration involve a numerical solving of Eq. (A2.20) and (A2.21)

for surface pressure, π, at the micelle surface. The micelle/water partition coefficients are calculated using Eq. (A2.22) and (A2.23).

There are limited experimental results of the solubilization isotherm for our interested systems in literature. Goto and Endo reported the experimental $K_{m/w}$ values of three parabens in SDS solutions as a function of drug concentration using gel filtration technique (Goto and Endo, 1978). We applied our extended surface-localized model to calculate the solubilization isotherms in these parabens-in-SDS systems in order to test the accuracy of the model. The results of the simulations of three parabens in SDS solutions are shown in Figures 5.14~5.16, where the ratio of $K_{m/w}$ at finite drug concentration (experimental) to that predicted by applying the dilute condition is plotted as a function of mole fraction of drug in micelles. In general, the model successfully predicts the overall trend of the micelle/water partitioning, but the deviations from the model increase with drug concentration. The experimental slopes for three parabens solubilized in SDS solutions were -1.77 (methylparaben), -1.84 (ethylparaben) and -1.87 (butylparaben) while the predicted slopes were -1.15 (methylparaben), -1.14 (ethylparaben) and -1.15 (butylparaben). The deviations of the predictions were between 35~39%. As has been experimentally observed in many other micelle solubilization systems (Christian et al., 1986; Lee et al., 1990; Goto and Endo, 1978; Croy and Kwon, 2005), micelle/water partition coefficients tend to decrease with increasing concentration. The drop of $K_{m/w}$ (experimental) with increasing drug concentration is likely mainly due to the nature of surface adsorption of solutes. As drug concentration in the system increases, it is likely that the density of solutes on the oil/water interface would approach a saturated state. Saturating the surface would be expected to lower the partitioning coefficient between interface and bulk water at higher solute concentration. For example, under saturated condition of solutes, the maximum mole ratios of drug to surfactant were 0.56 (methylparaben), 0.48 (ethylparaben) and 0.64 (butylparaben). The significant

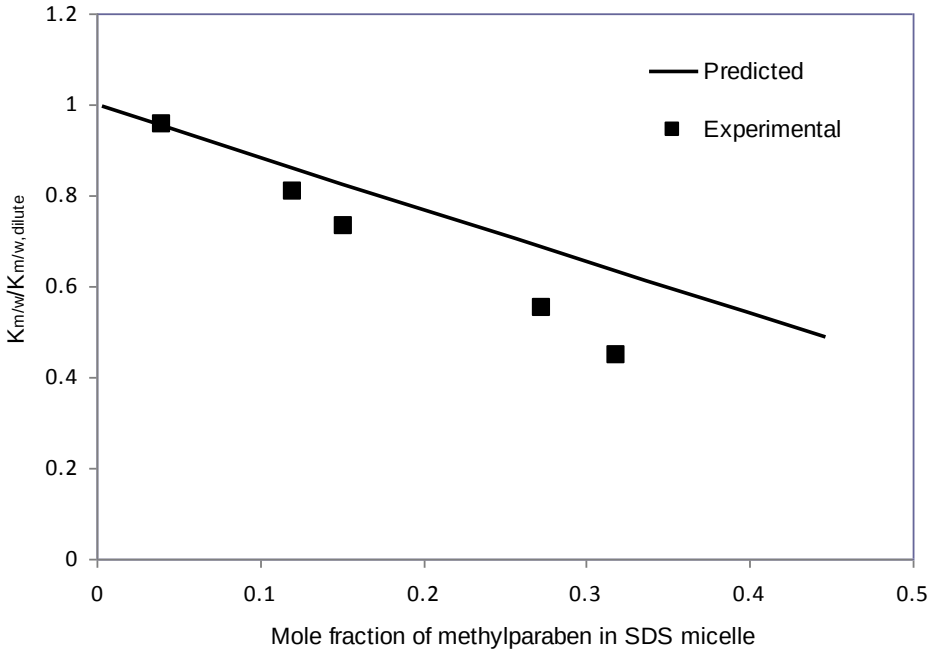

Figure 5.14, Experimental and predicted solubilization isotherms for methylparaben in SDS micelles. Experimental data are from Goto and Endo (Goto and Endo, 1978).

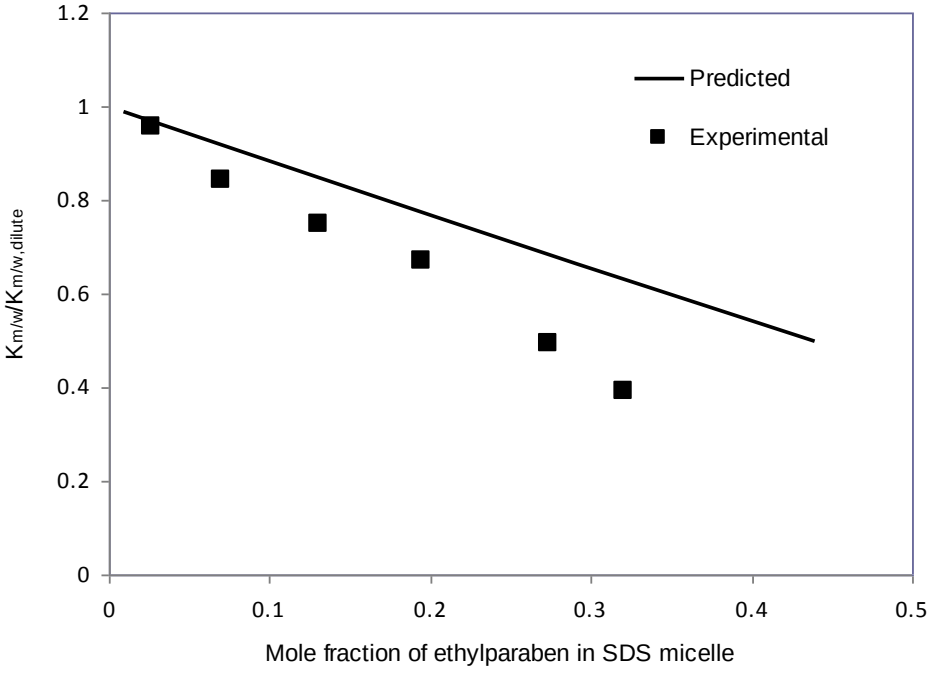

Figure 5.15, Experimental and predicted solubilization isotherms for ethylparaben in SDS micelles. Experimental data are from Goto and Endo (Goto and Endo, 1978).

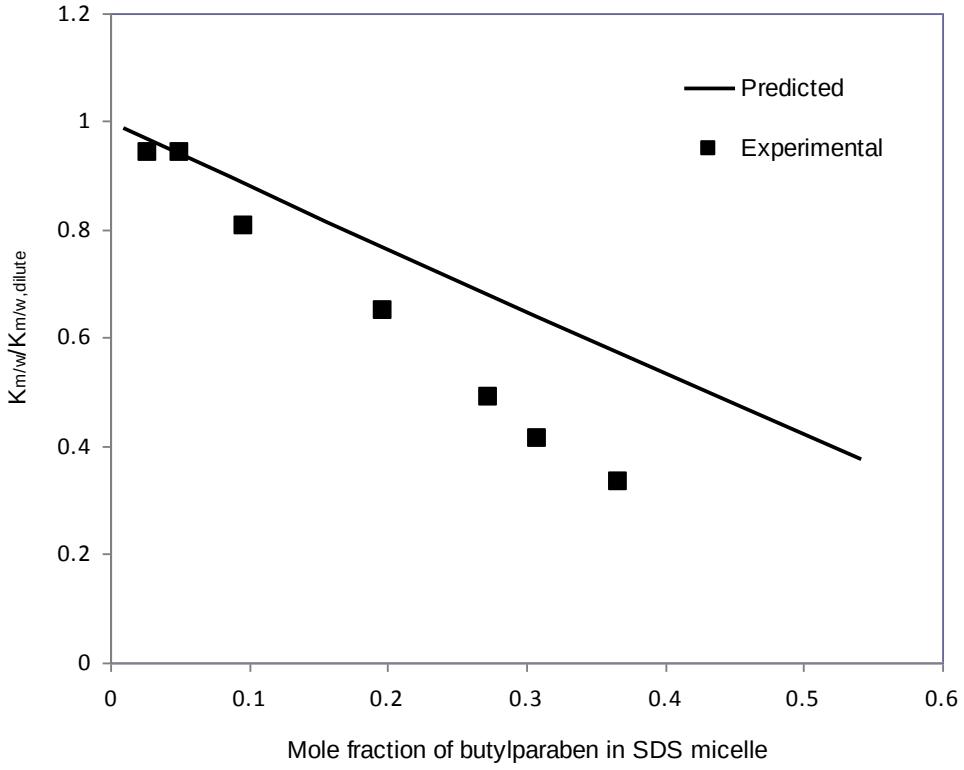

Figure 5.16, Experimental and predicted solubilization isotherms for butylparaben in SDS micelles. Experimental data are from Goto and Endo (Goto and Endo, 1978).

change in the composition of the micelle brought about by the high fraction of solute would induce an assembly that is far removed from that of a dilute solution. The assumption used in the model that micelle size was not affected by the solubilization of the drug would not be expected to be true given the dramatic changes in micelle structure. The model sensitivity test in section 5.3.4 showed even a small change in micelle size could produce significant changes in micelle/water partition coefficients. For instance, the deviation of 1Å in radius of SDS micelles could result in 28% changes in $K_{m/w}$ for methylparaben. The PGSE NMR studies in Chapter 7 will show there was no significant change in micelle size in the presence of solutes, but the conclusion only held within the experimental detection limit that was larger than 1Å. Another assumption of the model was the small changes in Laplace pressure, due to the presence of the solubilizates, were not considered in the co-adsorption between drugs and surfactants at the micelle surface. The assumption would hold at low drug concentration but would induce larger errors at high drug concentration and would likely contribute to the deviations of the predictions from experiments.

In addition to the parabens in SDS micelle systems, we also examined the micelle/water partition coefficients of all 9 model drugs in three surfactant systems at saturated condition. The calculated $K_{m/w}$ values under dilute and saturated conditions as well as experimental micelle/water partition coefficients are listed in Table 5.12 for comparison. The ratios between $K_{m/w}$ (saturated) and $K_{m/w}$ (dilute) were calculated and shown in Table 5.12. The ratios represented the effect of finite concentration of solute on the micelle/water partitioning. Interestingly, the majority of the ratios were quite close to 1: 16 out of 25 ratios were greater than 0.85 and another 4 ratios were between 0.7 and 0.85. For these systems, high drug concentration made little effect on the micelle/water partitioning coefficients. The predicted $K_{m/w}$ using dilute condition provided good estimations of the micelle/water partitioning at saturated drug concentrations. Only 5 out

of 25 ratios had smaller values than 0.7: 0.49 for methylparaben in SDS micelles, 0.52 for ethylparaben in SDS micelles, 0.32 for butylparaben in SDS micelles, 0.65 for methylparaben in DTAB micelles and 0.67 for ethylparaben in DTAB micelles. The influences of finite drug concentration on micelle/water partitioning were the greatest when the three parabens were solubilized in SDS solutions. The experimental ratios of $K_{m/w}$ between dilute and saturate conditions were 0.44 (methylparaben), 0.41 (ethylparaben) and 0.28 (butlyparaben) that were quite close to our predicted ratios. Another two cases when finite solute concentration had significant effects on $K_{m/w}$ values were methylparaben and ethylparaben solubilized in DTAB micelles. For the 5 cases which had the lowest ratios, the corresponding solubilization capacities were the highest among all 25 systems with the minimum of 0.47. The 4 systems that had the medium ratios of $K_{m/w}$(saturated)/$K_{m/w}$(dilute) between 0.7 and 0.85 also had quite high solubilization capacities that were between 0.22 and 0.42. The only exceptions that high solubilization capacity resulted in low ratio of $K_{m/w}$(saturated)/$K_{m/w}$(dilute) were methylparaben and ethylparaben in DM micelle systems. The solubilization capacities of DM micelles were 0.42 (methylparaben) and 0.36 (ethylparaben) but the ratios were both 0.85. Compared to ionic surfactants SDS and DTAB, the solubilization in nonionic DM micelles were less sensitive to the solute concentrations in micelles.

Figure 5.17 illustrates the comparisons between experimental and predicted micelle/water partition coefficients at the saturated solute concentrations. The overall predictions were in good agreements with experiments. Predicted $K_{m/w}$ did not deviate by more than a factor of 2 from the experimental values. Most of the predictions (17 out of 25) were within factor of 1.5 from the experiments. The R-square was 0.953. The results strongly supported the applicability of the surface-localized model to micellar solubilization.

Table 5.12, Calculated micelle/water partitioning coefficients under dilute condition (shown early in section 5.3.3 Table 5.5) and non-dilute condition (saturated solution) compared to experimental micelle/water partitioning coefficients (mainly under saturated condition). The ratios of $K_{m/w}$(saturated solution) and $K_{m/w}$(dilute condition) are listed.

		Km/w dilute	Km/w saturated	Ratio	Km/w exp.
Progesterone	SDS	5.25E+05	3.83E+05	0.73	3.69E+05
Testosterone	SDS	7.33E+04	6.31E+04	0.86	1.14E+05
11OH-prog*	SDS	5.84E+04	4.58E+04	0.78	6.75E+04
Diazepam	SDS	9.84E+04	7.19E+04	0.73	8.93E+04
Prazepam	SDS	2.82E+05	2.50E+05	0.89	4.03E+05
Temazepam	SDS	3.68E+04	2.86E+04	0.78	4.70E+04
Methylparaben	SDS	3.66E+03	1.78E+03	0.49	3.24E+03 (dilute) 1.42E+03 (saturat.)
Ethylparaben	SDS	8.82E+03	4.56E+03	0.52	8.51E+03 (dilute) 3.48E+03 (saturat.)
Butylparaben	SDS	9.62E+04	3.09E+04	0.32	7.24E+04 (dilute) 2.04E+04 (saturat.)
Progesterone	DTAB	2.27E+05	1.94E+05	0.85	1.79E+05
Testosterone	DTAB	2.98E+04	2.79E+04	0.94	5.40E+04
11OH-prog*	DTAB	2.29E+04	2.06E+04	0.90	3.57E+04
Diazepam	DTAB	4.64E+04	3.93E+04	0.85	2.94E+04
Prazepam	DTAB	1.27E+05	1.19E+05	0.94	8.76E+04
Temazepam	DTAB	1.89E+04	1.64E+04	0.87	1.67E+04
Methylparaben	DTAB	1.84E+03	1.20E+03	0.65	1.73E+03
Ethylparaben	DTAB	4.57E+03	3.06E+03	0.67	4.28E+03
Progesterone	DM	1.50E+05	1.36E+05	0.91	9.49E+04
Testosterone	DM	1.75E+04	1.69E+04	0.97	3.09E+04
11OH-prog*	DM	1.43E+04	1.34E+04	0.94	1.32E+04
Diazepam	DM	2.72E+04	2.50E+04	0.92	2.10E+04
Prazepam	DM	8.24E+04	7.96E+04	0.97	6.51E+04
Temazepam	DM	1.21E+04	1.13E+04	0.93	9.63E+03
Methylparaben	DM	8.28E+02	7.05E+02	0.85	1.16E+03
Ethylparaben	DM	2.24E+03	1.91E+03	0.85	2.85E+03

*Abbreviation of 11α-hydroxyprogesterone

5.3.7. Effect of Solutes on CMC of Micelles – Influence of Laplace Pressure

A very interesting phenomenon observed commonly during micelle studies is the reduction of critical micelle concentration (CMC) upon solubilization of drug. Goto and Endo systematically studied the CMC of SDS micelles as a function of aqueous concentrations of three parabens (Goto and Endo, 1978). In this section, we apply the Laplace pressure effect to quantitatively predict the decline of CMC with increasing drug concentrations. The detailed derivations of the model are shown in Appendix 2.3. The development of the theory can be divided into 2 steps: the first step is the introduction of solutes to micelle surface lowers the surface pressure and thus decreases the Laplace pressure; the second step is the surfactant molecules, subject to Laplace pressure, will have a lower transfer free energy from bulk water to micelle surface and thereby decreasing the CMC.

Figure 5.18 compares the predicted and experimental CMCs of SDS micelles as a function of aqueous concentrations of three parabens. The overall predictions are quite good. The model successfully predictes the decreasing trend of CMC with increasing drug concentration and also the slope of the CMC reduction with respective to drug concentration. Under the condition of equal solute concentration, butylparaben produced the greatest drop of CMC because that solute is the most surface active at oil/water interface. According to Eq. (A2.25) and (A2.26), the greatest negative transfer free energy of butylparaben (ΔG_{trans}=-31.4kJ/mol) could increase the surface pressure and lower the Laplace pressure to the greatest extent, resulting in the greatest drop in the CMC.

The successful predictions of the CMC~Conc. curves support the existence and importance of the Laplace pressure in micelle systems. The predictions are based on two assumptions: (1) the micelle size is not significantly affected by the addition of solutes;

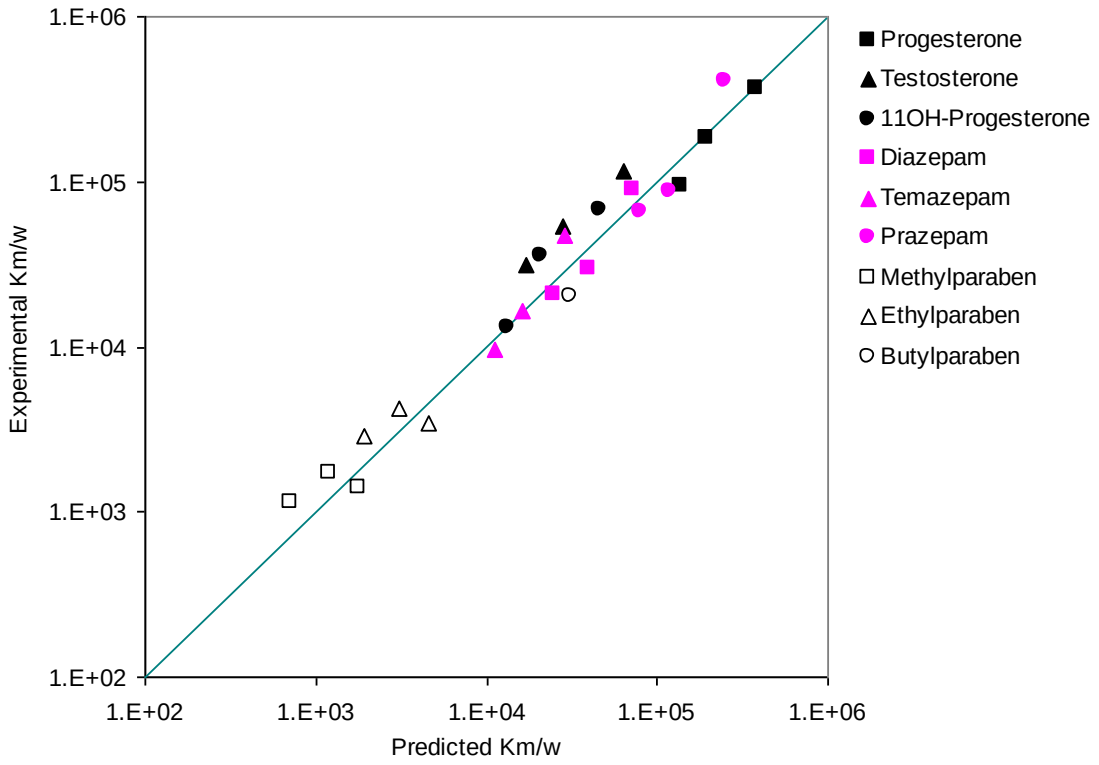

Figure 5.17, Comparison between experimental and predicted micelle/water partitioning coefficients ($K_{m/w}$) of 9 model drugs in 3 surfactant systems under saturated condition of drugs.

(2) The activity (free energy level) of surfactant at micelle surface is not changed with increasing solute concentration. The second assumption is important because it will change the monomer concentration of surfactant (CMC) and not the micelle structure as a consequence of the change of transfer free energy from bulk water to micelle surface.

5.4. CONCLUSION

A surface-localized thermodynamic model was successfully applied to predict the micelle/water partitioning coefficients of 9 model drugs in 3 micelle systems. The thermodynamic model was employed to calculate (1) the transfer free energies of model drugs from aqueous solution to oil/water interface; (2) the occupied areas of drugs at the oil/water interface. The greater the negative transfer free energy and the smaller the occupied interfacial areas by the drug molecules, the greater the micelle/water partition coefficients. For three model surfactants, the larger surface pressure at micelle surface correlated to lower solubilization capacity of the micelles. The successful predictions of micelle/water partitioning coefficients using surface-localized model support the following conclusions: (1) the model hydrophobic drugs are predominantly located at the surface region of the micelles; (2) the co-adsorption to the micelle surface by drugs and surfactants is the main mechanism of micellar solubilization; (3) the 2-D solution adsorption model is successfully applied to the hydrocarbon-water interface system and the relationship between drugs and surfactants is mainly pure competition without their specific interactions; (4) Laplace pressure exhibits a significant effect on micelle/water partitioning of the model drugs and can not be ignored.

The sensitivities of the predicted micelle/water partition coefficients to the chosen parameters were tested. The $K_{m/w}$ values were sensitive to the radius of the micelles with constant aggregation number of the micelles. Many parameter pairs were strongly

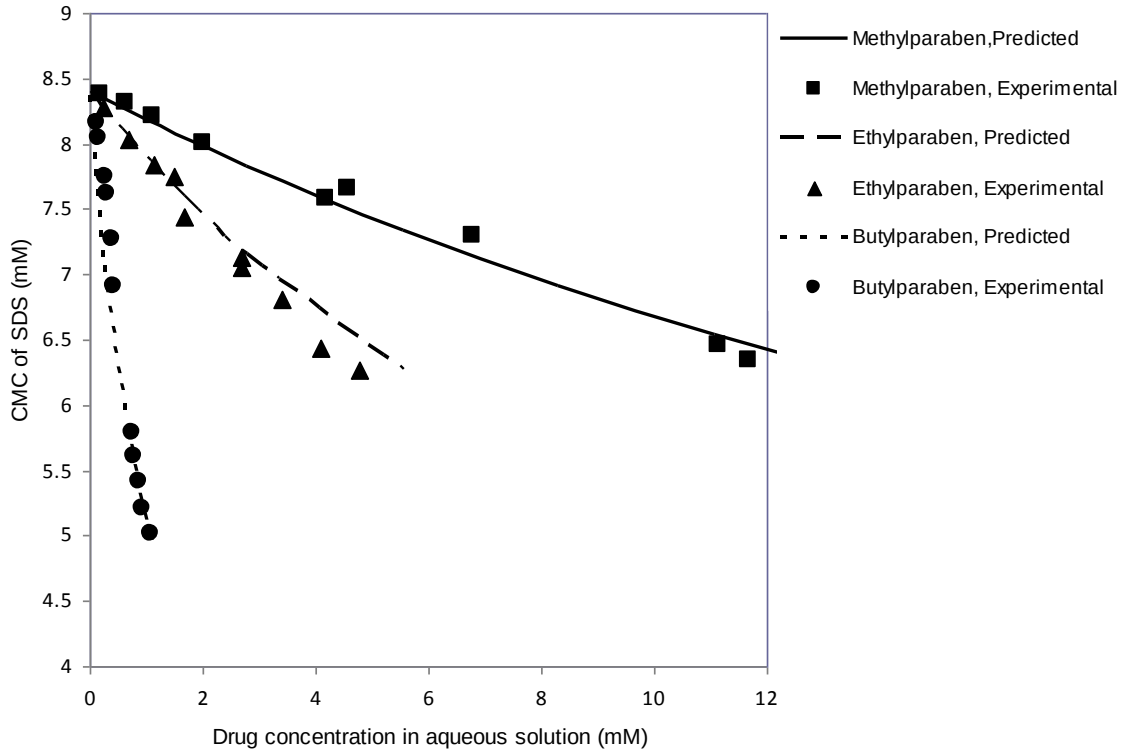

Figure 5.18, Predicted and experimental CMCs of SDS as a function of drug concentration in aqueous solutions. The experimental data are from Goto and Endo (Goto and Endo, 1978).

correlated with each other, for examples, aggregation number and radius of micelles, interfacial area occupied by drug molecules and transfer free energy of drug substance from water to oil/water interface. If the correlations of those parameter pairs were considered, the predicted micelle/water partitioning coefficients were not sensitive to the aggregation number of the micelles (50s~100 for SDS and DTAB, 113~130 for DM), interfacial area occupied by water molecules (7.6~10Å^2) and the interfacial area occupied by drug molecules (<10% variation). The insensitivity of the predictions to those chosen parameter reflected the robustness of the surface-localized model.

The model was extended to study some other micellar solubilization properties: salt effect, solubilization isotherm, CMC depression effect by solutes. The addition of salts to the surfactant solutions resulted in a decreased micelle/water partition coefficient for ionic micelle systems. This phenomenon could be explained by increasing aggregation number of micelles due to the screening of electrostatic forces between charged headgroups in the presence of salt while the micelle size was decreased. The model clearly showed the above changes could cause decrease in the micelle/water partition coefficients.

The surface-localized model was extended to finite solute concentration. The simulated solubilization isotherms for parabens solubilized in SDS micelles were compared to experiments from literature. The model successfully simulated the trend of $K_{m/w}$~C_{drug} curves but could not predict the slope of the curves accurately. The micelle/water partition coefficients of 9 model drugs in 3 micelle systems at saturated condition of model drugs were calculated and the results were in good agreements with experimental values.

The CMC of SDS micelles were observed to decrease with increasing concentration of parabens. The Laplace pressure acting on surfactant molecules were considered in the

thermodynamic model simulations. The quantitative predictions of CMC~C_{drug} curves coincided with experiments very well.

Chapter 6

Molecular Simulation Studies on the Orientations of Model Drugs at Oil/water Interface

6.1. INTRODUCTION

To understand the solubilization mechanism of hydrophobic drugs in micelle system, the location, orientation and amount of hydrophobic drugs solubilized in the lipid assembly are important factors to be considered. The three factors are interdependent. For instance, the maximum amount of drugs in micelles is dependent on the location and orientation of the model drugs in micelles.

The location and amount of model hydrophobic drugs in micelle systems have been extensively studied in last three chapters based on a framework of a thermodynamic model. A surface-localized thermodynamic model considering the co-adsorption of drug and surfactant molecules for micelle surface successfully predicted the micelle/water partition coefficients. Sensitivity analysis of the model illustrated that the areas occupied by model drugs at micelle surface could influence the micelle/water partitioning (Section 5.3.4.4). The larger occupied interfacial areas are correlated with less solubilized drugs in micelles. For example, a 10% increase in the area could decrease the micelle/water partition coefficient by 20% under assumption that other parameters, such as $\Delta G_{\text{water}\rightarrow\text{interface}}$, remain constant. The interfacial areas occupied by model drugs are dependent on the size and orientation of the drugs. Since the size of a specific drug is fixed, the orientation of the drug localized at the micelle surface would be important to the solubilization capacity. Understanding the orientation of drug substances in micelles may also be critical to the chemical stability of solubilized drugs because of the anisotropic local environment that may protect chemically-vulnerable functional groups.

So far, little is known about the orientation of model drugs at the micelle surface. In the literature, NMR technique was employed to detect the intermolecular interactions as well as microenvironment of different functional groups in order to infer the orientation of solubilizates in micelles (Hawrylak and Marangoni, 1999; Heins et al., 2007; Gjerde et al., 1998; Ueno and Asano, 1997; Nagaonkar and Bhagwat, 2006; Suratkar and Mahapatra, 2000;). These studies have advantages in probing selective regions of the solute molecule in aqueous or oil phases. The methods do not give detailed information such as the angles between the long axes of solutes with the oil/water interface. The angles would affect the interfacial areas occupied by model drugs and the micelle/water partition coefficients.

In this chapter, the experimental interfacial areas occupied by model drugs from the adsorption studies at dodecane/water interface (Section 5.3.1) were used to infer the orientation of the drugs at oil/water interface. A molecular simulation method was employed to calculate the possible cross-section areas of the drug molecules along any defined directions. By matching the calculated areas with experimental values and applying chemical intuition (considerations on hydrophilic/hydrophobic interactions and surface energies), the orientations of the drug molecules at oil/water interface, specifically the angles between the drug and interface, could be determined.

6.2. METHODS

6.2.1. Molecular Structures of Isolated Drug Molecules

There were three ways of obtaining three-dimensional molecular structures of single drug molecule. The following methods were taken in order:

(1) If the crystal structures of model drugs were reported in literature and the complete molecular structure information including the fractional coordinates of all atoms was

available, the molecular structures of the single drug molecule were extracted from the reported crystal structure data.

(2) If the crystal structures of model drugs were reported in literature and the partial molecular structures including only the fractional coordinates of heavy atoms were available, the partial molecular structures of the single drug molecule were extracted from the reported crystal structure data and hydrogen atoms were added afterwards employing Hyperchem® software (Hyperchem, 2001).

(3) If there was no reported crystal structure of model drugs that included the molecular details, the molecular structure was built and optimized using quantum chemistry software. In our studies, GaussView® software (Frisch et al., 2000) was employed to build the molecule according to its chemical structure and Gaussian03® software (Frisch et al., 2003) was used to optimize the structure based on minimum-energy principle. The calculation technique used in structure optimization was Hartree-Fock method combined with Pople's 6-31G** basis set.

6.2.2. Defining the Boundary of Isolated Molecules

To calculate the cross-section area of a molecule, the boundary of the molecule was defined as the "molecular shell". In our studies, an isosurface of electron densities of the molecule was used as the molecular boundary. The electronic structure of drug molecules was calculated using Hartree-Fock method with 6-31G** basis set. The calculations were carried out using Gaussian 2003 software. A three dimensional grid of electron densities for the drug molecules was generated from the electronic structures described as wave functions of electrons solved from Hartree-Fock equation. The resolutions of the grid were 10 points/Å along all three directions.

To define the molecular boundary, the isovalue of the isosurface of electron densities was chosen so as to match the enclosed volume of the isosurface to experimental partial molar volume of the drugs. The isovalue for electron densities was kept constant for all model drugs. The generation of isosurface from the 3-D grid of electron densities and the calculations of the enclosed volume by the isosurface were performed using self-written computer program with C language.

6.2.3. Calculation of Cross-section Areas along All Possible Directions

To make the calculation more convenient, the Cartesian coordinates of drug molecules were fixed while the orientations of oil/water interface were varied. The normal of the interface was used to describe the orientation of the plane and a pair of angles (θ, φ) was sufficient to represent all possible directions of the normal. The vector of the normal with angles (θ, φ) was ($\sin\theta\cos\varphi$, $\sin\theta\sin\varphi$, $\cos\theta$) ($0<\theta<\pi$, $0<\varphi<2\pi$). Once the orientation of the interface was defined, a series of planes parallel to the orientation would cut through the body of the molecular shell. For each plane, the cross-section area was calculated based on the intersection between the plane and the molecular shell. Among those cross-section areas corresponding to the parallel planes, the maximum area was chosen for the specific orientation. The above calculations were carried out for all possible orientations chosen as follows:

$$\begin{cases} \theta = \dfrac{\pi}{2n} i & i = 0 \sim n \\ \varphi = \begin{cases} 0 & for\ i = 0 \\ \dfrac{\pi}{2i} j & j = 1 \sim 4i \quad for\ i > 0 \end{cases} \end{cases} \tag{6.1}$$

The orientations shown in above equation only covered half of a sphere. Because the calculations had an inversion symmetry: the area calculated for orientation with normal (x, y, z) was same with the area for orientation (-x, -y, -z). Therefore half sphere is sufficient to represent all possible directions. The parameter *n* determined the resolution

of the orientations that was approximately $90^o/n$. The larger *n* corresponded to higher resolution. In our studies, a value of 18 was chosen for *n* with the resolution of the orientations equal to 5^o. The simulations were carried out using self-written C program.

6.2.4. Visualizations of the Molecules, Isosurfaces of Electron Densities, and Cutting Planes

The visualizations of the drug molecules, molecular shells, and the cutting planes that represented the oil/water interface were realized using OpenDX® software (OpenDX). A ball-and-stick model was used to show the molecular structure. Different atoms were color coded and had different radii. The molecular shells that represented the molecular boundaries were made half-transparent in order to illustrate the molecular structures inside. The intersection between the molecular boundary and the cutting plane was clearly demonstrated. The cutting plane was also mapped with electron densities. Areas with red color had highest electron density while areas with blue color had lowest electron density. The axes of 3-D Cartesian coordinates were shown beside the molecules with the gridlines. The scales had a unit of Å.

6.3. RESULTS AND DISCUSSION

6.3.1. Molecular Structures of Model Drugs

Of the model compounds, progesterone, testosterone, 17β-estradiol, 11α-hydroxyprogesterone, diazepam, temazepam and methylparaben had reported crystal structures that included complete molecular structures (Allen, 2002). The molecular structures could be extracted from those reported structure data. Another three drugs, oxazepam, prazepam and ethylparaben, had reported crystal structures that included partial molecular structures that only had coordinates of heavy atoms (Allen, 2002; Lin, 1986). These molecular structures were completed by adding hydrogen atoms using Hyperchem® software. Figure 6.1 uses prazepam as an example to illustrate the molecular structure extracted from literature without hydrogen atoms, Fig. 6.1a, and molecular structure with added hydrogen atoms using Hyperchem® program, Fig. 6.1b. Butylparaben has no reported crystal structure containing detailed molecular structure. The molecular structure of butylparaben was built according to its chemical structure using GaussView® program. One advantage of using GaussView to draw molecular structures was the program provided initial bond lengths and bond angles that were close to true values so that the following structure optimization calculations were more efficient. The molecular structure was optimized using Hartree-Fock/6-31G** method and the calculations were carried out using Gaussian03® software. The optimized structure of butylparaben is shown in Figure 6.2.

6.3.2. Determination of Molecular Boundaries

The molecular boundary was defined using an isosurface of electron densities of the molecules. The cut-off electron density, or the isovalue of the isosurface, was chosen so as to match the enclosed volume by the isosurface to the experimental occupied molecular volume. The experimental occupied volumes of model drugs were estimated

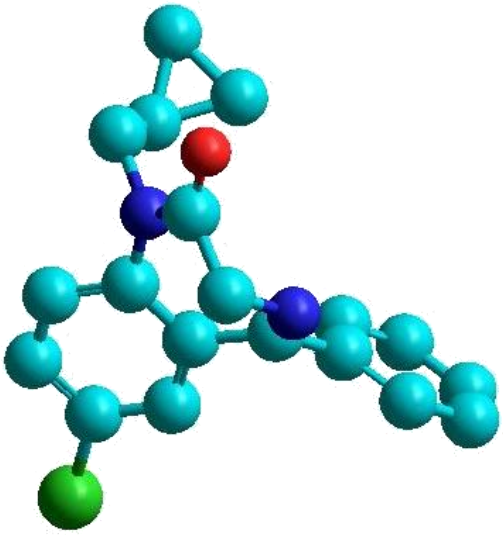

a

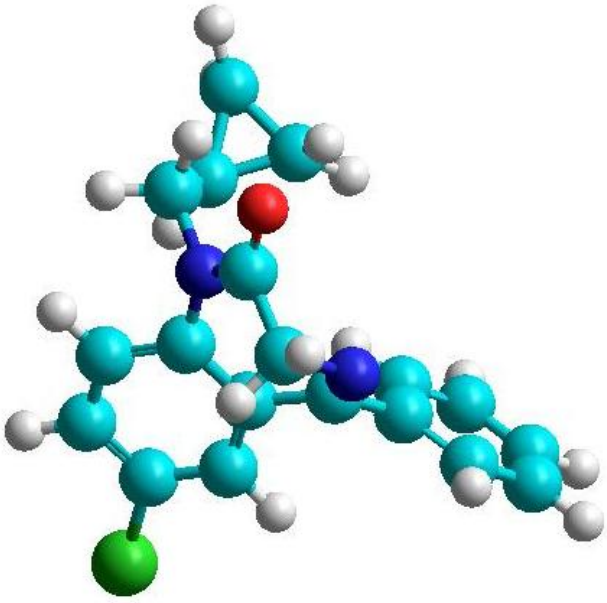

b

Figure 6.1, (a) The molecular structure of prazepam extracted from reported crystal structure (Allen, 2002) without coordinates of hydrogen atoms; (b) The molecular structure in (a) was added with hydrogen atoms using Hyperchem® software.

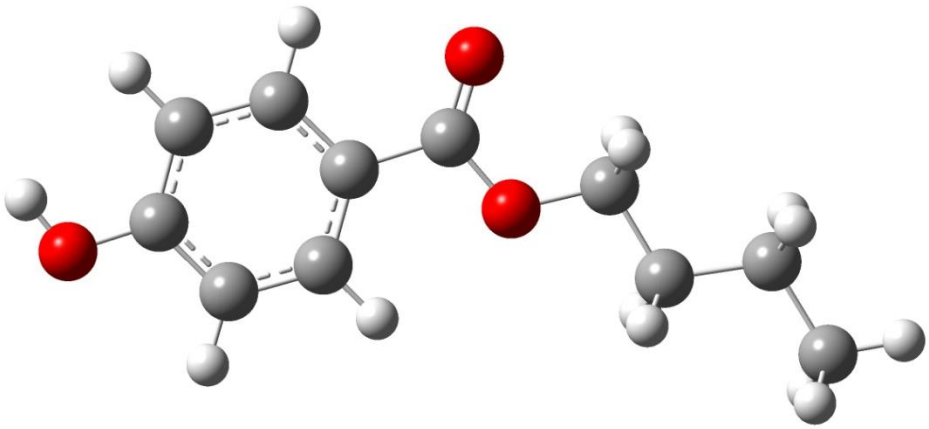

Figure 6.2, The optimized molecular structure of butylparaben using Hartree-Fock /6-31G** method with the aid of Gaussian03® program (Frisch et al., 2003).

using the reported crystal structures and the results shown in Table 5.1. In Table 6.1, the enclosed volumes by the isosurface of electron densities using different isovalues were calculated and compared with experimental occupied molecular volumes. Using least square fitting, the isovalue ρ=0.00065e/bohr^3 gave the best matches between calculations and experiments. The comparisons between calculated and experimental occupied volumes by isolated model drugs are shown in Figure 6.3. The predictions coincide well with the experimental results.

6.3.3. Determining Orientation of Model Drugs by Matching Calculated Interfacial Areas Occupied by Model Drugs to Experimental Areas

The theoretical areas occupied by model drugs at oil/water interface could be calculated as the cross-section areas of the molecular shells with a cutting plane representing the oil/water interface. Since the actual orientations of the model drugs at oil/water interface were unknown, exhaustive searches were carried out for all possible orientations. For each orientation, a cross-section area could be calculated and compared to the experimental value (see section 5.3.1). The matching between the calculations and experiments could indicate the possible orientations of the drugs at oil/water interface.

In our simulations, a fixed molecule with changing cutting planes was more convenient in calculating the cross-section areas than a fixed cutting plane with changing molecular positions and orientations. From the computational point of view, the above two cases were equivalent to each other.

The orientations of the cutting planes were described using two angles, θ and φ ($0<\theta<\pi$, $0<\varphi<2\pi$). A total number of 685 "molecular slices" with the resolution of 5^o were considered to calculate the corresponding cross-section areas. In Table 6.2, the

Table 6.1, The calculated occupied volumes of isolated molecules using different isovalues of the isosurfaces of electron densities compared to experimental occupied volumes for all model drugs.

Model drugs	The calculated occupied volumes of isolated molecules (Å³) using the following isovalue of electron density (e/bohr^3)						Experimental occupied volume(Å³)
	0.0005	0.00055	0.0006	0.00065	0.0007	0.0008	
progesterone	444.7	436.9	429.9	423.3	417.3	406.4	441.3
testosterone	416.9	408.9	402.3	396.3	390.7	380.6	406.9
17 β-estradiol	389.7	382.7	376.4	370.6	365.2	355.6	370.2
11OHprog*	457.8	450.0	442.9	436.4	430.3	419.4	450.7
diazepam	371.5	364.6	358.3	352.5	347.1	337.5	344.3
oxazepam	365.0	358.3	352.2	346.6	341.5	332.2	330.5
prazepam	447.6	439.5	432.1	425.4	419.1	407.7	417.7
temazepam	380.1	375.1	368.7	362.8	357.4	347.7	356.7
methylparaben	203.3	199.3	195.6	192.3	189.2	183.7	182.7
ethylparaben	238.1	233.4	229.1	225.1	221.5	215.0	213.8
butylparaben	289.9	284.2	279.0	274.2	269.9	262.0	259.2

*Abbreviation of 11α-hydroxyprogesterone

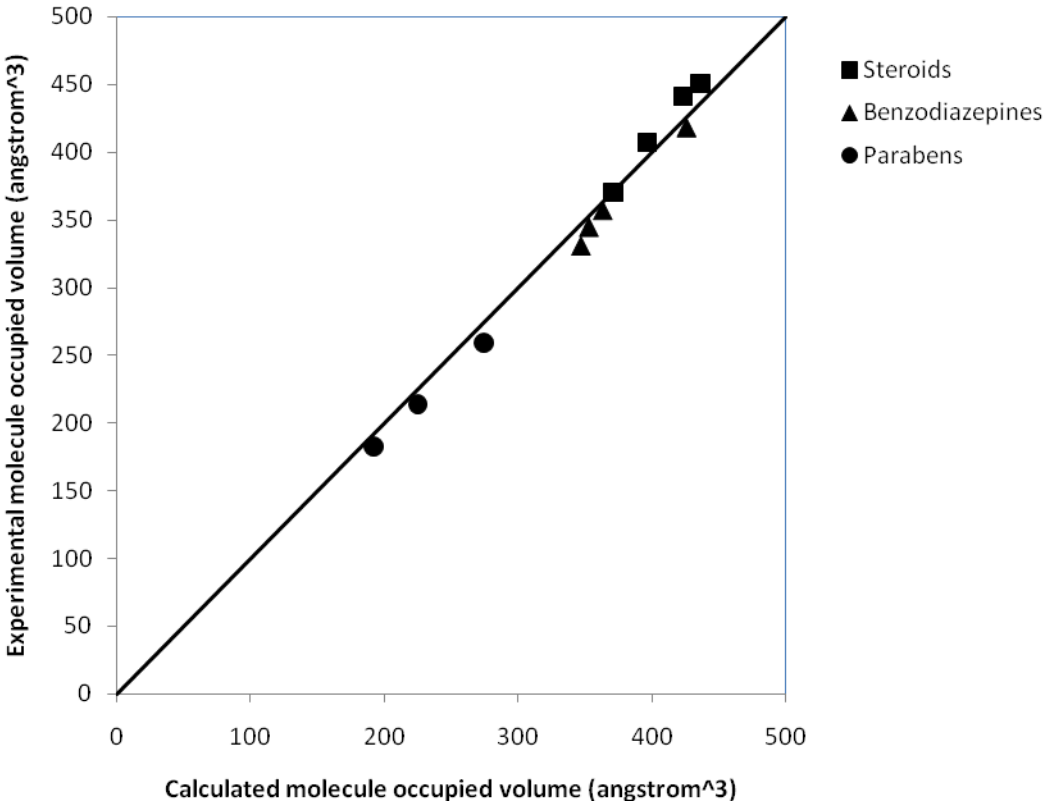

Figure 6.3, The comparisons between calculated and experimental occupied volumes by isolated model drug molecules. The calculated occupied volumes were based on a cut-off electron density of 0.00065e/bohr^3.

experimental areas are listed for comparisons. Figures 6.4~6.14 illustrate the orientations of model drugs at the oil/water interface (shown as the blue plane in the graph) when they are occupying maximum and minimum areas at the interface. Those calculated maximum and minimum cross-section areas are shown in Table 6.2. There were significant differences between the maximum and minimum areas with the ratio of a_{max}/a_{min} ranging from 1.7 (prazepam) to 3.3 (butylparaben) suggesting that the molecules would not be accurately described by simple spherical geometry.

When the data in Table 6.2 are examined, two trends are immediately apparent. All molecules in a single class tend to exhibit similar orientations. Each class of model solutes tends to exhibit characteristic orientation angles. For three benzodiazepines (oxazepam is not included because of the lack of accurate experimental areas occupied by oxazepam molecules), the experimental occupied areas by isolated molecules are not significantly different from the theoretical minimum occupied areas. Thus, it is concluded that benzodiazepines are likely orientated vertical to the oil/water interface. For three parabens, the experimental occupied areas are significantly larger than the minimum areas by 6~9Å^2 which suggests the long axes of paraben molecules deviate from the vertical orientation and form angles with the normal of the oil/water interface.

The estimated angles deviated from the normal are shown in the last column of Table 6.2. The angles were calculated between the long axis of the fixed molecule and all normals of the cutting planes that could produce the calculated cross-section areas within 1Å^2 from the experimental area. For the three parabens, the average angles are around 42^o. When steroids were studied, the experimental occupied areas are significantly larger than theoretical minimum areas by 18~25Å^2, corresponding to angle of about 54^o between the long axes of steroid molecules and the normal of the oil/water interface.

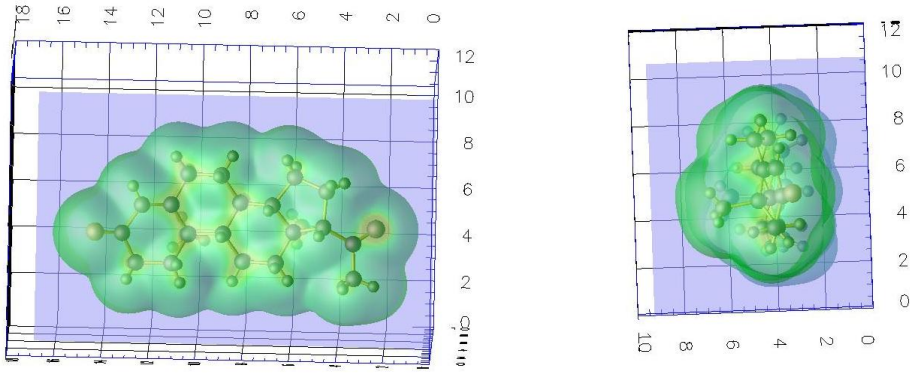

a b

Figure 6.4, The orientations of progesterone when it occupies the maximum (a) and minimum (b) areas at the oil-water interface which is illustrated using a blue color plane. The maximum projected area is 104.4Å² and the minimum projected area is 39.6 Å². The scales of axes have a unit of Å.

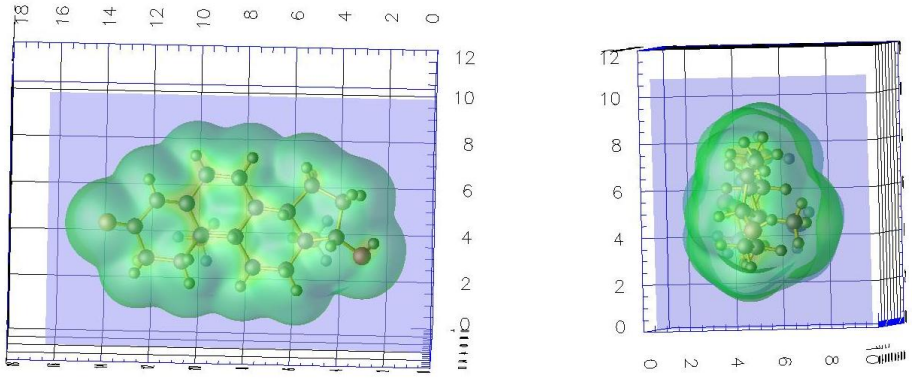

a b

Figure 6.5, The orientations of testosterone when it occupies the maximum (a) and minimum (b) areas at the oil-water interface which is illustrated using a blue color plane. The maximum projected area is 95.8Å² and the minimum projected area is 39.5Å². The scales of axes have a unit of Å.

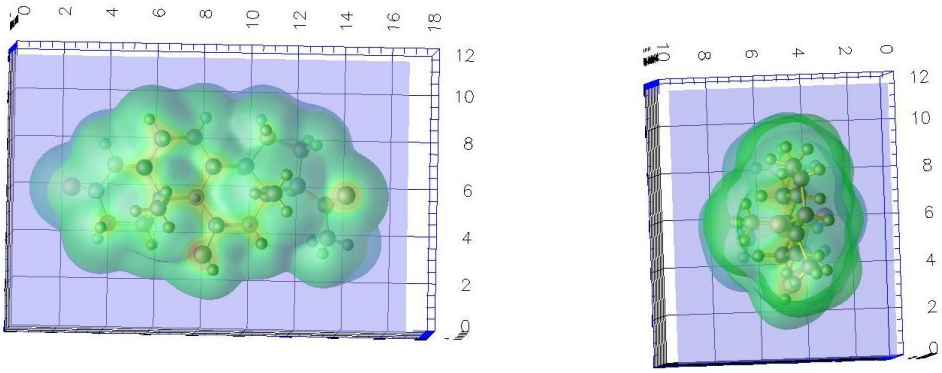

a b

Figure 6.6, The orientations of 11α-hydroxyprogesterone when it occupies the maximum (a) and minimum (b) areas at the oil-water interface which is illustrated using a blue color plane. The maximum projected area is 104.8Å² and the minimum projected area is 40.2Å². The scales of axes have a unit of Å.

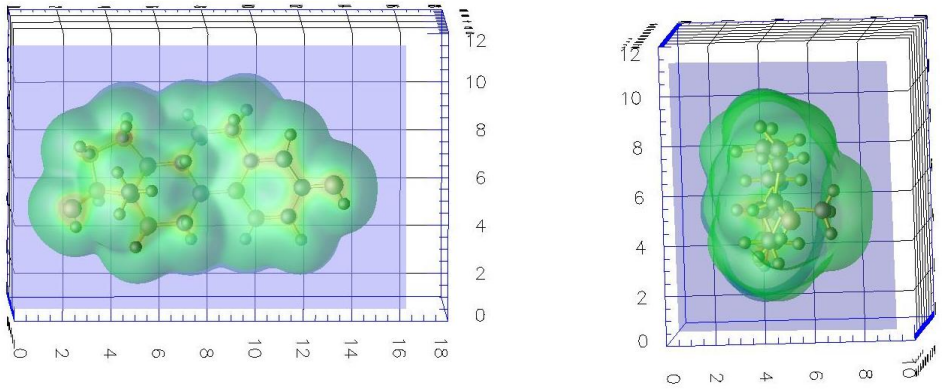

a b

Figure 6.7, The orientations of 17β-estradiol when it occupies the maximum (a) and minimum (b) areas at the oil-water interface which is illustrated using a blue color plane. The maximum projected area is 95.8Å² and the minimum projected area is 38.3Å². The scales of axes have a unit of Å.

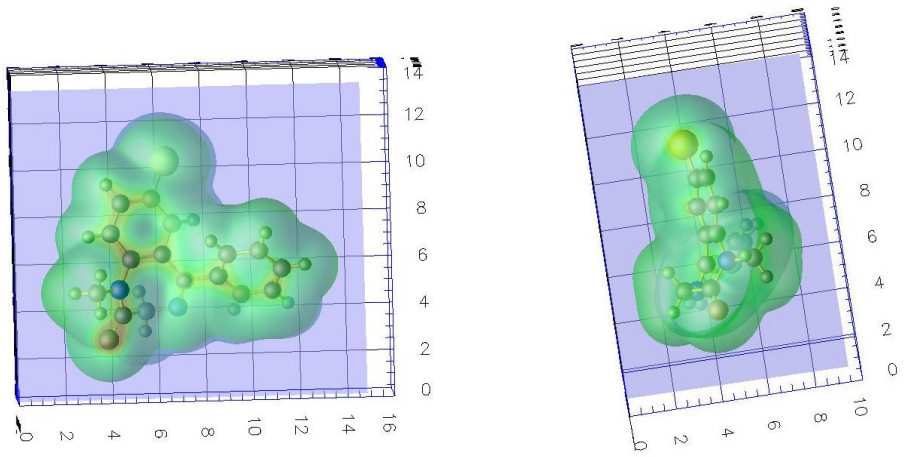

a b

Figure 6.8, The orientations of diazepam when it occupies the maximum (a) and minimum (b) areas at the oil-water interface which is illustrated using a blue color plane. The maximum projected area is 86.2Å² and the minimum projected area is 42.7Å². The scales of axes have a unit of Å.

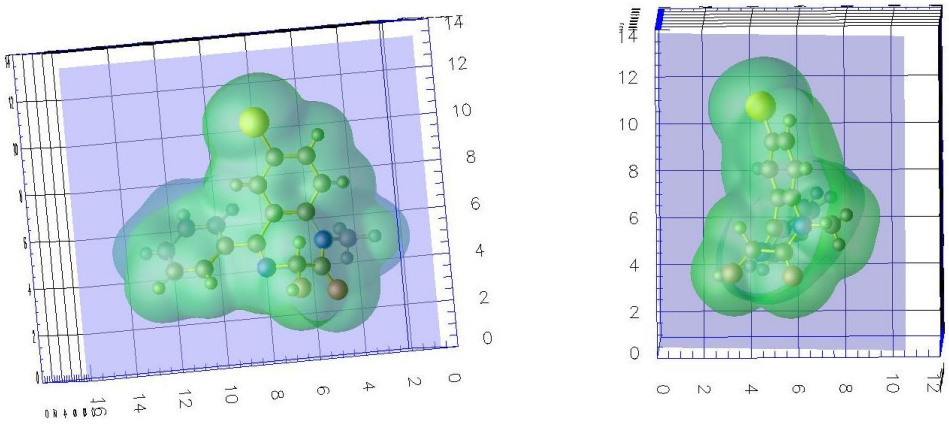

a b

Figure 6.9, The orientations of temazepam when it occupies the maximum (a) and minimum (b) areas at the oil-water interface which is illustrated using a blue color plane. The maximum projected area is 84.9Å² and the minimum projected area is 45.5Å². The scales of axes have a unit of Å.

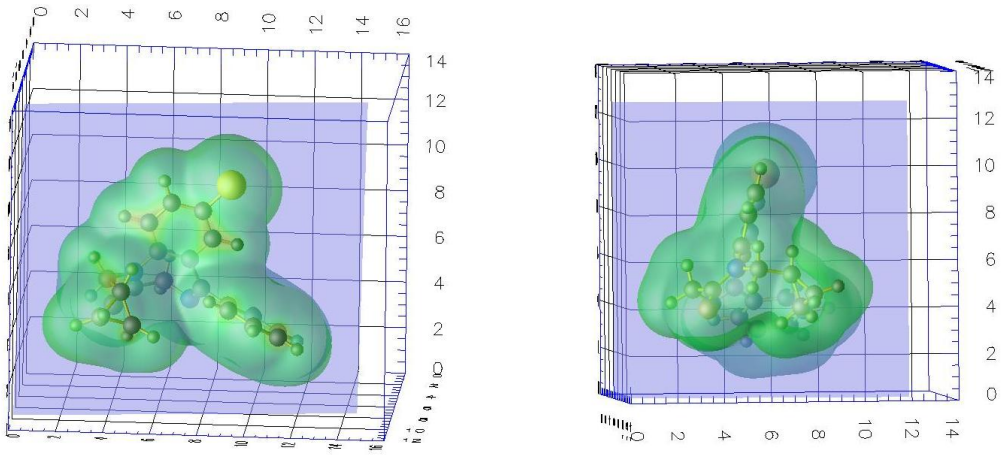

a b

Figure 6.10, The orientations of prazepam when it occupies the maximum (a) and minimum (b) areas at the oil-water interface which is illustrated using a blue color plane. The maximum projected area is 86.4Å² and the minimum projected area is 50.9Å². The scales of axes have a unit of Å.

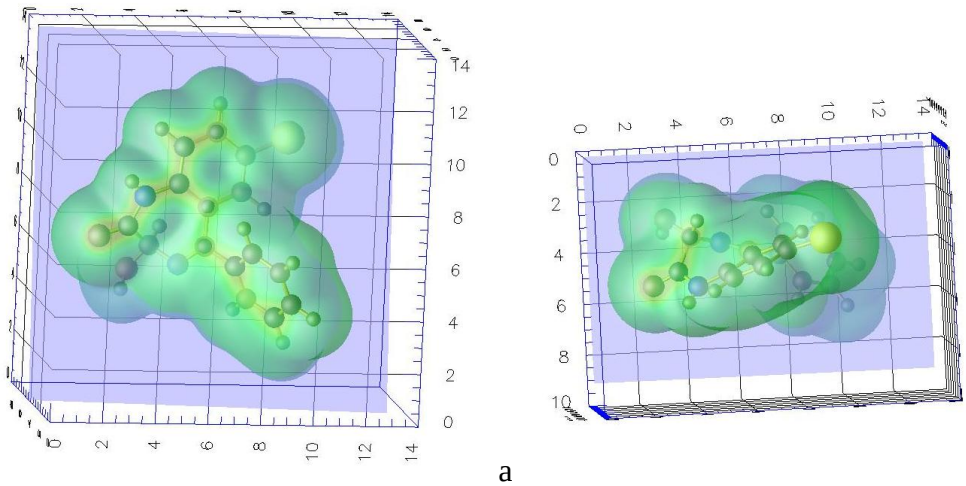

a b

Figure 6.11, The orientations of oxazepam when it occupies the maximum (a) and minimum (b) areas at the oil-water interface which is illustrated using a blue color plane. The maximum projected area is 83.7Å² and the minimum projected area is 44.8Å². The scales of axes have a unit of Å.

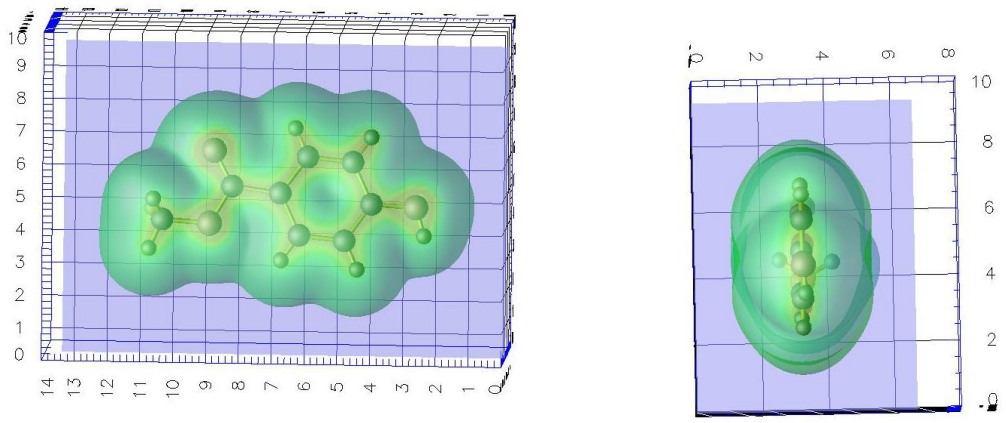

a b

Figure 6.12, The orientations of methylparaben when it occupies the maximum (a) and minimum (b) areas at the oil-water interface which is illustrated using a blue color plane. The maximum projected area is 62.0Å² and the minimum projected area is 24.5Å². The scales of axes have a unit of Å.

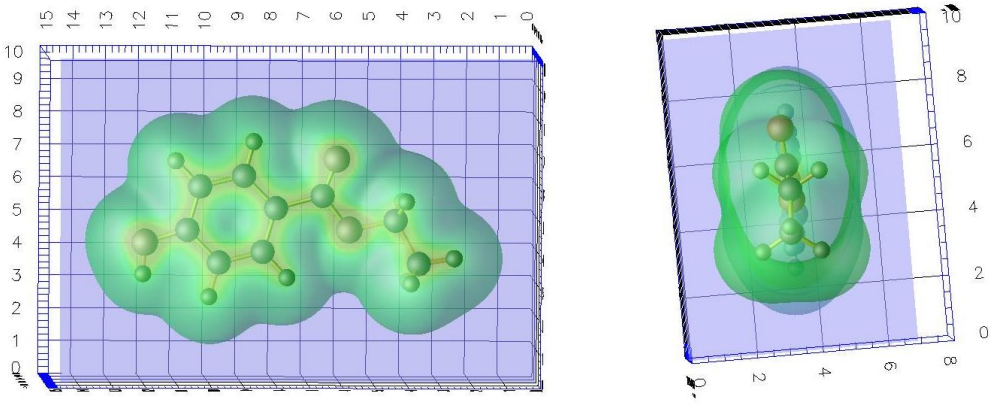

a b

Figure 6.13, The orientations of ethylparaben when it occupies the maximum (a) and minimum (b) areas at the oil-water interface which is illustrated using a blue color plane. The maximum projected area is 70.6Å² and the minimum projected area is 25.6Å². The scales of axes have a unit of Å.

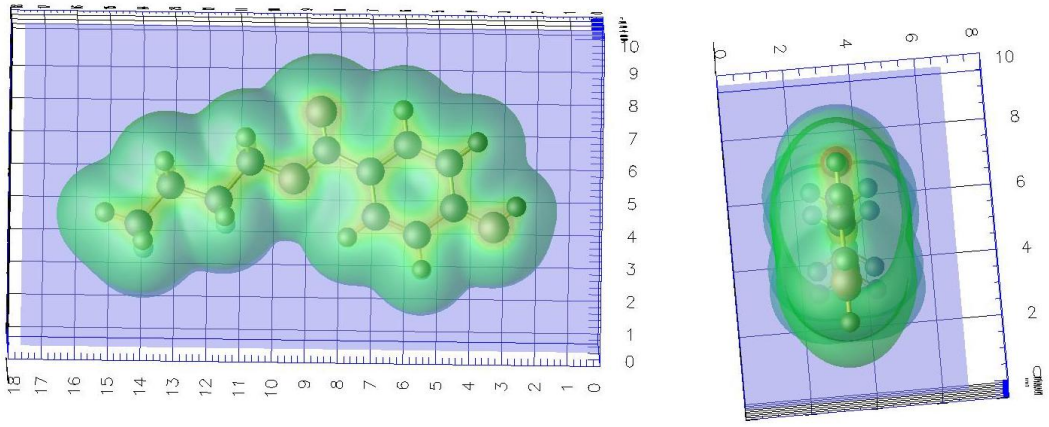

a b

Figure 6.14, The orientations of butylparaben when it occupies the maximum (a) and minimum (b) areas at the oil-water interface which is illustrated using a blue color plane. The maximum projected area is 82.9Å² and the minimum projected area is 25.4Å². The scales of axes have a unit of Å.

Table 6.2, The calculated maximum and minimum cross-section areas occupied by drug molecules at oil/water interface, a_{max} and a_{min}, compared to the experimental cross-section areas of molecules at oil/water interface, a_{exp}, reported in Table 5.2 (section 5.3.1); the estimated angles between long axes of model drugs and the normal of the oil/water interface and the calculated time-average interfacial areas occupied by drug molecules when the molecules are permitted to rotate freely at oil/water interface, $a_{average}$.

Drug	a_{max}(Å²)	a_{min}(Å²)	$a_{exp.}$(Å²)	Angles (°)	$a_{average}$(Å²)
Progesterone	104.4	39.6	58.0±4.4	49.5±3.9	64.8
Testosterone	95.8	39.5	59.8±4.9	55.8±5.4	62.5
11OHprog*	104.8	40.2	64.8±1.9	56.8±4.9	66.2
Diazepam	86.2	42.7	46.2±4.7	29.1±12.9	59.7
Temazepam	84.9	45.5	41.3±3.7	N/A	61.2
Prazepam	86.4	50.9	54.0±5.7	16.9±7.3	69.7
Methylparaben	62.0	24.5	31.9±4.0	47.3±3.1	38.0
Ethylparaben	70.6	25.6	31.8±4.6	38.4±3.0	42.0
Butylparaben	82.9	25.4	34.1±1.2	41.2±3.9	46.7
17β-estradiol	95.8	38.3	57.4±105.3	n.d.	59.5
Oxazepam	83.7	44.8	42.1±17.5	n.d.	59.3

*Abbreviation for 11α-hydroxyprogesterone

The estimated orientation angles could be rationalized by chemical intuition using the distribution of hydrophilic functional groups in the molecule of interest. Figure 6.15 shows a schematic of orientations of 3 series of model drugs at oil/water interface. Molecules of model drugs are illustrated using ellipsoids which have long and short axes. The small circles in the figure represent hydrophilic functional groups. The determining factor for the orientation of a molecule at oil/water interface is its free energy state; the molecule will choose an orientation that has the minimum free energy. There are two factors affecting the total free energy of a molecule at the oil/water interface. One modulating factor is the occupied area of the molecule. The larger occupied area of the molecule at oil/water interface, the larger the surface energy based on Eq. (A1.1). For other factors being equal, the molecule tends to take the minimum surface area to lower its surface energy. A second factor that influences the molecular orientation at oil/water interface is the distribution of hydrophilic functional groups of the molecule. Sequestering a polar (hydrophilic) functional group in a non-polar (hydrophobic) environment can be rather costly in terms of free energy. Molecular orientations that maximize the interactions of the polar functional groups with water tend to minimize the free energy. The two orientation factors may or may not conflict with each other. Obviously, when considered together, the effects of the two factors result in an orientation that will result in a minimum system free energy. In our studied system, benzodiazepines seem to have no conflict between the two factors. There are one or two hydrophilic functional groups (hydroxyl or carbonyl group) in each molecule that are adjacent to each other. As shown in Fig. 6.15a, the benzodiazepine molecules can take the minimum occupied interfacial area and, at the same time, maintain the hydrophilic functional groups in aqueous phase. For parabens, the two hydrophilic groups are far from each other as shown in Fig. 6.15b. It is not possible for the molecule to occupy a minimum surface area while simultaneously maintaining contact of the two hydrophilic groups with water. It seems reasonable to expect that the molecule will rotate from the

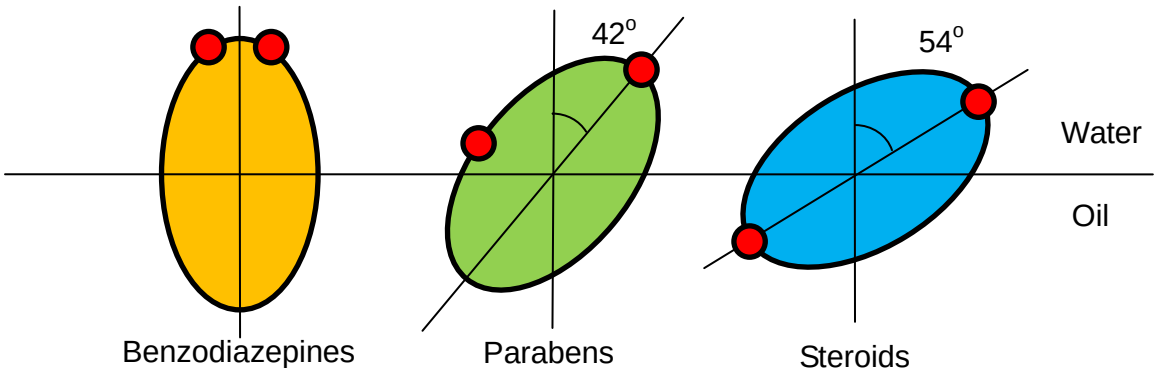

(a) (b) (c)

Figure 6.15, A schematic of orientations of three series of model drugs at oil/water interface. The molecules of model drugs are illustrated using ellipsoids that have long and short axes reflecting molecular shapes. The small circles represent the hydrophilic functional groups.

vertical orientation until the two hydrophilic groups are near/in the water phase. As a consequence, the long axes of parabens form an angle (~42^o) with the normal of the oil/water interface. For steroids, the two hydrophilic groups are at opposite ends of long axis of each molecule. Similar to parabens, the conflict between the two factors, maintaining the minimum surface area and keeping hydrophilic groups in water, will drive the molecules to deviate from the vertical orientation. Because the hydrophilic groups are more distantly separated in steroid molecules compared to the paraben molecules, the angles between long axes of drug molecules and the normal of oil/water interface are larger for steroids (~54^o) than those for parabens (~42^o).

In the above analysis, we considered the solute to occupy an area of the interface while in a static fixed orientation. In reality, the drug adsorption is a dynamic partitioning phenomenon. As a consequence, the orientation of drug molecules at the oil/water interface is unlikely fixed and would represent a time-average over different orientations. Solubilization of drug in micelle systems is known to be a dynamic partitioning phenomenon. The high exchange rate of molecules between the micelles and water (10^3~10^8/s (Lindman and Wennerstrom, 1980)) suggests the estimated orientations are time averages over possible orientations. The estimated angles between long axes of drugs and the normal of oil/water interface, e.g. 42^o for parabens and 54^o for steroids, are time average angles over their possible orientations. In the extreme case, the solute may freely rotate within the plane of the surface. The last column of Table 6.2 presents the average areas occupied by the solutes when allowed to freely rotate. When the average occupied areas are compared to experimental values, the experimental areas occupied by benzodiazepines and parabens are significantly smaller than the calculated average. For steroids the experimental areas occupied are close to the overall average when permitted to freely rotate. The results suggest steroids may have larger rotating degree of freedom at oil/water interface as compared to benzodiazepines and parabens.

The experimental studies on the occupied interfacial areas were carried out on a flat dodecane/water interface (Section 5.3.1). When attempting to correlate these findings to results at a micelle surface we must assume that the micelle surface curvature has no effect on the occupied area.

In these studies, rigid molecular structures (extracted from crystal structure) were employed, while, in solution state, the molecules had less restriction and could be flexible. For our model drugs, steroids molecules are all rigid and benzodiazepines are mainly rigid with a benzene ring at C_5 position having limited rotating ranges due to the steric hindrance. Parabens have flexible hydrocarbon chains but the determining factor of occupied surface areas is the rigid bulky resonance structure of the molecules. Therefore, the simplifications using rigid molecular structure will not introduce significant errors on the calculations of the areas occupied by drugs at the oil/water interface.

6.4. CONCLUSION

The orientations of model drugs at oil/water interface were estimated by comparing the experimental occupied areas of model drugs to the theoretical areas when model drugs were taking any possible orientations at oil/water interface. The theoretical occupied interfacial areas were carried out using molecular simulation methods: (1) the molecular boundary was defined using an isosurface of electron density; (2) the cross-section area of the molecule cut by a plane representing the oil/water interface was used as the occupied area corresponding to the specific orientation.

The orientations of model drugs at oil/water interface are different for different drug series but are similar within one series of model drugs. All three benzodiazepines are believed to take the vertical orientation at oil/water interface because the experimental

occupied areas are not significantly different from theoretical minimum areas. For parabens, the long axis of each drug molecule form an angle about 42^{o} with the normal of oil/water interface. For steroids, the angles between long axes of drug molecules and the normal of oil/water interface aere about 54^{o}.

The molecular orientations at oil/water interface are related to the distribution of hydrophilic functional groups of model drugs. If the hydrophilic groups are congregated at one end of molecular long axis, such as benzodiazepines, the molecules are likely taking vertical orientations that occupied minimum areas while maintaining hydrophilic groups in aqueous phase. If the hydrophilic groups are widely separated in the molecule, such as parabens and steroids, the solute cannot take the minimum surface areas and, at the same time, keep the hydrophilic groups in water. The long axes of those molecules would form angles with the normal of oil/water interface to reach the minimum of total free energy.

Chapter 7

NMR Studies on Inter-molecular Interactions in Micelles and Micellar Diffusivity

7.1. INTRODUCTION

Several spectroscopy-based methods, such as UV/vis, fluorescence, NMR, etc., have been used to determine the location of solubilizates in micelles (Sabate et al., 2001; Vermathen et al., 2000; Bromberg and Temchenko, 1999; Lebedeva et al., 2007; Ueno and Asano, 1997; Hawrylak and Marangoni, 1999). The thermodynamic-model-based approach of the present work has advantages in quantitative predictions of fractions of drugs located in different regions of micelles and micelle/water partitioning coefficients of model drugs. On the other hand, the method lacks detailed information of micellar solubilization, such as locations of specific functional groups in micelles, because the thermodynamic analysis treats one whole molecule as an elemental unit. The spectroscopic techniques could provide qualitative information such as the microenvironment of a functional group and explicit interactions between different function groups.

In Chapters 3~5 we have employed the thermodynamic-model-based method to determine the location of drugs in micelles and predict the partitioning of drugs between micelles and water phase. In this chapter, we will use 2-D and PGSE NMR techniques to study the microstructures of micelles solubilizing drugs. The inter-molecular interactions between surfactants and drugs are expected to be determining factors in the locations and orientations of drug molecules in micelles. For example, if the drugs were located at micelle surface, interactions between drugs and headgroups of surfactants would be expected. Specifically, the 2-D NMR techniques, including NOESY (Nuclear Overhauser Effect SpectroscopY) and ROESY (Rotating-frame nuclear Overhauser Effect

SpectroscopY), were employed to measure the interactions between surfactants and drugs in micellar aggregates. PGSE NMR technique can provide information on the translational diffusivities of particles which are correlated to the particle sizes. Here the PGSE NMR technique was mainly employed to detect the changes of micelle size with different drug concentrations and in the presence and absence of salts. The information of micellar size was used to test the validity of some assumptions in the thermodynamic model in Chapter 3~5. These studies provide complementary information on solubilization mechanism of micelle systems.

7.2. MATERIALS AND METHODS

7.2.1. MATERIALS

Progesterone (>99%), diazepam, temazepam, methylparaben (>99%), ethylparaben (>99%), butylparaben (>99%), sodium dodecyl sulfate (>99%), dodecyltrimethylammonium bromide (>99%) and dodecyle β-D-maltoside (>98%) were obtained from Sigma-Aldrich (St. Louis, MO). 11α-hydroxyprogesterone (>95%) was from Janssen Chimica (New Brunswick, NJ). D_2O (>99.9% isotopic purity) was purchased from Sigma-Aldrich. Three millimeter NMR tubes with a 500MHz rating were purchased from Norell (Landisville, NJ).

7.2.2. METHODS

7.2.2.1. 2D NMR (NOESY and ROESY) Methods

NOESY (Nuclear Overhauser Effect SpectroscopY) and ROESY (Rotating-frame nuclear Overhauser Effect SpectroscopY) were used to detect the inter-molecular interactions when the spatial distance between two protons is shorter than 5Å. NOESY measures the dipolar coupling between nuclear spins and is suitable for ‘small’ (MW<1000) and ‘large’ (MW>2000) molecules for which NOEs (nuclear Overhauser effect) are positive and negative respectively, but may fail for mid-sized molecules (Claridge, 1999). ROESY

observed transient NOEs in the rotating frame and is especially useful where the NOESY cross-peak signals are weak because the NOEs are near the transition between positive and negative. ROESY cross-peaks are always positive, but ROESY signal can also be interfered by other effects, such as TOCSY (TOtal Correlation SpectroscopY) transfer and COSY(COrelation SpectroscopY)-type cross-peak (Claridge, 1999).

Figure 7.1 shows the pulse sequences used in NOESY and ROESY experiments. The sequence of NOESY consists of three 90^o pulses. The evolution time, d2, would be systematically incremented to provide chemical shift information along the 2^{nd} dimension (F1 domain). The mixing time, τ_{mix}, is the duration for the spin-spin cross relaxation to occur and is kept constant in the experiments. The ROESY sequence includes a 90^o pulse following by a varied evolution time, d2, and a fixed mixing time, τ_{max}, when an alternating-phase spin-lock is applied to reduce TOCSY transfer (Hwang, 1992).

NOESY experiments were performed on a Varian Inova 400MHz NMR spectrometer (S/N S010883) equipped with a Highland Performa II gradient probe (S/N P003732). The acquisition and processing of the spectra were carried out using VNMR 6.1c software (Varian). D_2O was used as solvent for all the NMR experiments. The mixing time in NOESY measurements was 0.5~1.0s, and the relaxation delay, d1, was 6s. The experiments were acquired with 16 scans and 1024 complex data points for each of the 200 evolution delay time (d2). The spectral width was 4060Hz.

ROESY experiments were carried out on a Varian VNMR 500MHz NMR spectrometer (S/N 41312). The acquisition and processing of the spectra were carried out using VNMRJ 2.2c software (Varian). The mixing time in ROESY measurement was 0.2~0.3s. The relaxation delay, d1, was set to 3s and a homospoil gradient spoil sequence was employed prior to the d1 delay to achieve a less oscillatory steady-state for 2-D

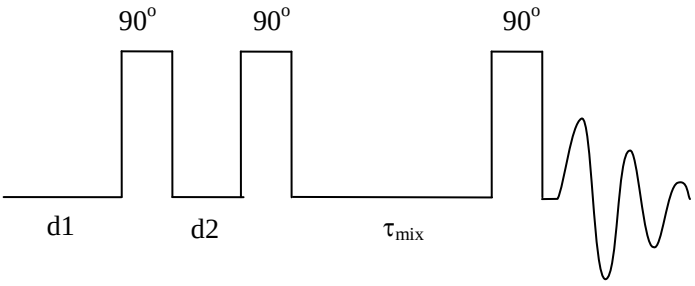

Pulse sequence used in NOESY experiments

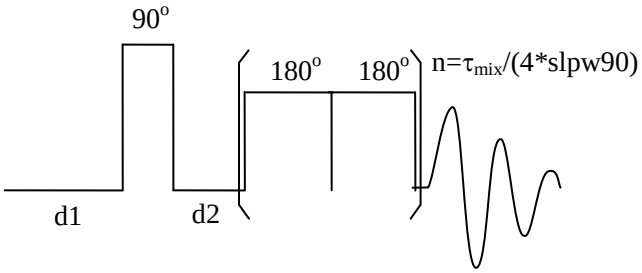

Pulse sequence used in ROESY experiments

Figure 7.1, The schematics of pulse sequences used in NOESY and ROESY experiments.

experiment (Varian Instrumental Manual, 2001). The experiments were acquired with 32 scans and 2048 complex data points for each of the 224 evolution delay time (d2). The spectral width was 5000Hz.

7.2.2.2. 2-D NMR Sample Preparations

Near-saturated concentrations of model drugs were employed in surfactant solutions with D_2O as solvent. The systems containing drugs and surfactant solutions were rotated at room temperature for 2 days to ensure complete dissolution. For the 400 MHz NMR instrument, about 0.75mL sample solutions were placed into 5mm NMR tubes. For the 500 MHz NMR instrument, about 0.25mL sample solutions were placed into 3mm NMR tubes.

7.2.2.3. PGSE NMR Method

Pulsed gradient spin echo (PGSE) NMR technique as a means of measuring diffusivity was first developed by Stejskal and Tanner (Stejskal and Tanner, 1965) based on the concept of nuclear spin echo brought by Hahn (Hahn, 1950) and Carr and Purcell (Carr and Purcell, 1954). Two magnetic field gradient pulses are employed, and they are essential for correlating the translational motion of nuclei to the NMR signal intensity. There are two commonly used pulse sequences: nonstimulated and stimulated PGSE pulse sequences, which are shown in Figure 7.2. Nonstimulated PGSE pulse sequence uses a 90^o pulse to start dephasing the magnetization followed by a 180^o pulse to rephrase the magnetization and realize an echoed signal. The stimulated pulse sequences utilize three successive 90^o pulses to bring about the same effect. In Figure 7.2, d0~d5 are acquisition delays. The spin echo condition requires: d0=d3 and d2=d4.

Stimulated spin echoes are often employed in system which has a short T_2 relaxation time and a slow diffusivity. For the micelle system, the diffusivity of micelle is much slower than that of monomer and the spin-spin coupling relaxation time (T_2) of nuclei in micelle

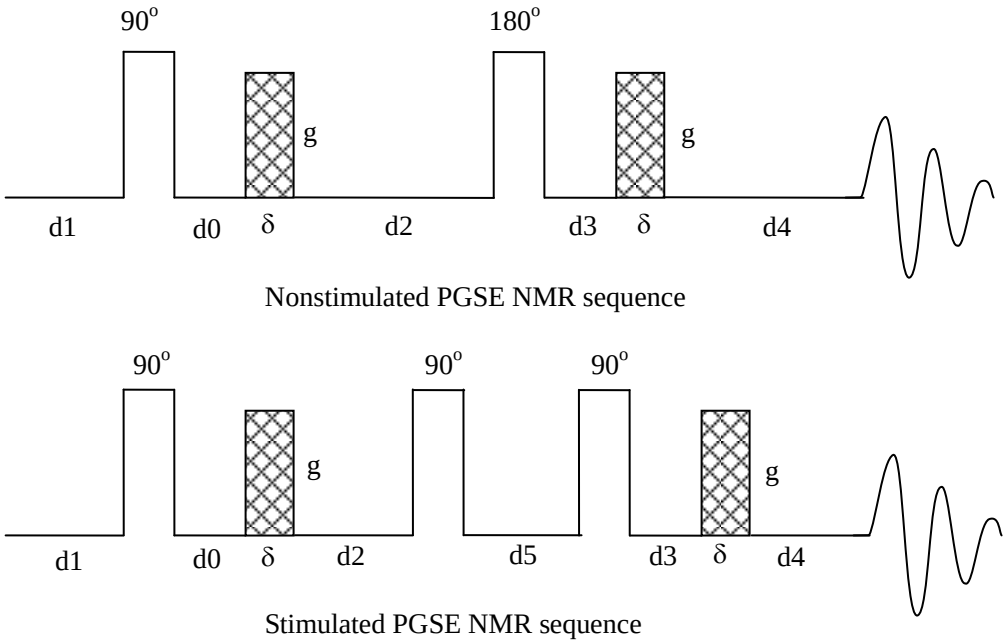

Figure 7.2, Schematics of nonstimulated and stimulated PGSE NMR sequences used in diffusivity measurements. The shaded bars represent the magnetic field gradient (along z direction) pulses with duration, δ, and intensity, g.

is also much shorter than that of monomer due to the molecular motional restriction in micelles.

For stimulated PGSE experiment, the equation used to determine the diffusivity can be written as:

$$I = I_0 \exp\left[-D\gamma^2 g^2 \delta^2 (\Delta - \delta/3)\right] \quad (7.1)$$

where I and I_0 are the measured NMR signal intensities in the presence and absence of magnetic field gradient; D is the diffusivity; γ is the gyromagnetic ratio (which is equal to $2.67515 \times 10^8 s^{-1}T^{-1}$ for proton); δ and g are the duration and intensity of the magnetic field gradient pulse along z direction; Δ is the diffusion time between two magnetic field gradients in the pulse sequence which is equal to $\delta + d2 + pw90 + d5 + pw90 + d3$ (see Figure 7.2; pw90 is the length of a 90^o pulse). In the experiment, δ and Δ are kept constant. By changing gradient strength, g, a series of signal intensity I are measured. Since the $\ln(I/I_0)$ and g^2 have good linear relationship, the slope is used to calculate the diffusion coefficient D.

The diffusivity measurements were carried out on a Varian Inova 400MHz Fourier Transform NMR spectrometer (S/N S010883) equipped with a Highland Performa II gradiet probe (S/N P003732). Thin-walled 3mm glass sample tubes were used in order to keep the sample within the linear region of the gradient coil. Compared to 5mm tube, the 3mm sample tube could also shorten the time to reach thermal equilibrium and inhibit the thermal convection that could affect the measured diffusivity (Antalek, 2002). The temperature of the measurements was controlled at 27.0 ± 0.1^oC. The samples were equilibrated inside the NMR probe for at least 15 minutes prior to the data collection. The trapezoidal gradient shape was utilized instead of the standard rectangular gradient in order to minimize the effects of eddy currents on diffusivity measurements (Price and Kuchel, 1991).

The instrument was calibrated using a standard solution containing 15mg/mL SDS in D_2O. The literature values of the diffusivities of dodecyl sulfate at 15mg/mL concentration are $0.976x10^{-10}m^2/s$ at 25^oC (Landman et al., 1984) and $1.70x10^{-10}m^2/s$ at 45^oC (Miller et al., 1994). The interpolated diffusion coefficient at 27^oC based on Arrhenius relationship was $1.05x10^{-10}m^2/s$. After the calibration our measured diffusivity of the standard was $(1.05\pm0.01)x10^{-10}m^2/s$. The diffusivity of the standard was measured both before and after each set of experiments. The intraday deviation of the diffusivities of standards was less than 1%. The advantage of using 15mg/mL SDS as the standard solution was the diffusivity value of the standard was close to the diffusivity of the samples while conventional standards, such as D_2O or dioxane, had values which were one order of magnitude higher than that of samples.

In our experiments, a value of 200ms was used for the delay time d5 which was the dominant term for the diffusion time, Δ. Delay time d2(=d4) was 10~20ms and d0(=d3) was 0.4ms. Pre-sequence time delay d1 should be 5 times greater than T_1 of species of interest so as to permit the magnetizations to return to their equilibrium positions. A delay time of 5s was chosen for d1. The length of 90^o pulse, pw90, ranged from 15.3 to 16.0μs when the transmitter power (tpwr) was set to 57 dB. The duration of the magnetic field gradient pulses, δ, was set to 5ms, and the strength of the gradient pulses, g, was varied from 5 to 27 Gauss/cm in 10 steps in most cases. The squares of gradient strengths, g^2, were chosen to be equally spaced between the minimum and maximum values. The minimum field gradient strength was set to 5 Gauss/cm instead of zero due to the poor performance at gradient strengths near zero, specifically significant phase distortion of spectra. The maximum gradient strength was varied between 22 and 30 Gauss/cm based on the gradient strength needed to cause an attenuation of NMR signal by about 90%. A trapezoidal shape of magnetic field gradient pulse was employed: a gradient ramp with

duration of 0.2ms was applied at the beginning and end of each gradient pulse in order to minimize the eddy current effect on signal fluctuation. Other parameters and their corresponding values included a sweep width of 6000 Hz, 16384 points for Fourier transform and 8~64 transients depending on the signal strength.

There were multiple NMR bands associated to each molecule, the drug or surfactant, in the system. Each band could be used to detect the diffusivity of the corresponding molecule. To improve the accuracy of the measurements, three bands were chosen for each molecule to detect the diffusivity separately. Since the measurement of each sample was repeated three times, the final determined diffusivity was an average of 3×3=9 measurements. The chosen NMR bands in diffusivity determinations for model drug and surfactant molecules are listed in Table 7.1. The chemical shifts of SDS, DTAB and butylparaben were in good agreements with the reported values in D_2O media (Hawrylak and Marangoni,1999; Suratkar and Mahapatra, 2000; Panicker, 2008).

7.2.2.4. PGSE NMR Sample Preparations

A known amount of model drugs was dissolved into surfactant solutions with D_2O as solvent to make near-saturated solutions of the drugs. The drug-surfactant solution systems were rotated for 2 days to ensure complete dissolution of the solid drugs. To prepare solutions with lower drug concentrations, the above samples were diluted 1.5~3 times with blank surfactant solutions (with same surfactant concentration). When salts were present, NaCl was weighed and added into surfactant solutions to make 0.15N concentration of NaCl. About 0.25mL sample solutions were place into 3mm NMR tube for diffusivity measurements.

Table 7.1, List of NMR bands of model drugs and surfactants used in diffusivity measurements.

Drug/Surfactant	Chemical shifts of NMR bands used in diffusivity measurements (ppm)
Progesterone	5.8, 2.2, 0.7
Diazepam	7.5, 7.2, 3.5
Methylparaben	7.9, 6.9, 3.9
Butylparaben	7.9, 6.9, 1.0
SDS	4.1, 1.3, 0.9
DTAB	3.2, 1.3, 0.9
DM	3.5~3.9, 1.3, 0.9

7.3 RESULTS AND DISCUSSION

7.3.1. Two-dimensional NMR

7.3.1.1. 2-D NMR for Steroids in Micelles

NOESY and ROESY NMR techniques were used as a means to study the locus of solubilization of model drugs in micelles. Figure 7.3 shows the ROESY spectrum for 3.5mg/mL 11α-hydroxyprogesterone in 15mg/mL SDS solutions. The corresponding 1-D spectrum is shown at both the top and left sides of the 2-D spectrum. There are several peaks identified as belonging to the steroid, such as 0.7, 2.0~2.7, 5.7ppm; one characteristic peak belonging to SDS, 0.9ppm; and at least three overlapped peaks having contributions from both the surfactant and drug, such as 1.3, 1.7, 4.0ppm. Many cross-peaks are present corresponding to short distance (<5Å) between two hydrogen atoms. Unfortunately, all the cross-peaks could be explained by intra-molecular interactions (surfactant-surfactant or drug-drug) and no evidence of inter-molecular interactions between surfactant and drug molecules was observed. Shown in Figure 7.4 is the ROESY spectrum for 1.9mg/mL 11α-hydroxyprogesterone in 20mg/mL DTAB solutions. Based on the 1-D spectrum, the peaks at 0.7, 2.0~2.7, 4.0, 5.7ppm are exclusively assigned to the drug; the peaks at 0.9, 3.2, 3.4ppm are assigned to DTAB and the peaks at 1.3, 1.8ppm are assigned to both the drug and surfactant due to the overlaps. Similar to 11α-hydroxyprogesterone-SDS systems, all observed cross-peaks correspond to intra-molecular interactions and no inter-molecular interaction between drug and surfactant molecules is evident. These results do not imply that the surfactant fails to solubilize the drug. The data in Section 3.3.1 clearly does illustrate the power of SDS to solubilize 11α-hydroxyprogesterone.

The ROESY experiments were carried out on 11α-hydroxyprogesterone (0.5mg/mL) in 20mg/mL DM solutions. The results are not shown. No cross-peak corresponding to inter-molecular interactions between drug and surfactant was observed. It is partly due to

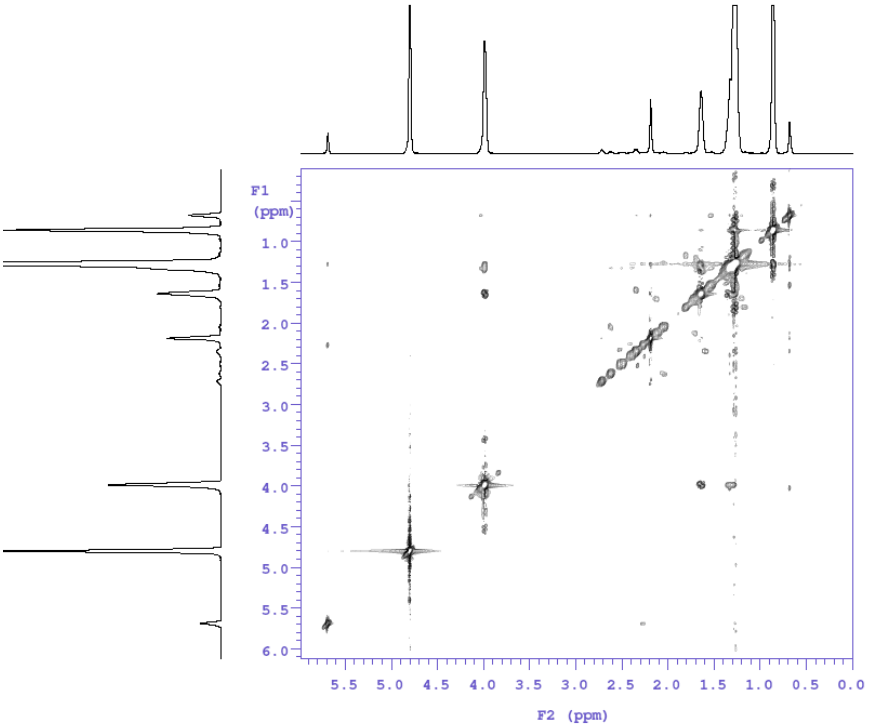

Figure 7.3, ROESY of 3.5mg/mL 11α-hydroxyprogesterone in 15mg/mL SDS.

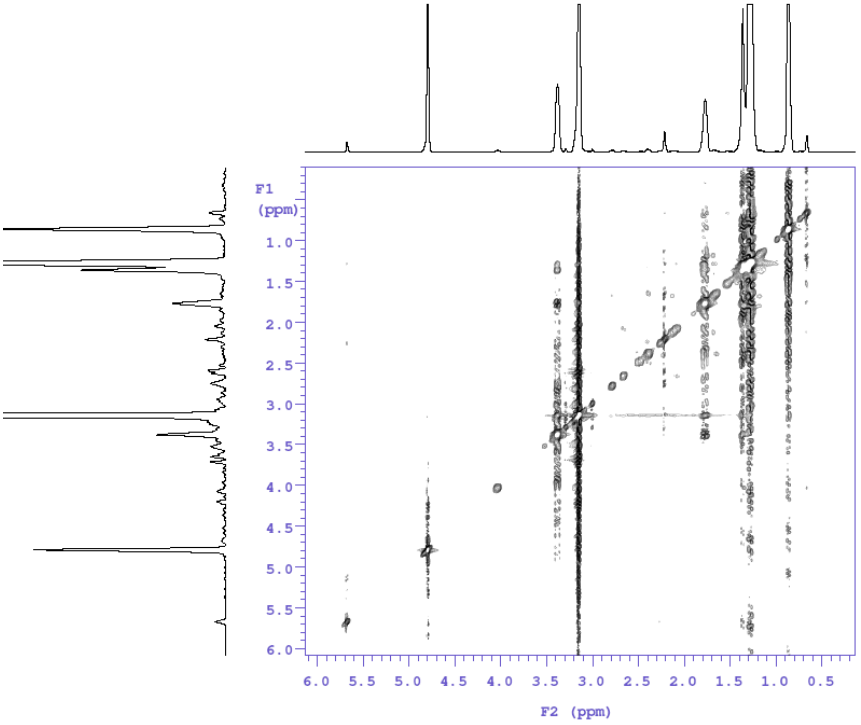

Figure 7.4, ROESY of 1.9mg/mL 11α-hydroxyprogesterone in 20mg/mL DTAB

the low drug concentration compared to the concentration of surfactant. As a result, the intra-molecular interactions of drug molecules may not be sufficiently detectable and only the cross-peaks between protons of surfactant molecules were observed.

Both ROESY and NOESY techniques were applied to 15mg/mL SDS solutions containing 2.6mg/mL progesterone with the results not shown here. The mixing time for ROESY experiment was 0.2s while the mixing time for NOESY experiments varied from 0.2 to 1.0s. But in all the 2-D spectra, no cross-peak related to inter-molecular interactions between drug and surfactant was seen.

In all the studied steroid-in-micelle systems, no evidence of interactions between steroid and surfactant molecules was observed. The possible reasons include: (1) In some systems, there are broad overlaps between characteristic peaks of the drug and surfactant. For example, in 11α-hydroxyprogesterone/SDS systems, there is only one peak exclusively assigned to surfactant (0.9ppm), which corresponds to the protons at the terminal methyl group of alkyl tail of SDS. As a consequence of 0.9ppm being the sole unambiguous peak, the outlined NMR methods will only detect an interaction between drug and the end of hydrophobic tail of SDS molecules. (2) The qualities of 2-D spectra were poor due to a significant t1-noise and the signal/noise ratio was significantly lowered. (3) The rotational movement of drug molecules in micelles can be sufficiently rapid that the distance between two protons of drug and surfactant cannot remain below 5Å on the NMR timescale. In Chapter 6 it was speculated that the steroids have larger degree of freedom at oil/water interface compared to benzodiazepines and parabens. This factor may contribute to the difficulties of detecting interactions between drugs and surfactants for SDS-steroid systems.

7.3.1.2. 2-D NMR for Parabens in Micelles

Figure 7.5 shows the ROESY spectrum of 4.9mg/mL methylparaben in 15mg/mL SDS solutions. The NMR bands at 0.9, 1.2, 1.6 and 4.0ppm are assigned to the methyl group, hydrocarbon chain (including 9 carbons adjacent to methyl group), β-protons and α-protons of the SDS. Methylparaben has characteristic peaks at 3.8ppm (methyl group), 6.9 and 7.9ppm (aromatic ring). The following cross-peaks corresponding to inter-molecular interactions between the drug and surfactant were observed: 0.9↔3.8ppm, 1.2↔3.8/6.9/7.9ppm, 1.6↔7.9ppm, 4.0↔7.9ppm (labeled by arrows in Fig. 7.5). A schematic representation, Figure 7.6, demonstrates how the interactions could be used to determine the location and orientation of drug molecules in micelles. The short distance between aromatic ring of methylparaben and α- and β-protons of SDS indicates the location of the aromatic ring in the vicinity of the head groups of the surfactant, and therefore the micelle surface. The interactions between methyl group of methylparaben and the terminal methyl group of the hydrophobic tail of SDS suggests the methyl group of methylparaben is pointing towards the micelle core. From the configuration derived from the inter-molecular interactions, the hydroxyl group of methylparaben must be pointing to the aqueous environment. To prove the observed interactions happened in the micelles but not in the solution state, such as from dimer complexes, the 2-D NMR spectrum was measured at surfactant concentration lower than the CMC. The spectrum of 1.0mg/mL methylparaben in 1.0mg/mL SDS solutions shows only cross-peaks corresponding to intra-molecular interactions and no cross-peak between the drug and surfactant (the spectrum is not shown).

Figure 7.7 shows the ROESY spectrum of 6.7mg/mL methylparaben in 20mg/mL DTAB solutions. There is no overlap between NMR bands of methylparaben and those of DTAB. The characteristic peaks of DTAB include 0.9ppm (methyl group at the end of

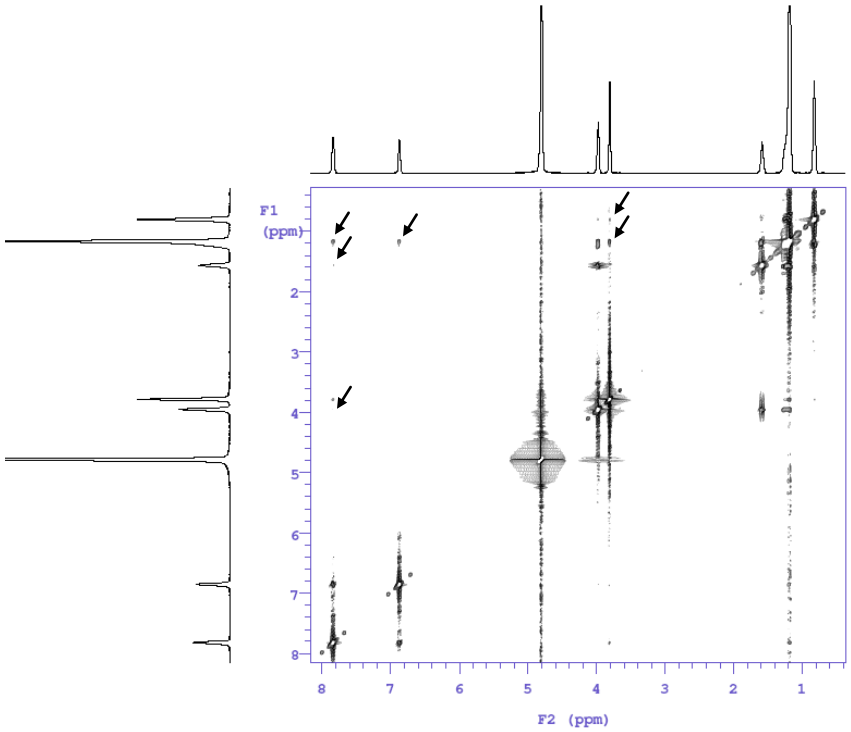

Figure 7.5, ROESY of 4.9mg/mL methylparaben in 15mg/mL SDS. The interested cross-peaks are labeled using arrows.

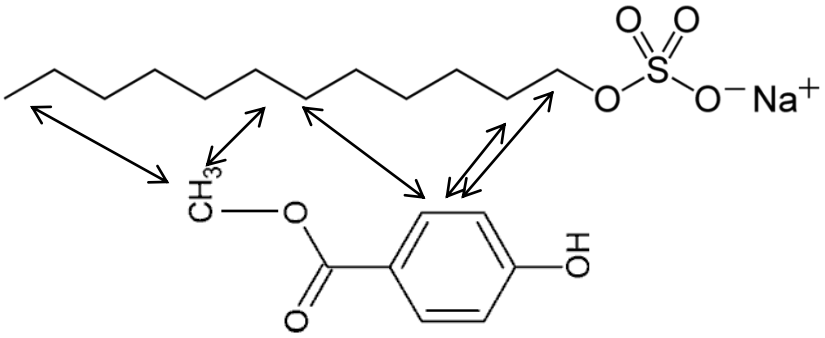

Figure 7.6, A schematic of inter-molecular interactions between methylparaben and SDS molecules detected by ROESY experiments (Fig. 7.5).

the hydrocarbon tail), 1.1~1.2ppm (hydrocarbon chain consisting of 9 carbons adjacent to methyl group), 1.6ppm (β-protons), 3.2ppm (methyl groups at the head group), and 3.8ppm (α-protons). The following cross-peaks between functional groups of methylparaben and DTAB were observed: 0.9↔3.8ppm, 1.1~1.2↔3.8/6.9/7.9ppm, 3.2↔6.9/7.9ppm (labeled using arrows in Fig. 7.7). Figure 7.8 is a schematic representation illustrating the specific interactions between methylparaben and DTAB in micelles. The aromatic ring of the drug is close to the head group of DTAB molecules while the methyl group of methylparaben is close to the end of hydrophobic tail of the surfactant. These observations are consistent with the conclusion that the aromatic ring and hydroxyl group of methylparaben are located at micelle surface while the methyl group of the drug points towards the micelle core.

Shown in Figure 7.9 is the NOESY spectrum of 3.7mg/mL methylparaben in 20mg/mL DM solutions. DM has characteristic bands at 0.9ppm (methyl group of the hydrophobic tail), 1.3ppm (hydrocarbon chain including 9 carbons adjacent to terminal methyl group), 1.6ppm (β-protons), 3.3~3.9, 4.3 and 5.3ppm (head group). Obviously, the broad band, 3.3~3.9ppm, of the head group overlaps with the sharp peak (3.8ppm) corresponding to the methyl group of methylparaben. No conclusive information can be obtained for interactions with the methyl group of methylparaben. The cross-peaks between 6.9/7.9ppm and 0.9/1.3/1.6/3.3~3.9ppm were observed which indicate the interactions between the aromatic ring of methylparaben and both the head group and hydrocarbon chain (including the terminal methyl group) of the surfactant. A schematic figure demonstrating the inter-molecular interactions is shown in Figure 7.10. These results suggest the drug and surfactant molecules may have more compact packing in DM micelles compared to that in ionic micelles. The ROESY experiments were carried out on the same system (methylparaben/DM system, results are not shown). No cross-peaks between the drug and surfactant were seen. This lack of response may be because the

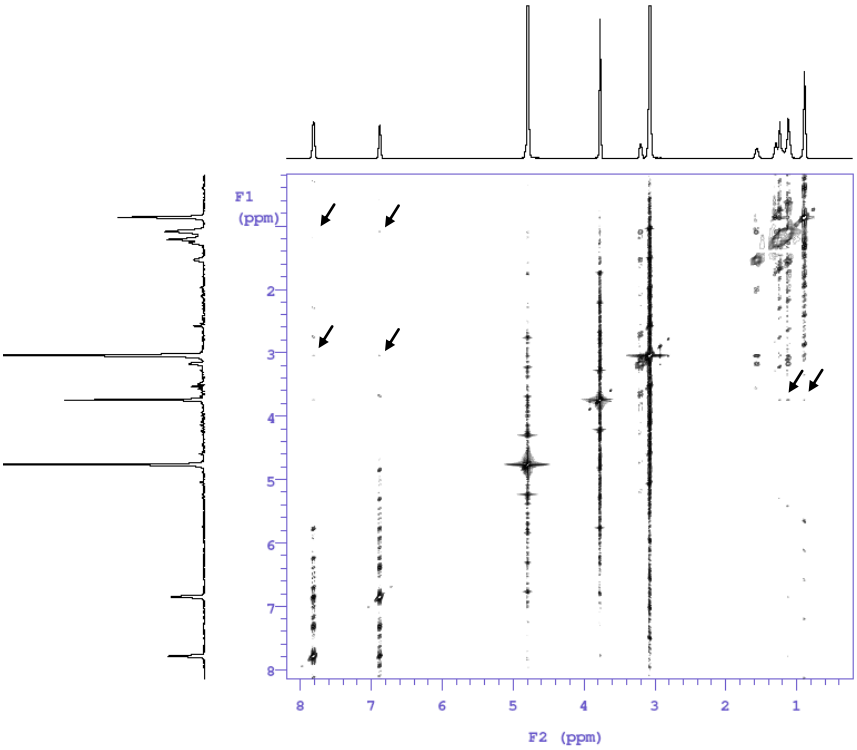

Figure 7.7, ROESY of 6.7mg/mL methylparaben in 20mg/mL DTAB. The interested cross-peaks are labeled using arrows.

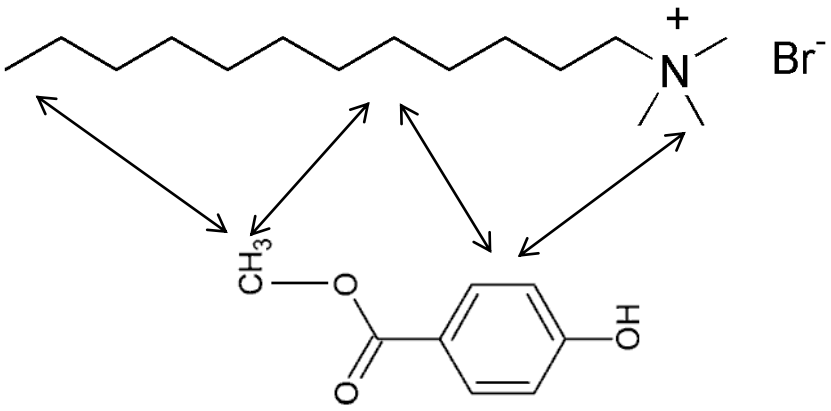

Figure 7.8, A schematic of inter-molecular interactions between methylparaben and DTAB molecules detected by ROESY experiments (Fig. 7.7).

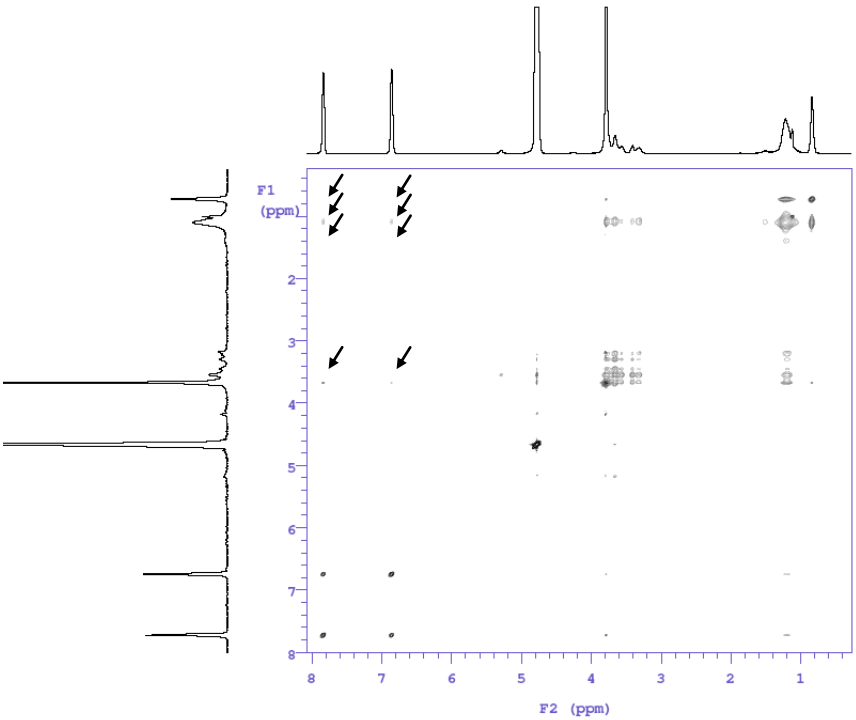

Figure 7.9, NOESY of 3.7mg/mL methylparaben in 20mg/mL DM. The interested cross-peaks are labeled using arrows.

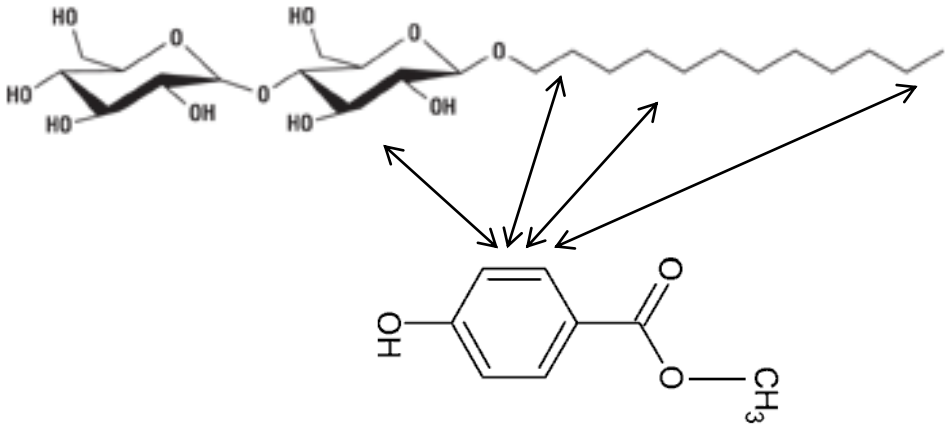

Figure 7.10, A schematic of inter-molecular interactions between methylparaben and DM molecules detected by NOESY experiments (Fig. 7.9).

cross-peak was significantly weakened by the much shorter spin-spin relaxation time (T_2=0.01~0.04s) for protons in DM micelles compared to the mixing time used in ROESY experiments (t_{mix}=0.3s).

Figure 7.11 is the ROESY spectrum of 3.7mg/mL ethylparaben in 15mg/mL SDS solutions. Ethylparaben has characteristic bands at 7.8 and 6.9ppm (aromatic ring), 4.3ppm (-CH_2- group), and 1.3ppm (methyl group). Compared to NMR bands of SDS, 4.0, 1.6, 1.2 and 0.8ppm, the methyl group band of the drug (1.3ppm) is very close to the peak of the hydrocarbon chain of SDS (1.2ppm) and is near the methyl group band of SDS (0.8ppm). When a small cross-peak (such as inter-molecular interactions) arises where two bands exhibit close chemical shifts, the signal is often difficult to be distinguished because of the t1-noise (along y-axis of Fig. 7.11) in a region close to the diagonal peaks of the 2-D spectrum. Therefore the interaction between methyl group of ethylparaben and alkyl chain of SDS is difficult to detect. On the other hand, from the off-diagonal cross-peaks, the following interactions between the drug and surfactant could be observed: the aromatic ring of ethylparaben with the alkyl chain of SDS (7.8/6.9ppm↔1.2ppm); the aromatic ring of the drug with the α-protons of SDS (7.8/6.9ppm↔4.0ppm). A schematic representation of the detected inter-molecular interactions between ethylparaben and SDS molecules is shown in Fig. 7.12. The results indicate the aromatic ring of ethylparaben is located between the head group and alkyl chain of the surfactant. The orientation of the model drug cannot be determined from the ROESY experiment.

Shown in Figure 7.13 is the ROESY spectrum of 5.8mg/mL ethylparaben in 20mg/mL DTAB solutions. Inter-molecular interactions included: the aromatic ring of ethylparaben with the hydrocarbon chain of DTAB (7.8/6.9ppm↔1.2ppm); the aromatic ring of the drug with the methyl groups in head group of DTAB (7.8/6.9ppm↔3.1ppm). The

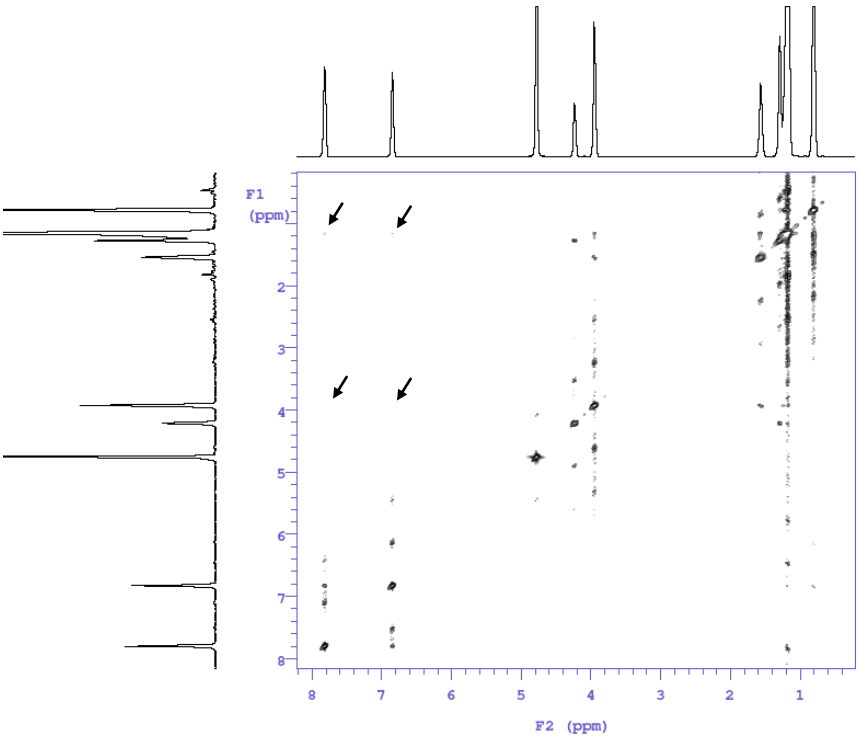

Figure 7.11, ROESY of 3.7mg/mL ethylparaben in 15mg/mL SDS. The interested cross-peaks are labeled using arrows.

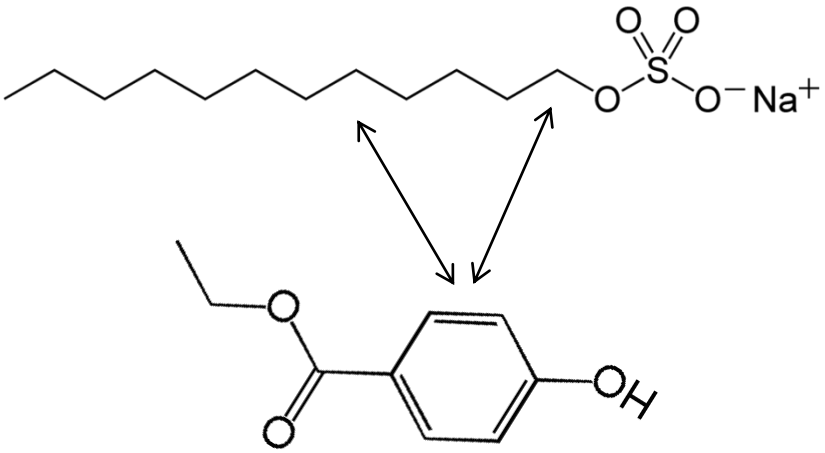

Figure 7.12, A schematic of inter-molecular interactions between ethylparaben and SDS molecules detected by ROESY experiments (Fig. 7.11).

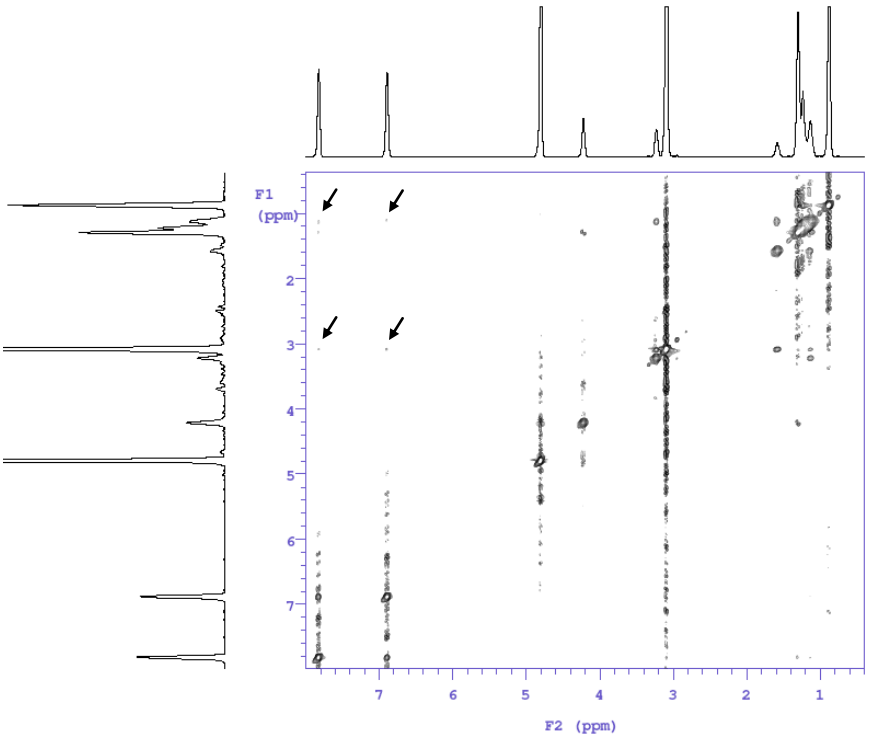

Figure 7.13, ROESY of 5.8mg/mL ethylparaben in 20mg/mL DTAB. The interested cross-peaks are labeled using arrows.

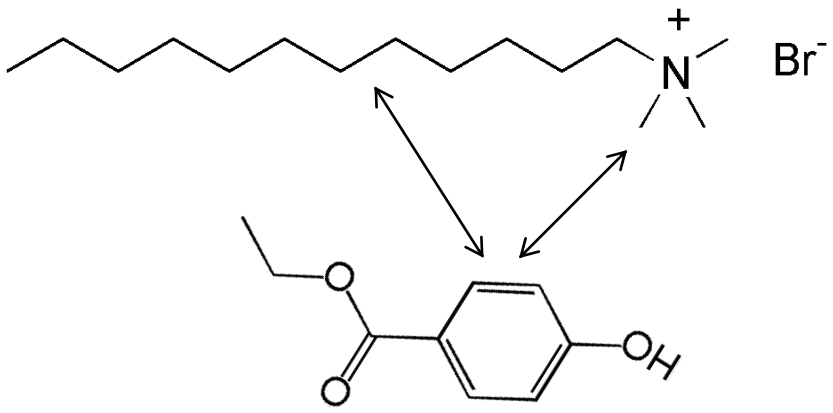

Figure 7.14, A schematic of inter-molecular interactions between ethylparaben and DTAB molecules detected by ROESY experiments (Fig. 7.13).

inter-molecular interactions are demonstrated in Figure 7.14. The aromatic ring of ethylparaben is close to both the head group and alkyl chain of the surfactant molecule which suggest the aromatic ring of the drug is near the surface of the DTAB micelles. Similar to that observed in ethylparaben/SDS system the 2-D NMR technique could not detect significant interaction between the methyl group of ethylparaben and the hydrophobic tail of DTAB. No conclusions concerning molecular orientation could be made.

Figure 7.15 is the ROESY spectrum of 5.0mg/mL butylparaben in 15mg/mL SDS solutions. Butylparaben has characteristic peaks at 7.8 & 6.9ppm (aromatic ring), 4.2ppm (α-protons), 1.7ppm (β-protons), 1.4ppm (γ-protons), and 0.9ppm (methyl group). The short spacing between the NMR bands of alkyl chain of butylparaben and the peaks of alkyl chain of SDS (4.0, 1.6, 1.2 and 0.8ppm) prevents unambiguous identification of interactions between alkyl chains of the drug and surfactant. On the other hand the cross-peaks between the aromatic ring of butylparaben (7.8/6.9ppm) and the alkyl chain (1.2ppm) or α-protons (4.0ppm) of SDS were observed. The corresponding interactions are illustrated in Figure 7.16 which suggests the aromatic ring of butylparaben is located between the head group and alkyl chain of the surfactant and therefore is in the vicinity of the micelle surface.

For all three parabens, the aromatic rings of the drug are shown to be close to micelle surface. When methylparaben is solubilized in ionic surfactant systems (SDS and DTAB), the methyl group of the drug is spatially close to the terminal methyl group of hydrophobic tail of the surfactant. The orientation of model solute could be determined: methyl group of methylparaben penetrats into the micelle core and the hydroxyl group of methylparaben must be on the micelle surface contacting water molecules. The location of methyl groups of ethylparaben and butylparaben in micelle could not be defined so

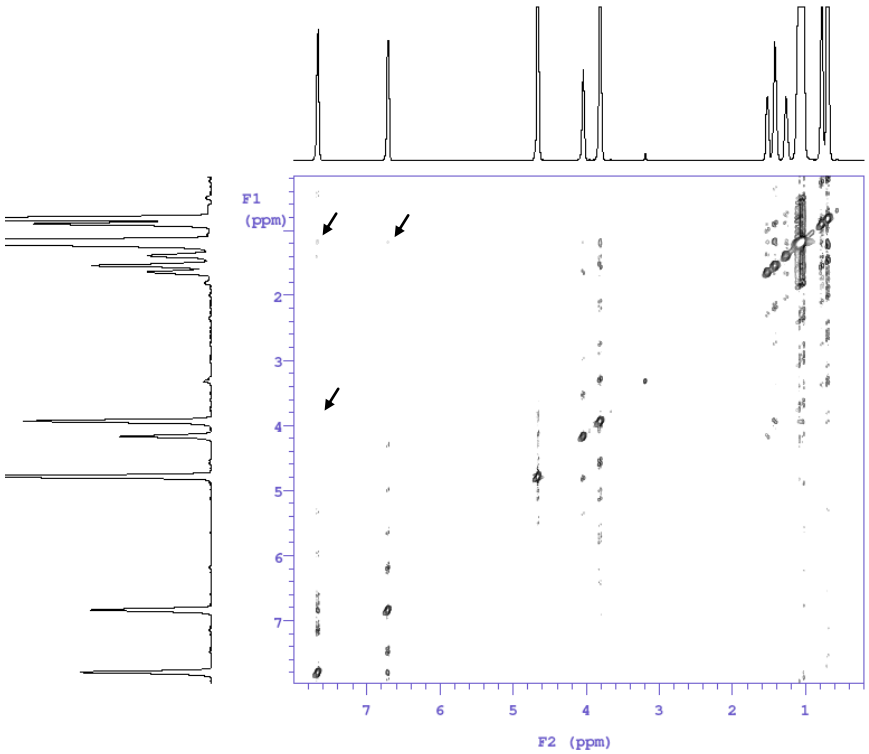

Figure 7.15, ROESY of 5.0mg/mL butylparaben in 15mg/mL SDS. The interested cross-peaks are labeled using arrows.

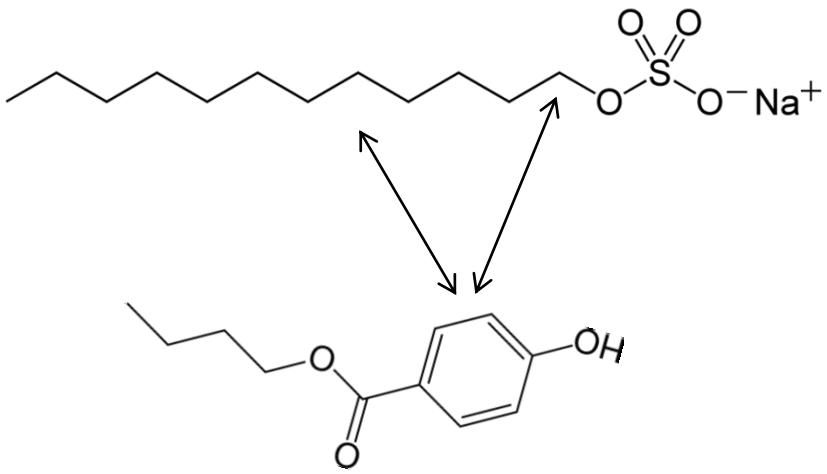

Figure 7.16, A schematic of inter-molecular interactions between butylparaben and SDS molecules detected by ROESY experiments (Fig. 7.15).

easily because the corresponding NMR peaks are close to the peaks of hydrophobic tail of surfactants. A weak cross-peak between two NMR bands that are near to each other in chemical shift is usually overwhelmed by the t1 noise in the 2-D NMR spectrum. In nonionic surfactant system, the interactions between the aromatic rings of methylparaben and all characteristic peaks of DM were observed. It may be due to the compact molecular packing in DM micelle.

7.3.1.3. 2-D NMR for Benzodiazepines in Micelles

Figure 7.17 shows the ROESY spectrum of 3.8mg/mL diazepam in 15mg/mL SDS solutions. The NMR bands assigned to diazepam have 7.6ppm (-8H, -9H), 7.5/7.4ppm (benzene ring connected to C-5), 7.1ppm (-6H), 4.6/3.8ppm ($-CH_2-$), and 3.4ppm ($-CH_3$). As marked with arrows in the figure, the observed cross-peaks between the drug and surfactant include 7.5↔1.2ppm, 7.5↔4.0ppm, 7.4↔1.2ppm, and 7.1↔1.2ppm. The corresponding intermolecular interactions are illustrated in Figure 7.18. The benzene ring connected to C-5 of diazepam is close to both the α-protons and alkyl chain of SDS molecule. The proton at C-6 position of diazepam is near the alkyl chain of SDS molecule in the micelles. These interactions indicate that part of diazepam molecule, e.g. the benzene ring at C-5, is near the head group of surfactant and therefore close to the micelle surface.

Shown in Figure 7.19 is the ROESY spectrum of 4.4mg/mL temazepam in 15mg/mL SDS. The characteristic peaks for temazepam have 7.6ppm (-8H, -9H), 7.5/7.4ppm (benzene ring connected to C-5), 7.1ppm (-6H), 3.4ppm ($-CH_3$). The observed cross-peaks are: 7.5↔1.2ppm, 7.5↔3.9ppm, 7.4↔1.2ppm, 7.4↔3.9ppm and 7.1↔1.2ppm (labeled using arrows in Fig. 7.19). The corresponding intermolecular interactions between temazepam and SDS molecules are shown in Figure 7.20. The benzene ring at C-5 position of temazepam is close to both the α-protons and alkyl chain

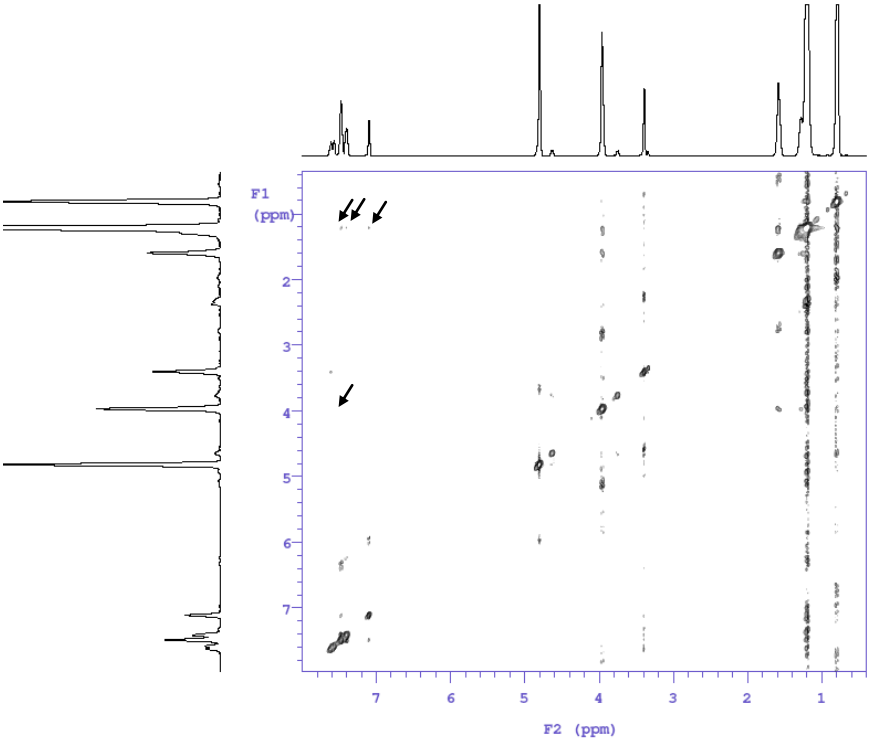

Figure 7.17, ROESY of 3.8mg/mL diazepam in 15mg/mL SDS. The interested cross-peaks are labeled using arrows.

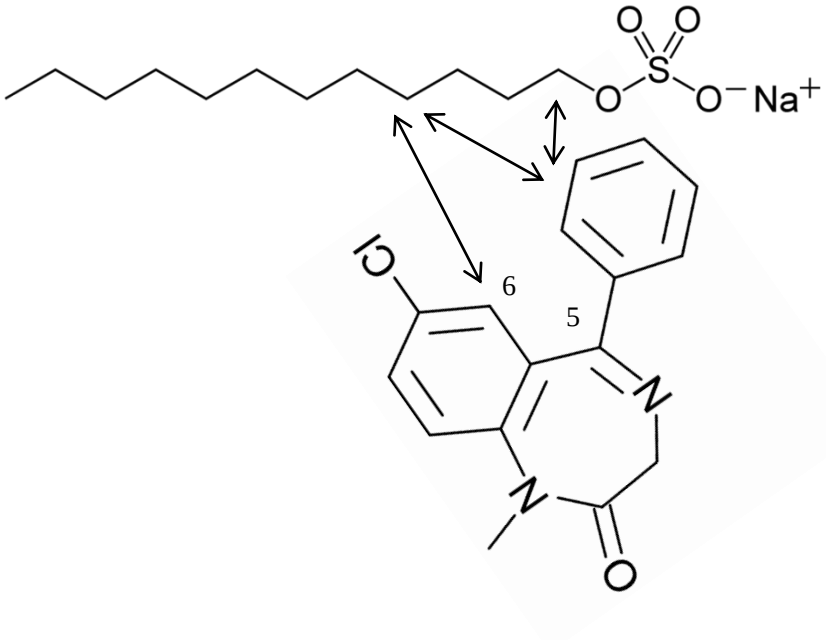

Figure 7.18, A schematic of inter-molecular interactions between diazepam and SDS molecules detected by ROESY experiments (Fig. 7.17).

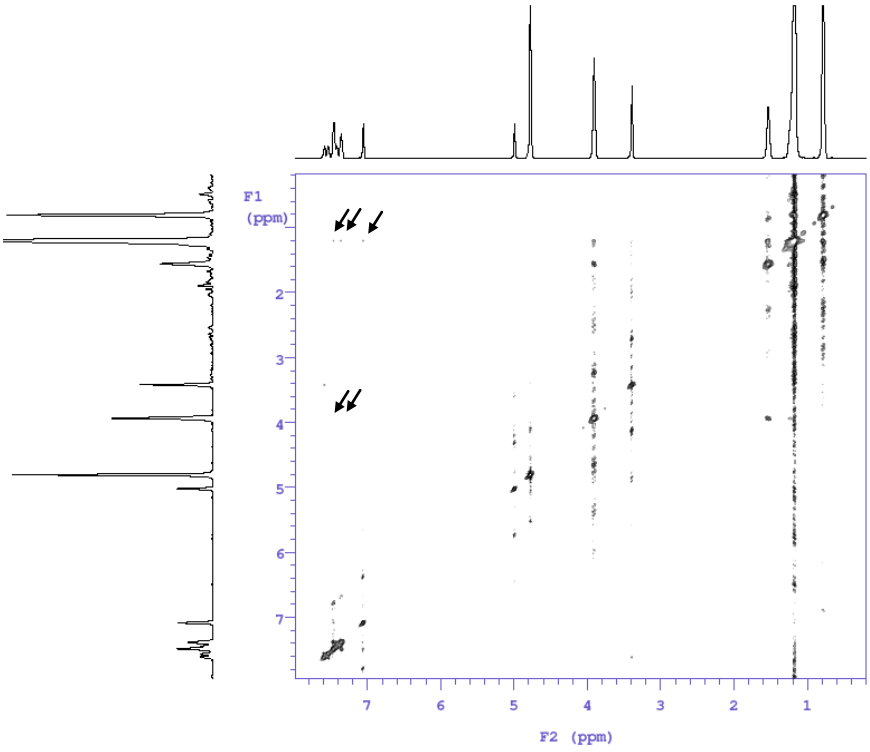

Figure 7.19, ROESY of 4.4mg/mL temazepam in 15mg/mL SDS. The interested cross-peaks are labeled using arrows.

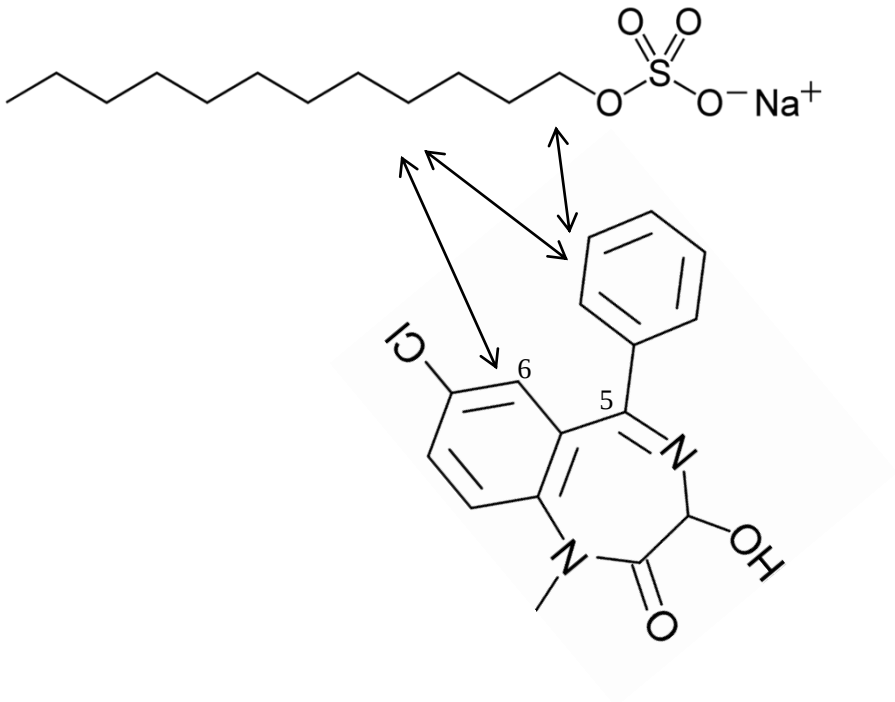

Figure 7.20, A schematic of inter-molecular interactions between temazepam and SDS molecules detected by ROESY experiments (Fig. 7.19).

of surfactant. The proton at C-6 position of temazepam is near alkyl chain of SDS molecule. These drug-surfactant interactions suggest part of temazepam molecules is close to the micelle surface, e.g. the benzene ring at C-5 position.

Figure 7.21 shows the ROESY spectrum of 1.6mg/mL temazepam in 20mg/mL DTAB solutions. The detected inter-molecular interactions include: the benzene ring at C-5 position of temazepam with the alkyl chain of DTAB (7.6/7.5↔1.3ppm); the benzene ring at C-5 of temazepam with the methyl groups at head group of DTAB (7.6↔3.1ppm); the proton at C-6 of temazepam with the alkyl chain of DTAB (7.2↔1.3ppm). Figure 7.22 shows the schematic representation of inter-molecular interactions between the drug and surfactant molecules. The benzene ring at C-5 of temazepam is near micelle surface due to the short distance between the benzene ring and head group of DTAB. The measured intermolecular interactions are not sufficient to determine the orientation of temazepam in the micelles.

ROESY spectrum of 0.7mg/mL temazepam in 20mg/mL DM solutions was measured with the results not shown here. No cross-peak corresponding to inter-molecular interaction was observed. The relatively low concentration of drug compared to the surfactant concentration and the short spin-spin relaxation time (T_2) of DM compared to the mixing time are two reasons for the failure of detecting inter-molecular interactions in the system.

In conclusion, when benzodiazepines are solubilized in ionic surfactant systems (SDS and DTAB), 2-D NMR method can detect the interactions between the benzene ring at C-5 position of benzodiazepines and both the head groups (α-protons of SDS or methyl groups at head group of DTAB) and alkyl chain of surfactant molecules. The results indicate the benzene ring at C-5 of the drug molecules are in the vicinity of the micelle

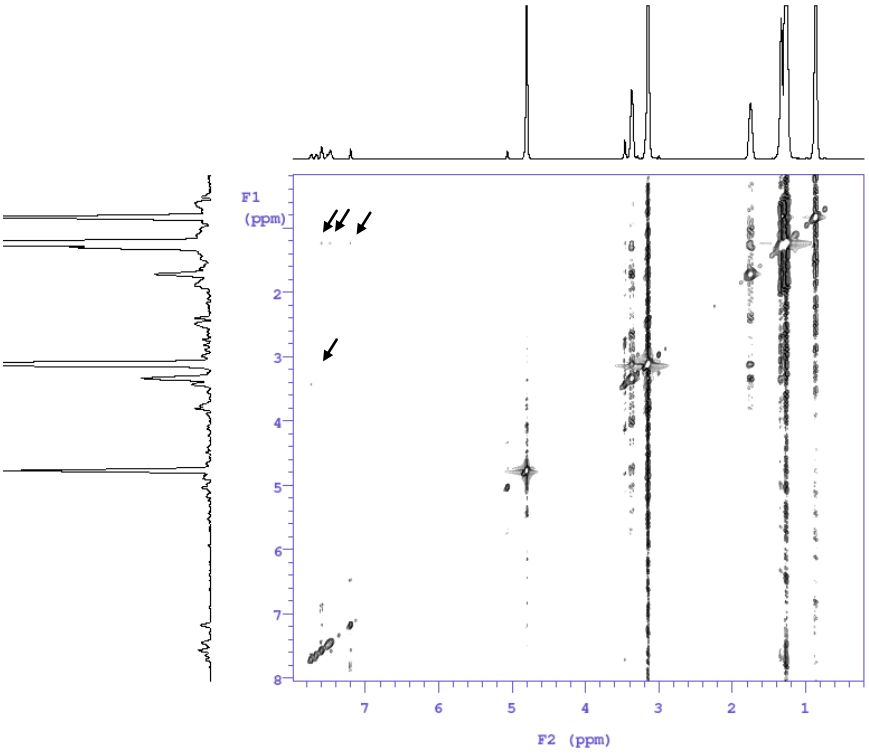

Figure 7.21, ROESY of 1.6mg/mL temazepam in 20mg/mL DTAB. The interested cross-peaks are labeled using arrows.

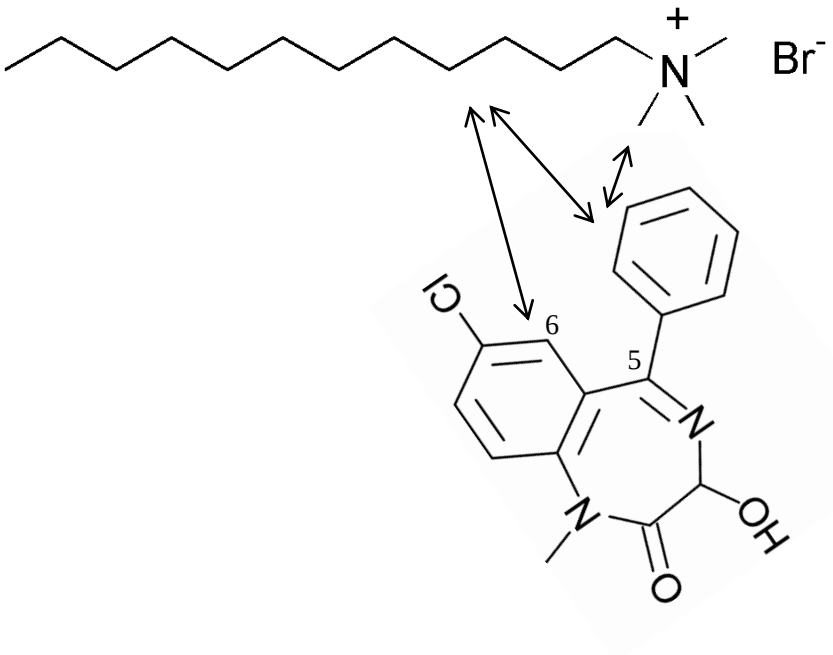

Figure 7.22, A schematic of inter-molecular interactions between temazepam and DTAB molecules detected by ROESY experiments (Fig. 7.21).

surface. Since some other functional groups of benzodiazepines, e.g. carbonyl and/or hydroxyl groups, are more hydrophilic than the benzene ring, it is very likely those hydrophilic groups are located at the micelle surface and contact with water molecules.

7.3.2. Pulse Gradient Spin-Echo (PGSE) NMR

PGSE NMR technique was employed to measure the diffusivity of drug or surfactant molecule in solutions. The diffusivity was correlated to particle size through Stokes-Einstein relation assuming the particle had a spherical shape:

$$D = \frac{k_B T}{6\pi\eta\, r} \tag{7.2}$$

where D is the diffusivity; k_B is the Boltzmann's constant (1.38×10^{-23} J/K); η is the viscosity of media; and r is the radius of the particle. Fortunately, the model micelles had a spherical shape (Yalkowski and Zografi, 1972) which satisfied the requirement of Stokes-Einstein relation. Since k_B, T and η are all constant or near constant in our study, the micelle size could be detected by measuring the diffusivity of the micelle.

For both the drug and surfactant, the measured diffusivities are comprised of two components, monomers and micelles. The total diffusivity could be expressed as:

$$D_{total} = f_{monomer} D_{monomer} + (1 - f_{monomer}) D_{micelle} \tag{7.3}$$

where D_{total}, $D_{monomer}$, $D_{micelle}$ are measured diffusivity, diffusivity of the monomer and diffusivity of the micelle, respectively; $f_{monomer}$ is the mole fraction of the drug or surfactant in monomer state in solutions. Only under conditions $f_{monomer} << 1$ and $f_{monomer} D_{monomer} << D_{total}$, the measured total diffusivity would reflect the diffusivity of micelle.

The micelle size was measured as a function of drug concentration in order to detect the extent to which the micelle size may change when drugs were solubilized.

7.3.2.1. Drugs Solubilized in SDS Micelles

Progesterone, diazepam and butylparaben were chosen as representatives of the three model drug series. The concentration of SDS was fixed at 15mg/mL. The measured diffusivities of drug molecules as a function of drug concentration are shown in Figure 7.23. Rearranging Eq. (7.3), the diffusivity of the micelle can be expressed as:

$$D_{micelle} = \frac{D_{total} - f_{monomer} D_{monomer}}{1 - f_{monomer}} \tag{7.4}$$

The diffusivity of progesterone monomer in D_2O has been reported as $(5.68\pm0.07)\times10^{-6}$ cm^2/s (Land, 2005). The diffusivity of the diazepam or butylparaben monomer was estimated based on approximate relationship:

$$D_{drug} = D_{progesterone}\left(\frac{V_{progesterone}}{V_{drug}}\right)^{1/3} \tag{7.5}$$

where D_{drug} and $D_{progestereone}$ are the diffusivities of the drug and progesterone monomers in D_2O; $V_{progesterone}$ and V_{drug} are molar volumes of the drug and progesterone. The molar volumes of the model drugs could be obtained from Table 5.1. The validity of Eq.(7.5) was tested by comparing the calculated diffusivity of methylparaben in D_2O (7.6×10^{-6} cm^2/s) to that of the measured value (7.4×10^{-6} cm^2/s). Applying Eq. (7.5), the diffusivities of diazepam and butylparaben monomers in D_2O were 6.2×10^{-6} and 6.8×10^{-6} cm^2/s, respectively.

The mole fraction of drug monomers as a function of total drug concentration could be estimated from the solubilization results in Chapter 3 (Table 3.2~3.4 and Fig. 3.14, 3.17 and 3.20). The $f_{monomer}$ values are 0.0027 for progesterone, 0.010 for diazepam and 0.033 for butylparaben. Substituting the values of $D_{monomer}$ and $f_{monomer}$ into Eq. (7.4), the measured diffusivities of SDS micelles are 6.8, 6.6 and 6.5×10^{-7} cm^2/s when progesterone, diazepam and butylparaben were used as the solubilizates. Using the average value of the

diffusivities, 6.6×10^{-7} cm^2/s, and viscosity of D_2O at 27°C (1.05cP) (Cho et al., 1999) in Eq. (7.2), the radius of SDS micelle is determined to be 32Å.

As shown in Fig. 7.23, for all three model drugs, the diffusivities of micelle exhibit no statistically significant changes in radius with varying drug concentration, indicating the micelle size remains constant even when solubilizing drugs. The results support the co-adsorption model of the drug and surfactant at micelle surface where micelle size remains constant.

In Figure 7.23, the effect of added electrolyte on the micelle size is also presented. In the presence of 0.15M NaCl in 15mg/mL SDS solutions, the total diffusivities of progesterone and diazepam are significantly larger than the diffusivities in the absence of salt. The mole fractions of drug monomers could be determined from the solubilization results in Chapter 3 (Table 3.5, Fig. 3.24). The $f_{monomer}$ values are 0.0040 for progesterone and 0.012 for diazepam. Eq. (7.4) was employed to determine the diffusivities of SDS micelles to be 7.7×10^{-7} (progesterone as solute) and 7.3×10^{-7} cm^2/s (diazepam as solute). Using Eq. (7.2), the micelle size is estimated to be 28Å, a value slightly smaller than the 32Å found in the absence of NaCl.

In may also be noted in Figure 7.23 that in the presence of 0.15M NaCl, the micelle size is not significantly changed with increasing drug concentration.

7.3.2.2. Drugs Solubilized in DTAB Micelles

Progesterone, diazepam and butylparaben were solubilized in 20mg/mL DTAB solutions. The diffusivities of drug molecules were measured as a function of drug concentration with results shown in Figure 7.24 and 7.25. Based on early studies on solubilization of

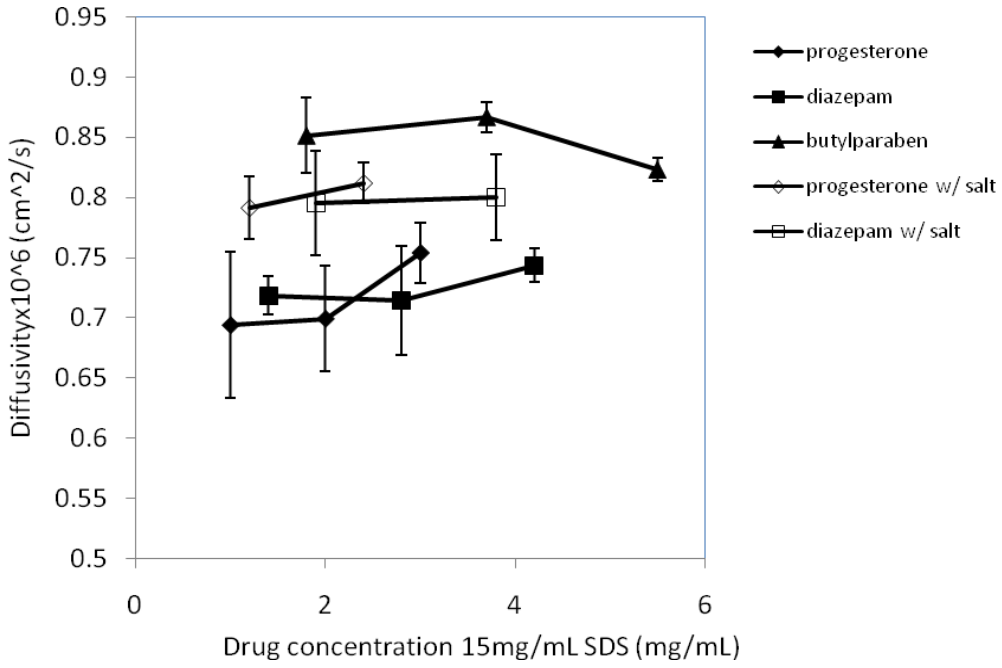

Figure 7.23, Diffusivities of progesterone, diazepam and butylparaben as a function of drug concentration in 15mg/mL SDS solutions in the absence and presence of 0.15M NaCl.

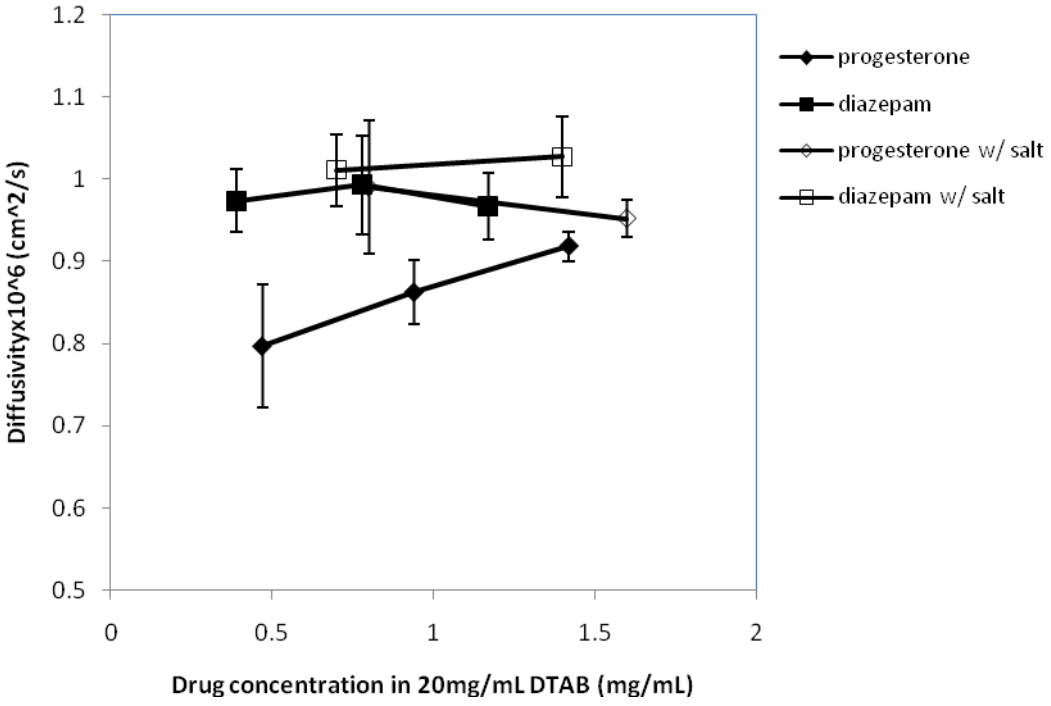

Figure 7.24, Diffusivities of progesterone and diazepam as a function of drug concentration in 20mg/mL DTAB solutions in the absence and presence of 0.15M NaCl.

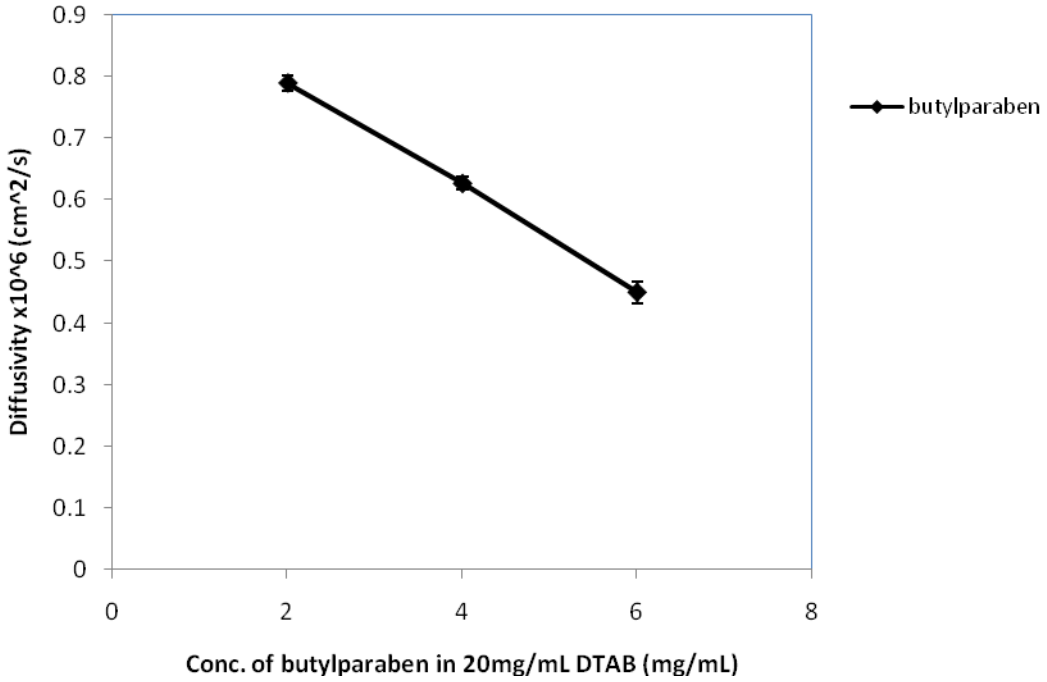

Figure 7.25, Diffusivities of butylparaben as a function of drug concentration in 20mg/mL DTAB solutions.

progesterone and diazepam in DTAB solutions (Table 3.2~3.3, Fig. 3.15 and 3.18), the mole fractions of drug monomers, $f_{monomer}$, are 0.0055 for progesterone and 0.033 for diazepam. The calculated diffusivities of DTAB micelles from Eq. (7.4) are 7.7×10^{-7} cm^2/s (progesterone as solute) and 7.9×10^{-7} cm^2/s (diazepam as solute). The hydrodynamic radius of DTAB micelle is calculated from Eq. (7.2) to be 27Å.

From Fig. 7.24, with increasing concentration of progesterone, the micelle size of DTAB was observed to decrease slightly, but significantly, due to the increase in diffusivity of the micelle. The student's t-test gives a two-tailed p-value of <0.01 (0.007) between the diffusivities at low (0.47mg/mL) and high (1.42mg/mL) concentrations of progesterone (using unequal variances because the measured diffusivity of a substance has a larger standard deviation at lower concentration of the substance). For diazepam, the radius of DTAB micelle has no significant change with increasing drug concentration. Both of the results suggested the solubilized drug may replace surfactant molecules during the solubilization process to keep micelle size constant or even decrease micelle size.

In our early solubilization studies (Chap. 3), it was observed that additon of butylparaben to DTAB solution could make the solutions cloudy indicating the disturbance of DTAB micelle structures. Here we investigated the size of newly formed assemblies by measuring the corresponding diffusivity. Figure 7.25 shows the diffusivity of butylparaben is dramatically decreased with increasing drug concentration in the DTAB solutions. When the concentration of butylparaben is increased from 2mg/mL to 6mg/mL, the diffusivity of butylparaben is decreased by 43%. The corresponding micelle size and micelle volume would increase by approximately 43% and 190%, respectively. The significant grow of micelle size may have resulted in phase transition of the system and the cloudy appearance of butylparaben in DTAB mixture.

The effect of added electrolyte on DTAB micelle size is shown in Fig. 7.24. In the presence of 0.15M NaCl in 20mg/mL DTAB solutions, the diffusivities of progesterone and diazepam were measured as a function of drug concentration. To estimate the contribution of drug monomers to total measured diffusivity, the mole fraction, $f_{monomer}$, was determined using the early solubilization results in the presence of salt (Table 3.5 and Fig. 3.25). The mole fraction of progesterone monomers is 0.0061 and the mole fraction of diazepam monomers is 0.032. The diffusivities of DTAB micelles are calculated from Eq. (7.4) to be 9.2×10^{-7} cm^2/s (progesterone as solute) and 8.4×10^{-7} cm^2/s (diazepam as solute). Using the average value of micelle diffusivities in Eq. (7.2), the estimated hydrodynamic radius of the DTAB micelle in the presence of 0.15M NaCl is 24Å which is smaller than the radius of the DTAB micelle in the absence of NaCl (27Å).

7.3.2.3. Drugs Solubilized in DM Micelles

Figure 7.26 shows the diffusivities of dodecyl β-D-maltoside (20mg/mL) as a function of concentration of model drugs, progesterone and diazepam. Due to the low solubilization capacity of DM micelles, the concentration of solubilized drugs is much lower than the surfactant concentration, resulting in weak NMR signals. The diffusivity measurements of drug molecules using those weak NMR signals exhibited large relative error (>10%) and were not used in micellar size determination. As an alternative, diffusivity of the DM micelle was determined by employing DM-associated NMR signals.

To estimate the diffusivity of the DM micelle using Eq. (7.4), the diffusivity of DM monomers was required. It may be inappropriate to extrapolate the diffusivity of DM monomer from the diffusion coefficient of progesterone using Eq. (7.5) because DM has a long chain structure while the structure of progesterone is bulky. The structural similarity between DM and SDS molecules enabled us to estimate the diffusivity of DM

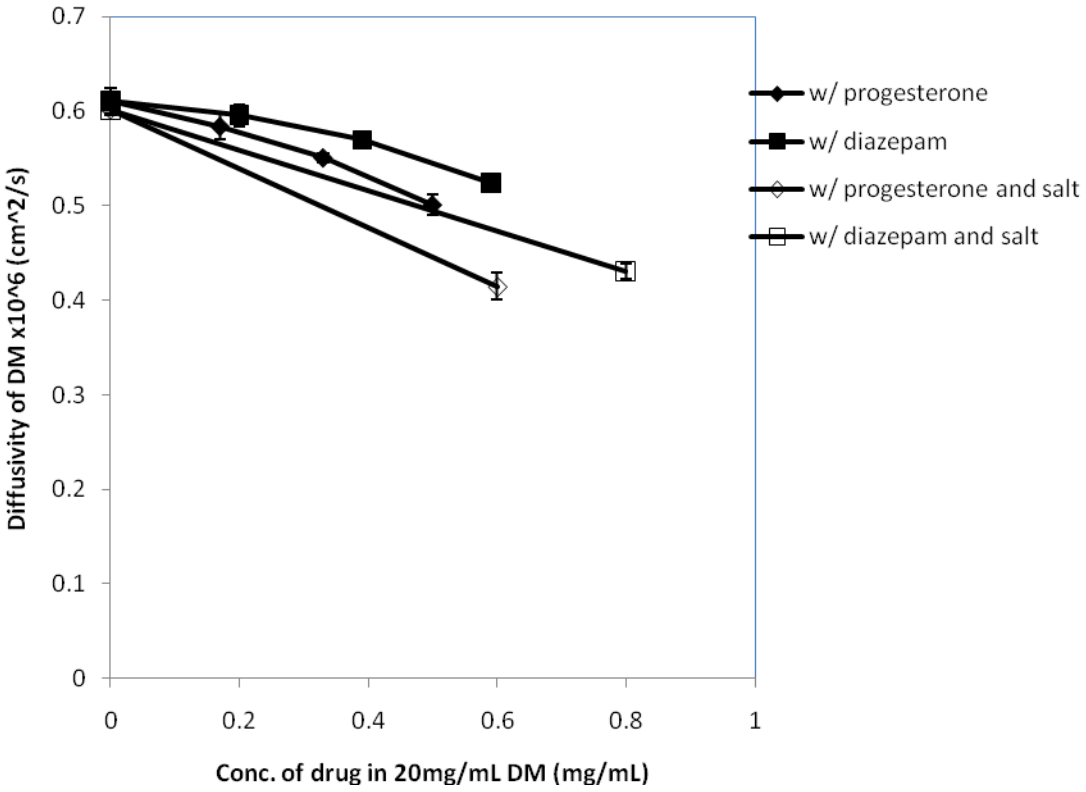

Figure 7.26, Diffusivities of DM as a function of drug concentration in 20mg/mL DM solutions in the absence and presence of 0.15M NaCl. Two model drugs, progesterone and diazepam, were used.

monomer based on diffusion coefficient of dodecyl sulfate monomer. The measured $D_{monomer}$ of dodecyl sulfate ion is 4.6×10^{-6} cm^2/s at SDS concentration below the CMC. The McGowan volumes of dodecyl sulfate and DM are calculated to be 361 and 651Å^3/molecule (McGowan, 1978), respectively. Employing Eq.(7.5), the estimated diffusivity of DM monomer is 3.8×10^{-6} cm^2/s. consequently, the diffusivity of DM micelle in the absence of drug is 6.0×10^{-7} cm^2/s. The hydrodynamic radius of DM micelle is calculated from Stokes-Einstein relation to be 35Å.

From Fig. 7.26, the diffusivity of micelles is significantly decreased in the presence of either progesterone or diazepam. When drug concentrations are raised to 0.5mg/mL for progesterone and 0.6mg/mL for diazepam, the diffusivities of DM micelles are decreased by 18% and 15%, respectively, that corresponds to increases of the micelle size by 18% (progesterone as solute) and 15% (diazepam as solute). The volume changes of DM micelles due to the solubilization of model drugs would be more dramatic: 64% (progesterone) and 52% (diazepam) increases. Assuming the drugs were simply added to DM micelles, the volumes of the micelles should be increased by only ~2.5% for progesterone and ~3% for diazepam. The measured volume changes of DM micelles are significantly larger than those based on the simple addition model, suggesting the aggregation number of DM micelle must be increased dramatically even in the presence of small amount of solubilized drug molecules.

The effect of adding 0.15M NaCl on the measured diffusivities of DM molecule as a function of concentration of model drugs, progesterone and diazepam, is shown also in Figure 7.26. In the absence of drug, the diffusivity of DM molecule in the presence of salts is not significantly different from that in the absence of salts, suggesting the micelle size does not change with added salts. The additions of 0.6mg/mL progesterone and 0.8mg/mL diazepam result in a decrease in the diffusivities of DM by 31% and 29%,

respectively. Similar to drug in DM micelle systems in the absence of salt, the micelle volumes are dramatically increased by 125% (progesterone as solute) and 115% (diazepam as solute) when solubilizing <4% (w/w) model drugs in micelles. Under these conditions, the aggregation number of DM micelle must be increased significantly with increasing drug concentration. Our early studies in Section 5.3.4.2 used the surface-localized thermodynamic model to demonstrate the solubilizations were not very sensitive to the aggregation number of DM micelles.

7.3.2.4. Support for Competition of the Drug and Surfactant at the Micelle Surface

In the interfacial tension experiments in the bulk state outlined in Chapter 4, competition between the drugs and surfactants for the dodecane/water clearly occurred. It is interesting to speculate whether the co-adsorption of drug and surfactant in the micelle might be described as a competition for micelle interface. If we hypothesize that the drugs are competing with surfactants at the micelle surface, the micelle size must not increase upon drug solubilization. Under the condition of constant micelle size, the drug molecule could replace surfactant molecule at micelle surface instead of simply adding to the micelle. The studies in Sections 7.3.2.1 and 7.3.2.2 showed the radii of SDS and DTAB micelles are not significantly increased with the increasing concentration of solubilizates, e.g. progesterone and diazepam, both in the absence and presence of 0.15N NaCl. In the case of progesterone in DTAB system (in the absence of NaCl), the micelles size is even significantly decreased with increasing drug concentration. These results would be consistent with the hypothesis that the added drugs to micelles may be replacing surfactant molecules due to the limited surface area of a micelle. Additional work would be necessary before a definitive conclusion of competition over co-adsorption could be drawn.

7.3.2.5. Possible Self-Association of Drug Molecules

Previously, we alluded to the assumption that the drug molecules do not self-associate in bulk solution. To test this assumption, we measured the diffusivities of the drug as a function of drug concentration. The results are shown in Figure 7.27. If the drug could self-associate at a certain drug concentration, the diffusivity of methylparaben as a function of drug concentration would exhibit a breakpoint connecting a constant diffusivity region and a descending curve with increasing drug concentration. The results in Figure 7.27 show that the diffusivity of methylparaben is independent of the drug concentration up to the aqueous solubility. The absolute diffusivity value of methylparaben could also rule out the formation of dimer or oligomer because the diffusivity of dimer or oligomer should be lower than 6.0×10^{-6} cm^2/s according to Eq. (7.5). The measured diffusivity is, in fact, higher at $7.3\pm0.1\times10^{-6}$ cm^2/s. Based on above analyses it may be concluded that methylparaben does not self-associate in aqueous solutions.

7.4. CONCLUSION

The two-dimensional NMR techniques including ROESY and NOESY were employed to probe the inter-molecular interactions between the drug and surfactant molecules in the micelles. In steroids/surfactants systems, the overlaps of NMR bands between solute molecules and hydrocarbon chains of surfactants (not including terminal methyl group) hindered the possible intermolecular interactions.

When parabens were solubilized in SDS and DTAB micelles, the interactions between aromatic rings of parabens and alkyl chains of surfactants as well as α-protons of SDS or methyl groups at head group of DTAB were clearly detected which indicated the aromatic rings of parabens were close to micelle surface. For methylparaben in SDS and DTAB systems, the methyl groups of the drug was found to be spatially close to the terminal

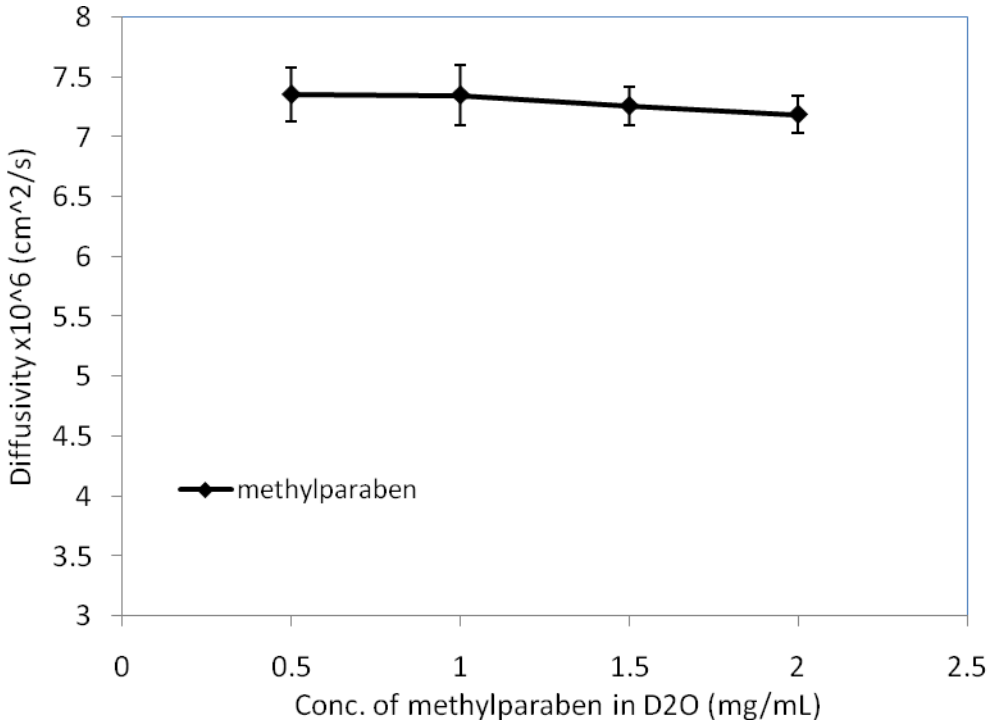

Figure 7.27, Diffusion coefficients of methylparaben in D_2O as a function of drug concentration.

methyl groups of alkyl chains of surfactants. Then the orientation of methylparaben in SDS/DTAB micelles was determined: the phenol group was likely located at micelle surface and the methyl group penetrated inside the micelles. For ethylparaben and butylparaben solubilized in SDS and DTAB micelle systems, the methyl groups of the drugs had chemical shifts close to that of methyl group in alkyl chain of surfactant which made the detection of corresponding cross-peaks difficult due to the big t1-noise. In methylparaben/DM system, the interactions between aromatic ring of the drug and many NMR bands of DM including head group, hydrocarbon chain and even the terminal methyl group of hydrophobic tail of DM. The nonspecific interactions may be due to the compact molecular packing in the nonionic micelles.

In benzodiazepine/surfactant systems, the interactions between benzene ring at C-5 position of benzodiazepines and both alkyl chain and head group (α-prontons in SDS or methyl groups at N-1 position of DTAB) of ionic surfactants were observed which suggested part of benzodiazepine molecule was located in the vicinity of the micelle surface. When benzodiazepines were solubilized in DM micelles, the relatively low solubilization capacity of the nonionic micelles resulted in a drug concentration much less than surfactant concentration. Therefore the cross-peaks between drug and surfactant, whose intensities were proportional to drug and surfactant concentrations, were too weak to be detected.

In all drug/surfactant systems where inter-molecular interactions were detected, there were some evidences that show part of solubilized drug was close to micelle surface. This finding supported our micellar surface solubilization picture based on the thermodynamic analyses in Chapter 3~5.

The PGSE NMR method was utilized to measure the diffusivity and size of the micelles in the presence of different drugs. The sizes of SDS micelles had no statistically significant change with increasing concentration of progesterone, diazepam or butylparaben. The phenomena are consistent with the hypothesis that added drug molecules may replace surfactant molecules in micelles to keep the micelle size constant in agreement with the existence of drug-surfactant competition for micelle surface. The sizes of DTAB micelles were either slightly decreased or unchanged with increasing concentration of progesterone or diazepam which also supported the co-adsorption of the drug and surfactant at the micelle surface. When butylparaben was added to DTAB solutions, the micelle size was significantly increased by up to 43%. The cloudy appearance of the solutions suggests a broad distribution of micelle sizes. For nonionic DM micelles, the solubilization of small amount of hydrophobic drug resulted in significant increase in micelle size and aggregation number.

The salt effect on micelle size was studied. The hydrodynamic radii of SDS and DTAB micelles were decreased in the presence of 0.15M NaCl while the hydrodynamic radii of DM micelles were not affected by salts. The sizes of SDS and DTAB micelles showed no significant change with increasing concentration of progesterone or diazepam in the presence of salts. The results indicate the co-adsorption of the drug and surfactant at micelle surface would happen even in the presence of salts. On the other hand, the sizes of DM micelles were significantly increased with added progesterone or diazepam in the presence of salts. It may be due to the decrease in Laplace pressure by the solubilized drug at micelle surface that let the surfactant move to micelle surface more easily.

Chapter 8

Conclusions and Future Work

In summary, the following experimental results have been obtained:

- For three series of model drugs in three micelle systems, the measured micelle/water partitioning coefficients were much larger than hydrocarbon/water partitioning coefficients, which indicated the core region of micelle was insufficient to solubilize the model hydrophobic drugs.
- Hydrocarbon/water interfacial tension could be significantly decreased in the presence of hydrophobic drugs, while the model drugs exhibited little or no surface activity at oil/air or water/air interface. The hydrophobic drugs could compete with surfactant molecules for the oil/water interface and the competition could be quantitatively simulated using thermodynamic model.
- A surface-localized thermodynamic model that considered the surfactant-drug co-adsorption at the micelle surface was successfully applied to predict the micelle/water partitioning coefficients of three series of model drugs in three micelle systems. The critical parameters in calculating micelle/water partitioning included the radii of micelles, surface activities of model drugs at oil/water interface ($\Delta G_{\text{water}\rightarrow\text{interface}}$) and surface pressure at the micelle surface.
- The surface-localized thermodynamic model successfully explained the salt effect on micellar solubilization, drug concentration dependency for micelle/water partitioning (solubilization isotherm), and surfactant CMC depression by solutes.
- Molecular simulations combined with experiments on drug adsorption at oil/water interface were employed to determine the orientation of drug at oil/water interface. The molecular orientations were strongly dependent on the distribution of

hydrophilic functional groups of model drugs.

- 2-D NMR (ROESY and NOESY) technique was able to detect some drug-surfactant interactions but also had limitations when strong overlaps of NMR peaks or low drug loading occurred.
- The measured diffusivities of micelles using PGSE NMR method showed insensitivity of micelle size (for ionic surfactants) to the solute concentration, which supported the drug-surfactant co-adsorption in micelles.

The overall goal of this dissertation is to probe the mechanism of drug solubilization in micelle systems. The work presented here provides a starting point for future studies that are laid out as followings:

- The surface-localized model could be extended to more complex mixed-micelle systems that are physiologically relevant, e.g. phospholipids/bile salts mixtures. The competitions between hydrophobic drugs and two surfactants for oil/water interface are expected.
- The surface adsorption of model drugs at oil/water interface could mimic biological membrane/water partitioning. Therefore, the permeability of drug through biological membrane may be correlated to the surface activities of the drug at hydrocarbon/water interface.
- The present work is mainly dealing with surfactants that have small headgroups. The micelle surface (oil/water interface) is the dominant locations for drugs. In practical applications, many nonionic surfactants have much larger headgroups that usually contain PEGylated chains, e.g. Tween80, VitaminE TPGS, CremophorEL, Solutol, etc. These bulky headgroups will introduce at least one more location for drug solubilization. A model that considers multi-locations will be proposed to predict the drug solubilization.

The progress on the mechanistic understanding and quantitative predictions on drug solubilization in micelle systems will provide a guideline for selecting solubilizing ingredients and speed up the drug formulation process.

APPENDICES

Appendix 1. Liquid-liquid Interfacial Adsorption by Two-dimensional Solution Model

Based on 2-D solution model, the chemical potential of a component of the interface can be expressed according to Butler's equation (Butler, 1932):

$$\mu_i^s = \mu_i^{s,0} + RT \ln\left(x_i^s f_i^s\right) - \gamma \cdot a_i \qquad \text{(A1.1)}$$

where μ_i is the chemical potential of component *i*, which could be water, drugs or surfactants; superscript *s* stands for surface; superscript 0 stands for standard state; *x* is the mole fraction based concentration; *f* is the activity coefficient; γ is the interfacial tension; and *a* is the partial molar interfacial area occupied by a molecule of component *i*. In the bulk phase the chemical potential could be written as:

$$\mu_i^l = \mu_i^{l,0} + RT \ln\left(x_i^l f_i^l\right) \qquad \text{(A1.2)}$$

where superscript *l* stands for bulk liquid. When the interface and bulk phase reach equilibrium the chemical potentials will be same:

$$\mu_i^s = \mu_i^l \qquad \text{(A1.3)}$$

In the absence of surface active species, the following relationship holds for solvent water:

$$\mu_{water}^{s,0} = \mu_{water}^{l,0} + \gamma_0 a_{water} \qquad \text{(A1.4)}$$

where γ_0 is the interfacial tension in the absence of surface active agents and a_{water} is the interfacial area occupied by a water molecule.

If the activity coefficients at the interface, f_i^s, are assumed to be unity for all molecules and f_i^l are assumed to be unity for neutral molecules, the above equations yield following relationships:

$$x^s_{water} = x^l_{water} \exp\left(-\frac{\pi a_{water}}{RT}\right) \cong \exp\left(-\frac{\pi a_{water}}{RT}\right) \quad \text{(A1.5a)}$$

$$x^s_{drug} = x^l_{drug} \exp\left(-\frac{\Delta G_{\text{water}\to\text{interface},drug}}{RT}\right)\exp\left(-\frac{\pi a_{drug}}{RT}\right) \quad \text{(A1.5b)}$$

$$x^s_{surfact} = \begin{cases} x^l_{surfact} \exp\left(-\frac{\Delta G_{\text{water}\to\text{interface},surfact}}{RT}\right)\exp\left(-\frac{\pi a_{surfact}}{RT}\right) & \text{for nonionic surfactant} \\ x^l_{surfact} f^l_{surfact} \exp\left(-\frac{\Delta G_{\text{water}\to\text{interface},surfact}}{RT}\right)\exp\left(-\frac{\pi a_{surfact}}{2RT}\right) & \text{for ionic surfactant} \end{cases} \quad \text{(A1.5c)}$$

where subscripts "water", "drug" and "surfact" represent water, drug and surfactant; $\Delta G_{\text{water}\to\text{interface}}$ is transfer free energy from bulk water to interface $\Delta G_{\text{water}\to\text{interface},i} = \mu_i^{s,0} - \mu_i^{l,0} - \gamma_0 a_i$; π is the surface pressure defined as interfacial tension difference between in the absence and presence of surfactant: $\pi = \gamma_0 - \gamma$. In Eq.(A1.5a), the mole fraction of bulk water, x^l_{water}, is chosen as 1 because $x^l_{surfact}, x^l_{drug}$ are both assumed to be much less than 1.

The total mole fractions of components occupying the surface will be equal to 1:

$$\begin{cases} x^s_{water} + x^s_{drug} + x^s_{surfact} = 1 & \text{(for nonionic surfactant)} \\ x^s_{water} + x^s_{drug} + 2x^s_{surfact} = 1 & \text{(for ionic surfactant)} \end{cases} \quad \text{(A1.6)}$$

The Eq.(A1.5a)~(A1.5c) are substituted into the appropriate equation (A1.6) in order to solve for surface pressure π. The final equation will have one of the following forms under selected conditions:

1) Only one type of ionic surfactant, e.g. SDS or DTAB, is present, Eq. (A1.6) becomes:

$$\exp\left(-\frac{\pi a_{water}}{RT}\right) + 2x^l_{surfact} f^l_{surfact} \exp\left(-\frac{\Delta G_{\text{water}\to\text{interface},surfact}}{RT}\right)\exp\left(-\frac{\pi a_{surfact}}{2RT}\right) = 1 \quad \text{(A1.7)}$$

2) Only one kind of nonionic surfactant or neutral drug is present, Eq. (A1.6) becomes:

$$\exp\left(-\frac{\pi a_{water}}{RT}\right)+x_i^l\exp\left(-\frac{\Delta G_{\text{water}\rightarrow\text{interface},i}}{RT}\right)\exp\left(-\frac{\pi a_i}{RT}\right)=1 \tag{A1.8}$$

where subscript *i* could be surfactant or drug.

3) Both ionic surfactant and neutral drug are present, Eq. (A1.6) becomes:

$$\begin{aligned}\exp\left(-\frac{\pi a_{water}}{RT}\right)+2x_{surfact}^l f_{surfact}^l\exp\left(-\frac{\Delta G_{\text{water}\rightarrow\text{interface},surfact}}{RT}\right)\exp\left(-\frac{\pi a_{surfact}}{2RT}\right)\\ +x_{drug}^l\exp\left(-\frac{\Delta G_{\text{water}\rightarrow\text{interface},drug}}{RT}\right)\exp\left(-\frac{\pi a_{drug}}{RT}\right)=1\end{aligned} \tag{A1.9}$$

4) Both nonionic surfactant and neutral drug are present, Eq. (A1.6) becomes:

$$\begin{aligned}\exp\left(-\frac{\pi a_{water}}{RT}\right)+x_{surfact}^l\exp\left(-\frac{\Delta G_{\text{water}\rightarrow\text{interface},surfact}}{RT}\right)\exp\left(-\frac{\pi a_{surfact}}{RT}\right)\\ +x_{drug}^l\exp\left(-\frac{\Delta G_{\text{water}\rightarrow\text{interface},drug}}{RT}\right)\exp\left(-\frac{\pi a_{drug}}{RT}\right)=1\end{aligned} \tag{A1.10}$$

The oil/water surface tension in the presence of one or two surface active components could be calculated by $\gamma=\gamma_0-\pi$ using the surface pressure solved from Eq. (A1.7)~(A1.10).

Another important property of surface adsorption is the surface pressure as a function of interfacial area per surfactant molecule, known as the π-A relationship. For ionic surfactant in the absence of drug, according to 2-D solution model, the interfacial area per surfactant (*A*) can be calculated as follows:

$$A = \frac{a_{water} x^s_{water} + a_{surfact} x^s_{surfact}}{x^s_{surfact}} = a_{surfact} + a_{water} \frac{x^s_{water}}{x^s_{surfact}} \qquad \text{(A1.11)}$$

Rearranging Eq. (A1.6), $x^s_{water} + 2x^s_{surfact} = 1$, to $x^s_{surfact} = (1 - x^s_{water})/2$. Substituting the expression for $x^s_{surfact}$ in Eq. (A1.5a) to Eq. (A1.11) the equivalent form of π-A relationship is obtained:

$$\begin{aligned} A &= a_{surfact} + a_{water} \frac{2x^s_{water}}{1 - x^s_{water}} \\ &= a_{surfact} + a_{water} \frac{2\exp\left(-\frac{\pi a_{water}}{RT}\right)}{1 - \exp\left(-\frac{\pi a_{water}}{RT}\right)} \\ &= a_{surfact} + 2\frac{a_{water}}{\exp\left(\frac{\pi a_{water}}{RT}\right) - 1} \end{aligned} \qquad \text{(A1.12)}$$

The above equation could be transformed to π-A relationship:

$$\pi = \frac{RT}{a_{water}} \ln\left(1 + \frac{2a_{water}}{A - a_{surfact}}\right) \qquad \text{(A1.13)}$$

For nonionic surfactant in the absence of drug, the π-A relationship is derived based on same principle:

$$A = a_{surfact} + \frac{a_{water}}{\exp\left(\frac{\pi a_{water}}{RT}\right) - 1} \qquad \text{(A1.14)}$$

$$\pi = \frac{RT}{a_{water}} \ln\left(1 + \frac{a_{water}}{A - a_{surfact}}\right) \qquad \text{(A1.15)}$$

Appendix 2. Surface-localized Thermodynamic Model

In Mukerjee's two-state model, solubility of drugs in the micelle system was expressed as a sum of contributions from two locations (Gumkowski, 1986).

$$\begin{aligned} K_{m/w} &= K_{m/w,core} + K_{m/w,surface} \\ &= K_{h/w}\exp[-PV/RT] + \frac{\Gamma A f}{X_w} \\ &= K_{h/w}\exp[-PV/RT]\left(1+\frac{\Gamma A f}{X_{core}}\right) \end{aligned} \tag{A2.1}$$

where $K_{m/w}$ and $K_{h/w}$ are micelle/water and hydrocarbon/water partitioning coefficients of drugs based on mole fraction; X_w and X_{core} are mole fraction-based concentrations of drug in aqueous phase and micellar core; P is Laplace pressure which is equal to $2\gamma/r$ for spherical micelle (γ is interfacial tension on micelle surface and r is radius of the micelle); V is partial molar volume of drug; f is relative adsorption potential of the drug to account for the effect of headgroups on adsorption; Γ is surface excess of the drug in hydrocarbon/water interface and is defined by the Gibbs isotherm:

$$\Gamma = -\frac{1}{RT}\frac{\partial\gamma}{\partial \ln C} \tag{A2.2}$$

A is micelle/water interfacial area per surfactant molecule and could be estimated by:

$$A = 4\pi r^2 \Big/ N_{aggr} \tag{A2.3}$$

where r is the radius of micelles and N_{aggr} is the aggregation number.

In the surface-localized model, the micelle/water partitioning coefficient could be expressed as:

$$\begin{aligned} K_{m/w} &= K_{m/w,core} + K_{m/w,surface} \\ &= K_{h/w}\exp[-PV/RT] + \frac{\Gamma A f}{X_w}\exp[-PV/RT] \\ &\approx \frac{\Gamma A f}{X_w}\exp[-PV/RT] \end{aligned} \tag{A2.4}$$

The intermediate step, the 2nd line of Eq. (A2.4), is equivalent to Mukerjee's two-state model, Eq. (A2.1). An assumption used in the model is the micelle surface is subjected to Laplace pressure. The assumption was implicitly employed in Mukerjee's two-state model but was not clearly stated. In our studied systems, the contributions of the micellar core to solubilization were assumed to be negligible and the micelle/water partitioning coefficient was expressed using the solubilization by micellar surface only. See Chapter 3 for experimental evidence to support this assumption.

A2.1. Dilute Solute Condition

The term Γ/X_w in Eq. (5.4) could be expressed by rearranging the Gibbs isotherm as:

$$\frac{\Gamma}{X_w} = -\frac{1}{X_w}\frac{\partial\gamma}{RT\partial \ln X_w} = -\frac{1}{RT}\frac{\partial\gamma}{\partial X_w} = \frac{1}{RT}\frac{\partial\pi}{\partial X_w} \tag{A2.5}$$

At infinite dilution of drug, the Eq. (A1.8) for neutral drug adsorbed at liquid-liquid interface can be simplified using $\Delta\pi \to 0, x^{l}_{drug} = \Delta X_w \to 0$

$$\begin{aligned} &1 - \frac{\Delta\pi \cdot a_{water}}{RT} + \Delta X_w \exp\left(-\frac{\Delta G_{\text{water}\to\text{interface,drug}}}{RT}\right) = 1 \\ \Rightarrow \quad &\frac{\Delta\pi}{\Delta X_w} = \frac{RT}{a_{water}}\exp\left(-\frac{\Delta G_{\text{water}\to\text{interface,drug}}}{RT}\right) \end{aligned} \tag{A2.6}$$

Substituting above equation to (A2.5), the term Γ/X_w is expressed in terms of free energy of transfer:

$$\frac{\Gamma}{X_w} = \frac{1}{RT}\frac{\partial\pi}{\partial X_w} = \frac{1}{a_{water}}\exp\left[-\frac{\Delta G_{\text{water}\to\text{interface,drug}}}{RT}\right] \tag{A2.7}$$

Relative adsorption potential *f* is defined as surface density of drugs in the presence of surfactants divided by surface density of drugs in the absence of surfactants:

$$f = \frac{\sigma'_{drug}(\text{in the presence of surfactant})}{\sigma_{drug}(\text{in the absence of surfactant})} = \frac{(\sigma'_{water} + \sigma'_{drug} + \sigma'_{surfact})}{(\sigma_{water} + \sigma_{drug})} \frac{x^s_{drug}(\text{in the presence of surfactant})}{x^s_{drug}(\text{in the absence of surfactant})} \quad \text{(A2.8)}$$

where σ and σ' are the surface density at dodecane/water interface in the absence and presence of surfactants; x^s is the mole fraction at the interface.

The mole fractions of the various components at the surface are related to the mole fractions in bulk liquid by Eq. (A1.5a, b, c). Using the equation set combined with infinite dilution condition ($\sigma_{drug}, \sigma'_{drug} \to 0$) and relationship Eq. (A1.6), the first term of Eq. (A2.8) could be simplified for nonionic surfactants:

$$\begin{aligned} \frac{(\sigma'_{water} + \sigma'_{drug} + \sigma'_{surfact})}{(\sigma_{water} + \sigma_{drug})} &= \frac{(\sigma'_{water} + \sigma'_{surfact})}{\sigma_{water}} \\ &= \frac{1/(x^s_{water} a_{water} + x^s_{surfact} a_{surfact})}{1/a_{water}} \\ &= \frac{a_{water}}{x^s_{water} a_{water} + (1 - x^s_{water}) a_{surfact}} \\ &= \frac{a_{water}}{\exp\left(-\frac{\pi a_{water}}{RT}\right) a_{water} + \left[1 - \exp\left(-\frac{\pi a_{water}}{RT}\right)\right] a_{surfact}} \end{aligned} \quad \text{(A2.9)}$$

Applying the equations (A1.5b), the second term in Eq. (A2.8) becomes:

$$\begin{aligned} \frac{x^s_{drug}(\text{w/surfactant})}{x^s_{drug}(\text{w/osurfactant})} &= \frac{x^l_{drug} \exp\left(-\frac{\Delta G_{\text{water}\to\text{interface, drug}}}{RT}\right) \exp\left(-\frac{(\gamma_0 - \gamma) a_{drug}}{RT}\right)}{x^l_{drug} \exp\left(-\frac{\Delta G_{\text{water}\to\text{interface, drug}}}{RT}\right) \exp\left(-\frac{(\gamma_0 - \gamma_0) a_{drug}}{RT}\right)} \\ &= \exp\left(-\frac{(\gamma_0 - \gamma) a_{drug}}{RT}\right) \end{aligned} \quad \text{(A2.10)}$$

Substituting the equations (A2.9) and (A2.10) into Eq. (A2.8), the relative adsorption potential becomes:

$$f = \frac{a_{water}}{a_{water}\exp\left(-\frac{\pi a_{water}}{RT}\right) + a_{surfact}\left[1-\exp\left(-\frac{\pi a_{water}}{RT}\right)\right]}\exp\left(-\frac{\pi a_{drug}}{RT}\right) \quad \text{(A2.11)}$$

Eq. (A2.11) is valid for nonionic surfactant. For ionic surfactant, such as SDS and DTAB, the relative adsorption potential could be written as:

$$f = \frac{a_{water}}{a_{water}\exp\left(-\frac{\pi a_{water}}{RT}\right) + \frac{a_{surfact}}{2}\left[1-\exp\left(-\frac{\pi a_{water}}{RT}\right)\right]}\exp\left(-\frac{\pi a_{drug}}{RT}\right) \quad \text{(A2.12)}$$

Substituting Eq. (A1.14)/(A1.12) and Eq. (A2.11)/(A2.12) into Eq. (A2.4), the micelle/water partitioning coefficient could be calculated as follows:

For nonionic surfactants:

$$\begin{aligned} K_{m/w} &= \frac{\Gamma A f}{X_w}\exp[-PV/RT] \\ &= \frac{1}{a_{water}}\exp\left[-\frac{\Delta G_{\text{water}\rightarrow\text{interface,drug}}}{RT}\right]\left[a_{surfact} + \frac{a_{water}}{\exp\left(\frac{\pi a_{water}}{RT}\right)-1}\right] \\ &\times \frac{a_{water}}{a_{water}\exp\left(-\frac{\pi a_{water}}{RT}\right) + a_{surfact}\left[1-\exp\left(-\frac{\pi a_{water}}{RT}\right)\right]}\exp\left(-\frac{\pi a_{drug}}{RT}\right)\exp\left[-\frac{PV}{RT}\right] \\ &= \frac{\exp\left(-\frac{\Delta G_{\text{water}\rightarrow\text{interface,drug}}}{RT}\right)\exp\left(-\frac{\pi a_{drug}}{RT}\right)\exp\left(-\frac{PV}{RT}\right)}{\left[1-\exp\left(-\frac{\pi a_{water}}{RT}\right)\right]} \end{aligned} \quad \text{(A2.13)}$$

For ionic surfactants:

$$K_{m/w} = \frac{2\exp\left(-\frac{\Delta G_{\text{water}\rightarrow\text{interface,drug}}}{RT}\right)\exp\left(-\frac{\pi a_{drug}}{RT}\right)\exp\left(-\frac{PV}{RT}\right)}{\left[1-\exp\left(-\frac{\pi a_{water}}{RT}\right)\right]} \qquad \text{(A2.14)}$$

The Eq. (A2.13) and (A2.14) are the operational equations employed to predict micelle/water partitioning coefficients.

A2.2. Non-dilute Solute Condition

When concentration of solute is finite, the definition of micelle/water partition coefficient is:

$$K_{m/w} = \frac{\left(\frac{x^s_{drug}}{x^x_{surfact} + x^s_{drug}}\right)}{x^l_{drug}} \qquad \text{(A2.15)}$$

Eq. (A1.5a, b, c) are modified to be applied to highly curved micelle surface:

$$x^s_{water} = x^l_{water}\exp\left(-\frac{\pi a_{water}}{RT}\right) \cong \exp\left(-\frac{\pi a_{water}}{RT}\right) \qquad \text{(A2.16a)}$$

$$x^s_{drug} = x^l_{drug}\exp\left(-\frac{\Delta G'_{\text{water}\rightarrow\text{interface,}drug}}{RT}\right)\exp\left(-\frac{\pi a_{drug}}{RT}\right) \qquad \text{(A2.16b)}$$

$$x^s_{surfact} = \begin{cases} x^l_{surfact}\exp\left(-\frac{\Delta G'_{\text{water}\rightarrow\text{interface,}surfact}}{RT}\right)\exp\left(-\frac{\pi a_{surfact}}{RT}\right) & \text{for nonionic surfactant} \\ x^l_{surfact} f^{\,l}_{surfact}\exp\left(-\frac{\Delta G'_{\text{water}\rightarrow\text{interface,}surfact}}{RT}\right)\exp\left(-\frac{\pi a_{surfact}}{2RT}\right) & \text{for ionic surfactant} \end{cases}$$

(A2.16c)

Eq. (A2.16a, b, c) have the same forms with Eq. (A1.5a, b, c) with the differences in the free energies of transfer from water to interface for drugs and surfactants. The $\Delta G'_{\text{water}\rightarrow\text{interface}}$ represents the transfer free energy from bulk water to highly curved

micelle surface. Because the drugs are subjected to Laplace pressure at micelle surface, the transfer free energy for drug is expressed as:

$$\Delta G'_{\text{water}\rightarrow\text{interface},drug} = \Delta G_{\text{water}\rightarrow\text{interface},drug} + PV \qquad \text{(A2.17)}$$

Since the *PV* term is positive, the free energy of transfer from water to micelle surface, $\Delta G'_{\text{water}\rightarrow\text{interface},drug}$, has less negative value than that for flat surface. Therefore, the drug is less surface active at micelle surface compared to flat oil/water interface.

For ionic surfactant, the $\Delta G'_{\text{water}\rightarrow\text{interface},surfact}$ can be determined using pure surfactant system in the absence of drugs. An equation similar to Eq. (A1.7) is obtained by substituting Eq. (A2.16a) and (A2.16c) into Eq. (A1.6):

$$\exp\left(-\frac{\pi a_{water}}{RT}\right) + 2x^{l}_{surfact} f^{l}_{surfact} \exp\left(-\frac{\Delta G'_{\text{water}\rightarrow\text{interface},surfact}}{RT}\right)\exp\left(-\frac{\pi a_{surfact}}{2RT}\right) = 1 \qquad \text{(A2.18)}$$

The surface pressure, π, at the micelle surface can be estimated according to Section 5.3.2. The monomer concentration in bulk water, $x^{l}_{surfact}$, is equal to CMC. Activity coefficient $f^{l}_{surfact}$ can be calculated using Eq. (4.3) and interfacial areas occupied by water and surfactants are shown in Section 4.3.3.2. The only unknown parameter is $\Delta G'_{\text{water}\rightarrow\text{interface},surfact}$ which could be determined by solving Eq. (A2.18).

Using same principle, the $\Delta G'_{\text{water}\rightarrow\text{interface},surfact}$ term for nonionic surfactant can be calculated using the following equation:

$$\exp\left(-\frac{\pi a_{water}}{RT}\right) + x^{l}_{surfact} \exp\left(-\frac{\Delta G'_{\text{water}\rightarrow\text{interface},surfact}}{RT}\right)\exp\left(-\frac{\pi a_{surfact}}{RT}\right) = 1 \qquad \text{(A2.19)}$$

When both ionic surfactant and neutral drug are present, the equations (A2.16a, b, c) are substituted into Eq. (1.6):

$$\exp\left(-\frac{\pi a_{water}}{RT}\right)+2x_{surfact}^{l}f_{surfact}^{l}\exp\left(-\frac{\Delta G'_{\text{water}\rightarrow\text{interface},surfact}}{RT}\right)\exp\left(-\frac{\pi a_{surfact}}{2RT}\right)+x_{drug}^{l}\exp\left(-\frac{\Delta G'_{\text{water}\rightarrow\text{interface},drug}}{RT}\right)\exp\left(-\frac{\pi a_{drug}}{RT}\right)=1 \quad \text{(A2.20)}$$

When both nonionic surfactant and neutral drug are present, the following equation is obtained by substituting Eq. (A2.16a, b, c) into Eq. (1.6):

$$\exp\left(-\frac{\pi a_{water}}{RT}\right)+x_{surfact}^{l}\exp\left(-\frac{\Delta G'_{\text{water}\rightarrow\text{interface},surfact}}{RT}\right)\exp\left(-\frac{\pi a_{surfact}}{RT}\right)+x_{drug}^{l}\exp\left(-\frac{\Delta G'_{\text{water}\rightarrow\text{interface},drug}}{RT}\right)\exp\left(-\frac{\pi a_{drug}}{RT}\right)=1 \quad \text{(A2.21)}$$

In Eq. (A2.20) or (A2.21), there is only one unknown parameter, the surface pressure (π). The equation is numerically solved for the surface pressure.

Now all the parameters in Eq. (2.16a, b, c) are known, the micelle/water partition coefficient is calculated by substituting Eq. (2.16b, c) into Eq. (2.15):

For ionic surfactant:

$$K_{m/w} = \frac{\left(\frac{x^{s}_{drug}}{x^{x}_{surfact} + x^{s}_{drug}} \right)}{x^{l}_{drug}}$$

$$= \frac{\left[\frac{x^{l}_{drug} \exp\left(-\frac{\Delta G'_{drug}}{RT} \right) \exp\left(-\frac{\pi a_{drug}}{RT} \right)}{x^{l}_{surfact} f^{l}_{surfact} \exp\left(-\frac{\Delta G'_{surfact}}{RT} \right) \exp\left(-\frac{\pi a_{surfact}}{2RT} \right) + x^{l}_{drug} \exp\left(-\frac{\Delta G'_{drug}}{RT} \right) \exp\left(-\frac{\pi a_{drug}}{RT} \right)} \right]}{x^{l}_{drug}}$$

$$= \frac{\exp\left(-\frac{\Delta G'_{drug}}{RT} \right) \exp\left(-\frac{\pi a_{drug}}{RT} \right)}{x^{l}_{surfact} f^{l}_{surfact} \exp\left(-\frac{\Delta G'_{surfact}}{RT} \right) \exp\left(-\frac{\pi a_{surfact}}{2RT} \right) + x^{l}_{drug} \exp\left(-\frac{\Delta G'_{drug}}{RT} \right) \exp\left(-\frac{\pi a_{drug}}{RT} \right)}$$

(A2.22)

For nonionic surfactant:

$$K_{m/w} = \frac{\exp\left(-\frac{\Delta G'_{drug}}{RT} \right) \exp\left(-\frac{\pi a_{drug}}{RT} \right)}{x^{l}_{surfact} \exp\left(-\frac{\Delta G'_{surfact}}{RT} \right) \exp\left(-\frac{\pi a_{surfact}}{RT} \right) + x^{l}_{drug} \exp\left(-\frac{\Delta G'_{drug}}{RT} \right) \exp\left(-\frac{\pi a_{drug}}{RT} \right)}$$

(A2.23)

The assumptions used for above derivations include:

(1) The solute and surfactant are ideally competing with each other for the micelle surface in the absence of specific interactions between the solute and surfactant molecules.

(2) The radius of micelles is not changed with addition of solutes to micelles.

(3) The transfer free energy of solute molecule from water to micelle surface is independent of solute concentration.

A2.3. The Effect of Finite Solute Concentration on CMC of Surfactants Using Laplace Pressure Concept

The CMC of micelle would be a function of the transfer free energy of surfactant molecule from bulk water to micelle surface. The following relationship holds:

$$\frac{CMC}{CMC_0} = \exp\left(\frac{\Delta G'_{\text{water}\rightarrow\text{interface}} - \Delta G'_{\text{water}\rightarrow\text{interface},0}}{RT}\right) \tag{A2.24}$$

where CMC and CMC_0 are the critical micelle concentrations in the presence and absence of solutes; $\Delta G'_{\text{water}\rightarrow\text{interface}}$ and $\Delta G'_{\text{water}\rightarrow\text{interface},0}$ are the transfer free energies of the surfactant from water to micelle surface in the presence and absence of solute.

The change in the transfer free energy is mainly due to the change in Laplace pressure acting on surfactant molecule.

$$\begin{aligned}\Delta G'_{trans} - \Delta G'_{trans,0} &= \left(\Delta G_{\text{water}\rightarrow\text{interface}} + PV\right) - \left(\Delta G_{\text{water}\rightarrow\text{interface}} + P_0 V\right) \\ &= \left(P - P_0\right)V = \left(\frac{2(\gamma_0 - \pi)}{r} - \frac{2(\gamma_0 - \pi_0)}{r}\right)V = -2\left(\pi - \pi_0\right)\frac{V}{r}\end{aligned} \tag{A2.25}$$

where P and P_0 are the Laplace pressures in the micelles in the presence and absence of solute; π_0 is the surface pressure at micelle surface in the absence of solute with the values for the model surfactants shown in Table 5.4; π is the surface pressure at micelle surface in the presence of model drugs and can be calculated in Section A2.2.

Substituting Eq. (A2.25) into Eq. (A2.24), the ratio CMC/CMC_0 is expressed as:

$$\frac{CMC}{CMC_0} = \exp\left(-\frac{2\Delta\pi \cdot V}{r \cdot RT}\right) \tag{A2.26}$$

Because of the usage of results in Section A2.2, the three assumptions used in that section are applied to the current question. There is one more assumption that the surfactant molecules are subject to Laplace pressure.

REFERENCES

Abraham, M.H., Chadha, H.S., Dixon, J.P., Rafols, C., Treiner, C., 1995, *J. Chem. Soc. Perkin Trans., 2*, p887.

Adams, M.L., Lavasanifar, A., Kwon, G.S., 2003, *J. Pharm. Sci.*, **92**, p1343.

Allen, F.H., 2002, *Acta Crystallogr. B*, **58**, p380

Allen, T.M., Hansen, C., Martin, F., Redemann, C., Yau-Young, A., 1991, *Biochim. Biophys. Acta*, **1066**, p29.

Alvarez-Nunez, F.A., Yalkowsky, S.H., 2000, *Int. J. Pharm.*, **200**, p217.

Amidon, G., Lennernas, H., Shah, V., Crison, 1995, *J., Pharm. Res.*, **12**, p413.

Anacker, E.W., Ghose, H.M., 1968, *J. Am. Chem. Soc.*, **90**, p3161.

Ansel, H.C., Popovich, N.G., Allen, Jr. L.V., 1995, in "Pharmaceutical Dosage Forms and Drug Delivery Systems", 6th Ed., Williams & Wilkins: Baltimore, Chapt 7.

Antalek, B., 2002, *Concepts Magn. Reson.*, **14**, p225.

Attwood, D., Florence, A.T., 1983, in "Surfactant Systems", Chapman & Hall: London and New York.

Bachofer, S.J., Simonis, U., Nowicki, T.A., 1991, *J. Phys. Chem.*, **95**, p480.

Barry, B.W., El Eini, D.I.D., 1976, *J. Pharm. Pharmcol.*, **28**, p210.

Bogusz, S., Venable, R.M., Pastor, R.W., 2000, *J. Phys. Chem. B*, **104**, p5462.

Bonfillon, A., Sicoli, F., Langevin, D., 1994, *J. Coll. Int. Sci.*, **168**, p497.

Blitzinger, H., Beier, H.G., 1933, *Kolloid-Z*, **64**, p160.

Bratt, P.J., Choudhury, H., Chowdhury, P.B., Gillies, D.G., Krebber, A.M.L., Sutcliffe, L.H., 1990, *J. Chem. Soc. Faraday Trans.*, **86**, p3313.

Bromberg, L., Temchenko, M., 1999, *Langmuir*, **15**, p8627.

Bucci, S., Fagotti, C., Degiorgio, V., Pianza, R., 1991, *Langmuir*, **7**, p824.

Bummer, P.M., 2004, *Crit. Rev. Ther. Drug Carr. Syst.*, **21**, p1.

Butler, J.A.V., 1932, *Proc. Roy. Soc. Ser. A*, **135**, p348.

Carr, H.Y., Purcell, E.M., 1954, *Phys. Rev.*, **94**, p630.

Chervinsky, D.S., Brecher, B.L., Hoelcle, M.J., 1993, *Anticancer Res.*, **13**, p93.

Cho, C.H., Urquidi, J., Singh, S., Robinson, G.W., 1999, *J. Phys. Chem. B*, **103**, p1991.

Christian, S.D., Tucker, EE., Smith, G.A., Bushong, D.S., 1986, *J. Coll. Interf. Sci.*, **113**, p439.

Christian, S.D., Scamehorn, J.F. Ed., 1995, in "Solubilization in Surfactant Aggregates", Marcel Dekker: New York.

Claridge, T.D.W., 1999, in "*High-Resolution NMR Techniques in Organic Chemistry*", Elsevier: New York, p278.

Craig, D.Q.M., Lievens, H.S.R., Pitt, K.G., 1993, *Int. J. Pharm.*, **96**, p147.

Croy, S.R., Kwon, G.S., 2005, *J. Pharm. Sci.*, **94**, p2345.

Dill, K.A., Flory, P.J., 1981, *Proc. Natl. Acad. Aci.*, **78**, p676.
Dill, K.A., 1982, *J. Phys. Chem.*, **86**, p1498.
Dill, K.A., Koppel, D.E., Cantor, R.S., Dill, J.D., Bendedouch, D., Chen, S.-H., 1984, *Nature*, **309**, p42.
Dintaman, J.M., Silverman, J.A., 1999, *Pharm. Res.*, **16**, p1550.
Donbrow, M., Molyneux, P., Rhodes, C.T., 1967, *J. Chem. Soc. A*, p561.
du Noüy, P. L., 1919, *J. Gen. Physiol.* **1**, p521.
Elworthy, P.H., Florence, A.T., Macfarlane, C.B., 1968, in "Solubilization by Surface-Active Agents", Chapman & Hall: London.
Engler, C., Dieckhoff, E., 1892, *Arch. Pharm.*, **230**, p561. Quoted by Attwood, D., Florence, A.T., 1983, in "Surfactant Systems", Chapman & Hall: London and New York.
Eriksson, J.C., Gillberg, G., 1966, *Acta Chem. Scand.*, **20**, p2019.
Fishbein, M., 1945, in "Medical Uses of Soap", Ed. Fishbein, M., Lippincott: Philadelphia.
Frisch, A., Nielsen, A.B., Holder, A.J., 2000, Gaussview Users Manual, Gaussian Inc., Pittsburgh.
Frisch, M.J. et al., 2003, Gaussian03, Gaussian, Inc., Pittsburgh, PA.
Gillap, W.R., Veiner,N.D., Gibaldi, M., 1968, *J. Coll. Interf. Sci.*, **26**, p232.
Gjerde, M.I., Nerdal, W., Hoiland, H., 1998, *Coll. Polym. Sci.*, **276**, p503.
Goldenberg, M.S., Bruno, L.A., Rennwantz, E.L., 1993, *J. Coll. Interf. Sci.*, **158**, p351.
Goto, A., Endo, F., 1978, *J. Coll. Interf. Sci.*, **66**, p26.
Griffin, W.C., 1949, *J Soc. Cosmetics Chemists*, **1**, p311.
Griffin, W.C., 1954, *J Soc. Cosmetics Chemists*, **5**, p1.
Grove, M., Mullertz, A., 2007, in "Oral Lipid-based Formulations: Enhancing the Bioavailability of Poorly Water-soluble Drugs", Hauss, D.J. (Ed.), Informa Healthcare Inc.: New York, p107.
Gumkowski, M.J., 1986, PhD thesis, University of Wisconsin.
Gursoy, R.N., Benita, S., 2004, *Biomed. Pharmacoth.*, **58**, p173.
Hiemenz, P.C., Rajagopalan, R., 1997, in "Principles of Colloid and Surface Chemistry", 3rd Ed., Marcel Dekker: New York, Chapter 8.
Hahn, E.L., 1950, *Phys. Rev.*, **80**, p580.
Hamid, I.A., Parrott, E.L., 1971, *J. Pharm. Sci.*, **60**, p901.
Hancock, B.C., Parks, M., 2000, *Pharm. Res.*, **17**, p397.
Hansch, C., Leo, A., Hoekman, D., 1995, in "Exploring QSAR". Vol.2, American Chemical Society: Washington, D.C.
Harkins, W.D., Jordan, H.F., 1930, *J. Am. Chem. Soc.*, **52**, p1751; Cupples, H.L., 1947, *J. Phys. Chem.*, **51**, p1341
Hartley, G.S., 1938, *J. Chem. Soc.*, p1968.
Hauss, D.J., 2007, *Adv. Drug Delivery Rev.*, **59**, p667.
Hawrylak, B.E., Marangoni, D.G., 1999, *Can. J. Chem.*, **77**, p1241

Haydon, D.A., Taylor, F.H., 1960, *Phil. Trans. Roy. Soc. London A*, **252**, p225.
Heins, A., Sokolowski, T., Stockmann, H., Schwartz, K., 2007, *Lipids*, **42**, p561.
Holm, R., Porter, C.J.H., Edwards, G.A., Mullertz, A. Kristensen, H.G. Charman, W.N., 2003, *Eur. J. Pharm. Sci.*, 20, p91.
Hwang, T.L., 1992, *J. Am. Chem. Soc.*, **114**, p3157.
HyperChem Release 7.0, 2001, Hypercube Inc., Gainesville, FL, USA.
Imae, T., Kamiya, R., Ikeda, S., 1985, *J. Coll. Interf. Sci.*, **108**, p215.
Jafvert, C.T., Van Hoof, P.L., Heath, J.K., 1994, *Water Res.*, **28**, p1009.
Joguparthi, V., 2007, PhD thesis, University of Kentucky.
Johnson, M.E., Blankschtein, D., Langer, R., 1995, *J. Pharm. Sci.*, **84**, p1144
Kamlet, M.J., Doherty, R.M., Carr, P.W., Mackay, D., Abraham, M.H., Taft, R.W., 1988, *Environ. Sci. Technol.*, **22**, p503.
Kawakami, K., Miyoshi, K., Ida, Y., 2004, *J. Pharm. Sci.*, **93**, p1471.
Khoo, S.M., Shackleford, D.M., Porter, C.J. Edwards G.A., Charman, W.N., 2003, *Pharm. Res.*, **20**, p1460.
Kim, B.-J., Im, S.-S., Oh S.-G., 2001, *Langmuir*, **17**, p565.
Kitagawa S, Ikarashi A, 2003, *Chem. Pharm. Bull.*, **51**, p1183.
Kuehne, W., 1868, in "Lehrbuch Physiol. Chem.". Quoted by McBain, M.E.L., Hutchinson, E., 1955, in "Solubilization and Related Phenomena", Academic Press: New York.
Land, L.M., 2005, PhD Thesis, University of Kentucky.
Landman, B., Puyal, M.-C., Kamenka, N., Rymden, R., Stilbs, P., 1984, *J. Phys. Chem.*, **88**, p5049.
Langmuir, I., 1917, *J. Am. Chem. Soc.*, **39**, p1848.
Lavasanifar, A., Samuel, J., Kwon, G.S., 2002, *Adv. Drug Deliv. Rev.*, **54**, p169.
Lebedeva, N., Ranganathan, R., Bales, B.L., 2007, *J. Phys. Chem. B*, **111**, p5781.
Lee, B.-H., Christian, S.D., Tucker, E.E., Scamehorn, J.F., 1990, *Langmuir*, **6**, p230
Li, P., Tabibi, S.E., Yalkowsky, S.H., 1999a, *J. Pharm. Sci.*, **88**, p507.
Li, P., Tabibi, S.E., Yalkowsky, S.H., 1999b, *J. Pharm. Sci.*, **88**, p945.
Li, P., Tabibi, S.E., Yalkowsky, S.H., 1998, *J. Pharm. Sci.*, **87**, p1535.
Lin, T., 1986, *J. Struct. Chem.*, **5**, p281.
Lin, T.-L., Chen, S.-H., Gabriel, N.E., Roberts, M.F., 1990, *J. Phys. Chem.*, **94**, p855
Lindblom, G., Lindman, B., Mandell, L., 1973, *J. Coll. Interf. Sci.*, 42, p400.
Lindman, B., Brun, B., 1973, *J. Coll. Interf. Sci.*, **42**, p388.
Lindman, B., Wennerstrom, H., 1980, in "Micelles. (Topics in Current Chemistry; 87)", Springer-Verlag: New York.
Lucassen-Reynders, E.H., 1981, in "Anionic Surfactants", Lucassen -Reynders, E.H. Ed., Marcel Dekker: New York, Chapt. 1.
Lundberg, B., 1980, *J. Pharm. Sci.*, **69**, p20.
MacKerell, A.D., 1995, *J. Phys. Chem.*, **99**, p1846.
Malcolmson, C., Lawrence, M.J., 1993, *J. Pharm. Pharmcol.*, **45**, p141.

Martin, A., 1993, in “Physical Pharmacy”, 4th Ed., Willaims & Wilkins: Baltimore, Chapt. 10.
Matsuoka, K. Ishii, S., Honda, C., Endo, K., Saito, A., Moroi, Y., Shibata, O., 2007, *Bull. Chem. Soc. Japan*, **80**, p2334.
McBain, J.W., McBain, M.E.L., 1936, *J. Am. Chem. Soc.*, **58**, p2610.
McGowan, J.C., 1978, *J. Appl. Chem. Biotech.*, **28**, p599.
Medrzycka, K., Zwierzykowski, W., 2000, *J. Coll. Int. Sci.*, **230**, p67.
Miller, D.D., Lenhart, W., Antalek, B.J., Williams, A.J., Hewitt, J.M., 1994, *Langmuir*, **10**, p68.
Moura, A.F., Freitas, L.C.G., 2005, *Chem. Phys. Lett.*, **411**, p474.
Mukerjee, P., 1964, *J. Coll. Sci.*, **19**, p722.
Mukerjee P., Cardinal, J., 1978, *J. Phys. Chem.*, **82**, p1620.
Mukerjee, P., 1979, In “Solution Chemistry of Surfactants”, Mittal, K.L. Ed., Plenum Press: New York, Vol. 1, p153.
Mukerjee, P., Ko, J.-S., 1992, *J. Phys. Chem.*, **96**, p6090.
Mulley, B.A., 1964, in “Advances in Pharmaceutical Sciences”, Academic Press: New York, Vol. 1, p87.
Mysels, K.J., 1986, *Langmuir*, **2**, p423.
Nagaonkar, U.C., Bhagwat, S.S., 2006, *J. Disp. Sci. Tech.*, **27**, p331.
Nakagawa, T., 1967, in “Nonionic Surfactants”, Schick, M.J. Ed., Dekker: New York, Chap. 17.
Ong, J.T. Manoukian, E., 1988, *Pharm. Res.*, **5**, p704.
OpenDX, http://www.opendx.org/
Palin, K.J., Wilson, C.G., 1984, *J. Pharm. Pharmacol.*, **36**, p641.
Panicker, L., 2008, *Current Trend in Biotech. Pharm.*, 2, p316.
Persoz, 1846, in “Traite Theoretique et Practique de L’impression des Tissues”, Vol. 1, p354. Quoted by McBain, M.E.L., Hutchinson, E., 1955, in “Solubilization and Related Phenomena”, Academic Press: New York.
Pierotti, R.A., 1965, *J. Phys. Chem.*, **69**, p281.
Pouton, C.W., 1997, *Adv. Drug Delivery Rev.*, **25**, p47.
Price, W.S., Kuchel, P.W., 1991, *J. Magn. Reson.*, **94**, p133.
Pyter, R., Ramachandran, C., Mukerjee, P., 1982, *J. Phys. Chem.*, **86**, p3206.
Rafati, A.A., Gharibi, H., Iloukhani, H., Safdari, L., 2003, *Phys. Chem. Liquids*, **41**, p227.
Ramachandran, C., Pyter, R.A., Mukerjee, P., 1982, *J. Phys. Chem.*, **86**, p3198
Rangel-Yagui, C.O., Pessoa-Jr, A., Tavares, L.C., 2005, *J. Pharm. Pharmceut. Sci.*, **8**, p147.
Reiss-Husson, F., Luzzati, V., 1964, *J. Phys. Chem.*, **68**, p3504.
Rodriguez, V.B., Henry, S.M., Hoffman, A.S., Stayton, P.S., Li, X.D., Pun, S.H., 2008, *J. Biomed. Optics*, **13**, p014025.
Rosen, M.J., 1981, *J. Coll. Interf. Sci.*, **79**, p587.
Rosen, M., 1989, in “Surfactants and Interfacial Phenomena”, 2nd ed., Wiley: New York.

Sabate, R., Gallardo, M., Estelrich, J., 2001, *J. Coll. Interf. Sci.*, **233**, p205.
Saket, M., 1996, *Alexandria J. Pharm. Sci.*, **10**, p138.
Shihab, F.A., Ebian, A.R., Mustafa, R.M., 1979, *Int. J. Pharm.*, **4**, p13.
Sjoblom, L., 1967, in "Solvent Properties of Surfactant Solutions" Ed. Shinoda, K., Marcel Dekker: New York, Chap. 5.
Smith, E.L., 1932, *J. Phys. Chem.* **36**, p1401, p1672, and p2455.
Smith, G.A., Christian, S.D., Tucker, E.E., Scamehorn, J.F., 1987, *Langmuir*, **3**, p598.
Smolinske, S.C., 1992, in "CRC Handbook of Food, Drug, ad Cosmetic Excipients", CRC Press: Boca Raton.
Soderman, O., Stilbs, P., Price, W.S., 2004, *Concepts Magn. Reson. A*, **23**, p121.
Stejskal, E.O., Tanner J.E., 1965, *J. Chem. Phys.*, **42,** p288.
Strickley, R.G., 2004, *Pharm. Res.*, **21**, p201.
Strickley, R.G., 2007, in Oral Lipid-based Formulations: Enhancing the Bioavailability of Poorly Water-soluble Drugs, Hauss, D.J. (Ed.), Informa Healthcare Inc., New York, p1.
Suratkar, V., Mahapatra, S., 2000, *J. Coll. Interf. Sci.*, **225**, p32.
Svens, S., Rosenholm, B., 1973, *J. Coll. Interf. Sci.*, **44**, p495.
Thevenot, C., Grassl, B., Bastiat, G., Binana, W., 2005, *Col. Surf. A*, **252**, p105.
Tieleman, D.P., van der Spoel, D., Berendsen, H.J.C., 2000, *J. Phys. Chem. B*, **104**, p6380.
Tokiwa, F., 1968, *J. Phys. Chem.*, **72**, p1214.
Tongaree, S., Flanagan, D.R. Poust, R.I., 1999, *Pharm. Dev. Tech.*, **4**, p571.
Treiner, C., Mannebach, M.H., 1987, *J. Coll. Interf. Sci.*, **118**, p243.
Turro, N.J., Yekta, A., 1978, *J. Am. Chem. Soc.*, **100**, p5951.
Ueno, M., Asano, H., 1997, in "Structure-Performance Relationships in Surfactants", Esumi, K., Ueno, M. Ed., Marcel Dekker Inc.: New York, p174.
USP, 2009, USP 32-NF 27, USP Convention: Rockville, MD, p663.
Valsaraj, K.T., Thibodeaux, L.J., 1990, *Separation Sci. Tech.*, **25**, p369.
Varian Instrumental Manual, 2001, VNMR 6.1C User Guide: Liquids NMR.
Vermathen, M., Louie, E.A., Chodosh, A.B., Ried, S., Simonis, U., 2000, *Langmuir*, **16**, p210.
Verzar, F., 1933, *Nutrit, Abs. Rev.*, **2**, p441.
Viernstein, H., Weiss-Greiler, P., Wolschann, P., 2003, *Int. J. Pharm.*, **256**, p85.
Wandel, C., Kim, R.B., Stein, M., 2003, *Clin. Pharmcol. Ther.*, **73**, p394.
Whitehead K, Mitragotri S, 2008, *Pharm. Res.*, **25**, p1412.
Wiedmann T.S., Kamel, L., 2002, *J. Pharm. Sci.*, **91**, p1743.
Yalkowsky, S.H., Zografi, G., 1972, *J. Pharm. Sci.*, **61**, p651.
Yalkowsky, S.H., 1999, in "Solubility and Solubilization", Oxford: New York.
Yalkowsky, S.H., He, Y., 2003, in "Handbook of Aqueous Solubility Data", CRC Press: Boca Raton, Fla.
Yoshioka, H., 1979, *J. Am. Chem. Soc.*, **101**, p28.

Zangenberg, N.H., Mullertz, A., Kristensen, H.G., Hovgaard, L., 2001a, *Euro J. Pharm. Sci.*, **14**, p115.
Zangenberg, N.H., Mullertz, A., Gjelstrup, K.H., Hovgaard, L., 2001b, *Euro J. Pharm. Sci.*, **14**, p237.
Zeppieri, S., Rodriguez, J., Lopez de Ramos, A.L., 2001, *J. Chem. Eng. Data*, **46**, p1086.
Zuidema, H.H., Waters, G.W., 1941, *Ind. Eng. Chem. (Anal.)* **13**, p312

Vita

Shaoxin Feng was born on June 8, 1974 in Liaoning, P. R. China. He received his Bachelor of Science degree (1996) and his Doctor of Philosophy degree (2001) in Condensed Matter Physics from Nankai University in Tianjin, P. R. China. He worked under the supervision of Dr. Datong Ding in the Department of Physics and his dissertation title was "*Energetic studies of point defects in ionic or semi-ionic crystals*". Before he joined the Department of Pharmaceutical Sciences Graduate Program at the University of Kentucky in the Fall of 2005, he did postdoctoral researches at the University of Illinois at Chicago under the supervision of Dr. Christoph Grein and Dr. Michael Flatte (2001~2003) and at the University of Kentucky under the supervision of Dr. Tonglei Li (2003~2005). Shaoxin was the recipient of Kentucky Opportunity Fellowship (2007-2008) and University of Kentucky Presidential Fellowship (2008-2009). Shaoxin is an author and a co-author on 12 peer-reviewed publications.

Publications:

1. Vijay Joguparthi, **Shaoxin Feng**, Brad Anderson, "Determination of intraliposomal pH and its effect on membrane partitioning and passive loading of a hydrophobic camptothecin, DB-67, *Int. J. Pharmaceutics*, Vol. 352, p17, 2008
2. Tonglei Li and **Shaoxin Feng**, "Empirically augmented density functional theory for predicting lattice energies of aspirin, acetaminophen polymorphs, and ibuprofen Homochiral and Racemic Crystals", *Pharmaceutical Research*, Vol. 23, p2326, 2006
3. **Shaoxin Feng** and Tonglei Li, "Predicting lattice energy of organic crystal by density functional theory with Empirically Corrected dispersion energy", *Journal of Chemical Theory and Computation*, Vol. 2, p149, 2006
4. Tonglei Li and **Shaoxin Feng**, "Study of crystal packing on the solid-state reactivity of indomethacin with density functional theory", *Pharmaceutical Research*, Vol. 22, p1964, 2005
5. **Shaoxin Feng** and Tonglei Li, "Understanding solid-state reactions of organic crystals with density functional theory-based concepts", *Journal of Physical Chemistry A*, Vol. 109, p7258, 2005
6. Tonglei Li, Shubin Liu, **Shaoxin Feng**, Clare E. Aubrey, "Face-integrated Fukui function: understanding wettability anisotropy of molecular crystal from density function theory", *J. Am. Chem. Soc.*, Vol. 127(5), p1364, 2005
7. **Shaoxin Feng**, Christoph H. Grein, Michael E. Flatté, "Effects of impurity scattering on electron-phonon resonance in semiconductor superlattice high-field transport", *Physical Review B*, Vol. 68(7), p085307, 2003

8. **Shaoxin Feng**, Baohui Li, Zhi Yang, Qinghua Jin, Zhenya Guo, Datong Ding, "Empirical calculations of the formation energies of point defects in lithium niobate", *J. Inorg. Mater.*, Vol. 18(2), p283, 2003

9. **Shaoxin Feng**, Baohui Li, Qinghua Jin, Zhenya Guo, Datong Ding, "Determination of empirical parameters of inter-ionic potentials for lithium niobate", *Acta Physica Sinica*, Vol. 49(12), p2433, 2000

10. **Shaoxin Feng**, Baohui Li, Qinghua Jin, Zhenya Guo, Datong Ding, "Empirical calculations of the formation energies of point defects in rutile TiO_2", *Acta Physica Sinica*, Vol. 49(7), p1307, 2000

11. Qinghua Jin, **Shaoxin Feng**, Zhenya Guo, Baohui Li, Datong Ding, "Calculations of the formation energies of point defects in alkaline earth fluorides", *Acta Physica Sinica*, Vol. 48(7), p1261, 1999

12. **Shaoxin Feng**, Qinghua Jin, Zhenya Guo, Baohui Li, Datong Ding, "Empirical parameterization of inter-ionic potentials for alkaline earth fluorides", *Acta Physica Sinica*, Vol. 47(11), p1811, 1998

Shaoxin Feng

Author

November 17, 2009

Date